UC Irvine
UC Irvine Electronic Theses and Dissertations

Title
Energy-Efficient Node Deployment in Wireless Sensor Networks

Permalink
https://escholarship.org/uc/item/1p70h70n

Author
Karimi Bidhendi, Saeed

Publication Date
2022

Peer reviewed|Thesis/dissertation

UNIVERSITY OF CALIFORNIA,
IRVINE

Energy-Efficient Node Deployment in Wireless Sensor Networks

DISSERTATION

submitted in partial satisfaction of the requirements
for the degree of

DOCTOR OF PHILOSOPHY

in Electrical Engineering and Computer Science

by

Saeed Karimi-Bidhendi

Dissertation Committee:
Chancellor's Professor Hamid Jafarkhani, Chair
Professor A. Lee Swindlehurst
Assistant Professor Yanning Shen

2022

DEDICATION

To my caring, patient, and supportive family

without whom this work would not have been possible.

TABLE OF CONTENTS

LIST OF FIGURES

LIST OF TABLES

ACKNOWLEDGMENTS

I would like to express my appreciation to my advisor, Prof. Hamid Jafarkhani, who has been an incredible mentor to me. His constant support and invaluable guidance paved the way for my graduate studies and I feel extremely fortunate to have him as my advisor. During my experience as a PhD candidate, I also had the privilege of collaborating with Prof. Yanning Shen from whom I learned a lot. I would like to thank both Prof. Yanning Shen and Prof. A. Lee Swindlehurst for serving in my thesis committee and their priceless support, time and review of this work.

Last but not least, I would like to express my gratitude to my parents for their unconditional love, support, and sacrifice. My father taught me that hard work pays off and my mother taught me to be patient and kind. Without their constant support and sacrifice, I would not have been able to acquire the achievements that I possess today. Finally, I would like to thank my brother who has always helped me with his indispensable guidance throughout both my academic and personal life.

VITA

Saeed Karimi-Bidhendi

EDUCATION

PhD in Electrical Engineering and Computer Science   **2022**
University of California, Irvine   *Irvine, CA*

MSc in Electrical Engineering and Computer Science   **2021**
University of California, Irvine   *Irvine, CA*

BSc in Electrical Engineering   **2015**
Sharif University of Technology   *Tehran, Iran*

BSc in Mathematical Sciences   **2015**
Sharif University of Technology   *Tehran, Iran*

RESEARCH EXPERIENCE

Graduate Research Assistant   **2015–2022**
University of California, Irvine   *Irvine, CA*

TEACHING EXPERIENCE

Teaching Assistant   **2015–2022**
University of California, Irvine   *Irvine, CA*

PROFESSIONAL EXPERIENCE

Software Engineering Intern   **2017**
PepperData Inc.   *Santa Clara, CA*

REFEREED JOURNAL PUBLICATIONS

S. Karimi-Bidhendi, J. Guo, and H. Jafarkhani, "Energy-Efficient Deployment in Static and Mobile Heterogeneous Multi-Hop Wireless Sensor Networks," *IEEE Transactions on Wireless Communications*, Dec. 2021.

Y. Shen, **S. Karimi-Bidhendi**, and H. Jafarkhani, "Distributed and Quantized Online Multi-kernel Learning," *IEEE Transactions on Signal Processing*, vol. 69, pp. 5496-5511, Sep. 2021.

S. Karimi-Bidhendi, J. Guo, and H. Jafarkhani, "Energy-Efficient Node Deployment in Heterogeneous Two-Tier Wireless Sensor Networks with Limited Communication Range," *IEEE Transactions on Wireless Communications*, vol. 20, no. 1, pp. 40-55, Sep. 2020.

S. Karimi-Bidhendi, A. Arafati, A.L. Cheng, Y. Wu, A. Kheradvar, and H. Jafarkhani, "Fully automated deep learning segmentation of pediatric cardiovascular magnetic resonance of patients with complex congenital heart diseases," *Journal of Cardiovascular Magnetic Resonance*, vol. 22, no. 1, pp. 1-24, Nov. 2020.

S. Ghasemi-Goojani, **S. Karimi-Bidhendi**, and H. Behroozi, "On the Capacity Region of Asymmetric Gaussian Two-Way Line Channel," *IEEE Transactions on Communications*, vol. 64, no. 9, pp. 3669-3682, Aug. 2016.

REFEREED CONFERENCE PUBLICATIONS

J. Guo, **S. Karimi-Bidhendi**, and H. Jafarkhani, "Energy-Efficient Node Deployment in Wireless Ad-hoc Sensor Networks," *IEEE International Conference on Communications*, pp. 1-6, Jul. 2020.

S. Karimi-Bidhendi, J. Guo, and H. Jafarkhani, "Using Quantization to Deploy Heterogeneous Nodes in Two-Tier Wireless Sensor Networks," *IEEE International Symposium on Information Theory*, pp. 1502-1506, Sep. 2019.

S. Karimi-Bidhendi, F. Munshi, and A. Munshi, "Scalable Classification of Univariate and Multivariate Time Series," *IEEE International Conference on Big Data*, pp. 1598-1605, Dec. 2018.

WORKSHOP PAPERS AND EXTENDED ABSTRACTS

S. Karimi-Bidhendi, A. Arafati, A. Cheng, Y. Wu, A. Kheradvar, and H. Jafarkhani, "Effect of the Down-Sampling Method on the Performance of Deep Learning Algorithms for Segmentation of CMR Images," *Society for Cardiovascular Magnetic Resonance (SCMR) Annual Scientific Sessions*, Feb. 2021.

S. Karimi-Bidhendi, A. Arafati, A. Cheng, Y. Wu, A. Kheradvar, and H. Jafarkhani, "Effect of the Synthetic Data Augmentation on the Performance of Deep Learning Algorithms for Segmentation of CMR Images," *Society for Cardiovascular Magnetic Resonance (SCMR) Annual Scientific Sessions*, Feb. 2021.

H. Liu, A. Liu, T. Li, **S. Karimi-Bidhendi**, Y. Yue, and A. Anandkumar, "Disentangling Causal Effects from Latent Confounders using Interventions," *NeurIPS Workshop on Causal Machine Learning*, Dec. 2019.

PATENT APPLICATIONS

H. Jafarkhani, **S. Karimi-Bidhendi**, and A. Kheradvar, "Synthetically Generating Medical Images using Deep Convolutional Generative Adversarial Networks," US Patent App. No. 17/214442, Mar. 2020.

ARXIV PREPRINTS

S. Karimi-Bidhendi and H. Jafarkhani, "Node Deployment in Heterogeneous Rayleigh Fading Sensor Networks," *preprint arXiv:2204.09172*, Apr. 2022.

A. Liu, H. Liu, T. Li, **S. Karimi-Bidhendi**, Y. Yue, and A. Anandkumar, "Disentangling Observed Causal Effects from Latent Confounders using Method of Moments," *preprint arXiv:2101.06614*, Jan. 2021.

ABSTRACT OF THE DISSERTATION

Energy-Efficient Node Deployment in Wireless Sensor Networks

By

Saeed Karimi-Bidhendi

Doctor of Philosophy in Electrical Engineering and Computer Science

University of California, Irvine, 2022

Chancellor's Professor Hamid Jafarkhani, Chair

With recent advances in communication, sensing, computing, and battery capacity, wireless sensor networks (WSNs) have emerged as a viable technology for monitoring and surveillance purposes in numerous applications such as precision agriculture, healthcare monitoring, and industrial monitoring. However, battery power depletion has remained the most pivotal factor in network failure since sensors are driven by battery that are infeasible to replenish, especially in hostile environments. This calls for innovative approaches for improving the energy-efficiency of WSNs and extending their lifetime.

Empirical measurements have demonstrated that wireless communication dominates the network's energy consumption. Node deployment plays a crucial role in energy-efficiency of the WSN since electromagnetic wave propagation dampens as a power law function of the distance between the transmitter and receiver. In this dissertation, by making a resemblance between network nodes/cells and quantization points/regions, I aim to find the optimal deployment, cell partitioning, and data routing that minimizes the wireless communication power consumption of these networks. In particular, I considered the effect of both large-scale path-loss signal attenuation and small-scale signal fading and modeled the node deployment problem as an optimization problem with the total power consumption of the network as its cost function. To tackle the resulting NP-hard optimization problem, I derived the necessary

conditions for optimal deployment, cell partitioning, and data routing under various network setups and environmental conditions. My theoretical results are then embedded in iterative algorithms to yield energy-efficient deployment and optimal intercommunication protocol for network nodes.

One of key contributions in this dissertation is addressing challenges that arise under various hardware settings, such as homogeneous versus heterogeneous and static versus mobile nodes, in addition to various network architectures, such as two-tier versus multi-hop. Simulation results show that, regardless of the distribution of events to be sensed by sensor nodes, the proposed deployment algorithms outperform previous state-of-the-art methods in the literature by a significant margin. In particular, the proposed algorithms improved these networks' energy efficiency and lifetime by up to a factor of two compared to existing work in the literature. This, in turn, reduces the cost of such networks and demonstrates their potential as a sustainable, rigorous, and cost-effective monitoring system.

Chapter 1

Using Quantization to Deploy Heterogeneous Nodes in Two-Tier Wireless Sensor Networks

1.1 Introduction

Wireless sensor networks (WSNs) have been widely used to gather data from the environment and transfer the sensed information through wireless channels to one or more fusion centers. Based on the network architecture, WSNs can be classified as either non-hierarchical WSNs in which every sensor node has identical functionality and the connectivity of network is usually maintained by multi-hop wireless communications, or hierarchical WSNs where sensor nodes play different roles as they are often divided into clusters and some of them are selected as cluster head or relay. WSNs can also be divided into either homogeneous WSNs [41, 21, 20, 10], in which sensors share the same capacity, e.g., storage, computation power, antennas, sensitivity etc., or heterogeneous WSNs where sensors have different capacities

[51, 38, 42, 79].

Energy consumption is a key bottleneck in WSNs due to limited energy resources of sensors, and difficulty or even infeasibility of recharging the batteries of densely deployed sensors. The energy consumption of a sensor node comes from three primary components: communication energy, computation energy and sensing energy. The experimental measurements show that, in many applications, the computation energy is negligible when it is compared to communication energy[4, 87]. Furthermore, for passive sensors, such as light sensors and acceleration sensors, the sensing energy is significantly small. Therefore, wireless communication dominates the sensor energy consumption in practice. There are three primary methods to reduce the energy consumption of radio communication in the literature: (1) topology control[64, 107], in which unnecessary energy consumption is avoided by properly switching awake and asleep states, (2) energy-efficient routing protocols [10, 48], that are designed to find an optimal path to transfer data, (3) power control protocols [58, 78], that save communication energy by adjusting the transmitter power at each node while keeping reliable communications. Another widely used method, Clustering [112, 58], attempts to balance the energy consumption among sensor nodes by iteratively selecting cluster heads. Unfortunately, above MAC protocols bring about a massive number of message exchanges because the geometry and/or energy information are required during the operation [112]. Also, the node deployment is known and fixed in the aforementioned energy saving approaches while it plays an important role in energy consumption of the WSNs.

In this paper, we study the node deployment problem in heterogeneous two-tier WSNs consisting of heterogeneous APs and heterogeneous FCs, with distortion defined as the total wireless communication power consumption. The optimal energy-efficient sensor deployment in homogeneous WSNs is studied in [41]. However, the homogeneous two-tier WSNs in [41] do not address various challenges that exist in the heterogeneous two-tier WSNs, e.g., unlike regular Voronoi diagrams for homogeneous WSNs, the optimal cells in heterogeneous WSNs

may be non-convex, not star-shaped or even disconnected, and the cell boundaries may not be hyperplanes. Another challenge that exists in the heterogeneous two-tier networks is that unlike the homogeneous case [41], or heterogeneous one-tier case [60], some nodes may not contribute to the energy saving. To the best of our knowledge, the optimal node deployment for energy efficiency in heterogeneous WSNs is still an open problem. Our main goal is to find the optimal AP and FC deployment to minimize the total communication energy consumption. By deriving the necessary conditions of the optimal deployments in such heterogeneous two-tier WSNs, we design a Lloyd-like algorithm to deploy nodes.

The rest of this paper is organized as follows: In Section 1.2, we introduce the system model and problem formulation. In Section 1.3, we study the optimal AP and FC deployment. A numerical algorithm is proposed in Section 1.4 to minimize the energy consumption. Section 1.5 presents the experimental results and Section 1.6 concludes the paper.

1.2 System Model and Problem Formulation

Here, we study the power consumption of the heterogeneous two-tier WSNs consisting of three types of nodes, i.e., homogeneous sensors, heterogeneous APs and heterogeneous FCs. The power consumption models for homogeneous WSNs are discussed in details in [41]. The main difference in this work is the heterogeneous characteristics of the APs and FCs. For the sake of completeness, we describe the system model for heterogeneous WSNs here in details. Given the target area $\Omega \subset \mathbb{R}^2$ which is a convex polygon including its interior, N APs and M FCs are deployed to gather data from sensors. Throughout this paper, we assume that $N \geq M$. Given the sets of AP and FC indices, i.e., $\mathcal{I}_{\mathcal{A}} = \{1, 2, ..., N\}$ and $\mathcal{I}_{\mathcal{B}} = \{1, 2, ..., M\}$, respectively, the index map $T : \mathcal{I}_{\mathcal{A}} \longrightarrow \mathcal{I}_{\mathcal{B}}$ is defined to be $T(n) = m$ if and only if AP n is connected to FC m. The AP and FC deployments are then defined by $P = (p_1, ..., p_N)$ and $Q = (q_1, ..., q_M)$, where $p_n, q_m \in \mathbb{R}^2$ denote the location of AP n and FC m, respectively.

3

Throughout this paper, we assume that each sensor only sends data to one AP. For each $n \in \mathcal{I}_\mathcal{A}$, AP n collects data from sensors in the region $R_n \subset \Omega$; therefore, for each AP deployment P, there exists an AP partition $\mathbf{R} = (R_1, ..., R_N)$ comprised of disjoint subsets of $\mathbb{R}^2$ whose union is Ω. The density of the data rate from the densely distributed sensors is denoted via a continuous and differentiable function $f : \Omega \longrightarrow \mathbb{R}^+$, i.e., the total amount of data gathered from the sensors in region R_n in one time unit is $\int_{R_n} f(w) dw$ [41].

We focus on the power consumption of sensors and APs, since FCs usually have reliable energy resources and their energy consumption is not the main concern. First, we discuss the APs' total power consumption. According to [51], power at the receiver of AP n is modeled as $\mathcal{P}^\mathcal{A}_{r_n} = \rho_n \int_{R_n} f(w) dw, n \in \mathcal{I}_A$, where ρ_n is AP n's power consumption coefficient for receiving data. For simplicity, we assume APs share the same receiving coefficient, i.e., $\rho_n = \rho$. Therefore, the sum of power consumption at receivers is a constant and does not affect the energy optimization and can be ignored in our objective function. In what follows, we focus on power consumption at AP transmitters. The *average-transmitting-power* (Watts) of AP n is defined to be $\mathcal{P}^\mathcal{A}_{t_n} = E^\mathcal{A}_{t_n} \Gamma^\mathcal{A}_n, \forall n \in \mathcal{I}_\mathcal{A}$, where $E^\mathcal{A}_{t_n}$ denotes the *instant-transmission-power* (Joules/second) of AP n, and $\Gamma^\mathcal{A}_n$ denotes the *channel-busy-ratio* for the channel of AP n to its corresponding FC, i.e., the percentage of time that the transmitter forwards data. According to [37, (2.7)], the instant-receive-power through free space is $\mathcal{P}^\mathcal{A}_{r_n} = \frac{\mathcal{P}^\mathcal{A}_{r_n} G_t G_r \lambda^2}{16\pi^2 d^2}$, where G_t is the transmitter antenna gain, G_r is the receiver antenna gain, λ is the signal wavelength, and d is the distance between the transmit and receive antennas. Let $\mathcal{N}_0$ be the noise power. In order to achieve the required SNR threshold γ at the receivers, i.e., $\frac{\mathcal{P}^\mathcal{A}_{r_n}}{\mathcal{N}_0} = \gamma$, the *instant-transmission-power* from AP n to FC $T(n)$ should be set to $E^\mathcal{A}_{t_n} = \eta^\mathcal{A}_{n,T(n)} ||p_n - q_{T(n)}||^2$, where $||.||$ denotes the Euclidean distance, $\eta^\mathcal{A}_{n,T(n)}$ is a constant determined by the antenna gain of AP n and the SNR threshold of FC $T(n)$. Since AP n gathers data from the sensors in R_n, the amount of data received from sensors in one time unit, i.e. the *average-receiver-data-rate*, is $\int_{R_n} f(w) dw$. It can be reasonably assumed that the AP transmitters only forward sensing data when the collected

4

data comes into the buffer. Therefore, the *channel-busy-ratio* is proportional to the *average-receiver-data-rate*, and can be written as $\Gamma_n^{\mathcal{A}} = \frac{\int_{R_n} f(w)dw.T/\zeta_{T(n)}^{\mathcal{A}}}{T} = \frac{\int_{R_n} f(w)dw}{\zeta_{T(n)}^{\mathcal{A}}}$, where $\zeta_{T(n)}^{\mathcal{A}}$ is the AP n's *instant-transmitter-data-rate* which is determined by the SNR threshold at the corresponding FC $T(n)$. Hence, we can rewrite the *average-transmitter-power* of AP n as $\mathcal{P}_{t_n}^{\mathcal{A}} = E_{t_n}^{\mathcal{A}} \Gamma_n^{\mathcal{A}} = \frac{\eta_{n,T(n)}^{\mathcal{A}}}{\zeta_{T(n)}^{\mathcal{A}}} ||p_n - q_{T(n)}||^2 \int_{R_n} f(w)dw$, and the total power consumption at AP transmitters is calculated by summing the *average-transmitter-powers* of APs:

$$
\begin{aligned}
\overline{\mathcal{P}}^{\mathcal{A}}(P,Q,\mathbf{R},T) &= \sum_{n=1}^{N} \mathcal{P}_{t_n}^{\mathcal{A}} \\
&= \sum_{n=1}^{N} \int_{R_n} \frac{\eta_{n,T(n)}^{\mathcal{A}}}{\zeta_{T(n)}^{\mathcal{A}}} ||p_n - q_{T(n)}||^2 f(w)dw
\end{aligned}
\tag{1.1}
$$

Second, we consider sensors' total transmitting power consumption. The total amount of data collected from the sensors inside the region $[w, w + dw]$ in one time unit is equal to $f(w)dw$ since the density of data rate $f(.)$ is approximately uniform on the extremely small region $[w, w + dw]$. Therefore, the sum of *channel-busy-ratios* of sensors in the infinitesimal region $[w, w + dw]$ is $\Gamma_n^{\mathcal{S}} = \frac{f(w)dw.T/\zeta_n^{\mathcal{S}}}{T} = \frac{f(w)dw}{\zeta_n^{\mathcal{S}}}$, where $\zeta_n^{\mathcal{S}}$ is sensors *instant-transmitter-data-rate*. We only consider the homogeneous sensors, i.e., sensors' antenna gains are identical. Moreover, sensors within $[w, w + dw]$ have approximately the same distance to the corresponding AP p_n, and thus have the same *instant-transmission-power* $E_{t_n}^{\mathcal{S}} = \eta_n^{\mathcal{S}} ||w - p_n||^2$, where $\eta_n^{\mathcal{S}}$ is a constant determined by sensors' common transmitter antenna gain, AP n's receiver antenna gain, and the SNR threshold of AP n. Therefore, the sum of *average-transmitter-powers* within the region $[w, w + dw]$ is equal to $\frac{\eta_n^{\mathcal{S}}}{\zeta_n^{\mathcal{S}}} ||p_n - w||^2 f(w)dw$. Since sensors in the region R_n send their data to AP n, the sum *average-transmitter-powers* of sensors in the target area Ω can be written as:

$$
\overline{\mathcal{P}}^{\mathcal{S}}(P,\mathbf{R}) = \sum_{n=1}^{N} \int_{R_n} \frac{\eta_n^{\mathcal{S}}}{\zeta_n^{\mathcal{S}}} ||p_n - w||^2 f(w)dw
\tag{1.2}
$$

The two-tier distortion is then defined as the Lagrangian function of Eqs. (1.1) and (1.2):

5

$$D\left(P,Q,\mathbf{R},T\right) = \overline{\mathcal{P}}^{\mathcal{S}}\left(P,\mathbf{R}\right) + \beta\overline{\mathcal{P}}^{\mathcal{A}}\left(P,Q,\mathbf{R},T\right) = \tag{1.3}$$

$$\sum_{n=1}^{N}\int_{R_n}\left(a_n||p_n - w||^2 + \beta b_{n,T(n)}||p_n - q_{T(n)}||^2\right)f(w)dw$$

where $a_n = \frac{\eta_n^{\mathcal{S}}}{\zeta_n^{\mathcal{S}}}$ and $b_{n,T(n)} = \frac{\eta_{n,T(n)}^{\mathcal{A}}}{\zeta_{T(n)}^{\mathcal{A}}}$. Our main objective in this paper is to minimize the two-tier distortion defined in Eq. (1.3) over the AP deployment P, FC deployment Q, cell partition $\mathbf{R}$ and index map T.

1.3 Optimal Node Deployment in Two-Tier WSNs

Let the optimal AP and FC deployments, cell partitions and index map be denoted by $P^* = (p_1^*, ..., p_N^*)$, $Q^* = (q_1^*, ..., q_M^*)$, $\mathbf{R}^* = (R_1^*, ..., R_N^*)$ and T^*, respectively. In what follows, we determine the properties of such an optimal node deployment $(P^*, Q^*, \mathbf{R}^*, T^*)$ that minimizes the two-tier distortion in (1.3). Note that the index map only appears in the second term of Eq. (1.3); thus, for any given AP and FC deployment P and Q, the optimal index map is given by:

$$T_{[P,Q]}(n) = \arg\min_{m} b_{n,m}||p_n - q_m||^2 \tag{1.4}$$

Eq. (1.4) implies that an AP may not be connected to its closest FC due to heterogeneity of the APs and FCs, and to minimize the two-tier distortion, AP n should be connected to FC m that minimizes the weighted distance $b_{n,m}||p_n - q_m||^2$. Inspired by definition of the two-tier distortion in (1.3), for each $n \in \mathcal{I}_{\mathcal{A}}$, the Voronoi cell V_n for AP and FC deployments P and Q, and index map T is defined as:

$$V_n(P, Q, T) \triangleq \{w : a_n||p_n - w||^2 + \beta b_{n,T(n)}||p_n - q_{T(n)}||^2$$

$$\leq a_k||p_k - w||^2 + \beta b_{k,T(k)}||p_k - q_{T(k)}||^2, \forall k \neq n\} \quad (1.5)$$

Ties are broken in favor of the smaller index to ensure that each Voronoi cell V_n is a Borel set. When it is clear from context, we write V_n instead of $V_n(P, Q, T)$. The collection

$$\mathbf{V}(P, Q, T) \triangleq (V_1, V_2, ..., V_N) \quad (1.6)$$

is referred to as the generalized Voronoi diagram. Note that unlike the regular Voronoi diagrams, the Voronoi cells defined in Eq. (1.5) may be non-convex, not star-shaped or even disconnected. The following proposition establishes that the generalized Voronoi diagram in (1.6) provides the optimal cell partitions, i.e., $\mathbf{R}^*(P, Q, T) = \mathbf{V}(P, Q, T)$.

Proposition 1. *For any partition of the target area Ω such as U, and any AP and FC node deployments such as P and Q and each index map T we have:*

$$D(P, Q, U, T) \geq D(P, Q, \mathbf{V}(P, Q, T), T) \quad (1.7)$$

The proof is provided in Appendix A.1. Note that given AP and FC deployments P and Q, the optimal index map and cell partitioning can then be determined by Eqs. (1.4) and (1.6). The following lemma demonstrates that in any optimal node deployment $(P^*, Q^*, \mathbf{R}^*, T^*)$, each FC contributes to the total distortion, i.e., adding an additional FC results in a strictly lower optimal two-tier distortion regardless of its weights $b_{n,M+1}$ as long as $M < N$ holds.

Lemma 1. *Let $(P^*, Q^*, \mathbf{R}^*, T^*)$ be the optimal node deployment for N APs and M FCs. Given an additional FC with parameters $b_{n,M+1}$ for every $n \in \mathcal{I}_A$, the optimal AP and FC deployments, index map and cell partitioning are denoted via $P' = (p'_1, p'_2, ..., p'_N)$, $Q' =$*

$\left(q'_1, q'_2, ..., q'_{M+1}\right)$, T' and $\mathbf{R}'$, respectively. Assuming $M < N$, we have:

$$D\left(P', Q', \mathbf{R}', T'\right) < D\left(P^*, Q^*, \mathbf{R}^*, T^*\right) \tag{1.8}$$

The proof is provided in Appendix A.2. While Lemma 1 indicates that each FC contributes to the distortion, same may not hold for some APs. As an example to show the existence of useless APs in the optimal deployment, consider two APs and one FC and one-dimensional target region $\Omega = [0,1]$ with parameters $a_1 = b_1 = 1$, $a_2 = b_2 = 100$, $\beta = 1$ and a uniform density function. We search the optimal deployments by Brute-force search. According to our simulation, the optimal deployments share the following properties: (i) Both FC and AP 1 are placed at the centroid of the target region, i.e., $q_1^* = p_1^* = 0.5$; (ii) AP 2's partition is empty, i.e., $V_2(P^*, Q^*, T_{[P^*,Q^*]}) = \varnothing$. Property (ii) implies that AP 2 does not contribute to the two-tier distortion of optimal node deployment. Let $v_n^*(P, Q, T) = \int_{R_n^*} f(w)dw$ be the Lebesgue measure (volume) of the region R_n^*, and $c_n^*(P, Q, T) = \frac{\int_{R_n^*} wf(w)dw}{\int_{R_n^*} f(w)dw}$ be the geometric centroid of the region R_n^*. When there is no ambiguity, we write $v_n^*(P, Q, T)$ and $c_n^*(P, Q, T)$ as v_n^* and c_n^*, respectively. Lemma 1 immediately leads to the following corollary.

Corollary 1. *Let $(P^*, Q^*, \mathbf{R}^*, T^*)$ be the optimal node deployment for N APs and M FCs. If $M \leq N$, then for each $m \in \mathcal{I}_{\mathcal{B}}$, $\sum_{n:T^*(n)=m} v_n^* > 0$.*

The proof can be found in Appendix A.3. The following proposition provides the necessary conditions for the optimal AP and FC deployments in the heterogeneous two-tier WSNs.

Proposition 2. *The necessary conditions for optimal deployments in the heterogeneous two-tier WSNs with the distortion defined in (1.3) are:*

$$
\begin{aligned}
p_n^* &= \frac{a_n c_n^* + \beta b_{n,T^*(n)} q_{T^*(n)}^*}{a_n + \beta b_{n,T^*(n)}} \\
q_m^* &= \frac{\sum_{n:T^*(n)=m} b_{n,m} p_n^* v_n^*}{\sum_{n:T^*(n)=m} b_{n,m} v_n^*}
\end{aligned}
\tag{1.9}
$$

The proof is provided in Appendix A.4. Corollary 1 implies that the denumerator of the second equation in (1.9) is positive; thus, q_m^* is well-defined. According to Eq. (1.9), the optimal location of FC m is the linear combination of the locations of its connected APs, and the optimal location of AP n is on the segment $\overline{c_n^* q_{T^*(n)}^*}$. In the next section, we use the properties derived in Propositions 1 and 2 and in Eq. (1.4), and design a Lloyd-like algorithm to find the optimal node deployment.

1.4   Node Deployment Algorithm

First, we quickly review the conventional Lloyd algorithm. Lloyd algorithm iterates between two steps: In the first step, the node deployment is optimized while the partitioning is fixed and in the second step, the partitioning is optimized while the node deployment is fixed. Although the conventional Lloyd Algorithm can be used to solve one-tier quantizers or one-tier node deployment problems as shown in [38], it cannot be applied to two-tier WSNs where two kinds of nodes are deployed. Inspired by the properties explored in Section III, we propose a heterogeneous two-tier Lloyd (HTTL) algorithm to solve the optimal deployment problem in heterogeneous two-tier WSNs and minimize the two-tier distortion defined in (1.3). Starting with a random initialization for node deployment $(P, Q, \mathbf{R}, T)$ in the target area Ω, our algorithm iterates between four steps: (i) Update the index map T according to Eq. (1.4); (ii) Obtain the cell partitioning according to Eq. (1.5) and update the value of volumes v_n and centroids c_n; (iii) Update the location of FCs according to Eq. (1.9); (iv) Update the location of APs according to Eq. (1.9). The algorithm continues until convergence. In Appendix A.5, we prove that the two-tier distortion will converge with HTTL algorithm. This procedure is summarized in Algorithm 1 below.

Algorithm 1: HTTL Algorithm

Input: Weights $\{a_n\}_{n \in \mathcal{I}_\mathcal{A}}$ and $\{b_{n,m}\}_{n \in \mathcal{I}_\mathcal{A}, m \in \mathcal{I}_\mathcal{B}}$. $\epsilon \in \mathbb{R}^+$.
Output: Optimal node deployment $(P^*, Q^*, \mathbf{R}^*, T^*)$.
  1: Randomly initialize the node deployment $(P, Q, \mathbf{R}, T)$.
  2: **do**
  3: Compute the two-tier distortion $D_{\text{old}} = D(P, Q, \mathbf{R}, T)$.
  4: Update the index map T according to Eq. (1.4).
  5: Update the AP partitioning $\mathbf{R}$ by selecting its nth region as the generalized Voronoi region in (1.5).
  6: Calculate the volumes $\{v_n\}_{n \in \mathcal{I}_\mathcal{A}}$ and centroids $\{c_n\}_{n \in \mathcal{I}_\mathcal{A}}$ of the AP partitioning $\mathbf{R}$.
  7: For each $m \in \mathcal{I}_\mathcal{B}$, move the FC m to $\frac{\sum_{n:T(n)=m} b_{n,m} p_n v_n}{\sum_{n:T(n)=m} b_{n,m} v_n}$.
  8: For each $n \in \mathcal{I}_\mathcal{A}$, move the AP n to $\frac{a_n c_n + \beta b_{n,T(n)} q_{T(n)}}{a_n + \beta b_{n,T(n)}}$.
  9: Update the two-tier distortion $D_{\text{new}} = D(P, Q, \mathbf{R}, T)$.
 10: **While** $\frac{D_{\text{old}} - D_{\text{new}}}{D_{\text{old}}} \geq \epsilon$
 11: **Return:** The node deployment $(P, Q, \mathbf{R}, T)$.

1.5   Experiments

We provide the experimental results in two heterogeneous two-tier WSNs: (i) WSN1: A heterogeneous WSN including 1 FC and 20 APs; (ii) WSN2: A heterogeneous WSN including 4 FCs and 20 APs. We consider the same target domain Ω as in [41, 42], i.e., $\Omega = [0, 10]^2$. The data rate density function is set to a uniform function, $f(\omega) = \frac{1}{\int_\Omega dA} = 0.01$. To evaluate the performance, 10 initial AP and FC deployments on Ω are generated randomly, i.e, every node location is generated with uniform distribution on Ω. In order to make a fair comparison to prior works, similar to the experimental setting in [41, 42], the maximum number of iterations is set to 100, FCs, APs, and geometric centroid of AP cells are denoted, respectively, by colored five-pointed stars, colored circles, and colored crosses. Other parameters are provided in Table 1.1. According to the parameters in Table 1.1, we divide APs into two groups: strong APs ($n \in \{1, \ldots, 10\}$) and weak APs ($n \in \{11, \ldots, 20\}$). Similarly, FCs are divided in strong

Table 1.1: Simulation Parameters

Parameters	$a_{1:10}$	$a_{11:20}$	$b_{1:4,1:2}$	$b_{1:4,3:4}$	$b_{5:20,1:2}$	$b_{5:20,3:4}$
Values	1	2	1	2	2	4

FCs ($m \in \{1, 2\}$) and weak FCs ($m \in \{3, 4\}$). To distinguish strong APs (or FCs) and weak APs (or FCs), we denote strong and weak nodes by solid and hollow symbols, respectively.

Like the experiments in [41], we compare the weighted power of our proposed algorithm with Minimum Energy Routing (MER) [37], Agglomerative Clustering (AC) [47], and Divisive Clustering (DC) [47] algorithms. AC and DC are bottom-up and top-down clustering algorithms, respectively. MER is a combination of Multiplicatively weighted Voronoi Partition [11] and Bellman-Ford algorithms [8, Section 2.3.4]. More details about MER, AC, and DC can be found in [41].
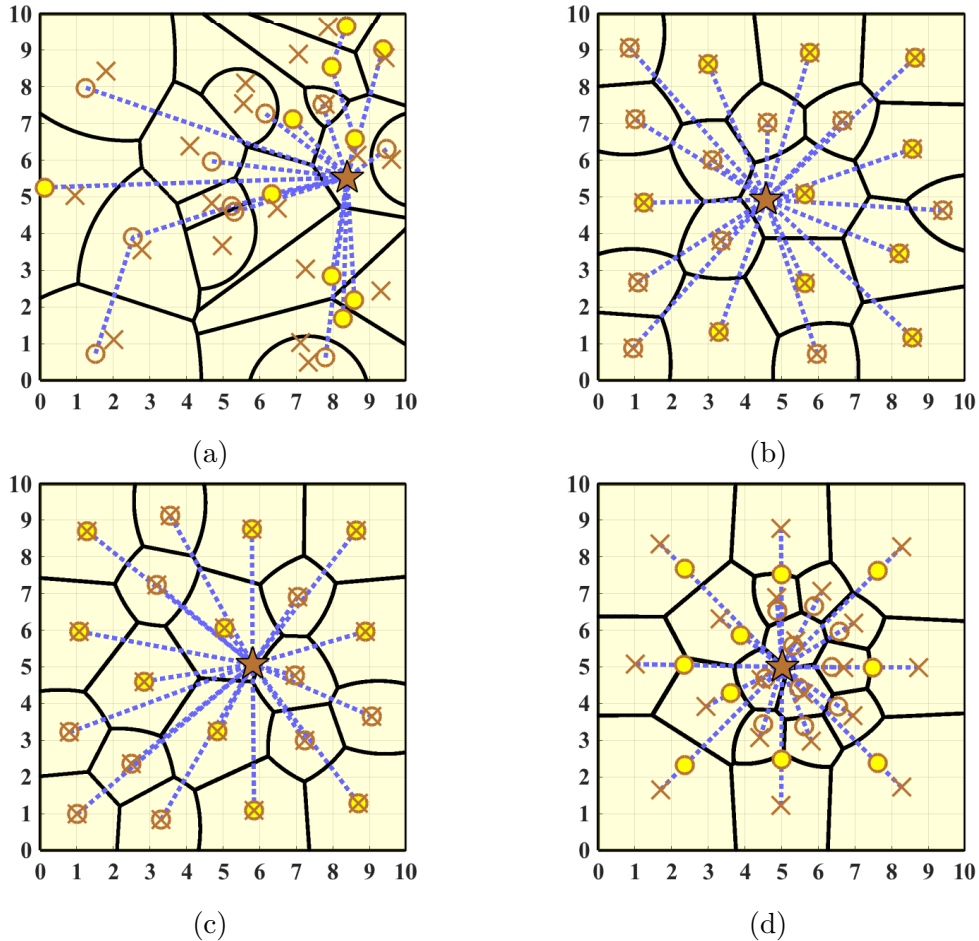
Figure 1.1: AP and FC deployments of different algorithms with $\beta = 0.25$ in WSN1. (a) MER. (b) AC (c) DC. (d) HTTL.

11
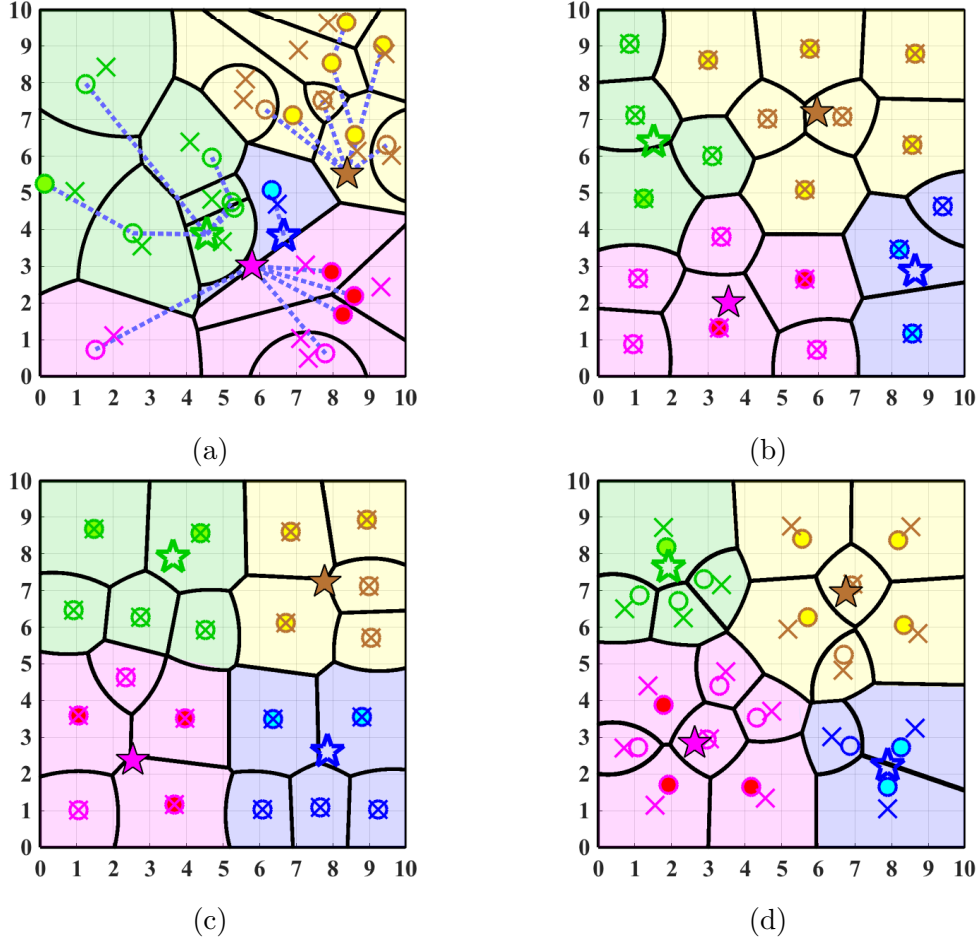
Figure 1.2: AP and FC deployments of different algorithms with $\beta = 0.25$ in WSN2. (a) MER. (b) AC (c) DC. (d) HTTL.

Figs. 1.1a, 1.1b, 1.1c, and 1.1d show final deployments of the four algorithms (MER, AC, DC, and HTTL) in WSN1. The multi-hop paths are denoted by blue dotted lines. As expected from Proposition 2, every AP is placed on the line between the connected FC and geometric center of its cell by running HTTL Algorithm. In addition, the HTTL Algorithm deploys weak APs close to the FC while strong APs are placed on outer regions. Figs. 1.2a, 1.2b, 1.2c, and 1.2d illustrate the final deployments of MER, AC, DC, and HTTL, in WSN2, respectively. Intuitively, strong FCs provide service to more APs compared to weak FCs in both AC and HTTL Algorithms. Moreover, by HTTL Algorithm, strong APs cover larger target regions compared to weak APs in Fig. 1.2d.

Figs. 1.3a and 1.3b show the weighted power comparison of different algorithms in WSN1 and
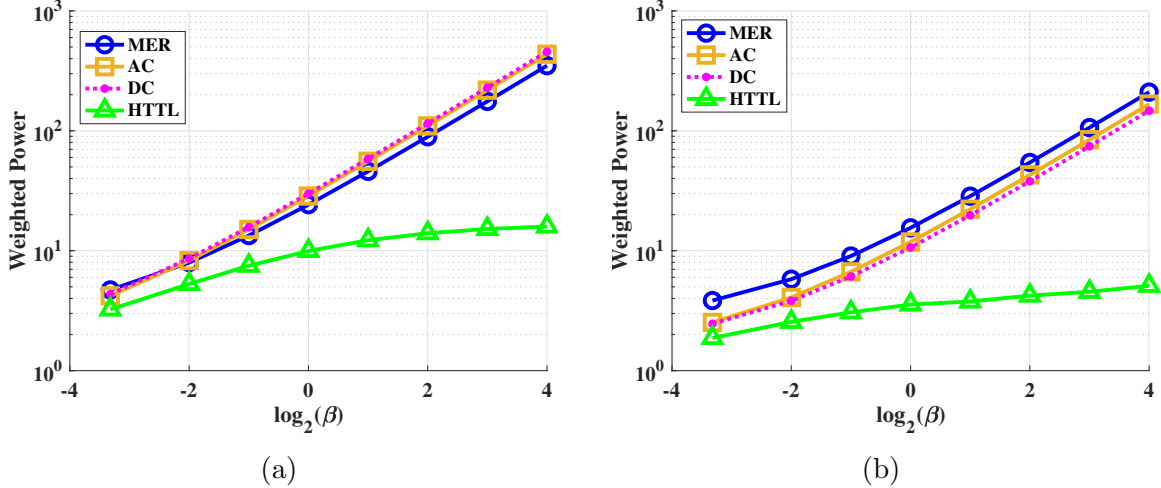
Figure 1.3: The weighted power comparison of different Algorithms. (a) WSN1. (b) WSN2.

WSN2. Obviously, our proposed algorithm, HTTL, outperforms the other three algorithms in both WSN1 and WSN2. In particular, the energy consumption gap between HTTL and other three algorithms increases as the FC energy consumption becomes more important (β increases).

1.6 Conclusion

A heterogeneous two-tier network which collects data from a large-scale wireless sensor to heterogeneous fusion centers through heterogeneous access points is discussed. We studied the minimum power that ensures reliable communication on such two-tier networks and modeled it as a quantization problem. Different from the homogeneous two-tier networks, a novel Voronoi Diagram is proposed to provide the best cell partition for the heterogeneous network. The necessary conditions of optimal node deployment imply that every access point should be placed between its connected fusion center and the geometric center of its cell partition. By defining an appropriate distortion measure, we proposed a heterogeneous two-tier Lloyd Algorithm (HTTL) to minimize the distortion. Simulation results show that HTTL algorithm greatly saves the weighted power or energy in a heterogeneous two-tier network.

13

Chapter 2

Energy-Efficient Node Deployment in Heterogeneous Two-Tier Wireless Sensor Networks with Limited Communication Range

2.1   Introduction

Wireless sensor networks (WSNs) have been widely used to gather data from the environment and transfer the sensed information through wireless channels to one or more fusion centers. Based on the network architecture, WSNs can be classified as either hierarchical or non-hierarchical WSNs. In hierarchical WSNs, sensors play different roles as they are often divided into clusters and some of them are selected as cluster heads or relays. In non-hierarchical WSNs every sensor has identical functionality and the connectivity of network is usually maintained by multi-hop wireless communications. WSNs can also be divided into

either homogeneous WSNs [40, 41, 21, 20, 10], in which sensors share the same capacity, e.g., storage, computation power, antennas, sensitivity etc., or heterogeneous WSNs where sensors have different capacities [51, 38, 42, 79].

Energy consumption is a key bottleneck in WSNs due to limited energy resources of sensors, and difficulty or even infeasibility of recharging the batteries of densely deployed sensors. The energy consumption of a sensor node comes from three primary components: communication energy, computation energy [114] and sensing energy. The experimental measurements show that, in many applications, the computation energy is negligible compared to communication energy[4, 87]. Furthermore, for passive sensors, such as light sensors and acceleration sensors, the sensing energy is significantly small. Therefore, wireless communication dominates the sensor energy consumption in practice. There are three primary methods to reduce the energy consumption of radio communication in the literature: (i) topology control[64, 107], in which unnecessary energy consumption is avoided by properly switching awake and asleep states, (ii) energy-efficient routing protocols [10, 48], that are designed to find an optimal path to transfer data, and (iii) power control protocols [58, 78], that save communication energy by adjusting the transmitter power at each node while keeping reliable communications. Another widely used method, Clustering [112, 58], attempts to balance the energy consumption among sensor nodes by iteratively selecting cluster heads. Unfortunately, the above MAC protocols bring about a massive number of message exchanges because the knowledge of geometry and/or energy is required during the operation [112, 61]. Also, the node deployment is known and fixed in these approaches while it plays an important role in energy consumption of the WSNs.

While WSNs provide a bridge between the physical and virtual information world, the collected data is not useful if it cannot be transmitted from sensors to access points and eventually to base stations. Connectivity, as a prominent necessity in WSNs, is widely studied under the binary communication model in [21] and [68, 106, 7, 98, 52, 113]. In the binary

communication model, each node can only communicate to other nodes within a certain range due to the limited transmission power. Note that connectivity is guaranteed when nodes are linked by wire lines; however, the same is not true for WSNs due to the limited available power in wireless communication. Many distributed sensor deployment algorithms, such as Lloyd Algorithm, do not take both power consumption and connectivity into account; therefore, they usually converge to a sub-optimal deployment in which nodes are divided into several disconnected components. For a one-tier WSN, the design of optimal deployment algorithms that consider connectivity and coverage is studied in [38]. While we consider a 2D deployment in this work, the case of 3D optimal deployment has been studied in [62, 43], and the applicability of the evolutionary algorithms to solve UAV deployment problems has been introduced in [93].

In this paper, we study the node deployment problem in heterogeneous two-tier WSNs consisting of heterogeneous APs and heterogeneous FCs, with and without communication power constraints. We consider the total wireless communication power consumption as the cost function. The optimal energy-efficient sensor deployment in homogeneous WSNs is studied in [41]. However, the homogeneous two-tier WSNs in [41] do not address various challenges that exist in the heterogeneous two-tier WSNs, e.g., unlike regular Voronoi diagrams for homogeneous WSNs, the optimal cells in heterogeneous WSNs may be non-convex, not star-shaped or even disconnected, and the cell boundaries may not be hyperplanes. Another challenge in the heterogeneous two-tier networks is that unlike the homogeneous case [41], or heterogeneous one-tier case [60], some nodes may not contribute to the energy saving. To the best of our knowledge, the optimal node deployment for energy efficiency in heterogeneous WSNs is still an open problem. Our main goal is to find the optimal AP and FC deployment to minimize the total communication power consumption. By deriving the necessary conditions of the optimal deployments in such heterogeneous two-tier WSNs, we design Lloyd-like algorithms to deploy nodes. In addition, we update the designed deployment algorithms to consider the effects of limited communication range. We also study the

16

trade-off between AP and sensor power consumption.

The rest of this paper is organized as follows: In Section 2.2, we introduce the system model and problem formulation. In Section 2.3, we study the optimal AP and FC deployment and provide the corresponding necessary conditions. A numerical algorithm is proposed in Section 2.4 to minimize the energy consumption. An analysis of AP and sensor power trade-off is provided in Section 2.5. In Section 2.6, an algorithm is proposed to maximize the network coverage and minimize the power consumption, simultaneously. Section 2.7 presents the experimental results and Section 2.8 concludes the paper.

2.2 System Model and Problem Formulation

Here, we study the power consumption of the heterogeneous two-tier WSNs consisting of three types of nodes, i.e., homogeneous sensors, heterogeneous APs and heterogeneous FCs. The power consumption models for homogeneous WSNs are discussed in details in [41]. The main difference in this work is the heterogeneous characteristics of the APs and FCs. For the sake of completeness, we describe the system model, as shown in Fig. 2.1, for heterogeneous WSNs here in details. Given the target area $\Omega \subset \mathbb{R}^2$ which is a convex polygon including its interior, N APs and M FCs are deployed to gather data from densely deployed sensors. Throughout this paper, we assume that $N \geq M$. Given the sets of AP and FC indices, i.e., $\mathcal{I}_{\mathcal{A}} = \{1, 2, ..., N\}$ and $\mathcal{I}_{\mathcal{B}} = \{1, 2, ..., M\}$, respectively, the index map $T : \mathcal{I}_{\mathcal{A}} \longrightarrow \mathcal{I}_{\mathcal{B}}$ is defined to be $T(n) = m$ if and only if AP n is connected to FC m. If AP n has no associated FC, we set $T(n) = -1$. Conversely, $T^{-1}(m)$ is defined to be the set of all AP indices n such that $T(n) = m$, and $|T^{-1}(m)|$ denotes the cardinality of this set. The AP and FC deployments are then defined by $P = (p_1, ..., p_N)$ and $Q = (q_1, ..., q_M)$, where $p_n, q_m \in \mathbb{R}^2$ denote the location of AP n and FC m, respectively. Throughout this paper, we assume that each sensor only sends data to one AP. For each $n \in \mathcal{I}_{\mathcal{A}}$, AP n collects data from sensors

17

in the region $R_n \subset \Omega$; therefore, for each AP deployment P, there exists an AP partition $\mathbf{R} = (R_1, ..., R_N)$ comprised of disjoint subsets of $\mathbb{R}^2$ whose union is Ω. The density of sensors is denoted via a continuous and differentiable function $f : \Omega \longrightarrow \mathbb{R}^+$. The total amount of data gathered from the sensors in region R_n in one time unit is $g \int_{R_n} f(w)dw$, where g is the bit-rate of the sensors. Due to the homogeneity of sensors, g is a constant [41].
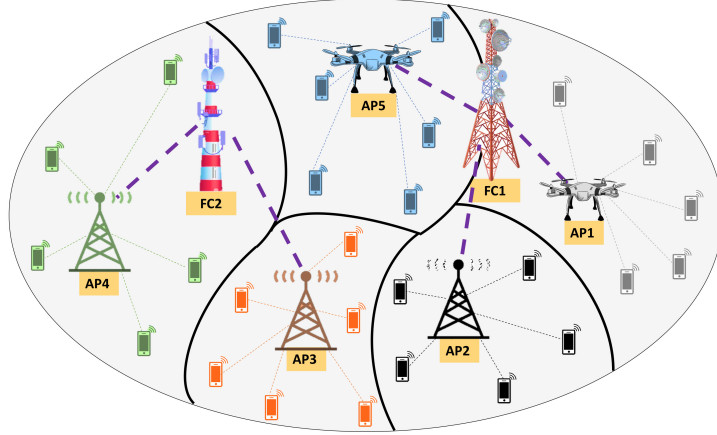
Figure 2.1: System model.

We focus on the power consumption of sensors and APs, since FCs usually have reliable energy resources and their energy consumption is not the main concern. First, we discuss the sensors' power consumption. As shown in [41], because of the path-loss, the instant transmission power is proportional to the square of the distance between the two nodes and a constant that depends on the characteristics of the two nodes, i.e., $a \times \|p_n - w\|^2$ for a sensor located at w that sends its data to AP n. According to [49], the parameter a is given as $a = \frac{P_{r-th}(4\pi)^2}{G_t G_r \lambda^2}$, where P_{r-th} is the minimum receiver power threshold, G_t and G_r are the transmitter and receiver antenna gains, respectively, and λ is the carrier signal wavelength. For homogeneous WSNs, all nodes in each tier have the same characteristics and therefore, the parameter a is the same and will not affect the optimization. However, in a heterogeneous WSN, the heterogeneity of APs causes nodes to have different antenna gains and SNR thresholds; therefore, the parameter a will be a function of the node index. Hence, the sensors' power consumption can be written as

$$\overline{\mathcal{P}}^{\mathcal{S}}(P, \mathbf{R}) = \sum_{n=1}^{N} \int_{R_n} a_n \|p_n - w\|^2 f(w) dw. \tag{2.1}$$

Similarly, for the AP's power consumption, the instant transmission power between AP n and FC $T(n)$ can be written as $b \times \|p_n - q_{T(n)}\|^2$ where the parameter b depends on the antenna gain and SNR threshold of FC $T(n)$ and antenna gain of AP n [49]. Hence, it is the same for homogeneous WSNs and will not affect the optimization. However, in a heterogeneous WSN, the heterogeneity of APs and FCs causes the parameter b to be a function of the node indices. Therefore, the APs' power consumption can be written as

$$\overline{\mathcal{P}}^{\mathcal{A}}(P, Q, \mathbf{R}, T) = \sum_{n=1}^{N} \int_{R_n} b_{n,T(n)} \|p_n - q_{T(n)}\|^2 f(w) dw. \tag{2.2}$$

Our goal in this work is to minimize the power consumptions in (2.1) and (2.2). However, as will be shown later, there is a trade-off between the two power consumptions. As such, one objective is to minimize the AP transmission power in (2.2) given a constraint on the sensor transmission power in (2.1). Mathematically, this results in the AP-Sensor power function defined as

$$A(s) \triangleq \inf_{(P,Q,\mathbf{R},T):\overline{\mathcal{P}}^{\mathcal{S}}(P,\mathbf{R}) \leq s} \overline{\mathcal{P}}^{\mathcal{A}}(P, Q, \mathbf{R}, T). \tag{2.3}$$

Similarly, one can define the Sensor-AP power function to minimize the sensor power in (2.1) given a constraint on the AP transmission power in (2.2) as follows:

$$S(a) \triangleq \inf_{(P,Q,\mathbf{R},T):\overline{\mathcal{P}}^{\mathcal{A}}(P,Q,\mathbf{R},T) \leq a} \overline{\mathcal{P}}^{\mathcal{S}}(P, \mathbf{R}). \tag{2.4}$$

The two-tier power consumption is then defined as the Lagrangian function of (2.2) and (2.1):

$$\overline{\mathcal{P}}\left(P,Q,\mathbf{R},T\right) = \overline{\mathcal{P}}^{\mathcal{S}}\left(P,\mathbf{R}\right) + \beta\overline{\mathcal{P}}^{\mathcal{A}}\left(P,Q,\mathbf{R},T\right) \qquad (2.5)$$

$$= \sum_{n=1}^{N} \int_{R_n} \left(a_n \|p_n - w\|^2 + \beta b_{n,T(n)} \|p_n - q_{T(n)}\|^2\right) f(w) dw.$$

Our main objective in this paper is to minimize the two-tier power consumption defined in (2.5) over the AP deployment P, FC deployment Q, cell partition $\mathbf{R}$ and index map T and study the behavior of the AP-Sensor power function.

2.3 Optimal Node Deployment in Two-Tier WSNs

As it is shown in (2.5), the two-tier power consumption depends on four variables P, Q, $\mathbf{R}$ and T. Therefore, our goal is to find the optimal AP and FC deployments, cell partitioning and index map, denoted by $P^* = (p_1^*, ..., p_N^*)$, $Q^* = (q_1^*, ..., q_M^*)$, $\mathbf{R}^* = (R_1^*, ..., R_N^*)$ and T^*, respectively, that minimizes the two-tier power consumption. Note that not only the variables P, Q, $\mathbf{R}$ and T are intertwined, i.e., the best value for each of them depends on the value of the other three variables, but also this optimization problem is NP-hard. Our approach is to design an iterative algorithm that optimizes the value of one variable while the other three variables are held fixed. To this end, first we derive the necessary conditions for optimal deployment at each step.

Note that the index map only appears in the second term of (2.5); thus, for any given AP and FC deployment P and Q, the optimal index map is given by:

$$T(n) = \arg\min_{m} b_{n,m} \|p_n - q_m\|^2. \qquad (2.6)$$

Ties are broken in favor of the smaller index for a unique mapping. Eq. (2.6) implies that

an AP may not be connected to its closest FC due to heterogeneity of the APs and FCs, and to minimize the two-tier power consumption, AP n should be connected to FC m that minimizes the weighted distance $b_{n,m}\|p_n - q_m\|^2$.

Next, we study the properties of optimal cell partitioning. For each $n \in \mathcal{I}_{\mathcal{A}}$, we define the Voronoi cell V_n for AP and FC deployments P and Q, and index map T as:

$$V_n(P,Q,T) \triangleq \{w : a_n\|p_n - w\|^2 + \beta b_{n,T(n)}\|p_n - q_{T(n)}\|^2$$

$$\leq a_k\|p_k - w\|^2 + \beta b_{k,T(k)}\|p_k - q_{T(k)}\|^2, \forall k \neq n\}. \quad (2.7)$$

Ties are broken in favor of the smaller index to ensure that each Voronoi cell V_n is a Borel set. When it is clear from the context, we write V_n instead of $V_n(P,Q,T)$. The collection

$$\mathbf{V}(P,Q,T) \triangleq (V_1, V_2, ..., V_N) \quad (2.8)$$

is referred to as the generalized Voronoi diagram. Note that unlike the regular Voronoi diagrams, the Voronoi cells defined in (2.7) may be non-convex, not star-shaped or even disconnected. The following proposition establishes that the generalized Voronoi diagram in (2.8) provides the optimal cell partitions, i.e., $\mathbf{R}^*(P,Q,T) = \mathbf{V}(P,Q,T)$ for a given P, Q, T.

Proposition 3. *For any partition of the target area Ω such as U, and any AP and FC node deployments such as P and Q and each index map T we have:*

$$\overline{\mathcal{P}}(P,Q,U,T) \geq \overline{\mathcal{P}}(P,Q,\mathbf{V}(P,Q,T),T). \quad (2.9)$$

The proof is provided in Appendix B.1.

Next, we aim to derive the necessary condition for optimal locations of APs and FCs. For this purpose, first we need to show that each FC contributes to the total power consumption in

an optimal node deployment, i.e., adding an additional FC results in a strictly lower optimal two-tier power consumption regardless of its weights $b_{n,M+1}$ as long as $M < N$ holds.

Lemma 2. *Let $(P^*, Q^*, \mathbf{R}^*, T^*)$ be the optimal node deployment for N APs and M FCs. Given an additional FC with parameters $b_{n,M+1}$ for every $n \in \mathcal{I_A}$, the optimal AP and FC deployments, index map and cell partitioning are denoted via $P' = (p'_1, p'_2, ..., p'_N)$, $Q' = (q'_1, q'_2, ..., q'_{M+1})$, T' and $\mathbf{R}'$, respectively. Assuming $M < N$, we have:*

$$\overline{\mathcal{P}}(P', Q', \mathbf{R}', T') < \overline{\mathcal{P}}(P^*, Q^*, \mathbf{R}^*, T^*). \tag{2.10}$$

The proof is provided in Appendix B.2.

Let $v_n^*(P, Q, T) = \int_{R_n^*} f(w)dw$ be the Lebesgue measure (volume) of the region R_n^*, and $c_n^*(P, Q, T) = \frac{\int_{R_n^*} w f(w)dw}{\int_{R_n^*} f(w)dw}$ be the geometric centroid of the region R_n^*. When there is no ambiguity, we write $v_n^*(P, Q, T)$ and $c_n^*(P, Q, T)$ as v_n^* and c_n^*, respectively. Lemma 2 immediately leads to the following corollary.

Corollary 2. *Let $(P^*, Q^*, \mathbf{R}^*, T^*)$ be the optimal node deployment for N APs and M FCs. If $M \leq N$, then for each $m \in \mathcal{I_B}$, $\sum_{n:T^*(n)=m} v_n^* > 0$.*

The proof is provided in Appendix B.3.

Lemma 2 and Corollary 2 are technical results that we need to prove the following proposition that provides the necessary conditions for the optimal AP and FC deployments in the heterogeneous two-tier WSNs.

Proposition 4. *The necessary conditions for optimal deployments in the heterogeneous two-tier WSNs with power consumption defined in (2.5) are:*

$$p_n^* = \frac{a_n c_n^* + \beta b_{n,T^*(n)} q_{T^*(n)}^*}{a_n + \beta b_{n,T^*(n)}},$$

$$q_m^* = \frac{\sum_{n:T^*(n)=m} b_{n,m} p_n^* v_n^*}{\sum_{n:T^*(n)=m} b_{n,m} v_n^*}.$$

(2.11)

The proof is provided in Appendix B.4.

Corollary 2 implies that the denominator of the second equation in (2.11) is positive; thus, q_m^* is well-defined. According to (2.11), the optimal location of FC m is the linear combination of the locations of its connected APs, and the optimal location of AP n is on the segment $\overline{c_n^* q_{T^*(n)}^*}$. While Lemma 2 indicates that each FC contributes to the power consumption, the same result may not hold for some APs. To show that under certain settings, an AP may not be useful, i.e., no sensor sends data to it, we use the sensor network in the following lemma as an example.

Lemma 3. *Consider two APs and one FC within the target region $\Omega = [0, 1]$ with parameters $b_{1,1} = \kappa \times a_1$, $b_{2,1} = \kappa \times a_2$ where κ is a positive constant, and a uniform density function. The necessary and sufficient condition for both APs to be useful is*

$$\sqrt{\frac{4\beta' + 1}{\beta' + 1}} - 1 \le \sqrt{\frac{a_1}{a_2}} \le \frac{1}{\sqrt{\frac{4\beta'+1}{\beta'+1}} - 1},$$

(2.12)

where $\beta' = \beta \times \kappa$. If the above condition holds, both APs are useful and the optimal two-tier power consumption is given by:

$$\overline{\mathcal{P}} = \frac{(4\beta' + 1)}{12(\beta' + 1)} \times \left(\frac{\sqrt{a_1 a_2}}{\sqrt{a_1} + \sqrt{a_2}} \right)^2.$$

(2.13)

Otherwise, all sensors send their data to the stronger AP and we have:

$$\overline{\mathcal{P}} = \frac{\min\left(a_1, a_2\right)}{12}. \tag{2.14}$$

The proof is provided in Appendix B.5.

In the next section, we use the properties derived in Propositions 1 and 2 and in (2.6), and design a Lloyd-like algorithm to find the optimal node deployment.

2.4 Node Deployment Algorithm

First, we quickly review the conventional Lloyd algorithm. Lloyd Algorithm iterates between two steps: In the first step, the node deployment is optimized while the partitioning is fixed and in the second step, the partitioning is optimized while the node deployment is fixed. Although the conventional Lloyd algorithm can be used to solve one-tier quantizers or one-tier node deployment problems as shown in [38], it cannot be applied to two-tier WSNs where two kinds of nodes are deployed. Inspired by the properties explored in Section III, we propose a heterogeneous two-tier Lloyd (HTTL) algorithm to solve the optimal deployment problem in heterogeneous two-tier WSNs and minimize the two-tier power consumption defined in (2.5). Starting with a random initialization for node deployment $(P, Q, \mathbf{R}, T)$ in the target area Ω, our algorithm iterates between four steps: (i) Update the index map T according to (2.6); (ii) Obtain the cell partitioning according to (2.7) and update the value of volumes v_n and centroids c_n; (iii) For each $m \in \mathcal{I}_\mathcal{B}$, if $T^{-1}(m)$ is not empty, update the location of FC m according to (2.11); otherwise, randomly select an index $m' \in \mathcal{I}_\mathcal{B}$ according to the distribution $P(m') = \frac{\left|T^{-1}(m')\right|}{N}$, and move FC m to a random location within $\bigcup_{n:T(n)=m'} R_n$; (iv) Update the location of APs according to (2.11). The algorithm continues until the stop criterion, $\frac{\overline{\mathcal{P}}_{\text{old}} - \overline{\mathcal{P}}_{\text{new}}}{\overline{\mathcal{P}}_{\text{old}}} \geq \epsilon$ is satisfied ($\overline{\mathcal{P}}_{\text{old}}$ and $\overline{\mathcal{P}}_{\text{new}}$ are the average powers in the previous

and current iterations, respectively.).

Proposition 5. *HTTL Algorithm is an iterative improvement algorithm, i.e., the Lagrangian function in (2.5) is non-increasing and the algorithm converges.*

The proof is provided in Appendix B.6.

2.5 AP-Sensor Power Function

Note that the Lagrangian two-tier power consumption defined in (2.5) is the unconstrained version of the constrained optimization problems defined in (2.3) and (2.4). Since the AP-Sensor power function and the Sensor-AP power function are dual of each other, in this section, we only study the properties of the AP-Sensor power function $A(s)$. An AP-Sensor power pair (s, a) is *achievable* if and only if there is a node deployment $(P, Q, \mathbf{R}, T)$ such that $\overline{\mathcal{P}}^{\mathcal{A}}(P, Q, \mathbf{R}, T) = a$ while $\overline{\mathcal{P}}^{\mathcal{S}}(P, \mathbf{R}) \leq s$. Moreover, a deployment $(P, Q, \mathbf{R}, T)$ is a *feasible* solution for the power pair (s, a) if and only if $\overline{\mathcal{P}}^{\mathcal{A}}(P, Q, \mathbf{R}, T) = a$ while $\overline{\mathcal{P}}^{\mathcal{S}}(P, \mathbf{R}) \leq s$. By definition, it is evident that every point above the curve $A(s)$ is also achievable. In what follows, we analyze the properties of the AP-Sensor power function. Without loss of generality, we assume that $a_1 \leq a_2 \leq \ldots \leq a_N$ holds. A $K-$level one-tier quantizer is a tuple $(X, \mathbf{R})$, i.e. the location of points $X = (x_1, \cdots, x_K)$ and the partitioning $\mathbf{R} = (R_1, \cdots, R_K)$ of the target region, such that x_i is the quantization point for all $\omega \in R_i$ and K is the number of sub-regions. Let D_K be the minimum distortion of a heterogeneous $K-$level one-tier quantizer in the space Ω with parameters $a_1, \ldots, a_K$, i.e., we have:

$$D_K = \min_{X, \mathbf{R}} \sum_{i=1}^{K} \int_{R_i} a_i \|x_i - w\|^2 f(w) dw, \tag{2.15}$$

where the minimum is over all node deployments $X = (x_1, \ldots, x_K)$ and partitioning $\mathbf{R} = (R_1, \ldots, R_K)$ of Ω.

Lemma 4. *Let N and M be the number of APs and FCs where $N > M$. Then, the AP-Sensor power function $A(s)$ is a non-increasing function with the domain $[D_N, +\infty)$ such that $A(s) > 0$ for $s \in [D_N, D_M)$ and $A(s) = 0$ for $s \in [D_M, +\infty)$.*

The proof is provided in Appendix B.7.

Lemma 4 characterizes the non-increasing property of $A(s)$ in addition to defining its domain based on the properties of a regular quantizer. For a fixed partitioning $\mathbf{R} = (R_1, \ldots, R_N)$, let $\mathcal{H}(\mathbf{R}) = \sum_{i=1}^{N} \int_{R_i} a_i \|c_i - w\|^2 f(w) dw$ where c_i is the centroid of the region R_i, i.e., $\mathcal{H}(\mathbf{R})$ is the minimum one-tier power consumption with parameters $a_1, \ldots, a_N$ for a fixed partitioning $\mathbf{R}$. For the special case of $M = 1$, the following lemma derives a closed-form solution for the AP-Sensor power function for any fixed partitioning of Ω.

Lemma 5. *For $Q = (q)$, $P = (p_1, \ldots, p_N)$, and fixed $\mathbf{R}$, define $A(s, \mathbf{R})$ to be:*

$$A(s, \mathbf{R}) \triangleq \inf_{(P,Q,T): \overline{\mathcal{P}}^{\mathcal{S}}(P,\mathbf{R}) \leq s} \overline{\mathcal{P}}^{\mathcal{A}}(P, Q, \mathbf{R}, T). \tag{2.16}$$

We have:

(i) The domain of $A(s, \mathbf{R})$ is $\{(s, \mathbf{R}) \,|\, s \geq \mathcal{H}(\mathbf{R})\}$.

(ii) If $b_{i,1} = \kappa a_i$ for $\kappa \in \mathbb{R}^+$ and each $i \in \mathcal{I}_{\mathcal{A}}$, when $(s, \mathbf{R}) \in \{(s, \mathbf{R}) \,|\, \mathcal{H}(\mathbf{R}) \leq s \leq \mathcal{J}(\mathbf{R})\}$, we have:

$$A(s, \mathbf{R}) = \kappa \left[\sqrt{\mathcal{J}(\mathbf{R}) - \mathcal{H}(\mathbf{R})} - \sqrt{s - \mathcal{H}(\mathbf{R})} \right]^2, \tag{2.17}$$

and $A(s, \mathbf{R}) = 0$ for $s \geq \mathcal{J}(\mathbf{R})$ where $\mathcal{J}(\mathbf{R})$ is defined as:

$$\mathcal{J}(\mathbf{R}) = \sum_{n=1}^{N} \int_{R_n} a_n \left\| \frac{\sum_{i=1}^{N} a_i v_i c_i}{\sum_{i=1}^{N} a_i v_i} - w \right\|^2 f(w) dw, \tag{2.18}$$

where v_i and c_i are volume and centroid of the region R_i, respectively.

The proof is provided in Appendix B.8.

In Section 2.7, we experimentally plot the AP-Sensor power function defined in (2.3) and verify the above properties. We conclude this section by deriving a closed-form formula for the AP-Sensor power function for the same setting used in Lemma 3.

Lemma 6. *Consider two APs and one FC within the target region $\Omega = [0, 1]$ with parameters $b_{1,1} = \kappa \times a_1$, $b_{2,1} = \kappa \times a_2$, and a uniform density function. If (2.12) holds, we have:*

$$A(s) = \kappa \left[\frac{1}{2} \left(\frac{\sqrt{a_1 a_2}}{\sqrt{a_1} + \sqrt{a_2}} \right) - \sqrt{s - \frac{1}{12} \left(\frac{\sqrt{a_1 a_2}}{\sqrt{a_1} + \sqrt{a_2}} \right)^2} \right]^2, \qquad (2.19)$$

for $\frac{1}{12} \left(\frac{\sqrt{a_1 a_2}}{\sqrt{a_1} + \sqrt{a_2}} \right)^2 \leq s < \frac{\min(a_1, a_2)}{12}$ and $A(s) = 0$ for $s \geq \frac{\min(a_1, a_2)}{12}$. If (2.12) does not hold, we have $A(s) = 0$ for any s.

The proof is provided in Appendix B.9.

Lemma 6 shows that $A(s)$ is not continuous at $s^* = \frac{\min(a_1, a_2)}{12}$ for this example. In addition, $A(s)$ is convex in the intervals $[0, s^*)$ and $[s^*, +\infty)$.

2.6   Limited Communication Range

Note that when sensors or APs have limited transmission power, not all APs can communicate with FCs. Similarly, only sensors within the sensing range of APs in the set $\{n | T(n) \neq -1\}$ can transmit their collected information to fusion centers. We consider a common power constraint σ^2 for homogeneous densely deployed sensors, and power constraints $\sigma_n^2, n \in \mathcal{I}_A$ for the heterogeneous APs. In other words, to maintain the connectivity of the network, a sensor at position w can forward its collected data to AP n, and AP n can

27

in turn sends the data to FC m if and only if:

$$a_n\|p_n - w\|^2 \le \sigma^2 \quad , \quad b_{n,m}\|p_n - q_m\|^2 \le \sigma_n^2, \tag{2.20}$$

or equivalently:

$$\|p_n - w\| \le \frac{\sigma}{\sqrt{a_n}} \quad , \quad \|p_n - q_m\| \le \frac{\sigma_n}{\sqrt{b_{n,m}}}. \tag{2.21}$$

Hence, we use the coverage defined by:

$$C(P,T) = \int_{\bigcup_{n:T(n)\ne -1} \mathcal{B}\left(p_n, \frac{\sigma}{\sqrt{a_n}}\right) \cap \Omega} f(w)dw \tag{2.22}$$

as a performance measure along with the two-tier power consumption in (2.5) when communication range is limited, where $\mathcal{B}(c,r) = \{\omega \mid \|\omega - c\| \le r\}$ is a disk centered at c with radius r. Note that HTTL Algorithm described in Section 2.4 can converge to a deployment in which (2.21) may not hold. Our main goal in this section is to find a proper deployment that not only minimizes the two-tier power consumption $\overline{\mathcal{P}}(P,Q,\mathbf{R},T)$ in (2.5), but also maximizes the total coverage $C(P,T)$ in (2.22). In what follows, we describe our approach in details.

Starting with an initial deployment $(P,Q,\mathbf{R},T)$, if $\left\{m \mid m \in \mathcal{I}_\mathcal{B}, q_m \in \mathcal{B}\left(p_n, \frac{\sigma_n}{\sqrt{b_{n,m}}}\right)\right\} \ne \varnothing$, then the index map T is updated as

$$T(n) = \underset{m:q_m \in \mathcal{B}\left(p_n, \frac{\sigma_n}{\sqrt{b_{n,m}}}\right)}{\arg\min} b_{n,m}\|p_n - q_m\|^2, \tag{2.23}$$

otherwise, we set $T(n) = -1$, indicating that AP n has no associated FC. Note that although some sensors in the region $R_n, n \in \mathcal{I}_\mathcal{A}$, may not be able to transmit their data to AP n due to their limited transmission power, we still partition the target region using the generalized

Voronoi diagram in (2.7) and (2.8) since it minimizes the two-tier power consumption given a fixed node deployment and index map. But instead of using all N APs for generalized Voronoi partitioning, we only use APs in the set $\{n|T(n) \neq -1\}$.
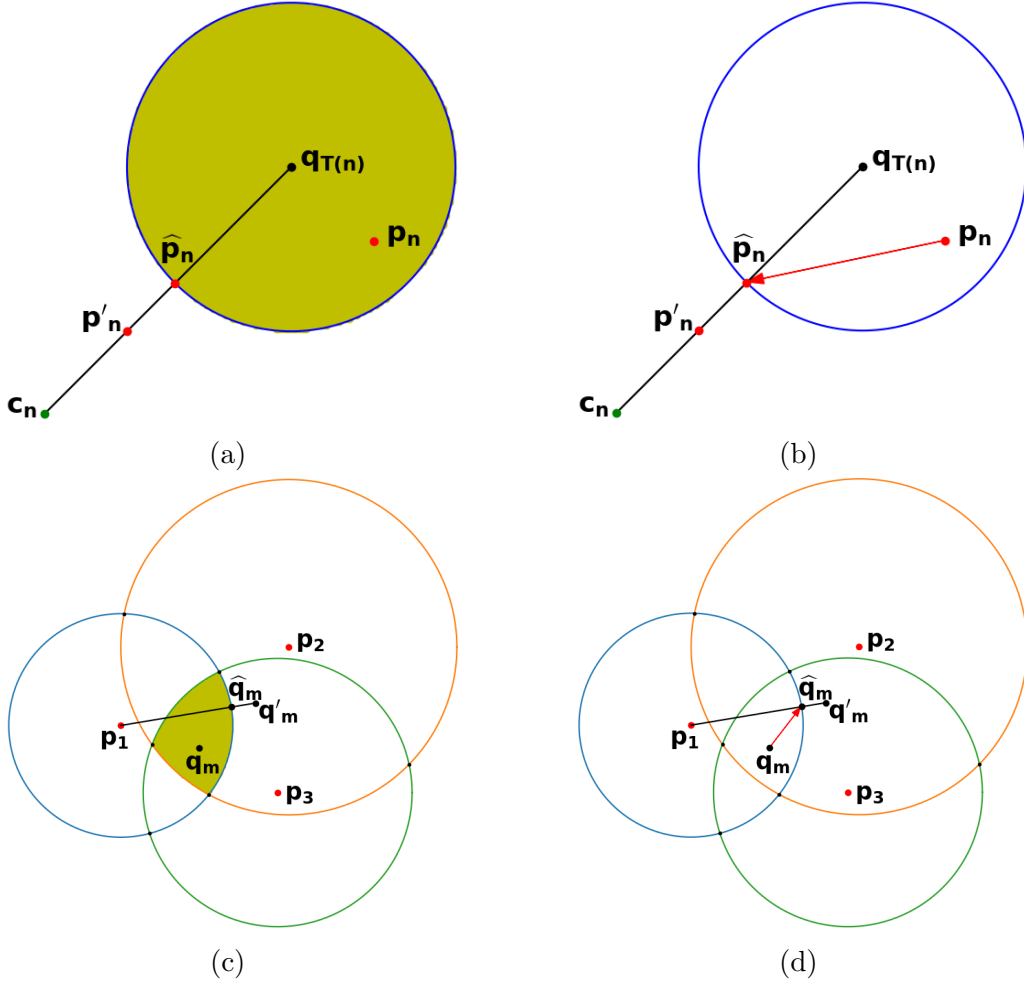
Figure 2.2: Optimal AP and FC movement. (a) Desired region for AP. (b) Optimal positioning of AP. (c) Desired region for FC. (d) Optimal positioning of FC.

For each AP in the set $\{n|T(n) = -1\}$, we randomly move AP inside the target region. Similarly, for each FC in the set $\{m|T^{-1}(m) = \varnothing\}$, we randomly relocate the FC inside Ω. For those APs that have an associated FC, Proposition 4 indicates that their current locations should be updated according to (2.11), as we did in Step 8 of the HTTL algorithm; however, as it is illustrated in Fig. 2.2a, the optimal location $p'_n = \frac{a_n c_n + \beta b_{n,T(n)} q_{T(n)}}{a_n + \beta b_{n,T(n)}}$ for AP n may lie outside the communication range of its corresponding FC, that we refer to as the

29

desired region for AP n. In that case, AP n is moved to the closest point to p'_n within its desired region, denoted by $\widehat{p}_n$, as it is shown in Fig. 2.2b. Similarly, (2.11) implies that FC m should be relocated to the position $q'_m = \frac{\sum_{n:T(n)=m} b_{n,m} p_n v_n}{\sum_{n:T(n)=m} b_{n,m} v_n}$, as we did in Step 7 of the HTTL algorithm; however, as it is illustrated in Fig. 2.2c, q'_m may lie outside the region, that we refer to as the *desired region* for FC m, in which all its associated APs can communicate. In that case, we move FC m to the closest point to q'_m within its desired region, denoted by $\widehat{q}_m$, as it is shown in Fig. 2.2d. Note that in order to find $\widehat{q}_m$, we only need to consider a finite number of points. The entire process to optimize the power for a limited communication range is summarized in Algorithm 1. Similar to HTTL Algorithm, each AP lies on the segment connecting its corresponding FC to the centroid of its region once the Limited-HTTL algorithm converges. The following lemma shows that Limited-HTTL Algorithm is an iterative improvement algorithm and converges.

Proposition 6. *Limited-HTTL Algorithm is an iterative improvement algorithm, i.e., the Lagrangian function in (2.5) is non-increasing and the algorithm converges.*

The proof is provided in Appendix B.10.

2.7   Experiments

Simulations are carried out for both synthetic and real-world datasets. For the synthetic data, we provide the experimental results in two heterogeneous two-tier WSNs: (i) WSN1: A heterogeneous WSN including 1 FC and 20 APs; (ii) WSN2: A heterogeneous WSN including 4 FCs and 20 APs. We consider the same target domain Ω as in [41, 42], i.e., $\Omega = [0, 10]^2$. Simulations are performed for two different data rate density functions, i.e., a uniform distribution $f(\omega) = \frac{1}{\int_\Omega dw} = 0.01$, and a mixture of Gaussian distribution:

Algorithm 2: Limited-HTTL Algorithm

Input: Weights $\{a_n\}_{n \in \mathcal{I}_\mathcal{A}}$ and $\{b_{n,m}\}_{n \in \mathcal{I}_\mathcal{A}, m \in \mathcal{I}_\mathcal{B}}$, $\beta \in \mathbb{R}^+$, powers σ^2 and $\sigma_n^2, n \in \mathcal{I}_\mathcal{A}$ and $\epsilon \in \mathbb{R}^+$.

Output: Optimal node deployment $(P^*, Q^*, \mathbf{R}^*, T^*)$.

1: Randomly initialize the node deployment $(P, Q, \mathbf{R}, T)$.
2: **do**
3: Compute the two-tier power consumption $\overline{\mathcal{P}}_{\text{old}} = \overline{\mathcal{P}}(P, Q, \mathbf{R}, T)$.
4: Update the index map T according to (2.23).
5: Use APs in the set $\{n | T(n) \neq -1\}$ for generalized Voronoi partitioning of Ω.
6: Calculate the volumes $\{v_n\}$ and centroids $\{c_n\}$ for each $n \in \{n | T(n) \neq -1\}$.
7: For each $m \in \mathcal{I}_\mathcal{B}$:
   – if $T^{-1}(m) \neq \varnothing$:
     • move FC m to the nearest point to $q'_m = \frac{\sum_{n:T(n)=m} b_{n,m} p_n v_n}{\sum_{n:T(n)=m} b_{n,m} v_n}$ inside its desired region.
   – else:
     • randomly select an index $m' \in \mathcal{I}_\mathcal{B}$ according to the distribution $P(m') = \frac{|T^{-1}(m')|}{N}$.
     • move FC m to a random location within the region $\bigcup_{n:T(n)=m'} R_n$.
8: $\forall n \in \mathcal{I}_\mathcal{A}$, move AP n to the nearest point to $p'_n = \frac{a_n c_n + \beta b_{n,T(n)} q_{T(n)}}{a_n + \beta b_{n,T(n)}}$ inside its desired region.
9: Update the two-tier power consumption $\overline{\mathcal{P}}_{\text{new}} = \overline{\mathcal{P}}(P, Q, \mathbf{R}, T)$.
10: **While** $\frac{\overline{\mathcal{P}}_{\text{old}} - \overline{\mathcal{P}}_{\text{new}}}{\overline{\mathcal{P}}_{\text{old}}} \geq \epsilon$
11: **Return:** The node deployment $(P, Q, \mathbf{R}, T)$.

$$f(\omega) = \frac{1}{2} \times \mathcal{N}\left(\begin{bmatrix} 3 \\ 3 \end{bmatrix}, \begin{bmatrix} 1.5 & 0 \\ 0 & 1.5 \end{bmatrix}\right) + \frac{1}{4} \times \mathcal{N}\left(\begin{bmatrix} 6 \\ 7 \end{bmatrix}, \begin{bmatrix} 2 & 0 \\ 0 & 2 \end{bmatrix}\right)$$

$$+ \frac{1}{4} \times \mathcal{N}\left(\begin{bmatrix} 7.5 \\ 2.5 \end{bmatrix}, \begin{bmatrix} 1 & 0 \\ 0 & 1 \end{bmatrix}\right). \quad (2.24)$$

To evaluate the performance, 10 initial AP and FC deployments on Ω are generated randomly, i.e, every node location is generated with uniform distribution on Ω. In order to make a fair comparison to prior work, similar to the experimental setting in [41, 42], the maximum number of iterations is set to 100, FCs and APs are denoted, respectively, by black and red circles. Other parameters are provided in Table 2.1. According to the parameters in Table 2.1, we divide APs into two groups: strong APs ($n \in \{1, \ldots, 10\}$) and weak APs ($n \in \{11, \ldots, 20\}$). Similarly, FCs are divided into strong FCs ($m \in \{1, 2\}$) and weak FCs ($m \in \{3, 4\}$).

Table 2.1: Simulation Parameters

WSN1				WSN2					
$a_{1:10}$	$a_{11:20}$	$b_{1:4,1}$	$b_{5:20,1}$	$a_{1:10}$	$a_{11:20}$	$b_{1:4,1:2}$	$b_{1:4,3:4}$	$b_{5:20,1:2}$	$b_{5:20,3:4}$
1	2	1	2	1	2	1	2	2	4

Like the experiments in [41], we compare the weighted power of our proposed algorithm with Minimum Energy Routing (MER) [37], Agglomerative Clustering (AC) [47], Divisive Clustering (DC) [47] algorithms, and Particle Swarm Optimization (PSO) [83]. PSO is a population-based stochastic algorithm for non-linear optimization. AC and DC are bottom-up and top-down clustering algorithms, respectively. MER is a combination of Multiplicatively weighted Voronoi Partition [11] and Bellman-Ford algorithms [8, Section 2.3.4]. More details about MER, AC, and DC can be found in [41]. When the communication range is limited, we further compare our method with two other algorithms, i.e., Improved Relay Node Placement (IRNP)[115], and Relay Node placement in Double tiered Wireless Sensor

Network (RNDWSN)[94]. IRNP and RNDWSN are node placement algorithms designed to maximize the network coverage. Note that if a small portion of sensors are covered by a particular node placement, since not many sensors will transfer data to fusion centers, the resulting power consumption will be small too. Therefore, our primary goal in node deployment with limited transmission power is to maximize the network coverage and minimize the power consumption, simultaneously.
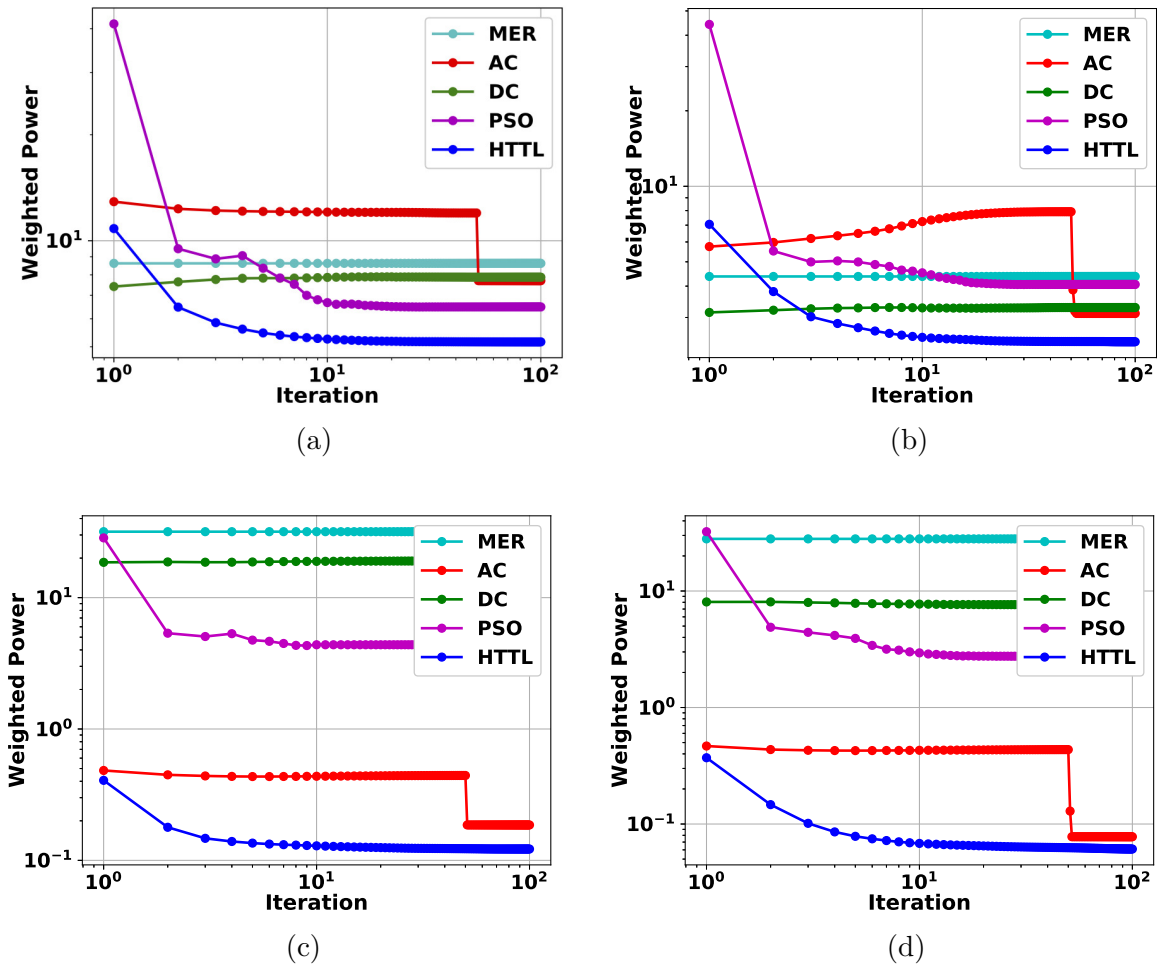
Figure 2.3: Weighted power versus iteration for different algorithms ($\beta = 0.25$). (a) WSN1/Uniform pdf, (b) WSN2/Uniform pdf, (c) WSN1/Mixture of Gaussian pdf, (d) WSN2/Mixture of Gaussian pdf.

The weighted power consumption over the iterations of MER, AC, DC, PSO and HTTL algorithms in WSN1 and WSN2 for $\beta = 0.25$ are shown in Figs. 2.3a and 2.3b for uniform data rate density function, and in Figs. 2.3c and 2.3d for the Gaussian mixture given
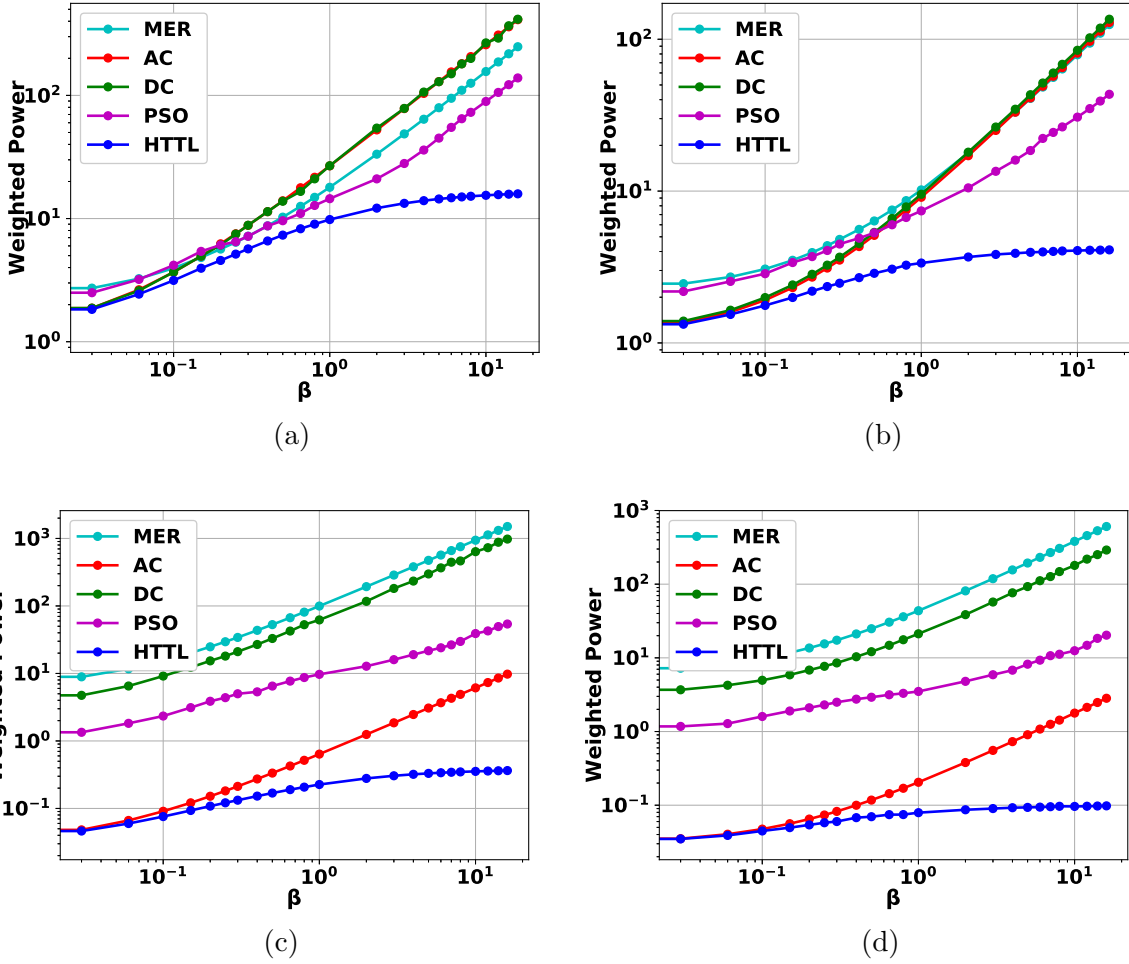
Figure 2.4: Power consumption of different two-tier WSNs/data rate density functions. (a) WSN1/Uniform pdf, (b) WSN2/Uniform pdf, (c) WSN1/Mixture of Gaussian pdf, (d) WSN2/Mixture of Gaussian pdf.

in (2.24). Weighted power consumption of MER, AC, DC, PSO and HTTL algorithms in WSN1 and WSN2 are illustrated in Figs. 2.4a and 2.4b for uniform data rate density function, and in Figs. 2.4c and 2.4d for the Gaussian mixture given in (2.24). Obviously, our proposed algorithm, HTTL, outperforms the other four algorithms in both WSN1 and WSN2. For instance, HTTL Algorithm yields the power consumption of 2.351 for WSN2, $\beta = 0.25$ and uniform data rate, which is lower than the values 4.371, 3.113, 3.253 and 4.063 obtained from MER, AC, DC and PSO algorithms, respectively. Similarly, for the case of WSN2 and mixture of Gaussian, HTTL Algorithm yields the power consumption of

0.058 which is lower than the values 15.484, 0.074, 7.677 and 2.301 obtained from MER, AC, DC and PSO algorithms, respectively. Unlike other methods, HTTL Algorithm exploits the trade-off between Sensor and AP power consumptions; hence, the energy consumption gap between HTTL and other algorithms increases as the AP energy consumption becomes more important (β increases). For $\beta = 0.25$, the final node deployment for WSN2 and the mixture of Gaussian data rate density function given in (2.24) is shown in Fig. 2.5 where APs, FCs and centroid of regions are denoted via red squares, black circle and crosses, respectively.
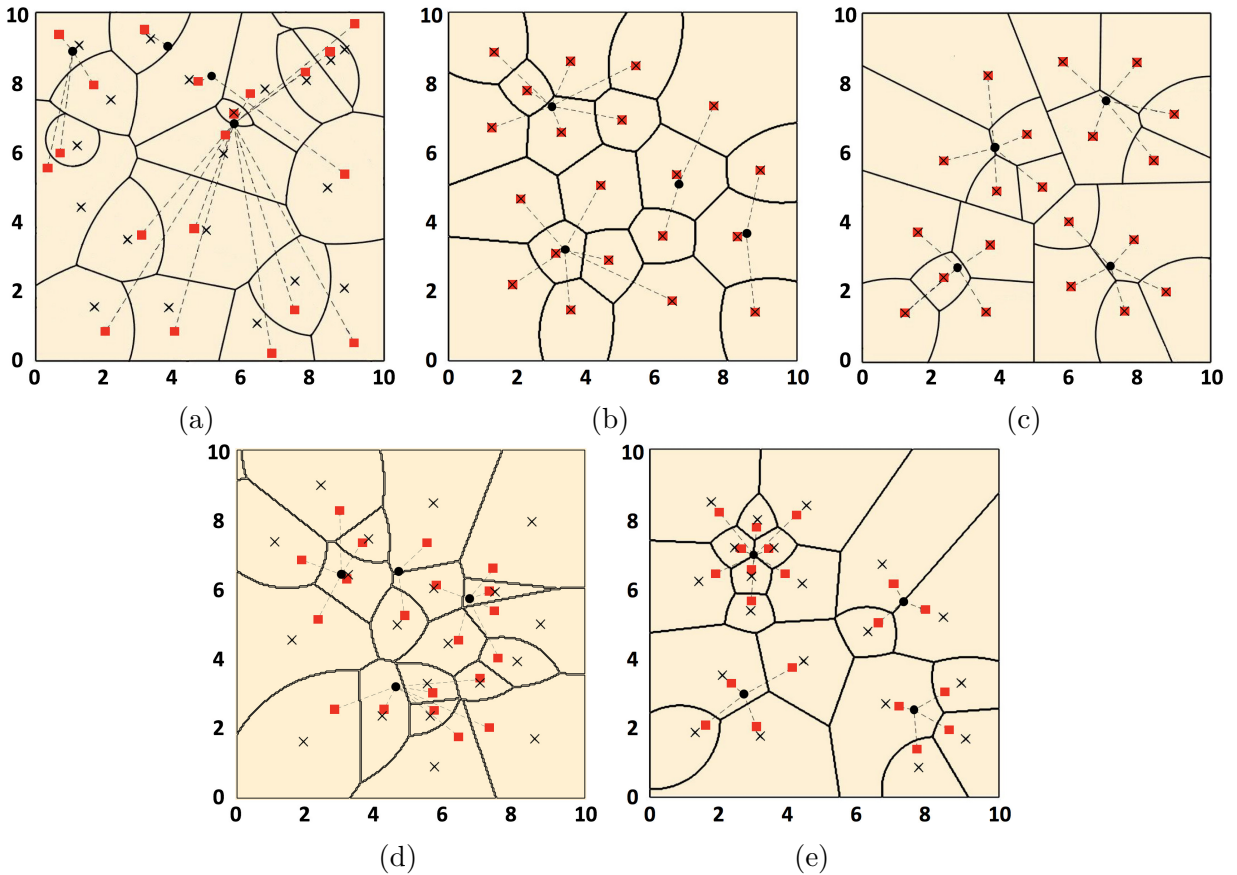
Figure 2.5: Node deployment for different algorithms with $\beta = 0.25$ in WSN2 and the mixture of Gaussian data rate density function. (a) MER (b) AC (c) DC (d) PSO (e) HTTL.

Note that the two-tier power consumption defined in (2.5) represents a trade-off between the Sensor power $\overline{\mathcal{P}}^{\mathcal{S}}$ and AP power $\overline{\mathcal{P}}^{\mathcal{A}}$, and this trade-off is illustrated as the AP-Sensor power functions for WSN1 and WSN2 in Figs. 2.6a and 2.6b for uniform data rate, and in Figs. 2.6c and 2.6d for the mixture of Gaussian data rate density function, respectively. For
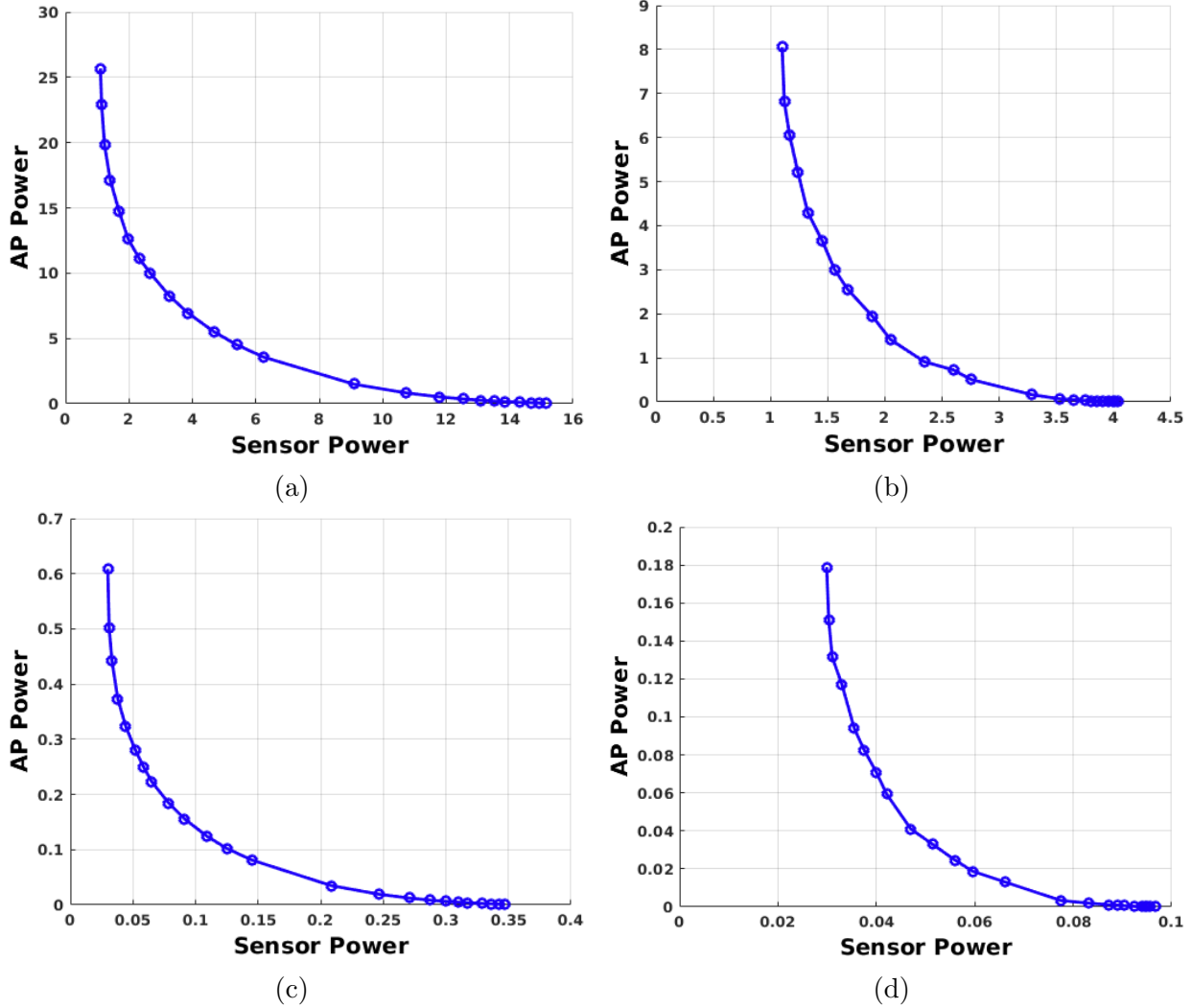
Figure 2.6: AP-Sensor power trade-off for HTTL Algorithm (a) WSN1/Uniform pdf, (b) WSN2/Uniform pdf, (c) WSN1/Mixture of Gaussian pdf, (d) WSN2/Mixture of Gaussian pdf.

small values of β, sensor power contributes to the two-tier power consumption more than AP power; hence, the optimal deployment tends to minimize $\overline{\mathcal{P}}^{\mathcal{S}}$, while $\overline{\mathcal{P}}^{\mathcal{A}}$ tends to be minimized in an optimal node placement for large values of β. Intuitively, moving APs towards the FCs, usually, will increase the average distance between sensors and APs, resulting in the increase of the sensor power. On the other hand, moving APs toward geometric centroids of their corresponding regions, usually, will increase their distances to the FCs, which leads to an increase in the AP power. This is shown in Fig. 2.6 where the AP-Sensor power function $A(s)$ decreases as s increases. Lemma 4 indicates that $A(s)$ is non-zero on the

intervals $[D_{20}, D_1)$ and $[D_{20}, D_4)$ for WSN1 and WSN2, respectively. Simulations show that AP-sensor power function is a piece-wise continuous convex function, as we demonstrated earlier for the setting in Lemma 6.

Table 2.2: Power Constraint Parameters

Parameters	σ^2	$\sigma^2_{1:4}$	$\sigma^2_{5:10}$	$\sigma^2_{11:20}$
Values	4	25	16	9

Next, we consider a transmission power constraint on sensors and APs. The value of parameters σ^2 and $\sigma^2_n, n \in \mathcal{I}_\mathcal{A}$ in (2.20) are provided in Table 2.2. According to Table 2.2, strong APs ($n \in \{1, \ldots, 10\}$) also tend to have more available power than weak APs ($n \in \{11, \ldots, 20\}$).
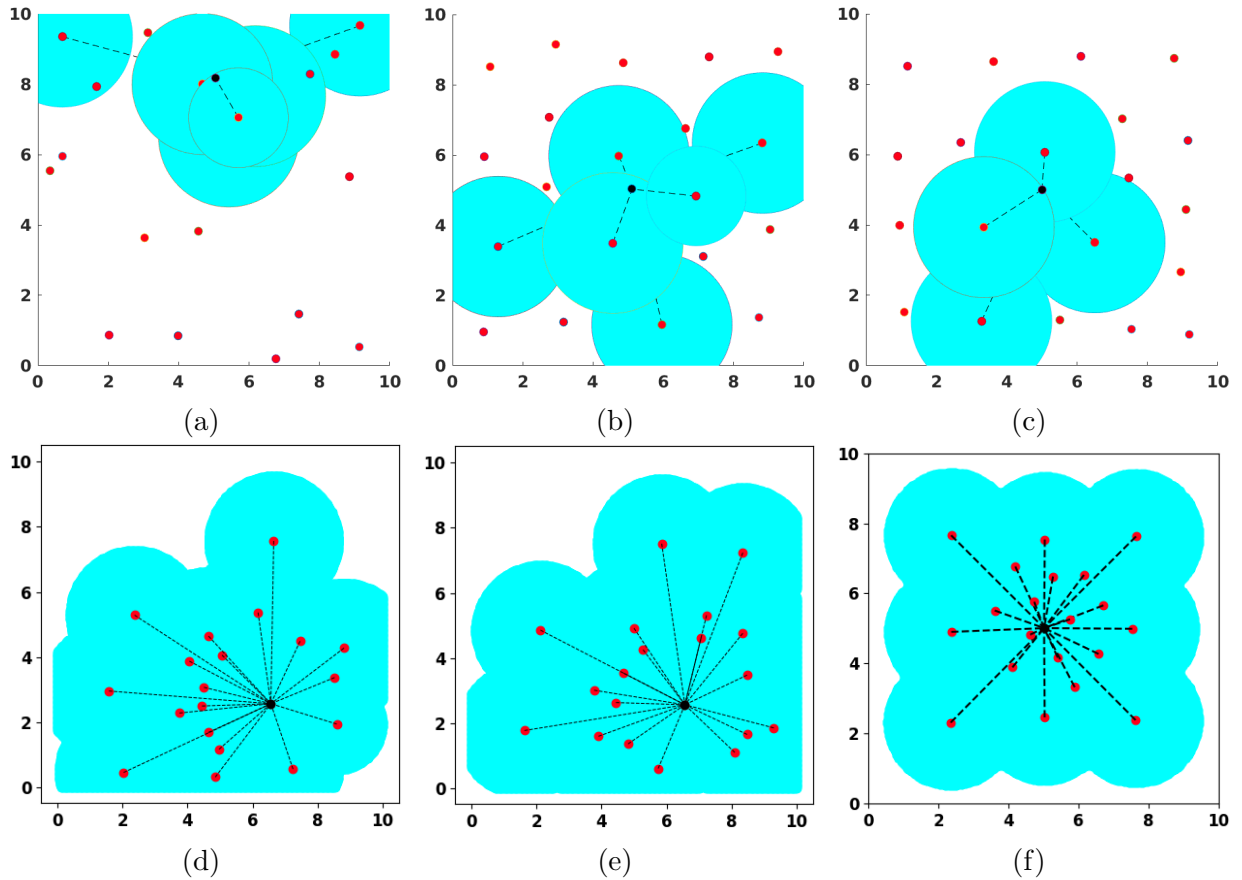
Figure 2.7: Node deployment for different algorithms with $\beta = 0.25$ in WSN1 and uniform data rate density function. (a) MER (b) AC (c) DC (d) RNDWSN (e) IRNP (f) Limited-HTTL.

Table 2.3: Coverage and power comparison for uniform data rate density function.

	MER	AC	DC	RNDWSN	IRNP	Limited-HTTL
WSN1						
Power	1.1287	2.1812	1.3972	4.0105	4.4258	3.2151
Coverage	33.90%	53.01%	40.31%	74.13%	80.04%	78.26%
WSN2						
Power	0.8843	2.3309	2.6340	3.9463	4.7733	2.1305
Coverage	38.55%	82.26%	91.79%	81.48%	95.09%	94.66%
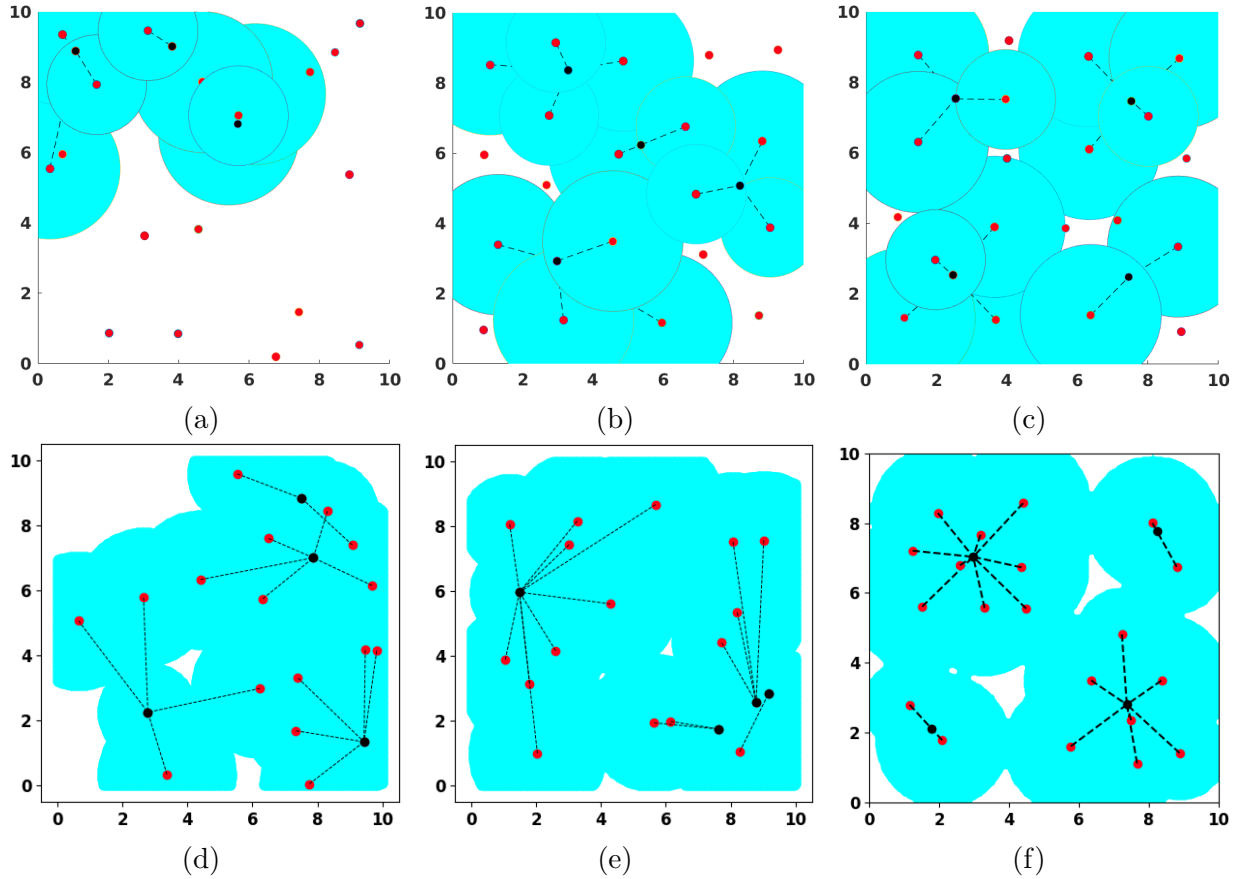
Figure 2.8: Node deployment for different algorithms with $\beta = 0.25$ in WSN2 and uniform data rate density function. (a) MER (b) AC (c) DC (d) RNDWSN (e) IRNP (f) Limited-HTTL.

Figs. 2.7 and 2.8 illustrate the optimal node deployment and covered area for different algorithms in WSN1 and WSN2, respectively, with $\beta = 0.25$ and uniform data rate density function. The two-tier power consumption and coverage of different algorithms for $\beta = 0.25$ and uniform data rate density function are summarized in Table 2.3. IRNP Algorithm

Table 2.4: Coverage and power comparison for the mixture of Gaussian data rate.

	MER	AC	DC	RNDWSN	IRNP	Limited-HTTL
WSN1						
Power	1.6810	2.3428	1.5385	4.9187	4.4630	2.2659
Coverage	43.24%	75.72%	63.04%	92.45%	92.12%	91.68%
WSN2						
Power	1.5285	1.6436	1.6676	4.0627	3.5923	1.1565
Coverage	46.43%	98.64%	97.13%	95.34%	99.32%	98.11%
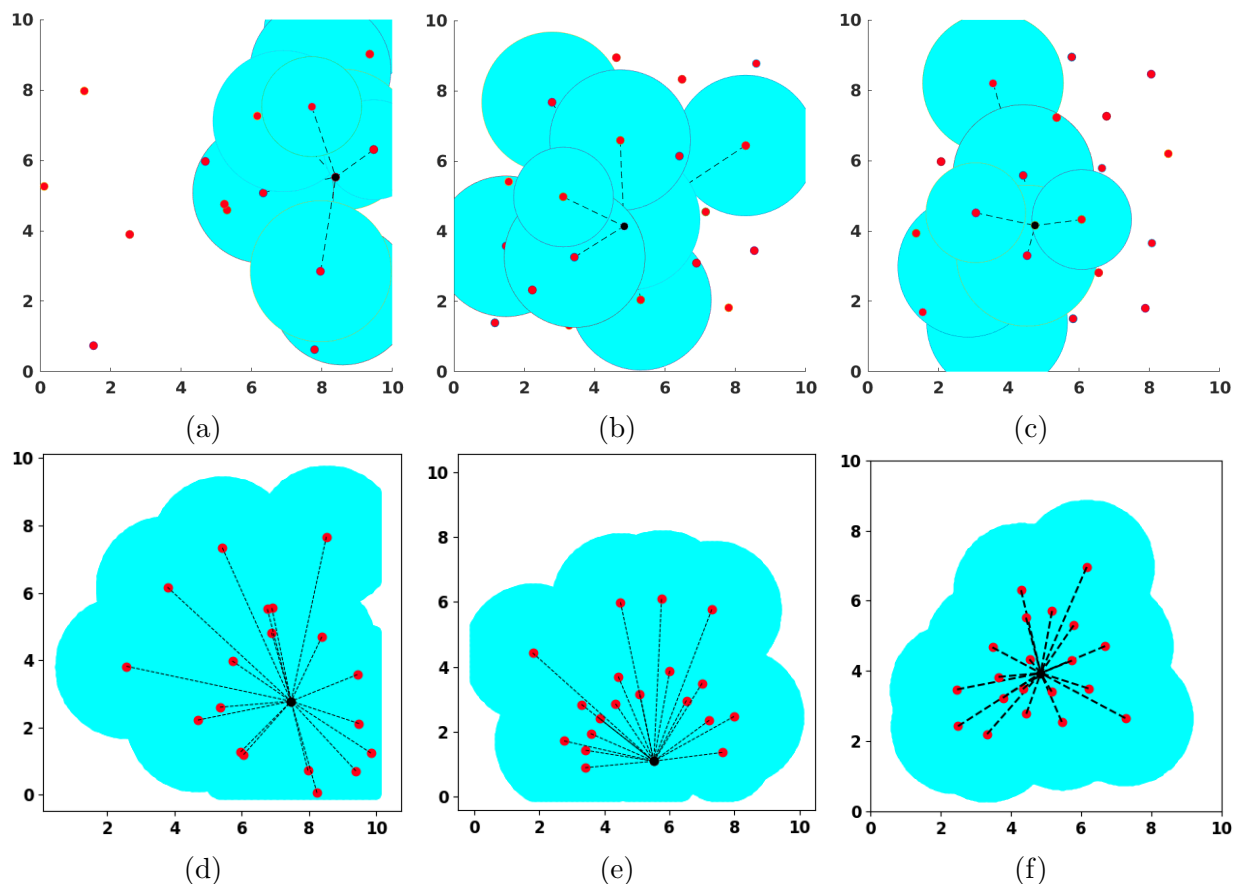
Figure 2.9: Node deployment for different algorithms with $\beta = 0.25$ and the mixture of Gaussian data rate density function in WSN1. (a) MER (b) AC (c) DC (d) RNDWSN (e) IRNP (f) Limited-HTTL.

yields the maximum coverage in WSN1; however, the 1.78% improvement in the coverage over our proposed Limited-HTTL Algorithm comes at the cost of 38% increase in power consumption. Our algorithm also outperforms RNDWSN Algorithm in terms of both power and coverage. Similarly, although IRNP Algorithm results in less than 1% improvement
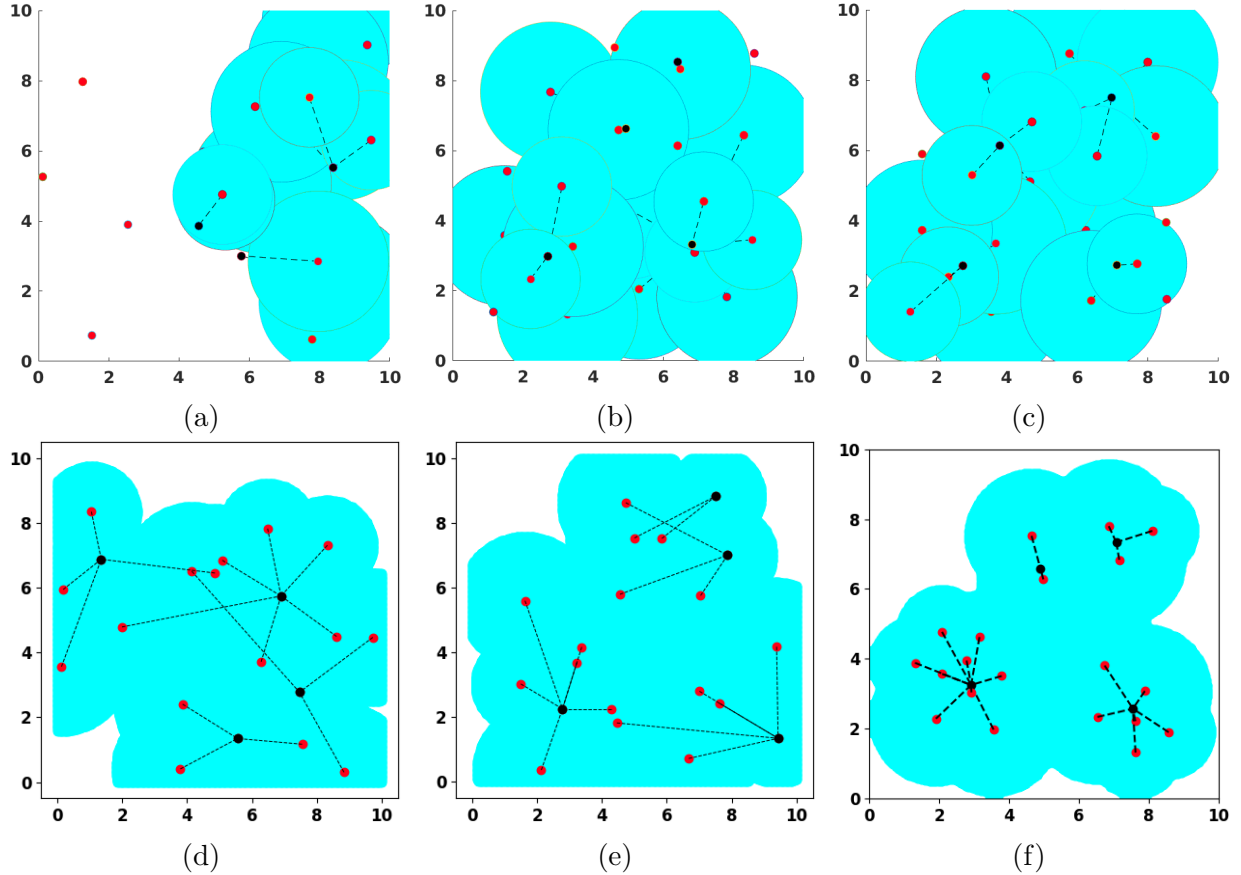
Figure 2.10: Node deployment for different algorithms with $\beta = 0.25$ and the mixture of Gaussian data rate density function in WSN2. (a) MER (b) AC (c) DC (d) RNDWSN (e) IRNP (f) Limited-HTTL.

in coverage compare to Limited-HTTL Algorithm in WSN2, it consumes more than twice power used by our proposed algorithm. Limited-HTTL Algorithm also outperforms the other algorithms in terms of both coverage and power consumption in WSN2.

Figs. 2.9 and 2.10 show the optimal node deployment and covered area for different algorithms in WSN1 and WSN2, respectively, with $\beta = 0.25$ and data rate density function given in (2.24). The two-tier power consumption and coverage of different methods for $\beta = 0.25$ and Gaussian mixture data rate density function given in (2.24) are summarized in Table 2.4. RNDWSN and IRNP algorithms result in less than 1% improvement in coverage compare to Limited-HTTL Algorithm in WSN1; however, their power consumption is about twice that of our proposed algorithm. Similar results for AC and IRNP algorithms in WSN2 show that

Table 2.5: Simulation Parameters

$a_{1:20}$	$a_{21:40}$	Parameters (pWatt/m^2)		$b_{9:40,1:4}$	$b_{9:40,5:8}$
		$b_{1:8,1:4}$	$b_{1:8,5:8}$		
1	2	1	2	2	4
		Power Constraints (milliWatt)			
	σ^2	$\sigma^2_{1:8}$	$\sigma^2_{9:20}$	$\sigma^2_{21:40}$	
	6.4	19.6	14.4	10.0	

Table 2.6: Coverage and power (Watt) comparison for the climate data.

	MER	AC	DC	RNDWSN	IRNP	Limited-HTTL
Power	0.7052	1.0169	0.8846	1.1978	1.3788	0.9151
Coverage	60.14%	82.17%	78.32%	76.57%	89.51%	96.15%

about 1% increase in the coverage obtained over Limited-HTTL Algorithm leads to 42% and 210% increase in power consumption, respectively. Finally, our proposed algorithm outperforms DC and RNDWSN methods in terms of both coverage and power consumption in WSN2. Note that when communication range is limited, MER Algorithm usually yields poor performance since many APs fall outside the communication range of their corresponding FC, and they cannot transfer their collected data from sensors to fusion centers.

To evaluate the performance of our method in real world applications, we conduct experiments on the daily weather data of the Colorado state, i.e. precipitation, relative humidity, temperature etc. Sensory data is obtained with the same rate from 286 locations that form a 13×22 grid across Colorado. We consider a heterogeneous WSN with 40 APs and 8 FCs. The power constraints and other parameter values are provided in Table 2.5 [49].

Table 2.6 summarizes the two-tier power consumption and coverage of different methods. Our method outperforms AC, RNDWSN and IRNP algorithms in terms of both total coverage and power consumption. While providing lower power, MER Algorithm yields poor performance since many sensory locations fall outside the communication range of their nearby APs. Finally, DC Algorithm yields 3% improvement in power consumption although it provides a significantly lower coverage value compared with our algorithm.

2.8 Conclusion

A heterogeneous two-tier network which collects data from a large-scale wireless sensor to heterogeneous fusion centers through heterogeneous access points is discussed. We studied the minimum power that ensures reliable communication on such two-tier networks and modeled it as an optimization problem. Different from the homogeneous two-tier networks, a novel Voronoi Diagram is proposed to provide the best cell partition for the heterogeneous network. The necessary conditions of optimal node deployment imply that every access point should be placed between its connected fusion center and the geometric center of its cell partition. By defining an appropriate power consumption measure, we proposed a heterogeneous two-tier Lloyd Algorithm (HTTL) to minimize the power consumption. Simulation results show that HTTL Algorithm greatly saves the weighted power or energy in a heterogeneous two-tier network. When communication range is limited, our novel Limited-HTTL Algorithm ensures that all APs are active. Simulation results show that our algorithms provide superior results, in terms of both power consumption and network coverage.

Chapter 3

Energy-Efficient Node Deployment in Wireless Ad-hoc Sensor Networks

3.1   Introduction

Recent developments in wireless communications, digital electronics and computational power have enabled a large number of applications of wireless ad-hoc sensor networks (WASNs) in various fields such as agriculture and industry to name a few. In a general WASN, spatially dispersed sensors collect data, e.g. temperature, sound, pressure and radio signals from the physical environment, and then forward the gathered information to one or more fusion centers (FCs).

In order to collect accurate data from the physical surroundings, high sensing quality or sensitivity is required. In general, sensing quality diminishes as the distance between the sensor and its target point increases [73, 74, 45, 13, 50, 108]. Thus, two distance-dependent measures, i.e., sensing coverage [73, 92, 120, 111, 106] and sensing uncertainty [13, 60, 38, 39, 98, 22, 63] are widely studied in the literature to evaluate the sensing quality. In the binary

coverage model [73, 92, 120, 111, 106], each sensor node can only detect the events within its sensing radius. Then, sensing coverage represents the percentage of events that is covered by at least one sensor [73, 92, 120, 111]. Another common model, centroidal Voronoi tessellation, formulates the sensing quality as a source coding problem with sensing uncertainty as its distortion [13, 60, 38, 39, 98, 22, 63]. Sensing uncertainty reflects the distortion of a quantizer, and provides a distance-based measure of sensing quality [22, 63, 41, 21].

Energy efficiency is another key metric in WASNs as it is inconvenient or even infeasible to recharge the batteries of numerous and densely deployed sensors. In general, wireless communication, sensing and data processing are three primary energy consumption components of a static node. However, in many WASN applications, wireless communication dominates the node energy consumption [4, 87]. There are four primary energy saving methods for WASNs in the literature: (i) topology control [64, 107], in which unnecessary energy consumption is reduced by properly switching the nodes' states between sleeping and working; (ii) clustering [112, 58] which is used to balance the energy consumption among nodes in one-hop communication models by iteratively selecting cluster heads; (iii) energy-efficient routing [15, 34, 9], a widely used method that attempts to find the optimal routing paths to forward data to FCs while the communication cost between two nodes are held fixed; and (iv) deployment optimization that plays an important role in the energy consumption of WASNs since the communication cost between two nodes depends on their distance. Our previous works [41, 55] proposed Lloyd-like algorithms to save communication energy in homogeneous and heterogeneous WASNs by optimizing the node deployment. Nonetheless, a pre-existing network infrastructure, which only includes two-hop communications, is a basic assumption in [41, 55]. Compared to one-hop and two-hop communications, the generalized multi-hop communications can, on average, reduce the transmission distance and save more energy. However, to the best of our knowledge, the optimal node deployment with generalized multi-hop communications in WASNs is still an open problem.

In this paper, we study the node deployment problem in WASNs with arbitrary multi-hop routing algorithms. Our primary goal is to find the optimal FC and sensor deployment to minimize both sensing uncertainty and total energy consumption of the network. By deriving the routing-dependent necessary conditions of the optimal deployments in such WASNs, we design a Lloyd-like algorithm to deploy nodes.

The rest of this paper is organized as follows: In Section 3.2, we introduce the system model and problem formulation. In Section 3.3, we study the optimal FC and sensor deployment for a given routing algorithm. A numerical algorithm is proposed in Section 3.4 to optimize the node deployment. Section 3.5 presents the experimental results and Section 3.6 concludes the paper.

3.2   System model and problem formulation

We consider a wireless ad-hoc sensor network consisting of M homogeneous FCs and N homogeneous sensors over a target region $\Omega \in \mathbb{R}^2$. Let $\mathcal{I}_S = \{1, \ldots, N\}$ and $\mathcal{I}_F = \{N + 1, \ldots, N + M\}$ denote the set of node indices for sensors and FCs, respectively. When $i \in \mathcal{I}_S$, Node i refers to Sensor i; however, when $i \in \mathcal{I}_F$, Node i refers to FC $(i - N)$. Let $\mathbf{P} = (p_1, \ldots, p_N, p_{N+1}, \ldots, p_{N+M})^T \in \mathbb{R}^{(N+M) \times 2}$ be the node deployment, where $p_i \in \Omega$ denotes the location of Node i. Throughout this paper, we assume that each event within the target region is sensed by only one sensor. Therefore, for each $i \in \mathcal{I}_S$, Sensor i monitors the events occurred in the cell $W_i \subseteq \Omega$, and $\mathbf{W} = (W_1, \ldots, W_N)$ provides a cell partitioning of Ω. According to [41], the frequency of random events taking place over Ω is modeled via a continuous and differentiable spatial density function $f(\omega) : \Omega \to \mathbb{R}^+$. Therefore, the amount of data generated at Sensor i during a unit of time is given by $\Gamma(W_i) = \kappa \int_{W_i} f(\omega) d\omega$ where κ is a positive constant, [41]. The data collected by each sensor node is forwarded to other nodes in the network until it eventually reaches to one or more fusion centers.

According to [15], this WASN can be modeled as a directed acyclic graph $\mathcal{G}(\mathcal{I}_S \bigcup \mathcal{I}_F, \mathcal{E})$ where $\mathcal{E}$ is the set of directed links (n, k) such that $n \in \mathcal{I}_S$ and $k \in \mathcal{I}_S \bigcup \mathcal{I}_F$. In particular, sensors and FCs are source nodes and sink nodes of this network, respectively, and there is no cycle in the flow network since each cycle can be eliminated by reducing the flows along the cycle without influencing the in-flow and out-flow links to that cycle. We define $\mathbf{F} = [F_{i,j}]_{N \times (N+M)}$ to be the flow matrix, where $F_{i,j}$ is the amount of data transmitted through the link (i, j) in the unit time. Since $\mathbf{F}$ depends on the cell partitioning $\mathbf{W}$, we can define the normalized flow matrix as follows:

$$
\mathbf{S} = \overbrace{\begin{bmatrix} s_{1,1} & s_{1,2} & \cdots & s_{1,N+M} \\ s_{2,1} & s_{2,2} & \cdots & s_{2,N+M} \\ \vdots & \vdots & \ddots & \vdots \\ s_{N,1} & s_{N,2} & \cdots & s_{N,N+M} \end{bmatrix}}^{N+M} \Bigg\} N, \tag{3.1}
$$

where $s_{i,j} \triangleq \frac{F_{i,j}}{\sum_{j=1}^{N+M} F_{i,j}}$ is the ratio of in-flow data to Node i that is transmitted to Node j.
The normalized flow matrix $\mathbf{S}$ satisfies the following properties:

(a) $s_{i,j} \in [0, 1]$;[1]

(b) $\sum_{j=1}^{N+M} s_{i,j} = 1, \forall i \in \{1, \ldots, N\}$;

(c) No cycle: if there exists a path $l_0 \to l_1 \to \cdots \to l_K$, i.e., $\prod_{k=1}^{K} s_{l_{k-1}, l_k} > 0$, then we have $s_{l_K, l_0} = 0$. In particular, $s_{ii} = 0, \forall i \in \{1, \ldots, N\}$.

Since the flow $F_{i,j}$ can be determined by the cell partitioning $\mathbf{W}$ and normalized flow ma-

---

[1] For time-invariant routing algorithms, such as Bellman-Ford Algorithm [34, 9], the flows construct a tree-structured graph in which each node has only one successor. Under such a circumstance, the normalized flow from Node i to Node j is either 0 or 1, i.e., $s_{i,j} \in \{0, 1\}$. However, the time-variant routing algorithms, such as Flow Augmentation Algorithm [15], will generate different flows during different time periods. As a result, the overall normalized flow from Node i to Node j can be a real number between 0 and 1, i.e., $s_{i,j} \in [0, 1]$.

trix $\mathbf{S}$, in the remaining of this paper we use $\mathbf{F}(\mathbf{W}, \mathbf{S})$ instead of $\mathbf{F}$. Let $F_i(\mathbf{W}, \mathbf{S}) \triangleq$ $\sum_{j=1}^{N+M} F_{i,j}(\mathbf{W}, \mathbf{S})$ be the total flow originated from Node i. Since the in-flow to each sensor, say i, should be equal to the out-flow, we have $\sum_{j=1}^{N} F_{j,i}(\mathbf{W}, \mathbf{S}) + \Gamma(W_i) = \sum_{j=1}^{N+M} F_{i,j}(\mathbf{W}, \mathbf{S})$. In what follows, we provide an example to elucidate how to calculate $F(\mathbf{W}, \mathbf{S})$ in terms of $\mathbf{W}$ and $\mathbf{S}$.

Example 1. We consider a WASN with three sensor nodes and one FC, i.e., $N = 3$ and $M = 1$. The parameter κ is set to 4. For a cell partitioning $\mathbf{W}$ with cell volumes $v(W_1) = v(W_2) = 0.25$, $v(W_3) = 0.5$, and the normalized flow matrix $\mathbf{S} = \begin{bmatrix} 0 & 0.5 & 0.5 & 0 \\ 0 & 0 & 0.4 & 0.6 \\ 0 & 0 & 0 & 1 \end{bmatrix}$,

the corresponding flow network is illustrated in Fig. 3.1.
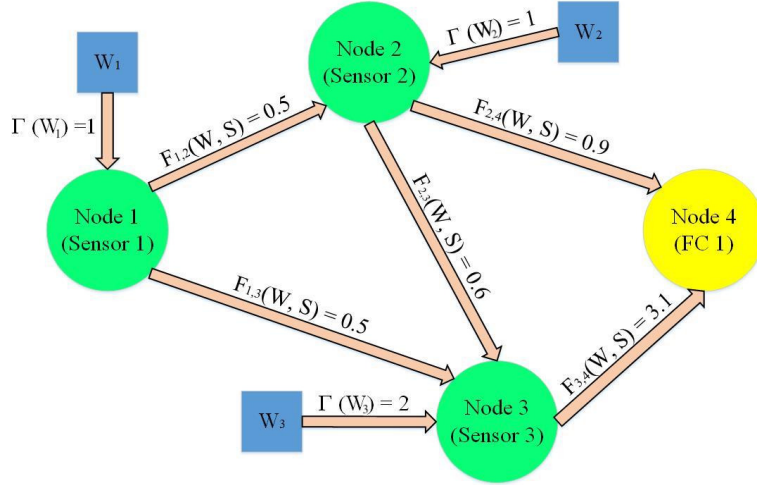
Figure 3.1: Example 1

The amount of data generated from each sensor node can be calculated as: $\Gamma(W_1) = \kappa v(W_1) = 1$, $\Gamma(W_2) = \kappa v(W_2) = 1$, and $\Gamma(W_3) = \kappa v(W_3) = 2$. As a leaf node, Sensor 1 does not receive data from any other sensor nodes, and only transmits its sensed data; thus, $F_1(\mathbf{W}, \mathbf{S}) = \Gamma(W_1) = 1$. The flows from Sensor 1 are then $F_{1,2}(\mathbf{W}, \mathbf{S}) = s_{1,2} \times F_1(\mathbf{W}, \mathbf{S}) = 0.5$ and $F_{1,3}(\mathbf{W}, \mathbf{S}) = s_{1,3} \times F_1(\mathbf{W}, \mathbf{S}) = 0.5$, respectively. Sensor 2's flows come from $F_{1,2}(\mathbf{W}, \mathbf{S})$ and the data gathered from the region W_2. Hence, $F_2(\mathbf{W}, \mathbf{S}) = \Gamma(W_2) + F_{1,2}(\mathbf{W}, \mathbf{S}) = 1.5$.

Therefore, the flows from Sensor 2 are $F_{2,3}(\mathbf{W}, \mathbf{S}) = s_{2,3} \times F_2(\mathbf{W}, \mathbf{S}) = 0.6$ and $F_{2,4}(\mathbf{W}, \mathbf{S}) = s_{2,4} \times F_2(\mathbf{W}, \mathbf{S}) = 0.9$. Similarly, for Sensor 3, we have $F_3(\mathbf{W}, \mathbf{S}) = \Gamma(W_3) + F_{1,3}(\mathbf{W}, \mathbf{S}) + F_{2,3}(\mathbf{W}, \mathbf{S}) = 3.1$; hence, the unique flow from Sensor 3 is $F_{3,4}(\mathbf{W}, \mathbf{S}) = s_{3,4} \times F_3(\mathbf{W}, \mathbf{S}) = 3.1$.

We focus on power consumption of sensors since FCs are usually equipped with reliable energy sources and their power consumption is not the main concern. The average power consumption through link (i, j) consists of two components: (i) average transmitter power, $\overline{\mathcal{P}}_{i,j}^T$; and (ii) average receiver power, $\overline{\mathcal{P}}_{i,j}^R$. As shown in [41], because of the free-space path-loss, the instant transmission power is proportional to the square of distance between nodes i and j. Therefore, Sensor i's average transmitter power through link (i, j) is modeled as $\overline{\mathcal{P}}_{i,j}^T = \beta \|p_i - p_j\|^2 F_{i,j}(\mathbf{W}, \mathbf{S})$ where the coefficient β depends on the characteristics of nodes i and j [41]. In homogeneous WASNs, all nodes share the same characteristics; thus, the coefficient β is the same for all links (i, j). According to [51], Sensor j's average receiver power through link (i, j) can be modeled as $\overline{\mathcal{P}}_{i,j}^R = \rho F_{i,j}(\mathbf{W}, \mathbf{S})$, where ρ is a constant coefficient for receiving data. In sum, the average power consumption over link (i, j) can be written as

$$
\begin{aligned}
\overline{\mathcal{P}}_{i,j}(\mathbf{P}, \mathbf{W}, \mathbf{S}) &= \overline{\mathcal{P}}_{i,j}^T + \overline{\mathcal{P}}_{i,j}^R \\
&= \begin{cases} \left(\beta\|p_i - p_j\|^2 + \rho\right) F_{i,j}(\mathbf{W}, \mathbf{S}), & j \in \mathcal{I}_S \\ \left(\beta\|p_i - p_j\|^2\right) F_{i,j}(\mathbf{W}, \mathbf{S}), & j \in \mathcal{I}_F \end{cases}
\end{aligned}
\tag{3.2}
$$

and the total power consumption can be written as

$$
\begin{aligned}
\overline{\mathcal{P}}(\mathbf{P}, \mathbf{W}, \mathbf{S}) &= \sum_{i=1}^{N} \sum_{j=1}^{N+M} \overline{\mathcal{P}}_{i,j}(\mathbf{P}, \mathbf{W}, \mathbf{S}) \\
&= \sum_{i=1}^{N} \left[\sum_{j=1}^{N+M} \beta\|p_i - p_j\|^2 F_{i,j}(\mathbf{W}, \mathbf{S}) + \rho \sum_{j=1}^{N} F_{i,j}(\mathbf{W}, \mathbf{S}) \right].
\end{aligned}
\tag{3.3}
$$

According to [13, 60, 38, 39, 98, 22, 63], for a given node deployment $\mathbf{P}$ and cell partitioning $\mathbf{W}$, the sensing uncertainty can be formulated as:

$$\mathcal{H}(\mathbf{P}, \mathbf{W}) = \sum_{n=1}^{N} \int_{W_n} \|p_n - \omega\|^2 f(\omega) d\omega. \tag{3.4}$$

Our main goal is to minimize the power consumption and sensing uncertainty defined in (3.3) and (3.4), respectively. However, as will be shown in Section 3.5, there is a trade-off between sensing uncertainty and power consumption. Intuitively, sensing uncertainty is minimized when sensors are located on the centroid of their corresponding regions; however, this will usually increase the pair-wise distance between nodes which leads to an increase in power consumption. Therefore, one objective is to minimize the sensing uncertainty given a constraint on the total power consumption, or vice versa. This constrained optimization can equivalently be formulated as the following Lagrangian cost function:

$$
\begin{aligned}
D(\mathbf{P}, \mathbf{W}, \mathbf{S}) &= \mathcal{H}(\mathbf{P}, \mathbf{W}) + \lambda \overline{\mathcal{P}}(\mathbf{P}, \mathbf{W}, \mathbf{S}) \\
&= \sum_{i=1}^{N} \int_{W_i} \|p_i - \omega\|^2 f(\omega) d\omega + \lambda \rho \sum_{i=1}^{N} \sum_{j=1}^{N} F_{i,j}(\mathbf{W}, \mathbf{S}) \\
&+ \sum_{i=1}^{N} \sum_{j=1}^{N+M} \left(\lambda \beta \|p_i - p_j\|^2 \right) F_{i,j}(\mathbf{W}, \mathbf{S}),
\end{aligned}
\tag{3.5}
$$

where $\lambda \geq 0$, i.e. the Lagrangian multiplier, makes a trade-off between sensing uncertainty and total power consumption. Our main goal in this paper is to minimize the cost function defined in (3.5) over the node deployment $\mathbf{P}$, cell partitioning $\mathbf{W}$, and the normalized flow matrix $\mathbf{S}$.

3.3 Optimal node deployment in WASNs

As it is shown in (3.5), the cost function depends on three variables $\mathbf{P}$, $\mathbf{W}$ and $\mathbf{S}$. Therefore, our goal is to find the optimal node deployment, cell partitioning and the normalized flow matrix, denoted by $\mathbf{P}^* = (p_1^*, \ldots, p_{N+M}^*)$, $\mathbf{W}^* = (W_1^*, \ldots, W_N^*)$ and $\mathbf{S}^* = [s_{i,j}^*]_{N \times (N+M)}$,

respectively, that minimizes the cost function. Note that not only the optimal values of these variables depend on each other, but also the optimization problem is NP-hard. We aim to design an iterative algorithm that optimizes the value of one variable while the other two variables are held fixed. To accomplish this goal, we study the necessary conditions for optimal deployment at each step. Let

$$
e_{i,j}(\mathbf{P}) \triangleq \frac{\overline{\mathcal{P}}_{i,j}(\mathbf{P}, \mathbf{W}, \mathbf{S})}{F_{i,j}(\mathbf{W}, \mathbf{S})} = \begin{cases} \beta \|p_i - p_j\|^2 + \rho, & j \in \mathcal{I}_S \\ \beta \|p_i - p_j\|^2, & j \in \mathcal{I}_F \end{cases} \tag{3.6}
$$

be the Link (i,j)'s energy cost (Joules/bit). Without loss of generality, we assume that Sensor i's collected data goes through K_i paths $\{L_k^{(i)}(\mathbf{S})\}_{k \in \{1,\dots,K_i\}}$, where $L_k^{(i)}(\mathbf{S}) = l_{k,0}^{(i)} \rightarrow l_{k,1}^{(i)} \rightarrow \cdots \rightarrow l_{k,J_k^{(i)}}^{(i)}$, $l_{k,0}^{(i)} = i$, $l_{k,J_k^{(i)}}^{(i)} \in \mathcal{I}_F$, and $J_k^{(i)}$ is the number of nodes on the k-th path except Node i. Then, the data rate (bits/s) and the path cost (Joules/bit) corresponding to the k-th path can be written as

$$
\mu_k^{(i)}(\mathbf{W}, \mathbf{S}) = F_i(\mathbf{W}, \mathbf{S}) \prod_{j=1}^{J_k^{(i)}} s_{l_{k,j-1}^{(i)}, l_{k,j}^{(i)}}, \tag{3.7}
$$

and

$$
\bar{e}_k^{(i)}(\mathbf{P}, \mathbf{S}) = \sum_{j=1}^{J_k^{(i)}} e_{l_{k,j-1}^{(i)}, l_{k,j}^{(i)}}(\mathbf{P}), \tag{3.8}
$$

respectively. Note that $\sum_k \mu_k^{(i)}(\mathbf{W}, \mathbf{S}) = F_i(\mathbf{W}, \mathbf{S})$ which means the data from Node i eventually reaches one or more FCs. Sensor i's power coefficient, denoted by $g_i(\mathbf{P}, \mathbf{S})$, is then defined to be the energy consumption (Joules/bit) for transmitting 1 bit data from Sensor i to the FCs, i.e, we have:

$$g_i(\mathbf{P}, \mathbf{S}) = \frac{\sum_{k=1}^{K_i} \mu_k^{(i)}(\mathbf{W}, \mathbf{S})\overline{e}_k^{(i)}(\mathbf{P}, \mathbf{S})}{F_i(\mathbf{W}, \mathbf{S})}$$

$$= \sum_{k=1}^{K_i} \left[\prod_{j=1}^{J_k^{(i)}} s_{l_{k,j-1}^{(i)}, l_{k,j}^{(i)}} \left(\sum_{j=1}^{J_k^{(i)}} \beta \left\| p_{l_{k,j-1}^{(i)}} - p_{l_{k,j}^{(i)}} \right\|^2 + \rho \left(J_k^{(i)} - 1 \right) \right) \right]. \qquad (3.9)$$

Note that the term $F_i(\mathbf{W}, \mathbf{S})$ is canceled in (3.9), indicating that power coefficient $g_i(\mathbf{P}, \mathbf{S})$ is independent of $\mathbf{W}$. In what follows, we provide an example to clarify how to calculate the sensor power coefficients.

Example 2. Consider the WASN described in Fig. 3.1, and let $\mathbf{P} = ((0,0), (0,1), (1,0), (1,1))$, $\beta = 1$ and $\rho = 1$. We aim to find Sensor 1's power coefficient $g_1(\mathbf{P}, \mathbf{S})$. The link energy costs for this network can be calculated as $e_{1,2}(\mathbf{P}) = e_{1,3}(\mathbf{P}) = 2$, $e_{2,3}(\mathbf{P}) = 3$, and $e_{2,4}(\mathbf{P}) = e_{3,4}(\mathbf{P}) = 1$. Note that Sensor 1's data goes through the following 3 paths: $L_1^{(1)}(\mathbf{S}) = 1 \rightarrow 2 \rightarrow 4$, $L_2^{(1)}(\mathbf{S}) = 1 \rightarrow 3 \rightarrow 4$, and $L_3^{(1)}(\mathbf{S}) = 1 \rightarrow 2 \rightarrow 3 \rightarrow 4$. The data rate through the above paths are, respectively, $\mu_1^{(1)}(\mathbf{W}, \mathbf{S}) = F_1(\mathbf{W}, \mathbf{S}) \times s_{1,2} \times s_{2,4} = 0.3F_1(\mathbf{W}, \mathbf{S})$, $\mu_2^{(1)}(\mathbf{W}, \mathbf{S}) = F_1(\mathbf{W}, \mathbf{S}) \times s_{1,3} \times s_{3,4} = 0.5F_1(\mathbf{W}, \mathbf{S})$, and $\mu_3^{(1)}(\mathbf{W}, \mathbf{S}) = F_1(\mathbf{W}, \mathbf{S}) \times s_{1,2} \times s_{2,3} \times s_{3,4} = 0.2F_1(\mathbf{W}, \mathbf{S})$. Moreover, we can calculate the path costs using (3.8) as follows: $\overline{e}_1^{(1)}(\mathbf{P}) = e_{1,2}(\mathbf{P}) + e_{2,4}(\mathbf{P}) = 3$, $\overline{e}_2^{(1)}(\mathbf{P}) = e_{1,3}(\mathbf{P}) + e_{3,4}(\mathbf{P}) = 3$, and $\overline{e}_3^{(1)}(\mathbf{P}) = e_{1,2}(\mathbf{P}) + e_{2,3}(\mathbf{P}) + e_{3,4}(\mathbf{P}) = 6$. Then, Sensor 1's power coefficient is $g_1(\mathbf{P}, \mathbf{S}) = 0.3 \times 3 + 0.5 \times 3 + 0.2 \times 6 = 3.6$.

Note that the average power consumption for transmitting Sensor i's data is $g_i(\mathbf{P}, \mathbf{S})\Gamma(W_i) = g_i(\mathbf{P}, \mathbf{S})\kappa \int_{W_i} f(\omega)d\omega$. Thus, the total power consumption (3.3) can be rewritten as:

$$\overline{\mathcal{P}}(\mathbf{P}, \mathbf{W}, \mathbf{S}) = \sum_{i=1}^{N} g_i(\mathbf{P}, \mathbf{S})\kappa \int_{W_i} f(\omega)d\omega. \qquad (3.10)$$

Therefore, the cost function in (3.5) can be rewritten as:

$$D(\mathbf{P}, \mathbf{W}, \mathbf{S}) = \mathcal{H}(\mathbf{P}, \mathbf{W}) + \lambda \overline{\mathcal{P}}(\mathbf{P}, \mathbf{W}, \mathbf{S})$$

$$= \sum_{i=1}^{N} \int_{W_i} \left(\|p_i - \omega\|^2 + \lambda \kappa g_i(\mathbf{P}, \mathbf{S}) \right) f(\omega) d\omega. \tag{3.11}$$

Now, given the node deployment $\mathbf{P}$ and normalized flow matrix $\mathbf{S}$, the optimal cell partitioning is equal to:

$$\mathcal{V}_i(\mathbf{P}, \mathbf{S}) = \{\omega | \ \|p_i - \omega\|^2 + \lambda \kappa g_i(\mathbf{P}, \mathbf{S}) \le \|p_j - \omega\|^2 + \lambda \kappa g_j(\mathbf{P}, \mathbf{S}), \forall j \ne i\}, i \in \mathcal{I}_S. \tag{3.12}$$

Moreover, given the link costs $\{e_{ij}(\mathbf{P})\}$s and generated sensing data rates $\{\Gamma(W_i)\}$s, the total power consumption can be minimized by Bellman-Ford Algorithm [34, 9]. For convenience, we represent the functionality of Bellman-Ford Algorithm by $\mathcal{R}(\mathbf{P}, \mathbf{W})$, where $\mathbf{P}$ and $\mathbf{W}$ are inputs and $\mathbf{S}$ is the output, i.e., $\mathcal{R}(\mathbf{P}, \mathbf{W}) = \arg\min_{\mathbf{S}} \overline{\mathcal{P}}(\mathbf{P}, \mathbf{W}, \mathbf{S})$. Since sensing uncertainty $\mathcal{H}(\mathbf{P}, \mathbf{W})$ is independent of $\mathbf{S}$, we have:

$$\mathcal{R}(\mathbf{P}, \mathbf{W}) = \arg\min_{\mathbf{S}} \mathcal{H}(\mathbf{P}, \mathbf{W}) + \lambda \overline{\mathcal{P}}(\mathbf{P}, \mathbf{W}, \mathbf{S})$$

$$= \arg\min_{\mathbf{S}} D(\mathbf{P}, \mathbf{W}, \mathbf{S}). \tag{3.13}$$

The optimal flow matrix for a given $\mathbf{P}$ and $\mathbf{W}$ is then $\mathbf{F}(\mathbf{W}, \mathcal{R}(\mathbf{P}, \mathbf{W}))$. The following theorem provides the necessary conditions for the optimal deployment.

Theorem 3.1. The necessary conditions for the optimal deployments in the WASNs with the cost defined in (3.5) are

$$p_i^* = \frac{c_i^* v_i^* + \lambda \beta \left(\sum_{j=1}^{N+M} F_{i,j}^* p_j^* + \sum_{j=1}^{N} F_{j,i}^* p_j^* \right)}{v_i^* + \lambda \beta \left(\sum_{j=1}^{N+M} F_{i,j}^* + \sum_{j=1}^{N} F_{j,i}^* \right)}, \qquad \forall i \in \mathcal{I}_S \tag{3.14}$$

$$p_i^* = \frac{\sum_{j=1}^{N} F_{j,i}^* p_j^*}{\sum_{j=1}^{N} F_{j,i}^*}, \qquad \forall i \in \mathcal{I}_F \tag{3.15}$$

$$\mathbf{W}^* = \mathcal{V}(\mathbf{P}^*, \mathbf{S}^*), \tag{3.16}$$

$$\mathbf{S}^* = \mathcal{R}(\mathbf{P}^*, \mathbf{W}^*), \tag{3.17}$$

where $v_i^* = \int_{\mathcal{V}_i(\mathbf{P}^*,\mathbf{S}^*)} f(\omega)d\omega$ and $c_i^* = \frac{\int_{\mathcal{V}_i(\mathbf{P}^*,\mathbf{S}^*)} \omega f(\omega)d\omega}{\int_{\mathcal{V}_i(\mathbf{P}^*,\mathbf{S}^*)} f(\omega)d\omega}$ are the Lebesgue measure (volume) and geometric centroid of the region $\mathcal{V}_i(\mathbf{P}^*, \mathbf{S}^*)$, respectively, and $F_{i,j}^* = F_{i,j}(\mathbf{W}^*, \mathbf{S}^*)$ is the optimal flow from Node i to Node j.

The proof of Theorem 3.1 is provided in Appendix C.1. Let $\mathcal{N}_i^P(\mathbf{S}) \triangleq \{j | F_{j,i}(\mathbf{W}, \mathbf{S}) > 0\}$ be the set of Node i's predecessors, and $\mathcal{N}_i^S(\mathbf{S}) \triangleq \{j | F_{i,j}(\mathbf{W}, \mathbf{S}) > 0\}$ be the set of Node i's successors. Hence, (3.14) and (3.15) can be simplified as

$$p_i^* = \frac{c_i^* v_i^* + \lambda\beta \left(\sum_{j \in \mathcal{N}_i^S(\mathbf{S}^*)} F_{i,j}^* p_j^* + \sum_{j \in \mathcal{N}_i^P(\mathbf{S}^*)} F_{j,i}^* p_j^* \right)}{v_i^* + \lambda\beta \left(\sum_{j \in \mathcal{N}_i^S(\mathbf{S}^*)} F_{i,j}^* + \sum_{j \in \mathcal{N}_i^P(\mathbf{S}^*)} F_{j,i}^* \right)} \tag{3.18}$$

for each $i \in \mathcal{I}_S$, and

$$p_i^* = \frac{\sum_{j \in \mathcal{N}_i^P(\mathbf{S}^*)} F_{j,i}^* p_j^*}{\sum_{j \in \mathcal{N}_i^P(\mathbf{S}^*)} F_{j,i}^*} \tag{3.19}$$

for each $i \in \mathcal{I}_F$, respectively. In other words, Sensor i's optimal location is a linear combination of its geometric centroid, predecessors, and successors while FC i's optimal location is a linear combination of its predecessors.

3.4   Routing-aware Lloyd Algorithm

First, we quickly review Lloyd Algorithm [69]. Lloyd Algorithm iterates between two steps: (i) Voronoi partitioning and (ii) Moving each node to the geometric centroid of its corresponding Voronoi region. Although the conventional Lloyd Algorithm can be used for one-tier quantizers or one-tier node deployment tasks, it cannot be applied to WASNs with multi-hop wireless communications. Based on the properties explored in Section 3.3, we design a Routing-aware Lloyd (RL) Algorithm to optimize the node deployment in WASNs and minimize the cost function in (3.5). To avoid a poor initial deployment, first, we design a quantizer with N (M) points for the spatial density function $f(\omega)$ and place the sensors (FCs) on the corresponding centroids. This results in an even distribution of sensors among FCs as the initial deployment. RL Algorithm then iterates between three steps: (i) Update the node deployment $\mathbf{P}$ according to (3.14) and (3.15); (ii) run Bellman-Ford Algorithm to update the normalized flow matrix $\mathbf{S}$ and obtain the sensor power coefficients $g_i(\mathbf{P}, \mathbf{S})$ and the flow matrix $\mathbf{F}(\mathbf{W}, \mathbf{S})$; and (iii) update the cell partitioning $\mathbf{W}$ according to (3.16) and update the value of volumes v_n and centroids c_n. The algorithm continues until the stop criterion, $\frac{D_{\mathrm{old}} - D_{\mathrm{new}}}{D_{\mathrm{old}}} \geq \epsilon$ is satisfied (D_{old} and D_{new} are the cost functions in the previous and current iterations, respectively).

Theorem 3.2. RL Algorithm is an iterative improvement algorithm, i.e., the cost function is non-increasing and the algorithm converges.

The proof of Theorem 3.2 is provided in Appendix C.2.

3.5   Performance Evaluation

We provide the experimental results for two WASNs: (i) WASN1: A WASN including 1 FC and 20 sensors; (ii) WASN2: A WASN including 4 FCs and 40 sensors. To make a

fair comparison, we use the same target region and density function as in [41, 55], i.e., $\Omega = [0, 10]^2$ and $f(\omega) = \frac{1}{\int_\Omega d\omega} = 0.01$. Other parameters are set as follows: $\beta = 1$, $\rho = 0.1$, $\kappa = 1$, $\epsilon = 10^{-6}$.

To the best of our knowledge, this is the first work to consider both sensing uncertainty and power consumption in WASNs. Bellman-Ford Algorithm [34, 9] is the best routing algorithm to minimize the total energy consumption, but it does not take node deployment into account. To compare with Bellman-Ford Algorithm, we apply random deployment and Lloyd Algorithm [69] for the node deployment part. Random deployment + Bellman-Ford (RBF) employs Bellman-Ford Algorithm on 100 random node deployments and selects the best one. Similarly, Lloyd + Bellman-Ford (LBF) first applies Lloyd Algorithm to both FCs and Sensors to obtain a node deployment with small cost, and then employs Bellman-Ford Algorithm to reduce the average power. Furthermore, we compare RL with Combining Lloyd (CL) [41] which combines two Lloyd-like algorithms to optimize the node deployment with one-hop communications.
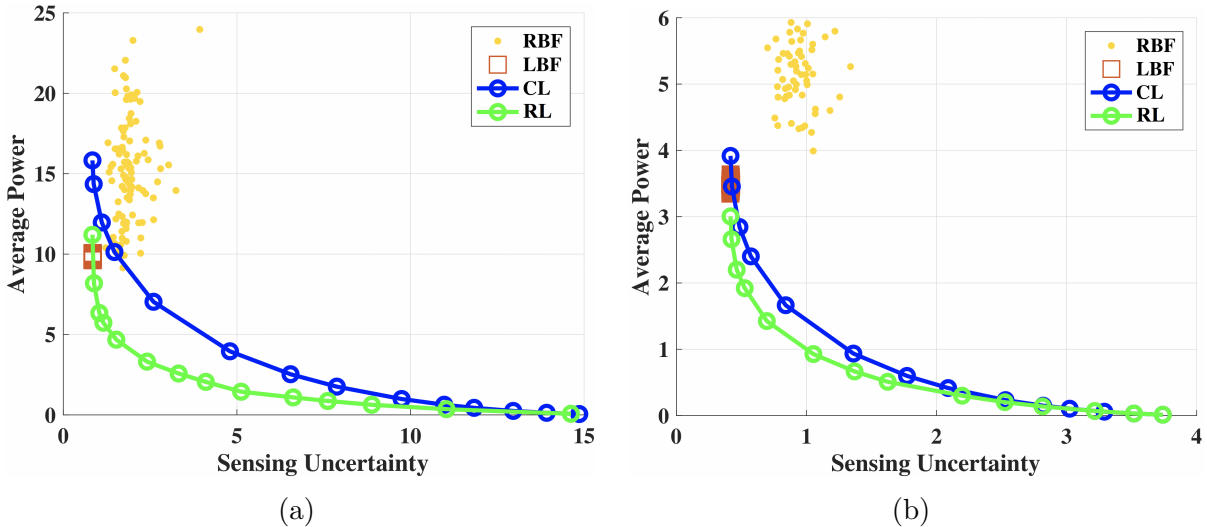
Figure 3.2: Performance comparison for different algorithms: (a) WASN1 (B) WASN2.

Performance results for different values of $\lambda \in \{0, 0.05, 0.15, 0.25, 0.5, 1, 1.5, 2, 3, 4, 5, 7, 10, 16\}$ are provided in Fig. 3.2. Note that the trade-off between sensing uncertainty and power consumption, represented by the constant parameter λ, is taken into account in both CL

and RL algorithms. However, RBF and LBF algorithms are independent of λ. In particular, since LBF determines the node deployment by Lloyd Algorithm before employing Bellman-Ford Algorithm, LBF's performance is almost independent of the initial deployments, and its experimental results in Fig. 3.2 converge to a point with small sensing uncertainty but large power consumption. For small values of λ, the cost function in (3.5) favors the sensing uncertainty over power consumption, which leads to the points on the left-hand side of the RL curve in Fig. 3.2. Similarly, large values of λ results in points on the right-hand side of the RL curve. Overall, the proposed RL algorithm outperforms other algorithms by saving more power and reducing more sensing uncertainty, in addition to providing a trade-off.[2]

The node deployments of the four algorithms (RBF, LBF, CL, and RL) in WASN1 with $\lambda = 0.25$ are illustrated in Figs. 3.3a, 3.3b, 3.3c, and 3.3d. FCs and sensors are denoted by five-pointed stars and circles, respectively. Flows are denoted by black dotted lines. As shown in Fig. 3.3, cell partitions in LBF, CL and RL algorithms tend to have similar shapes; however, RBF does not result in a similar pattern. Moreover, sensors in Fig. 3.3b are placed on top of their corresponding centroids while sensors in Fig. 3.3c are placed between their corresponding FC and centroid. However, in Fig. 3.3d, location of each sensor depends on its centroid, predecessors, and successors, as provided in Theorem 3.1. Note that in Figs. 3.3b, 3.3c and 3.3d, sensors inside each cluster tend to be close to each other with their FC in the middle; however, the same relationship does not appear in Fig. 3.3a. Besides, CL only uses one-hop communications, i.e., sensors are directly connected to the FC while other algorithms utilize multi-hop communications to reduce the average power. The corresponding cost function given $\lambda = 0.25$ for RBF, LBF, CL, and RL are, respectively, 3.82, 3.25, 4.00, 2.59; thus, our RL Algorithm achieves a lower cost function and outperforms other algorithms.

Similar results for WASN2 can be found in Fig. 3.4. The distortion of RL in WASN2, i.e.,

---

[2]To better exhibit the performance of LBF, CL, RL, we do not show the results of RBF with excessive powers ($\overline{\mathcal{P}} > 6$) in Fig. 3.2.
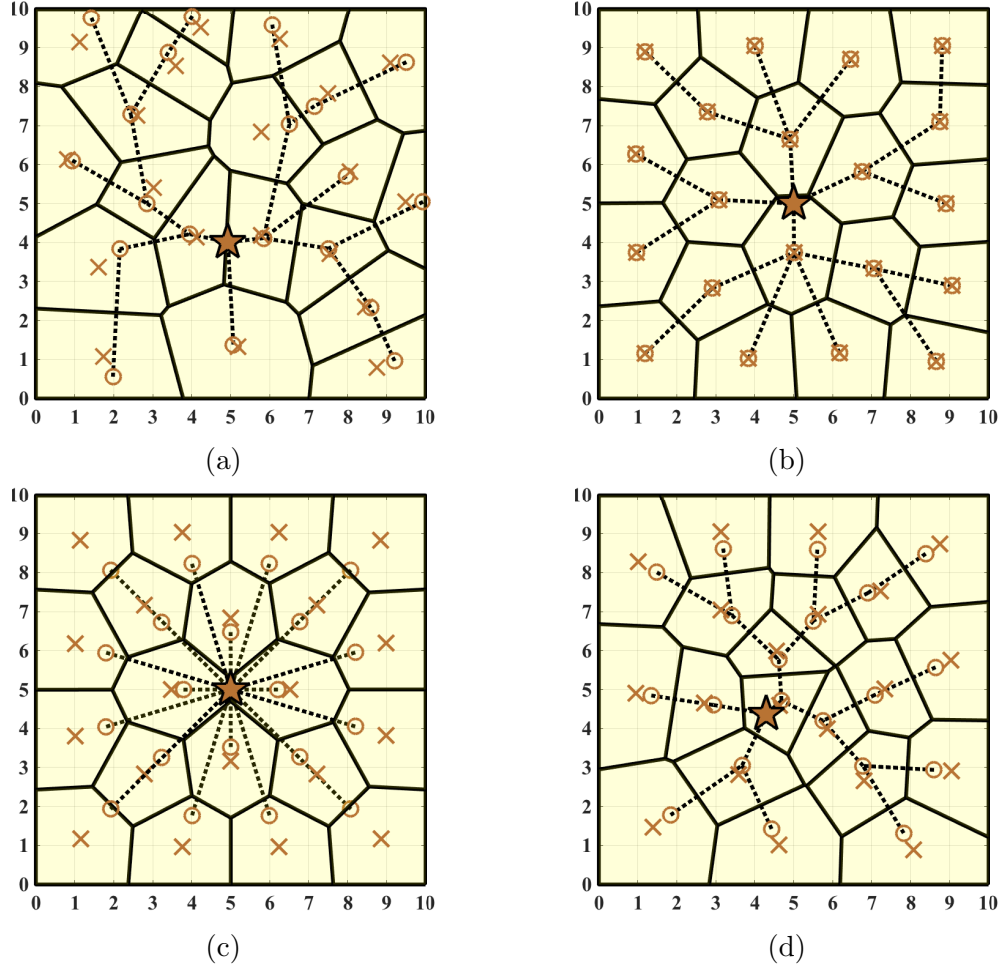
Figure 3.3: Node deployments of different algorithms with $\lambda = 0.25$ in WASN1: (a) RBF (b) LBF (c) CL (d) RL.

1.01, is smaller than that of RBF, LBF and CL (1.87, 1.25, 1.17). Note that in Figs. 3.4b, 3.4c and 3.4d, sensors inside each cluster tend to be close to each other with their FC in the middle; however, the same relationship does not appear in Fig. 3.4a.

3.6 Conclusions and Discussion

In this paper, we formulated the node deployment in WASNs as an optimization problem to make a trade-off between sensing uncertainty and energy consumption. The necessary conditions for the optimal deployment imply that each sensor location should be a linear
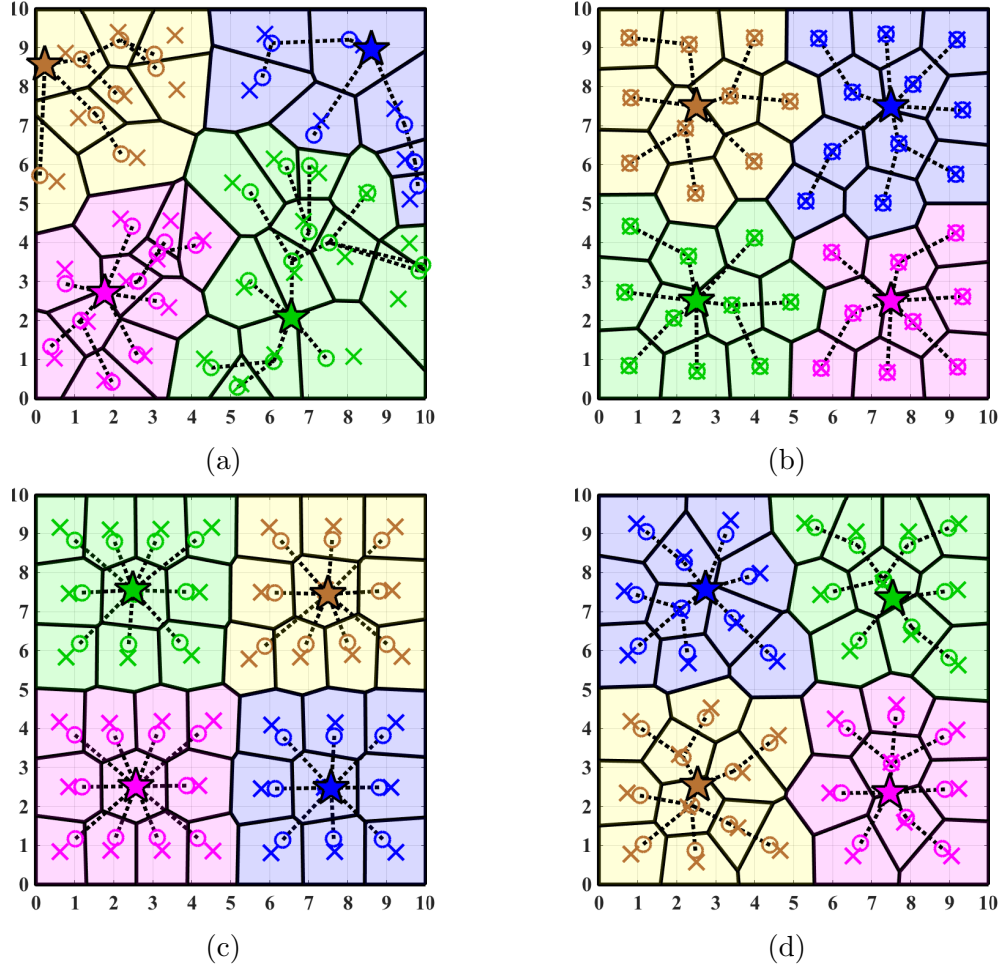
Figure 3.4: Node deployments of different algorithms with $\lambda = 0.25$: (a) RBF (b) LBF (c) CL (d) RL.

combination of its centroid, predecessors and successors. Based on these necessary conditions, we proposed a Lloyd-like algorithm to minimize the total cost. Our experimental results show that the proposed algorithm significantly reduces both sensing uncertainty and energy consumption. Although we only considered Bellman-Ford Algorithm as the routing algorithm in this paper, the proposed system model in Section 3.2 can be applied to arbitrary routing algorithms, such as Flow Augmentation Algorithm [15] (a network lifetime maximization routing algorithm). The optimal deployment with maximum network lifetime will be our future work.

Chapter 4

Energy-Efficient Deployment in Static and Mobile Heterogeneous Multi-Hop Wireless Sensor Networks

4.1 Introduction

Wireless sensor networks (WSNs) consist of small and low-cost sensor devices used to monitor the environment and transfer the sensed information through wireless channels to dedicated fusion centers. WSNs can be classified into either homogeneous WSNs [40, 41, 21, 20, 10], in which network nodes share the same characteristics such as storage, antennas, sensitivity etc., or heterogeneous WSNs where network nodes have different characteristics [55, 51, 56, 79, 42, 38]. Based on the network architecture, WSNs can be divided into either hierarchical WSNs, where network nodes are often grouped into clusters with some of them chosen to be cluster heads, or non-hierarchical WSNs where sensors have identical functionality and multi-hop wireless communication is used to maintain the connectivity of the network. Wireless sensor

nodes can also be classified as either static [56, 38], in which each network node remains at its deployed position, or mobile where network nodes can move to their optimal locations to improve the energy efficiency and sensing quality of WSNs [39, 98, 120, 19]. In general, there are three fundamental elements to specify for a WSN: (i) node deployment, i.e., the location of network nodes; (ii) cell partitioning, i.e., the region that each network node monitors; and (iii) data routing, i.e., the path that each sensory data takes to reach fusion centers. Not only should a proper network design algorithm jointly optimize over node deployment, cell partitioning, and data routing, but also it should be applicable to heterogeneous WSNs and be extendable to both static and mobile network nodes.

In [40, 41], we studied the optimal deployment in homogeneous WSNs; however, the homogeneous setting does not address many challenges that are inherent in heterogeneous WSNs, e.g., unlike regular Voronoi diagrams in homogeneous WSNs, the optimal cells in heterogeneous WSNs may be non-convex, not star-shaped, or even disconnected and the cell boundaries may not be hyperplanes. In [55, 56, 42, 38, 39], we studied the energy-efficient deployment for heterogeneous WSNs; however, the network is restricted to a one-tiered or two-tiered architecture while an efficient data routing through multi-hop communication can substantially improve the total energy consumption. Thus, our prior studies along with the majority of the work in the literature, as we will explore in the next section, fall short on one or more of the desired properties discussed above; namely, they may not consider the heterogeneous nature of network nodes, lack a rigorous radio energy model for the communication energy consumption, assume a specific network architecture, and consider only a static or mobile setting.

The primary motivation and key characteristic of this work over the existing literature is that not only do we incorporate the heterogeneity of network nodes into our system model and make no assumption about the network's architecture, but also we consider a radio energy model, where the electromagnetic wave propagation dampens as a power law function

60

of the distance between the transmitter and receiver, and develop deployment algorithms that are applicable to both static and mobile WSNs. In particular, we study the optimal deployment in heterogeneous multi-hop WSNs consisting of homogeneous densely deployed sensors, heterogeneous APs, and heterogeneous FCs, to minimize the wireless communication power consumption with and without movement energy constraints. Our contributions in this paper are multifold:

- We consider a radio energy model based on large scale fading and line-of-sight path loss signal attenuation that incorporates the heterogeneous characteristics of network nodes without any a priori assumption about the network's architecture, location of nodes, etc;

- We provide theoretical necessary conditions for an optimal deployment, cell partitioning, and data routing design for both static and mobile heterogeneous WSNs to minimize the power consumption;

- We design energy-efficient algorithms to jointly optimize node deployment, cell partitioning, and data routing that satisfy the necessary conditions and prove their convergence.

The rest of the paper is organized as follows: In Section 4.2, we present an overview of the existing literature on WSN deployment. In Section 4.3, we provide the system model. In Section 4.4, we study the optimal deployment in static heterogeneous multi-hop WSNs and propose an iterative algorithm based on the derived necessary conditions. The analysis of optimal deployment with network's total movement energy constraint is provided in Section 4.5. In Section 4.6, we study an energy-efficient deployment that guarantees a given network's lifetime in mobile WSNs. Experimental results are provided in Section 4.7 and Section 4.8 concludes the paper.

4.2 Related Work

Energy efficiency is a key determinant in longevity of the WSNs since sensors have limited energy resources and it is difficult or infeasible to recharge the batteries of densely deployed sensors. In general, many factors contribute to the energy consumption of the WSNs, e.g., communication energy, movement energy, sensing energy, and computation energy [114, 49]. Empirical measurements have shown that the data processing and computation energy as well as sensing energy for passive sensors are negligible compared to communication energy [87]. Thus, wireless communication dominates the energy consumption in static sensors in practice while movement energy dominates the energy consumption in mobile wireless sensor networks [56, 105].

Several methods have been proposed in the literature to reduce the energy consumption of wireless communication in WSNs. Examples include methods that circumvent the excess energy consumption by appropriately switching sensors between awake and asleep states [107], calibrating the transmission power of sensors while a reliable communication is maintained [58], and finding optimal paths to transfer data from sensors to fusion centers [10]. The common drawback of these approaches is that the deployment is assumed to be known and fixed; however, because the required transmission power is polynomially proportional to the distance between the transmitter and the receiver, a proper deployment can significantly affect the energy consumption of WSNs.

There are two types of deployment techniques proposed in the literature to optimize the energy consumption of WSNs: random deployment and deterministic deployment. Random deployment is often used in harsh or inaccessible environments where deterministic deployment is not feasible. Examples include Constant Diffusion [110], Hybrid Diffusion [91], and Discontinuous Diffusion [90] in which network nodes are scattered in the target region according to a given probability density function. Since network nodes are not usually placed

at their optimal locations due to the stochastic nature of these methods, the performance of random-based deployment falls short compared to the deterministic deployment. Deterministic deployment approaches aim to calculate the optimal location of network nodes that achieves a desired objective. These methods can be classified into four different categories, as we have summarized below:

1. *Grid-based methods:* Examples include [97, 86, 31, 71] in which the locations of network nodes are determined based on a grid shape such as triangular, rectangular, or hexagonal grid pattern. These methods are favorable due to their simplicity; however, they consider a homogeneous setting and do not account for the heterogeneity of network nodes; thus, they perform poorly when the WSN is comprised of nodes with different characteristics [31, 24]. In addition, they do not account for connectivity and are only applicable to static nodes.

2. *Force-based methods:* Examples include [117, 26, 66] in which a set of attractive, repulsive or null virtual forces act on network nodes based on their distance from each other. These methods offer adequate coverage and are applicable to mobile nodes; however, they suffer from nodes' oscillations problem [12], shortened network lifetime due to invalid movements [119], high computational complexity, and do not scale well with the number of nodes. Moreover, they yield undesirable performance for heterogeneous WSNs since virtual forces do not consider the heterogeneity of nodes.

3. *Geometry-based methods:* Examples include Delaunay triangulation and Voronoi-based algorithms such as [2, 104, 36, 99, 70] in which the target region is partitioned into a set of unique polygons, one for each network node, such that each point within a polygon is closest to that network node compared to any other node residing in other polygons. While the intuition of closeness in the sense of Euclidean distance makes sense for homogeneous nodes, it has been shown to fail for heterogeneous WSNs in which the best partitioning heavily depends on nodes' characteristics [56]. Our

63

proposed algorithms in this paper fall into this category of deployment methods.

4. *Meta-heuristic methods:* Examples include ant colony optimization [25, 65], artificial bee colony [80], particle swarm optimization [14], genetic algorithm [116, 44], and simulated annealing [28] in which various optimization tools are used to find nodes' locations. These methods are designed to achieve high coverage rates, but they are sensitive to node failure and suffer from high power consumption [32], high computational complexity, and low convergence rate. Additionally, fine-tuning the hyperparameters for these algorithms is very challenging since a slight variation can result in different network behavior.

To the best of our knowledge, the energy-efficient deployment in heterogeneous multi-hop WSNs is still an open problem. In the remainder of this paper, we study such networks in details.

4.3 System Model

In this section, we study the system model of heterogeneous multi-hop WSNs, as shown in Fig. 4.1, consisting of three types of nodes: homogeneous sensors, heterogeneous APs and heterogeneous FCs. Given the target region $\Omega \in \mathbb{R}^2$ which is a convex polygon including its interior, N APs and M FCs are deployed to collect information from densely deployed sensors. Let $\mathcal{I}_\mathcal{A} = \{1, \cdots, N\}$ and $\mathcal{I}_\mathcal{F} = \{N+1, \cdots, N+M\}$ denote the set of node indices for APs and FCs, respectively. If $n \in \mathcal{I}_\mathcal{A}$, Node n refers to AP n; however, when $n \in \mathcal{I}_\mathcal{F}$, Node n refers to FC $(n-N)$. The location of Node n is denoted by $p_n \subset \Omega$ and collectively the node deployment is denoted by $\mathbf{P} = (p_1, \cdots, p_N, p_{N+1}, \cdots, p_{N+M})$. Throughout this paper, we assume that each sensor only sends data to one AP; therefore, for each $n \in \mathcal{I}_\mathcal{A}$, AP n gathers data from sensors within the region $W_n \subseteq \Omega$, and $\mathbf{W} = (W_1, \cdots, W_N)$ provides

a set partitioning of the target region. The density of sensors is denoted via a continuous and differentiable function $f : \Omega \longrightarrow \mathbb{R}^+$. The total amount of data collected from sensors within the region W_n in one time unit is $R_b \int_{W_n} f(\omega) d\omega$, where the bit-rate R_b is a constant due to the homogeneity of sensors [41]. For each $n \in \mathcal{I}_\mathcal{A}$, the volume and centroid of the region W_n is defined as $v(W_n) \triangleq \int_{W_n} f(\omega) d\omega$ and $c(W_n) \triangleq \frac{\int_{W_n} \omega f(\omega) d\omega}{\int_{W_n} f(\omega) d\omega}$, respectively. The data gathered from each sensor is forwarded to other nodes in the network until it eventually reaches to one or more FCs.
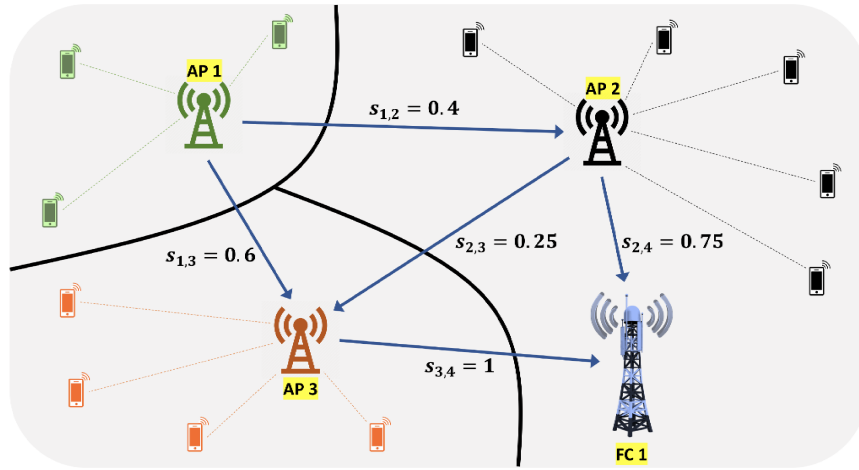
Figure 4.1: System model.

As shown in Fig. 4.1, the network can be regarded as a directed acyclic graph $\mathcal{G}(\mathcal{I}_\mathcal{A} \bigcup \mathcal{I}_F, \mathcal{E})$ where APs and FCs are source and sink nodes, respectively, and $\mathcal{E}$ is the set of directed edges (i, j) such that $i \in \mathcal{I}_\mathcal{A}$ and $j \in \mathcal{I}_\mathcal{A} \bigcup \mathcal{I}_\mathcal{F}$ [15]. Note that any cycle in the network's graph can be removed by reducing the flow of data along the cycle without changing the in-flow and out-flow links to that cycle. Let $\mathbf{F} = [F_{i,j}]_{N \times (N+M)}$ be the flow matrix, where $F_{i,j}$ is the amount of data transmitted through the link (i, j) in one time unit. Since the in-flow to each AP, say i, should be equal to the out-flow, we have $\sum_{j=1}^{N} F_{j,i} + R_b \int_{W_i} f(\omega) d\omega = \sum_{j=1}^{N+M} F_{i,j}$. For $i \in \mathcal{I}_\mathcal{A}$, we define $F_i \triangleq \sum_{j=1}^{N+M} F_{i,j}$ to be the total flow originated from AP i. Let $\mathbf{S} = [s_{i,j}]_{N \times (N+M)}$ be the normalized flow matrix, where $s_{i,j} \triangleq \frac{F_{i,j}}{\sum_{j=1}^{N+M} F_{i,j}}$ is the ratio of the in-flow data to AP i that is transmitted to node j. The normalized flow matrix $\mathbf{S}$ satisfies the

following properties: (a) $s_{i,j} \in [0,1]$;[1] (b) $\sum_{j=1}^{N+M} s_{i,j} = 1$, $\forall i \in \{1, \cdots, N\}$; (c) No cycle: if there exists a path in the network's graph such as $l_0 \to l_1 \to \cdots \to l_K$, i.e., $\prod_{k=1}^{K} s_{l_{k-1}, l_k} > 0$, then we have $s_{l_K, l_0} = 0$. In particular, we have $s_{i.i} = 0$, $\forall i \in \{1, \cdots, N\}$. Since the flow matrix $\mathbf{F}$ can be uniquely determined by the set partitioning $\mathbf{W}$ and the normalized flow matrix $\mathbf{S}$, in the remaining of this paper, we use the notation $\mathbf{F}(\mathbf{W}, \mathbf{S})$ instead of $\mathbf{F}$. The following example describes how to calculate $\mathbf{F}(\mathbf{W}, \mathbf{S})$ in terms of $\mathbf{W}$ and $\mathbf{S}$.

Example 1. We consider a heterogeneous multi-hop WSN with three APs and one FC, i.e. $N = 3$ and $M = 1$, and the bit-rate $R_b = 20$. For a cell partitioning $\mathbf{W}$ with cell volumes $v(W_1) = v(W_2) = 0.3$, $v(W_3) = 0.4$, and the normalized flow matrix $S = [s_{i,j}]_{N \times (N+M)}$ with non-zero entries $s_{1,2} = 0.4$, $s_{1,3} = 0.6$, $s_{2,3} = 0.25$, $s_{2,4} = 0.75$ and $s_{3,4} = 1$, the corresponding flow network is illustrated in Fig. 4.1. The amount of data generated from sensors within each cell can be calculated as: $\Gamma(W_1) = R_b v(W_1) = 6$, $\Gamma(W_2) = R_b v(W_2) = 6$, and $\Gamma(W_3) = R_b v(W_3) = 8$. AP 1 does not receive data from any other AP, and only transmits its collected sensed data; thus, $F_1(\mathbf{W}, \mathbf{S}) = \Gamma(W_1) = 6$. The flows from AP 1 are then $F_{1,2}(\mathbf{W}, \mathbf{S}) = s_{1,2} \times F_1(\mathbf{W}, \mathbf{S}) = 2.4$ and $F_{1,3}(\mathbf{W}, \mathbf{S}) = s_{1,3} \times F_1(\mathbf{W}, \mathbf{S}) = 3.6$, respectively. AP 2's flows come from $F_{1,2}(\mathbf{W}, \mathbf{S})$ and the data gathered from the region W_2. Hence, $F_2(\mathbf{W}, \mathbf{S}) = \Gamma(W_2) + F_{1,2}(\mathbf{W}, \mathbf{S}) = 8.4$. Therefore, the flows from AP 2 are $F_{2,3}(\mathbf{W}, \mathbf{S}) = s_{2,3} \times F_2(\mathbf{W}, \mathbf{S}) = 2.1$ and $F_{2,4}(\mathbf{W}, \mathbf{S}) = s_{2,4} \times F_2(\mathbf{W}, \mathbf{S}) = 6.3$. Similarly, for AP 3, we have $F_3(\mathbf{W}, \mathbf{S}) = \Gamma(W_3) + F_{1,3}(\mathbf{W}, \mathbf{S}) + F_{2,3}(\mathbf{W}, \mathbf{S}) = 13.7$; hence, the unique flow from AP 3 is $F_{3,4}(\mathbf{W}, \mathbf{S}) = s_{3,4} \times F_3(\mathbf{W}, \mathbf{S}) = 13.7$.

In what follows, we formulate the wireless communication power consumption of the network. Also, we focus on the power consumption of sensors and APs, since FCs are usually supplied with reliable energy sources and their power consumption is not the main concern. First, we

---

[1]For time-invariant routing algorithms, such as Bellman-Ford Algorithm [34, 9], the flows construct a tree-structured graph in which each node has only one successor. Under such circumstances, the normalized flow from Node i to Node j is either 0 or 1, i.e., $s_{i,j} \in \{0, 1\}$. However, the time-variant routing algorithms, such as Flow Augmentation Algorithm [15], generate different flows during different time periods. As a result, the overall normalized flow from Node i to Node j can be a real number between 0 and 1, i.e., $s_{i,j} \in [0, 1]$.

focus on the sensor's power consumption. According to [41], due to the path-loss, the instant transmission power is equal to the square of the distance between the two nodes multiplied by a constant that depends on the characteristics of both nodes, i.e., $\eta \times \|p_n - \omega\|^2$ for a sensor positioned at ω that transmits its data to AP n, $n \in \mathcal{I}_\mathcal{A}$. As shown in [49], the parameter η is given by $\eta = \frac{P_{th}(4\pi)^2}{R_b G_t G_r \lambda_c^2}$, where P_{th} is the minimum receiver power threshold for successful reception, R_b is the bit-rate, G_t and G_r are the antenna gains of the transmitter and receiver, respectively, and λ_c is the carrier signal wavelength. In the homogeneous setting, all nodes have the same characteristics; thus, the parameter η is the same and will not affect the optimization. However, in a heterogeneous multi-hop WSN, AP nodes can have different antenna gains and SNR thresholds; hence, the parameter η will be a function of the node index. Therefore, the sensors' transmission power consumption can be written as

$$\overline{\mathcal{P}}_\mathcal{S}^T(\mathbf{P}, \mathbf{W}) = \sum_{n=1}^{N} \int_{W_n} \eta_n \|p_n - \omega\|^2 R_b f(\omega) d\omega. \tag{4.1}$$

Similarly, the instant transmission power from Node i to Node j can be written as $\beta \times \|p_i - p_j\|^2$ where the parameter β depends on the antenna gain and SNR threshold of Node j and the antenna gain of Node i [49]. Therefore, it is the same for the homogeneous setting and will not affect the optimization. However, in a heterogeneous multi-hop WSN, the heterogeneity of the nodes causes the parameter β to be a function of the node indices. Hence, the average transmission power through link (i, j) is equal to $\beta_{i,j} \|p_i - p_j\|^2 F_{i,j}(\mathbf{W}, \mathbf{S})$, and the APs' total transmission power consumption can be written as

$$\overline{\mathcal{P}}_\mathcal{A}^T(\mathbf{P}, \mathbf{W}, \mathbf{S}) = \sum_{i=1}^{N} \sum_{j=1}^{N+M} \beta_{i,j} \|p_i - p_j\|^2 F_{i,j}(\mathbf{W}, \mathbf{S}). \tag{4.2}$$

According to [51], power at the receiver of AP n can be modeled as $\sum_{i=1}^{N} \rho_n F_{i,n}(\mathbf{W}, \mathbf{S}) + \rho_n R_b \int_{W_n} f(\omega) d\omega$, where ρ_n is the power consumption coefficient for receiving data at AP n, and depends on digital coding, modulation and filtering of the signal before transmission

[49]. Therefore, the APs' total receiver power consumption can be written as:

$$\overline{\mathcal{P}}_{\mathcal{A}}^{R}\left(\mathbf{W},\mathbf{S}\right) = \sum_{n=1}^{N} \rho_n \left[\sum_{i=1}^{N} F_{i,n}\left(\mathbf{W},\mathbf{S}\right) + R_b \int_{W_n} f(\omega)d\omega \right]. \tag{4.3}$$

Thus, the total communication power consumption of the multi-hop WSN can be written as:

$$\mathcal{D}\left(\mathbf{P},\mathbf{W},\mathbf{S}\right) = \overline{\mathcal{P}}_{\mathcal{S}}^{T}\left(\mathbf{P},\mathbf{W}\right) + \lambda \left[\overline{\mathcal{P}}_{\mathcal{A}}^{T}\left(\mathbf{P},\mathbf{W},\mathbf{S}\right) + \overline{\mathcal{P}}_{\mathcal{A}}^{R}\left(\mathbf{W},\mathbf{S}\right) \right], \tag{4.4}$$

where the Lagrangian multiplier $\lambda \geq 0$ provides a trade-off between the sensor and AP power consumption. Our main objective in this paper is to minimize the multi-hop power consumption defined in (4.4) over the node deployment $\mathbf{P}$, cell partitioning $\mathbf{W}$, and the normalized flow matrix $\mathbf{S}$ in both static and mobile WSNs with constrained movement energy.

4.4 Optimal Node Deployment in Static Heterogeneous Multi-Hop WSNs

As shown in (4.4), the total power consumption depends on three variables $\mathbf{P}$, $\mathbf{W}$ and $\mathbf{S}$. Thus, our goal is to find the optimal AP and FC deployments, cell partitioning and normalized flow matrix, denoted by $\mathbf{P}^* = \left(p_1^*, \cdots, p_N^*, p_{N+1}^*, \cdots, p_{N+M}^*\right)$, $\mathbf{W}^* = \left(W_1^*, \cdots, W_N^*\right)$ and $\mathbf{S}^* = \left[s_{i,j}^*\right]_{N\times(N+M)}$, respectively, that minimizes the multi-hop power consumption. Note that not only the variables $\mathbf{P}$, $\mathbf{W}$ and $\mathbf{S}$ are interdependent, i.e., the optimal value for each of them depends on the value of the other two variables, but also this optimization problem is NP-hard. Our aim is to design an iterative algorithm that optimizes the value of one variable while the other two variables are held fixed. For this purpose, first we introduce a few concepts, and then we derive the necessary conditions for optimal deployment at each

step.

Without loss of generality, we assume that AP n's gathered data goes through K_n paths in the network's graph before it reaches to one or more fusion centers. We denote these paths by $\left\{L_k^{(n)}(\mathbf{S})\right\}_{k \in \{1, \cdots, K_n\}}$, where $L_k^{(n)}(\mathbf{S}) = l_{k,0}^{(n)} \to l_{k,1}^{(n)} \to \cdots \to l_{k,J_k^{(n)}}^{(n)}$, $l_{k,0}^{(n)} = n$, $l_{k,i}^{(n)} \in \mathcal{I}_\mathcal{A}$ for $i \in \{0, \cdots, J_k^{(n)} - 1\}$, $l_{k,J_k^{(n)}}^{(n)} \in \mathcal{I}_\mathcal{F}$ and $J_k^{(n)}$ is the number of nodes on the k-th path excluding Node n. The portion of the total flow originated from AP n that goes through the k-th path can then be calculated as

$$\mu_k^{(n)}(\mathbf{W}, \mathbf{S}) = F_n(\mathbf{W}, \mathbf{S}) \prod_{i=1}^{J_k^{(n)}} s_{l_{k,i-1}^{(n)}, l_{k,i}^{(n)}}. \tag{4.5}$$

In particular, we have $\sum_{k=1}^{K_n} \mu_k^{(n)}(\mathbf{W}, \mathbf{S}) = F_n(\mathbf{W}, \mathbf{S})$ that indicates the data from AP n eventually reaches to one or more FCs. Next, for each link (i, j) in the network's graph, we define the energy cost (Watt/bit) to be:

$$e_{i,j}(\mathbf{P}) \triangleq \begin{cases} \beta_{i,j} \|p_i - p_j\|^2 + \rho_j, & \text{if } j \in \mathcal{I}_\mathcal{A} \\ \beta_{i,j} \|p_i - p_j\|^2, & \text{if } j \in \mathcal{I}_\mathcal{F}. \end{cases} \tag{4.6}$$

Hence, we define the path cost corresponding to the k-th path from AP n to FCs as:

$$\bar{e}_k^{(n)}(\mathbf{P}, \mathbf{S}) = \sum_{i=1}^{J_k^{(n)}} e_{l_{k,i-1}^{(n)}, l_{k,i}^{(n)}}(\mathbf{P}). \tag{4.7}$$

Now, AP n's power coefficient, denoted by $g_n(\mathbf{P}, \mathbf{S})$ is defined to be the power consumption (Joules/bit) for transmitting 1 bit data from AP n to the FCs, i.e., we have:

$$g_n(\mathbf{P}, \mathbf{S}) = \frac{\sum_{k=1}^{K_n} \mu_k^{(n)}(\mathbf{W}, \mathbf{S}) \bar{e}_k^{(n)}(\mathbf{P}, \mathbf{S})}{F_n(\mathbf{W}, \mathbf{S})} \tag{4.8}$$

$$= \sum_{k=1}^{K_n} \left[\prod_{i=1}^{J_k^{(n)}} s_{l_{k,i-1}^{(n)}, l_{k,i}^{(n)}} \left(\sum_{j=1}^{J_k^{(n)}} \beta_{l_{k,j-1}^{(n)}, l_{k,j}^{(n)}} \left\| p_{l_{k,j-1}^{(n)}} - p_{l_{k,j}^{(n)}} \right\|^2 + \sum_{j=1}^{J_k^{(n)}-1} \rho_{l_{k,j}^{(n)}} \right) \right]. \tag{4.9}$$

Note that the term $F_n(\mathbf{W}, \mathbf{S})$ is canceled in (4.8), implying that power coefficient $g_n(\mathbf{P}, \mathbf{S})$ is independent of $\mathbf{W}$. Below we provide an example to clarify how to calculate the AP power coefficients.

Example 2. Consider the WSN described in Example 1, and let $\mathbf{P} = ((0, 0), (0, 1), (1, 0), (1, 1))$, $\beta_{i,j} = 1$ and $\rho_i = 1$ for all $i \in \mathcal{I}_\mathcal{A}$ and $j \in \mathcal{I}_\mathcal{A} \bigcup \mathcal{I}_\mathcal{F}$. We aim to find AP 1's power coefficient $g_1(\mathbf{P}, \mathbf{S})$. The link energy costs for this network can be calculated as $e_{1,2}(\mathbf{P}) = e_{1,3}(\mathbf{P}) = 2$, $e_{2,3}(\mathbf{P}) = 3$, and $e_{2,4}(\mathbf{P}) = e_{3,4}(\mathbf{P}) = 1$. Note that AP 1's data goes through the following 3 paths: $L_1^{(1)}(\mathbf{S}) = 1 \to 2 \to 4$, $L_2^{(1)}(\mathbf{S}) = 1 \to 3 \to 4$, and $L_3^{(1)}(\mathbf{S}) = 1 \to 2 \to 3 \to 4$. The data rate through the above paths are, respectively, $\mu_1^{(1)}(\mathbf{W}, \mathbf{S}) = F_1(\mathbf{W}, \mathbf{S}) \times s_{1,2} \times s_{2,4} = 0.3 F_1(\mathbf{W}, \mathbf{S})$, $\mu_2^{(1)}(\mathbf{W}, \mathbf{S}) = F_1(\mathbf{W}, \mathbf{S}) \times s_{1,3} \times s_{3,4} = 0.6 F_1(\mathbf{W}, \mathbf{S})$, and $\mu_3^{(1)}(\mathbf{W}, \mathbf{S}) = F_1(\mathbf{W}, \mathbf{S}) \times s_{1,2} \times s_{2,3} \times s_{3,4} = 0.1 F_1(\mathbf{W}, \mathbf{S})$. Moreover, we can calculate the path costs using (4.7) as follows: $\bar{e}_1^{(1)}(\mathbf{P}) = e_{1,2}(\mathbf{P}) + e_{2,4}(\mathbf{P}) = 3$, $\bar{e}_2^{(1)}(\mathbf{P}) = e_{1,3}(\mathbf{P}) + e_{3,4}(\mathbf{P}) = 3$, and $\bar{e}_3^{(1)}(\mathbf{P}) = e_{1,2}(\mathbf{P}) + e_{2,3}(\mathbf{P}) + e_{3,4}(\mathbf{P}) = 6$. Then, AP 1's power coefficient is $g_1(\mathbf{P}, \mathbf{S}) = 0.3 \times 3 + 0.6 \times 3 + 0.1 \times 6 = 3.3$.

To derive the necessary condition for an optimal cell partitioning, first, we need to rewrite the objective function in (4.4).

Lemma 7. *For the AP power coefficient defined in (4.8), we have:*

$$\sum_{n=1}^{N} g_n(\mathbf{P}, \mathbf{S}) R_b \int_{W_n} f(\omega) d\omega = \sum_{i=1}^{N} \left[\sum_{j=1}^{N+M} \beta_{i,j} \|p_i - p_j\|^2 F_{i,j}(\mathbf{W}, \mathbf{S}) + \sum_{j=1}^{N} \rho_j F_{i,j}(\mathbf{W}, \mathbf{S}) \right].$$
$$(4.10)$$

The proof is provided in Appendix D.1. Using Lemma 7, the objective function is:

$$\mathcal{D}(\mathbf{P}, \mathbf{W}, \mathbf{S}) = \sum_{n=1}^{N} \int_{W_n} \left(\eta_n \|p_n - \omega\|^2 R_b + \lambda g_n(\mathbf{P}, \mathbf{S}) R_b + \lambda \rho_n R_b \right) f(\omega) d\omega. \qquad (4.11)$$

Now, we study the properties of the optimal cell partitioning. For each $n \in \mathcal{I}_\mathcal{A}$, the Voronoi

cell $\mathcal{V}_n$ for a node deployment $\mathbf{P}$ and normalized flow matrix $\mathbf{S}$ is defined to be:

$$\mathcal{V}_n(\mathbf{P},\mathbf{S}) \triangleq \left\{\omega : \eta_n\|p_n-\omega\|^2 + \lambda g_n(\mathbf{P},\mathbf{S}) + \lambda\rho_n \leq \eta_k\|p_k-\omega\|^2 + \lambda g_k(\mathbf{P},\mathbf{S}) + \lambda\rho_k, \forall k \neq n\right\}. \tag{4.12}$$

Ties are broken in the favor of the smaller index to ensure that each Voronoi cell $\mathcal{V}_n$ is a Borel set. For brevity, we write $\mathcal{V}_n$ instead of $\mathcal{V}_n(\mathbf{P},\mathbf{S})$ when it is clear from the context. The collection

$$\mathcal{V}(\mathbf{P},\mathbf{S}) = (\mathcal{V}_1, \mathcal{V}_2, \cdots, \mathcal{V}_N) \tag{4.13}$$

is referred to as the generalized Voronoi diagram [56]. Note that in contrast to the regular Voronoi diagrams, the Voronoi cells defined in (4.12) can be non-convex, not star-shaped and even disconnected. The following proposition indicates that given a node deployment $\mathbf{P}$ and normalized flow matrix $\mathbf{S}$, the generalized Voronoi diagram provides the optimal cell partitioning.

Proposition 7. *For any node deployment* $\mathbf{P}$, *cell partitioning* $\mathbf{W}$ *and normalized flow matrix* $\mathbf{S}$, *we have:*

$$\mathcal{D}(\mathbf{P},\mathbf{W},\mathbf{S}) \geq \mathcal{D}(\mathbf{P},\mathcal{V}(\mathbf{P},\mathbf{S}),\mathbf{S}). \tag{4.14}$$

The proof is provided in Appendix D.2. Now, given the link costs $\{e_{i,j}(\mathbf{P})\}$s and generated sensing data rate from each cell partition, the total multi-hop power consumption can be minimized by Bellman-Ford Algorithm [34, 9]. For convenience, we show the functionality of Bellman-Ford Algorithm by $\mathcal{R}(\mathbf{P},\mathbf{W})$, where $\mathbf{P}$ and $\mathbf{W}$ are inputs and $\mathbf{S}$ is the output, i.e., $\mathcal{R}(\mathbf{P},\mathbf{W}) = \arg\min_{\mathbf{S}}\left[\overline{\mathcal{P}}_{\mathcal{A}}^T(\mathbf{P},\mathbf{W},\mathbf{S}) + \overline{\mathcal{P}}_{\mathcal{A}}^R(\mathbf{W},\mathbf{S})\right]$. Since the sensors' power consumption is independent of $\mathbf{S}$, we have:

$$\mathcal{R}\left(\mathbf{P},\mathbf{W}\right) = \arg\min_{\mathbf{S}} \overline{\mathcal{P}}_{\mathcal{S}}^{T}\left(\mathbf{P},\mathbf{W}\right) + \lambda\left[\overline{\mathcal{P}}_{\mathcal{A}}^{T}\left(\mathbf{P},\mathbf{W},\mathbf{S}\right) + \overline{\mathcal{P}}_{\mathcal{A}}^{R}\left(\mathbf{W},\mathbf{S}\right)\right]$$

$$= \arg\min_{\mathbf{S}} \mathcal{D}\left(\mathbf{P},\mathbf{W},\mathbf{S}\right). \tag{4.15}$$

Hence, the optimal flow matrix for a given $\mathbf{P}$ and $\mathbf{W}$ is $\mathbf{F}\left(\mathbf{W}, \mathcal{R}\left(\mathbf{P},\mathbf{W}\right)\right)$. For notational brevity, we define the point $z_i\left(\mathbf{P},\mathbf{W},\mathbf{S}\right)$, or z_i for short, to be:

$$z_i = \frac{\eta_i R_b v_i c_i + \lambda\left(\sum_{j=1}^{N+M} \beta_{i,j} F_{i,j} p_j + \sum_{j=1}^{N} \beta_{j,i} F_{j,i} p_j\right)}{\eta_i R_b v_i + \lambda\left(\sum_{j=1}^{N+M} \beta_{i,j} F_{i,j} + \sum_{j=1}^{N} \beta_{j,i} F_{j,i}\right)}, \qquad \forall i \in \mathcal{I}_{\mathcal{A}} \tag{4.16}$$

$$z_i = \frac{\sum_{j=1}^{N} \beta_{j,i} F_{j,i} p_j}{\sum_{j=1}^{N} \beta_{j,i} F_{j,i}}. \qquad \forall i \in \mathcal{I}_{\mathcal{F}} \tag{4.17}$$

The following theorem provides the necessary conditions for the optimal deployment.

Proposition 8. *The necessary conditions for the optimal deployments in heterogeneous multi-hop WSNs with communication power consumption defined in (4.4) are*

$$p_i^* = z_i^*, \qquad \forall i \in \mathcal{I}_{\mathcal{A}} \bigcup \mathcal{I}_{\mathcal{F}} \tag{4.18}$$

$$\mathbf{W}^* = \mathcal{V}\left(\mathbf{P}^*, \mathbf{S}^*\right), \tag{4.19}$$

$$\mathbf{S}^* = \mathcal{R}\left(\mathbf{P}^*, \mathbf{W}^*\right), \tag{4.20}$$

where $z_i^* = z_i\left(\mathbf{P}^*, \mathbf{W}^*, \mathbf{S}^*\right)$ is given by Eqs. (4.16) and (4.17).

The proof of Proposition 8 is provided in Appendix D.3.

Note that depending on the cell partitioning and normalized flow matrix, there may not be any flow through some links in the network's graph. Let $\mathcal{N}_i^P(\mathbf{S}) \triangleq \{j | F_{j,i}(\mathbf{W},\mathbf{S}) > 0\}$ be the set of Node i's predecessors, and $\mathcal{N}_i^S(\mathbf{S}) \triangleq \{j | F_{i,j}(\mathbf{W},\mathbf{S}) > 0\}$ be the set of Node i's

successors. We can then simplify Eq. (4.18) as:

$$p_i^* = \frac{\eta_i R_b v_i^* c_i^* + \lambda \left(\sum\limits_{j \in \mathcal{N}_i^S(\mathbf{S}^*)} \beta_{i,j} F_{i,j}^* p_j^* + \sum\limits_{j \in \mathcal{N}_i^P(\mathbf{S}^*)} \beta_{j,i} F_{j,i}^* p_j^* \right)}{\eta_i R_b v_i^* + \lambda \left(\sum\limits_{j \in \mathcal{N}_i^S(\mathbf{S}^*)} \beta_{i,j} F_{i,j}^* + \sum\limits_{j \in \mathcal{N}_i^P(\mathbf{S}^*)} \beta_{j,i} F_{j,i}^* \right)}, \qquad \forall i \in \mathcal{I}_\mathcal{A} \qquad (4.21)$$

$$p_i^* = \frac{\sum\limits_{j \in \mathcal{N}_i^P(\mathbf{S}^*)} \beta_{j,i} F_{j,i}^* p_j^*}{\sum\limits_{j \in \mathcal{N}_i^P(\mathbf{S}^*)} \beta_{j,i} F_{j,i}^*}, \qquad \forall i \in \mathcal{I}_\mathcal{F}. \qquad (4.22)$$

In other words, AP i's optimal location is a linear combination of its geometric centroid, predecessors, and successors while FC i's optimal location is a linear combination of its predecessors.

In what follows, first, we quickly review the conventional Lloyd Algorithm [69], then we propose an algorithm to optimize the communication power consumption defined in Eq. (4.4) for heterogeneous multi-hop WSNs. Lloyd Algorithm iterates between two steps: (i) Voronoi partitioning and (ii) Moving each node to the geometric centroid of its corresponding Voronoi region. Although the conventional Lloyd Algorithm can be used for one-tier quantizers or one-tier node deployment tasks [38], it cannot be applied to WSNs with multi-hop wireless communications. Based on the properties explored in this section, we design a Routing-aware Lloyd (RL) Algorithm, as outlined in Algorithm 3, to optimize the node deployment in heterogeneous multi-hop WSNs and minimize the objective function in (4.4).

Proposition 9. *RL Algorithm is an iterative improvement algorithm, i.e., the objective function is non-increasing and the algorithm converges.*

The proof of Proposition 9 is provided in Appendix D.4.

Algorithm 3: Routing-aware Lloyd Algorithm

Result: Optimal node deployment $\mathbf{P}$, cell partitioning $\mathbf{W}$ and normalized flow matrix $\mathbf{S}$.

Input: Convergence error threshold $\epsilon \in \mathbb{R}^+$;

do

    – Calculate the objective function $\mathcal{D}_{\mathrm{old}} = \mathcal{D}\left(\mathbf{P}, \mathbf{W}, \mathbf{S}\right)$;

    1. Update the cell partitioning $\mathbf{W}$ according to the Eq. (4.19);

    2. Update the normalized flow matrix $\mathbf{S}$ using to the Bellman-Ford algorithm;

    3. Update the node deployment $\mathbf{P}$ as follows:

$$p_n = \frac{\eta_n R_b v_n c_n + \lambda\left(\sum_{j=1}^{N+M} \beta_{n,j} F_{n,j} p_j + \sum_{j=1}^{N} \beta_{j,n} F_{j,n} p_j\right)}{\eta_n R_b v_n + \lambda\left(\sum_{j=1}^{N+M} \beta_{n,j} F_{n,j} + \sum_{j=1}^{N} \beta_{j,n} F_{j,n}\right)}, \qquad \forall n \in \mathcal{I}_{\mathcal{A}}$$

$$p_n = \frac{\sum_{j=1}^{N} \beta_{j,n} F_{j,n} p_j}{\sum_{j=1}^{N} \beta_{j,n} F_{j,n}}, \qquad \forall n \in \mathcal{I}_{\mathcal{F}}$$

    – Calculate the objective function $\mathcal{D}_{\mathrm{new}} = \mathcal{D}\left(\mathbf{P}, \mathbf{W}, \mathbf{S}\right)$;

while $\frac{\mathcal{D}_{\mathrm{old}} - \mathcal{D}_{\mathrm{new}}}{\mathcal{D}_{\mathrm{old}}} \geq \epsilon$;

4.5 The Node Deployment with a Total Energy Constraint in Mobile WSNs

4.5.1 Problem formulation

In Section 4.4, we studied the scenario where nodes are directly placed at the optimal locations calculated via RL Algorithm. However, here we study mobile heterogeneous multi-hop WSNs in which each node moves from its initial position to its optimal location that minimizes the communication power consumption in (4.4) while the total movement energy consumption of the network is constrained. More precisely, given the linear model for movement energy consumption in [102], for each $n \in \mathcal{I}_{\mathcal{A}} \bigcup \mathcal{I}_{\mathcal{F}}$, Node n's movement energy can be modeled as:

$$E_n\left(\mathbf{P}\right) = \zeta_n \|p_n - \tilde{p}_n\|, \tag{4.23}$$

where the moving cost parameter ζ_n depends on Node n's energy efficiency, p_n and $\tilde{p}_n$ are its destination and initial locations, respectively. Therefore, the total movement energy consumption of the network is

$$E\left(\mathbf{P}\right) = \sum_{n=1}^{N+M} E_n\left(\mathbf{P}\right) = \sum_{n=1}^{N+M} \zeta_n \|p_n - \tilde{p}_n\|. \tag{4.24}$$

Our main objective in this section is to minimize the multi-hop communication power consumption in Eq. (4.4) while the total movement energy is limited, i.e., the constrained optimization problem is defined as

$$\underset{\mathbf{P},\mathbf{W},\mathbf{S}}{\text{minimize}}\, \mathcal{D}\left(\mathbf{P}, \mathbf{W}, \mathbf{S}\right), \tag{4.25}$$

$$\text{s.t.} \quad E\left(\mathbf{P}\right) \leq \gamma \tag{4.26}$$

where $\gamma \geq 0$ is the maximum movement energy consumption of the network.

4.5.2 The Optimal Node Deployment

Here, we aim to find the optimal node deployment $\mathbf{P}^*$, cell partitioning $\mathbf{W}^*$ and normalized flow matrix $\mathbf{S}^*$ that minimizes the total multi-hop communication power consumption while the movement energy consumption is constrained. Note that the movement energy in (4.26) is independent of the cell partitioning and normalized flow matrix; therefore, the generalized Voronoi diagram and Bellman-Ford Algorithm, represented in Eqs. (4.13) and (4.15), respectively, still provide the optimal cell partitioning and normalized flow matrix. Now, we discuss the optimal node deployment for the constrained optimization problem in Eqs.

(4.25) and (4.26).

Lemma 8. *Let* $\mathbf{P}^*$, $\mathbf{W}^*$ *and* $\mathbf{S}^*$ *be the optimal node deployment, cell partitioning and normalized flow matrix for the constrained optimization problem in Eqs. (4.25) and (4.26). We have:*

$$p_i^* = \delta_i \times \tilde{p}_i + (1 - \delta_i) \times z_i^*, \qquad \forall i \in \mathcal{I}_\mathcal{A} \bigcup \mathcal{I}_\mathcal{F} \tag{4.27}$$

where $\delta_i \in [0, 1]$ *and* $\tilde{p}_i$ *is the initial location of Node* i.

The proof is provided in Appendix D.5.

Lemma 8 states that the optimal location for Node i is on the line connecting its initial position to the point $z_i^* = z_i\left(\mathbf{P}^*, \mathbf{W}^*, \mathbf{S}^*\right)$. Note that this is in contrast to the optimal node deployment without movement energy constraint in Section 4.4, i.e., $p_i^* = z_i^*$, as shown in Proposition 8. The difference is because of the constraint in Eq. (4.26). Intuitively, for $\gamma = 0$ we have $\delta_i = 1$ for all $i \in \mathcal{I}_\mathcal{A} \bigcup \mathcal{I}_\mathcal{F}$, i.e., each node will remain at its initial position since there is zero total available movement energy. However, for sufficiently large enough γ, we have $\delta_i = 0$, i.e., $p_i^* = z_i^*$ for all $i \in \mathcal{I}_\mathcal{A} \bigcup \mathcal{I}_\mathcal{F}$. In general, nodes can be classified into two groups based on whether they have positive moving distance or they stand still. Let $\mathcal{I}_d = \{n \mid \|p_n - \tilde{p}_n\| > 0, \forall n \in \mathcal{I}_\mathcal{A} \bigcup \mathcal{I}_\mathcal{F}\}$ and $\mathcal{I}_s = \{n \mid \|p_n - \tilde{p}_n\| = 0, \forall n \in \mathcal{I}_\mathcal{A} \bigcup \mathcal{I}_\mathcal{F}\}$ be the set of dynamic and static nodes, respectively. The following theorem provides the necessary condition for the optimal node deployment in multi-hop WSNs with total movement energy constraint:

Proposition 10. *Let* $\mathbf{P}^*, \mathbf{W}^*$ *and* $\mathbf{S}^*$ *be the optimal node deployment, cell partitioning and normalized flow matrix for the constrained optimization problem in Eqs. (4.25) and (4.26). Then:*

$$\chi_n^* = \chi_m^* \geq \chi_k^*, \qquad\qquad \forall n, m \in \mathcal{I}_d, k \in \mathcal{I}_s \tag{4.28}$$

$$p_n^* = \tilde{p}_n + \Gamma_n^* \times \left[1 - \frac{\max\left(0, \sum_{i \in \mathcal{I}_d} \zeta_i \|\Gamma_i^*\| - \gamma\right)}{\|\Gamma_n^*\| \times \frac{\psi_n^*}{\zeta_n} \times \sum_{i \in \mathcal{I}_d} \frac{\zeta_i^2}{\psi_i^*}} \right], \qquad \forall n \in \mathcal{I}_d \qquad (4.29)$$

where $\Gamma_n^* = z_n^* - \tilde{p}_n$ and ψ_n^* is defined to be

$$\psi_n^* \triangleq \begin{cases} \eta_n R_b v_n^* + \lambda \left[\sum_{k=1}^{N+M} \beta_{n,k} F_{n,k}^* + \sum_{k=1}^{N} \beta_{k,n} F_{k,n}^* \right], & \text{if } n \in \mathcal{I}_\mathcal{A} \\ \lambda \sum_{k=1}^{N} \beta_{k,n} F_{k,n}^*, & \text{if } n \in \mathcal{I}_\mathcal{F} \end{cases} \qquad (4.30)$$

and the moving efficiency χ_n^* is defined as

$$\chi_n^* = \frac{\psi_n^* \|p_n^* - z_n^*\|^2}{\zeta_n \|p_n^* - z_n^*\|} = \frac{\psi_n^*}{\zeta_n} \|p_n^* - z_n^*\|, \qquad \forall n \in \mathcal{I}_\mathcal{A} \bigcup \mathcal{I}_\mathcal{F} \qquad (4.31)$$

to reflect Node n's ability to reduce the communication power consumption by movement.

The proof is provided in Appendix D.6. Proposition 10 captures the intuition in Lemma 8 that in an optimal deployment, Node n is located on the line connecting its initial position $\tilde{p}_n$ to the point z_n^*, for all $n \in \mathcal{I}_\mathcal{A} \bigcup \mathcal{I}_\mathcal{F}$. Furthermore, for a sufficiently large enough available movement energy γ, say $\gamma \geq \sum_{i \in \mathcal{I}_d} \zeta_i \|\Gamma_i^*\|$, we have $p_n^* = z_n^*$ for all $n \in \mathcal{I}_d$. Based on the necessary conditions in Proposition 10, we propose a Movement-Efficient Routing-aware Lloyd (MERL) Algorithm, as outlined in Algorithm 4, to optimize the node deployment in heterogeneous multi-hop WSNs with constrained movement energy, and minimize the objective function in Eqs. (4.25) and (4.26).

Proposition 11. *MERL Algorithm is an iterative improvement algorithm, i.e., the objective function is non-increasing and the algorithm converges.*

The proof of Proposition 11 is provided in Appendix D.7.

Algorithm 4: Movement-Efficient Routing-aware Lloyd Algorithm

---

Result: Optimal node deployment $\mathbf{P}$, cell partitioning $\mathbf{W}$ and normalized flow matrix $\mathbf{S}$.

Input: Initial node deployment $\tilde{\mathbf{P}}$, convergence error threshold $\epsilon \in \mathbb{R}^+$;

do

    – Calculate the objective function $\mathcal{D}_{\text{old}} = \mathcal{D}\left(\mathbf{P}, \mathbf{W}, \mathbf{S}\right)$;

    1. Update the cell partitioning $\mathbf{W}$ according to the Eq. (4.19);

    2. Update the normalized flow matrix $\mathbf{S}$ using to the Bellman-Ford algorithm;

    3. Set $\mathcal{I}_d = \{1, \cdots, N + M\}$ and calculate $r_n \triangleq \left[1 - \frac{\max\left(0, \sum_{i \in \mathcal{I}_d} \zeta_i \|\Gamma_i\| - \gamma\right)}{\|\Gamma_n\| \times \frac{\psi_n}{\zeta_n} \times \sum_{i \in \mathcal{I}_d} \frac{\zeta_i^2}{\psi_i}} \right]$,

    $\forall n \in \mathcal{I}_d$;

    4. **while** $\exists n \in \mathcal{I}_d$ such that $r_n \leq 0$ **do**

        4.1. Update $\mathcal{I}_d = \mathcal{I}_d - \bigcup_{r_n \leq 0} n$;

        4.2. Update $\{r_n\}_{n \in \mathcal{I}_d}$;

    5.

$$p_n = \tilde{p}_n + \Gamma_n \times \left[1 - \frac{\max\left(0, \sum_{i \in \mathcal{I}_d} \zeta_i \|\Gamma_i\| - \gamma\right)}{\|\Gamma_n\| \times \frac{\psi_n}{\zeta_n} \times \sum_{i \in \mathcal{I}_d} \frac{\zeta_i^2}{\psi_i}} \right] \times \mathbf{1}_{\mathcal{I}_d}(n), \qquad \forall n \in \mathcal{I}_{\mathcal{A}} \bigcup \mathcal{I}_{\mathcal{F}};$$

    – Calculate the objective function $\mathcal{D}_{\text{new}} = \mathcal{D}\left(\mathbf{P}, \mathbf{W}, \mathbf{S}\right)$;

while $\frac{\mathcal{D}_{\text{old}} - \mathcal{D}_{\text{new}}}{\mathcal{D}_{\text{old}}} \geq \epsilon$;

4.6 The Node Deployment with a Network Lifetime Constraint in Mobile WSNs

4.6.1 Problem formulation

In Section 4.5, we studied the node deployment with a total movement energy constraint, which can be seen as a resource allocation problem. This is because we can calculate how much movement energy each node requires once an optimal deployment is obtained. In this section, we focus on minimizing the communication power consumption given a constraint on the network lifetime. Let ν_n be the residual movement energy on Node n, and α_n be the power consumption for Node n after relocation. To ensure a network lifetime of T, the

following condition

$$\nu_n - E_n(\mathbf{P}) \geq \alpha_n T, \qquad \forall n \in \mathcal{I}_\mathcal{A} \bigcup \mathcal{I}_\mathcal{F} \tag{4.32}$$

has to be satisfied. Hence, the network lifetime of T can be achieved by setting a maximum individual movement energy consumption for each node. Here, our main objective is to find the optimal node deployment for the following constrained optimization problem:

$$\underset{\mathbf{P},\mathbf{W},\mathbf{S}}{\text{minimize}} \, \mathcal{D}(\mathbf{P},\mathbf{W},\mathbf{S}) \tag{4.33}$$

$$\text{s.t.} \quad E_n(\mathbf{P}) \leq \gamma_n, \qquad \forall n \in \mathcal{I}_\mathcal{A} \bigcup \mathcal{I}_\mathcal{F} \tag{4.34}$$

where $\gamma_n = \nu_n - \alpha_n T$ is the maximum individual movement energy consumption of Node n.

4.6.2   The Optimal Node Deployment

Here, our goal is to find the optimal node deployment $\mathbf{P}^*$, cell partitioning $\mathbf{W}^*$ and normalized flow matrix $\mathbf{S}^*$ that minimizes the multi-hop communication power consumption while each individual movement energy consumption is constrained. The following theorem provides the necessary condition for optimal node deployment in the constrained optimization problem in Eqs. (4.33) and (4.34).

Proposition 12. *Let $\mathbf{P}^*$, $\mathbf{W}^*$ and $\mathbf{S}^*$ be the optimal node deployment, cell partitioning and normalized flow matrix for the constrained optimization problem in Eqs. (4.33) and (4.34). Then,*

$$p_n^* = \tilde{p}_n + \Gamma_n^* \times \min\left(1, \frac{\gamma_n}{\zeta_n \|\Gamma_n^*\|}\right), \qquad \forall n \in \mathcal{I}_\mathcal{A} \bigcup \mathcal{I}_\mathcal{F} \tag{4.35}$$

where $\Gamma_n^* = z_n^* - \tilde{p}_n$.

The proof of Proposition 12 is provided in Appendix D.8. Based on the optimal condition in Proposition 12, we design the Lifetime-Optimized Routing-aware Lloyd (LORL) Algorithm, as outlined in Algorithm 5, to optimize the node deployment in heterogeneous multi-hop WSNs with network lifetime constraint, and minimize the objective function in Eqs. (4.33) and (4.34).

Algorithm 5: Lifetime-Optimized Routing-aware Lloyd Algorithm

---

Result: Optimal node deployment $\mathbf{P}$, cell partitioning $\mathbf{W}$ and normalized flow matrix $\mathbf{S}$.

Input: Initial node deployment $\tilde{\mathbf{P}}$, convergence error threshold $\epsilon \in \mathbb{R}^+$;

do

    – Calculate the objective function $\mathcal{D}_{\text{old}} = \mathcal{D}\left(\mathbf{P}, \mathbf{W}, \mathbf{S}\right)$;

    1. Update the cell partitioning $\mathbf{W}$ according to the Eq. (4.19);

    2. Update the normalized flow matrix $\mathbf{S}$ using to the Bellman-Ford algorithm;

    3. $p_n = \tilde{p}_n + \Gamma_n \times \min\left(1, \frac{\gamma_n}{\zeta_n \|\Gamma_n\|}\right),$ $\forall n \in \mathcal{I}_{\mathcal{A}} \bigcup \mathcal{I}_{\mathcal{F}}$;

    – Calculate the objective function $\mathcal{D}_{\text{new}} = \mathcal{D}\left(\mathbf{P}, \mathbf{W}, \mathbf{S}\right)$;

while $\frac{\mathcal{D}_{\text{old}} - \mathcal{D}_{\text{new}}}{\mathcal{D}_{\text{old}}} \geq \epsilon$;

Proposition 13. *LORL Algorithm is an iterative improvement algorithm, i.e., the objective function is non-increasing and the algorithm converges.*

The proof of Proposition 13 is provided in Appendix D.9.

4.7 Experiments

Simulations are carried out for a heterogeneous wireless sensor network consisting of 30 APs and 3 FCs. We consider a square field of size 10km $\times$ 10km, i.e., $\Omega = [0, 10000]^2$. Simulations are performed for two different sensor density functions, a uniform distribution $f\left(\omega\right) = \frac{1}{\int_\Omega d\omega} = 10^{-8}$ and a mixture of Gaussian where sensors are distributed according to:

$$f(\omega) = \frac{1}{2} \times \mathcal{N}\left(\begin{bmatrix} \mu_1^{(1)} \\ \mu_2^{(1)} \end{bmatrix}, \begin{bmatrix} \Sigma_{1,1}^{(1)} & 0 \\ 0 & \Sigma_{2,2}^{(1)} \end{bmatrix}\right) + \frac{1}{4} \times \mathcal{N}\left(\begin{bmatrix} \mu_1^{(2)} \\ \mu_2^{(2)} \end{bmatrix}, \begin{bmatrix} \Sigma_{1,1}^{(2)} & 0 \\ 0 & \Sigma_{2,2}^{(2)} \end{bmatrix}\right)$$
$$+ \frac{1}{4} \times \mathcal{N}\left(\begin{bmatrix} \mu_1^{(3)} \\ \mu_2^{(3)} \end{bmatrix}, \begin{bmatrix} \Sigma_{1,1}^{(3)} & 0 \\ 0 & \Sigma_{2,2}^{(3)} \end{bmatrix}\right),$$

where $\mu_1^{(1)} = 3,000$, $\mu_2^{(1)} = 3,000$, $\Sigma_{1,1}^{(1)} = 1.5 \times 10^6$, $\Sigma_{2,2}^{(1)} = 1.5 \times 10^6$, $\mu_1^{(2)} = 6,000$, $\mu_2^{(2)} = 7,000$, $\Sigma_{1,1}^{(2)} = 2 \times 10^6$, $\Sigma_{2,2}^{(2)} = 2 \times 10^6$, $\mu_1^{(3)} = 7,500$, $\mu_2^{(3)} = 2,500$, $\Sigma_{1,1}^{(3)} = 10^6$, $\Sigma_{2,2}^{(3)} = 10^6$. All homogeneous densely deployed sensors share the transmitter antenna gain of $G_{t_{\text{sensor}}} = 1$. We consider a radio bit-rate of $R_b = 1$Mbps and assume that the wavelength of the carrier signal is $\lambda_c = 0.3$m. In order for APs and FCs to receive the signal without error, the received power at each point $n \in \mathcal{I_A} \bigcup \mathcal{I_F}$ should be greater than some threshold P_{th_n}. Moreover, the transceiver electronics in each AP n consumes ρ_n J/bit for digital coding, modulation, and filtering before signal transmission. Table 4.1 summarizes the values of P_{th_n} and ρ_n for all APs and FCs [49].

Let us denote the transmitter antenna gain of AP n by G_{t_n}. In addition, for each point $n \in \mathcal{I_A} \bigcup \mathcal{I_F}$, let G_{r_n} be its receiver antenna gain. Table 4.2 summarizes the values of the transmitter and receiver antenna gains for all nodes [49].

Note that parameters η_i and $\beta_{i,j}$, for all $i \in \mathcal{I_A}$ and $j \in \mathcal{I_A} \bigcup \mathcal{I_F}$, can be calculated using the explained experimental setup. For example, we have $\eta_7 = \frac{P_{th_7} \times (4\pi)^2}{R_b G_{t_{\text{sensor}}} G_{r_7} \lambda_c^2} = \frac{10^{-8} \times (4\pi)^2}{10^6 \times 1 \times 2 \times (0.3)^2} = 8.77$ pJ/bit/m^2 and $\beta_{10,20} = \frac{P_{th_{20}} \times (4\pi)^2}{R_b G_{t_{10}} G_{r_{20}} \lambda_c^2} = \frac{6 \times 10^{-9} \times (4\pi)^2}{10^6 \times 2 \times 2 \times (0.3)^2} = 2.63$ pJ/bit/m^2. For performance evaluation, 10 initial AP and FC deployments are generated randomly on Ω, i.e., the location of each node is generated according to a uniform distribution on Ω. The maximum number of iterations for all algorithms is set to 200 and the Lagrangian multiplier is set to $\lambda = 0.25$.

Table 4.1: Simulation parameters

minimum received power (nW)				electronics energy dissipation (nJ/bit)		
$P_{th_{1:15}}$	$P_{th_{16:30}}$	$P_{th_{31}}$	$P_{th_{32:33}}$	$\rho_{1:7}$	$\rho_{8:16}$	$\rho_{17:30}$
10	6	6	10	40	50	60

Table 4.2: Transmitter and receiver antenna gains

transmitter antenna gain		receiver antenna gain	
$G_{t_{1:7,15:22}}$	$G_{t_{8:14,23:30}}$	$G_{r_{1:3,8:11,15:18,23:26,31:32}}$	$G_{r_{4:7,12:14,19:22,27:30,33}}$
1	2	1	2

4.7.1   Static Heterogeneous Multi-Hop WSNs

We compare the total weighted communication power consumption of our proposed RL Algorithm with Cluster-Formation (CF) Algorithm [17], Global Algorithm [100], Gradient-SA (GSA) Algorithm [28], HTTL Algorithm [56], MWCDS Algorithm [27], PSO Algorithm [23], Rhombus Algorithm [97], and SHMS Algorithm [54]. To reduce the number of hops that data packets have to travel to reach the fusion centers, the Cluster-Formation algorithm employs a graph theoretic approach to optimize both the number of clusters and their corresponding diameters. The Global algorithm deploys network nodes such that the average Euclidean distance between access points and their corresponding fusion centers is minimized. Starting with a dense triangular grid deployment, the GSA algorithm first removes those nodes with least coverage; then, it moves the boundary nodes toward the gradient direction that maximizes the covered area. For a two-tier hierarchy of APs and FCs, the HTTL algorithm iteratively updates the deployment, cell partitioning, and connections between APs and FCs while the flow of data from each sensor to its corresponding FC is mediated by exactly one access point. MWCDS Algorithm aims to deploy the minimum number of network nodes such that the resulting network is both connected and energy efficient. PSO is a population-based iterative algorithm for finding the optimal deployment and minimizing the non-linear

Table 4.3: Weighted power comparison for the uniform sensor density function

CF	Global	GSA	HTTL	MWCDS	PSO	Rhombus	SHMS	RL
15.49	14.98	17.28	12.80	17.12	19.98	16.21	22.39	**10.12**

Table 4.4: Weighted power comparison for the mixture of Gaussian sensor density function

CF	Global	GSA	HTTL	MWCDS	PSO	Rhombus	SHMS	RL
7.07	6.81	9.49	6.23	9.38	9.97	14.65	16.62	**5.58**

objective function. Rhmobus Algorithm uses a rhombus-based grid search for an energy-aware deployment that maximizes the coverage as well. For a given deployment, the SHMS algorithm determines the connections between APs and FCs such that the maximum energy consumed by each network node is minimized.

The weighted power consumption of Cluster-Formation, Global, GSA, HTTL, MWCDS, PSO, Rhombus, SHMS, and RL algorithms for the uniform sensor density function are summarized in Table 4.3. The RL algorithm outperforms other algorithms and achieves a lower weighted communication power consumption. Note that although the HTTL algorithm proposed in [56] deploys nodes based on the necessary conditions of optimality, the network architecture is restricted to a two-tier hierarchy while the RL algorithm simultaneously optimizes over the deployment and data routing. As a result, the deployment based on the RL algorithm results in a WSN that saves about 21% of the energy compared to that of the HTTL Algorithm.

Table 4.4 summarizes the weighted communication power consumption of Cluster-Formation, Global, GSA, HTTL, MWCDS, PSO, Rhombus, SHMS, and RL algorithms for the mixture of Gaussian sensor density function. The RL algorithm results in a power consumption of 5.58 Watts and outperforms other methods. Furthermore, the RL algorithm leads to a network architecture that exhaust its available communication energy in a time period that is longer by about 10% of that of HTTL Algorithm, the second best algorithm. Fig. 4.2

Figure 4.2: Node deployment for different algorithms and the mixture of Gaussian sensor density function. (a) Cluster-Formation (b) Global (c) HTTL (d) MWCDS (e) PSO (f) Rhombus (g) SHMS (h) RL.

shows the optimal deployment for different algorithms where APs and FCs are denoted by red squares and black circles, respectively.

4.7.2 Mobile Heterogeneous Multi-Hop WSNs with a Total Movement Energy Constraint

The underlying assumption in all deployment strategies studied in Section 4.7.1 is that the optimal locations are calculated offline and then APs and FCs are placed at the corresponding positions. However, in many applications, e.g., when the target region is a hostile environment, static deployment is not feasible. Instead, network nodes are initially deployed in the target region, e.g., by airdropping them using drones or manual placement in an accessible sub-region of the field and then each AP or FC moves to its optimal location based on the initial deployment and available movement energy. When the total available movement

Table 4.5: Moving cost parameters (J/m)

$\zeta_{1:8}$	$\zeta_{9:22}$	$\zeta_{23:30}$	ζ_{31}	ζ_{32}	ζ_{33}
2	4	6	4	5	6

energy is limited, which is the focus of this section, the optimization problem is translated into a resource allocation problem where the optimal energy supply for each AP or FC is determined such that the resulting total communication power consumption after optimal deployment is minimized. In Section 4.7.3, we study the performance evaluation when the available movement energy is predetermined and the optimization problem is translated to that of enhancing the network lifetime.

The same experimental setup described at the beginning of Section 4.7 and in Tables 4.1 and 4.2 is used for the simulations. Furthermore, Table 4.5 provides the moving cost parameters ζ_n for all $n \in \mathcal{I}_\mathcal{A} \bigcup \mathcal{I}_\mathcal{F}$. We consider a total available movement energy of $\gamma = 40,000$ Joules for the constrained objective function in Eqs. (4.25) and (4.26).

We compare the total weighted communication power consumption of our proposed MERL Algorithm with BCBS Algorithm [30], Lloyd-α Algorithm [98], OMF Algorithm [19], VCOND Algorithm [36], and VFA Algorithm [120]. BCBS Algorithm augments the iterative procedure of Lloyd Algorithm to maximize the network's coverage and minimize network nodes' movement. The Lloyd-α algorithm applies a penalty term to the Lloyd algorithm to reduce the movement steps and save traveling energy while guaranteeing the convergence property. The OMF algorithm optimizes the movement plan for nodes such that each region in the network has a minimum number of nodes to relay the data to fusion centers while the sum of network nodes' traveling distances is minimized. The VCOND algorithm iteratively partitions the target region according to the Voronoi diagram and relocates each network node based on the net virtual force coming from vertices and edges of its corresponding Voronoi cell. The VFA algorithm uses attractive and repulsive virtual forces on nodes such that not only every two network nodes in the final deployment maintain a minimum distance from

Table 4.6: Weighted power comparison

Sensor Density Function	BCBS	Lloyd-α	OMF	VCOND	VFA	MERL
uniform	24.35	29.12	27.35	27.92	27.85	**14.49**
mixture of Gaussian	15.94	17.38	17.29	15.32	18.76	**7.64**

each other, but also the communication distances are minimized by avoiding network nodes to be located very far from each other. For a fair comparison, the same initial deployment is used for all algorithms.

The weighted communication power consumption of BCBS, Lloyd-α, OMF, VCOND, VFA, and MERL algorithms for the uniform sensor density function are summarized in Table 4.6. All algorithms exhausted the available movement energy γ to move the AP and FC nodes from their initial deployment to their designated optimal locations. The MERL algorithm leads to a deployment that consumes communication energy in a rate that is almost half of other algorithms. The superior performance of the MERL algorithm is due to the optimal energy allocation among APs and FCs, as it is implicit in Eq. (4.29). Note that if the total movement energy γ is large enough, e.g., $\gamma \geq \sum_{i=1}^{N+M} \zeta_i \|\tilde{p}_i - z_i^*\|$, then the performance of the MERL algorithm will converge to that of the RL algorithm. However, since the value of γ in our experiments is not large enough, some APs and FCs will run out of their allocated movement energy and MERL algorithm leads to a communication power consumption that is larger than that of the RL algorithm in Section 4.7.1.

Table 4.6 also summarizes the weighted communication power consumption of BCBS, Lloyd-α, OMF, VCOND, VFA, and MERL algorithms for the mixture of Gaussian sensor density function. The MERL algorithm significantly outperforms other methods and leads to a communication power consumption that is less than half of what other algorithms achieve. This is because the MERL algorithm can optimally adapt to any underlying sensor density function $f(\omega)$ and deploy APs and FCs accordingly, as we studied in Section 4.5. Fig. 4.3 shows the final deployment for different algorithms where APs and FCs are denoted by red squares and black circles, respectively.
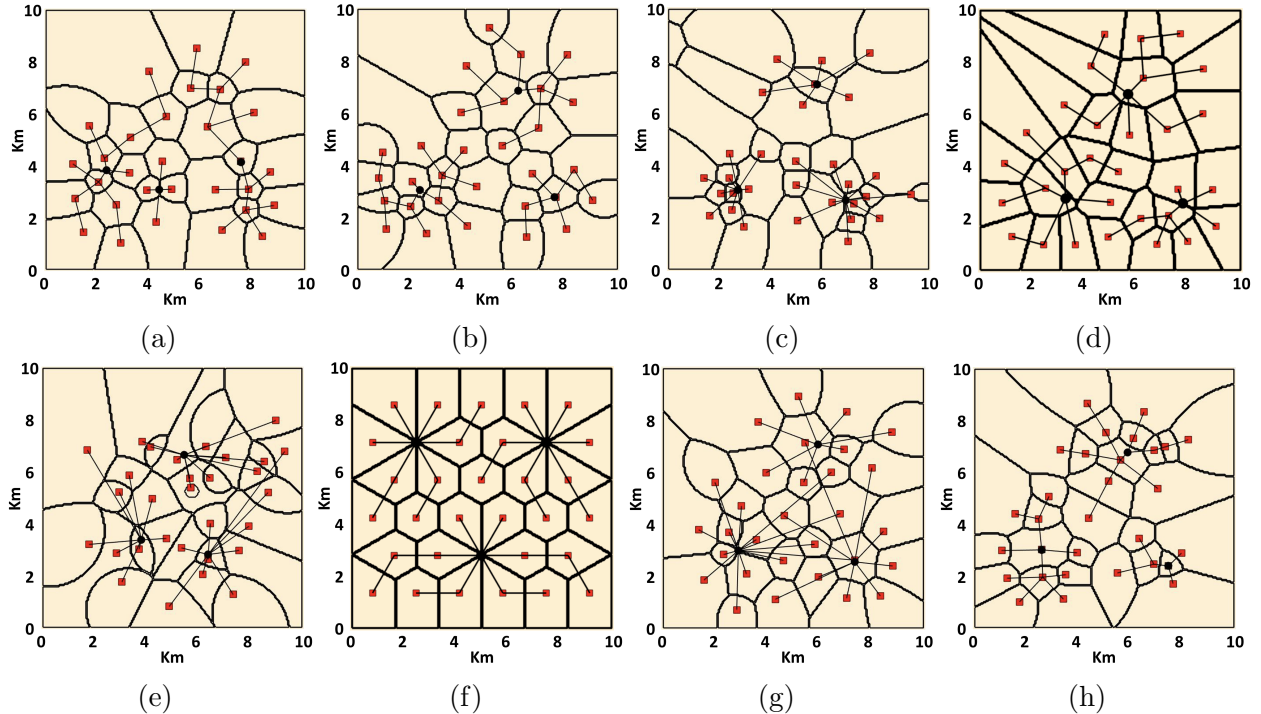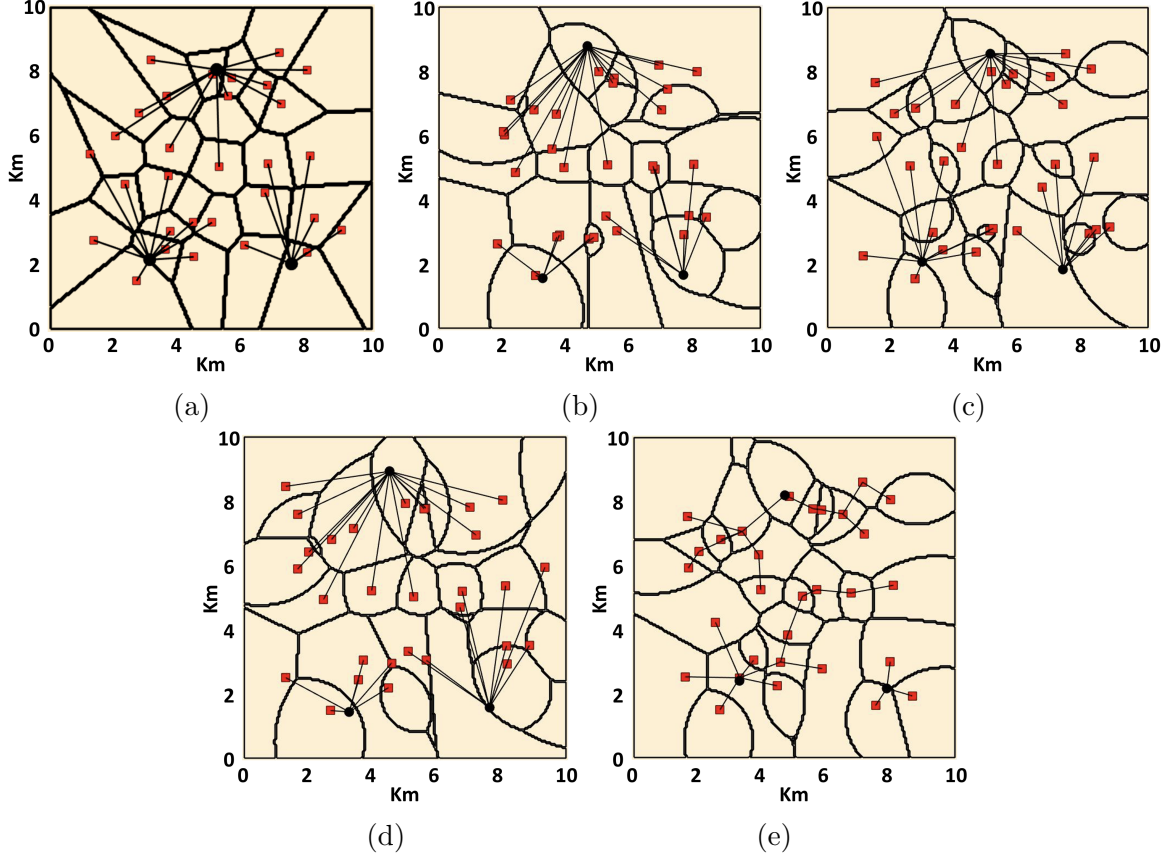
Figure 4.3: Node deployment for different algorithms and the mixture of Gaussian sensor density function. (a) BCBS (b) Lloyd-α (c) OMF (d) VFA (e) MERL.

4.7.3 Mobile Heterogeneous Multi-Hop WSNs with a Network Lifetime Constraint

While we studied the performance evaluation of mobile WSNs under a total movement energy constraint in Section 4.7.2, here, we focus on enhancing the network lifetime, which necessitates APs and FCs to have individual movement energy constraints, as formulated in Eqs. (4.33) and (4.34). We use the same experimental setup as described at the beginning of Section 4.7 and in Tables 4.1, 4.2, and 4.5 for performance evaluation. In addition, Table 4.7 provides the maximum individual movement energy consumption γ_n for all $n \in \mathcal{I}_\mathcal{A} \bigcup \mathcal{I}_\mathcal{F}$.

Table 4.7: Movement energy constraints (J)

$\gamma_{1:8}$	$\gamma_{9:22}$	$\gamma_{23:30}$	γ_{31}	γ_{32}	γ_{33}
800	1100	1400	2000	2400	2600

We compare the weighted communication power consumption of our proposed LORL Algorithm with those of BCBS Algorithm, Lloyd-α Algorithm, OMF Algorithm, and VFA Algorithm described in Section 4.7.2. For a fair comparison, the same initial deployment as in Section 4.7.2 is used for all algorithms.

The weighted communication power consumption of BCBS, Lloyd-α, OMF, VCOND, VFA, and LORL algorithms for the uniform sensor density function are provided in Table 4.8. The LORL algorithm outperforms other methods and achieves a significantly lower power consumption. For instance, the LORL algorithm leads to a deployment in which the network consumes its residual energy with a rate that is less than 70% of that of the VFA algorithm. This in turn prolongs the network lifetime, which is a prominent factor in wireless sensor networks.

Table 4.8: Weighted power comparison

Sensor Density Function	BCBS	Lloyd-α	OMF	VCOND	VFA	LORL
uniform	28.74	27.64	30.12	29.78	25.24	**17.33**
mixture of Gaussian	20.21	17.24	20.12	16.55	14.60	**9.59**

Table 4.8 also summarizes the power consumption of different algorithms for the mixture of Gaussian sensor density function. LORL Algorithm achieves a power consumption of 9.59 Watts and outperforms other methods. Fig. 4.4 shows the final deployment of different algorithms where APs and FCs are denoted by red squares and black circles, respectively.

The sum of individual movement energies in Table 4.7, i.e. $\sum_{i=1}^{N+M} \gamma_i$, is equal to the value of γ in Section 4.7.2. In other words, Table 4.7 represents one exemplary distribution of the total movement energy γ among APs and FCs; however, it is different from the optimal energy allocation provided by the MERL algorithm in Section 4.7.2. The results in Tables 4.6
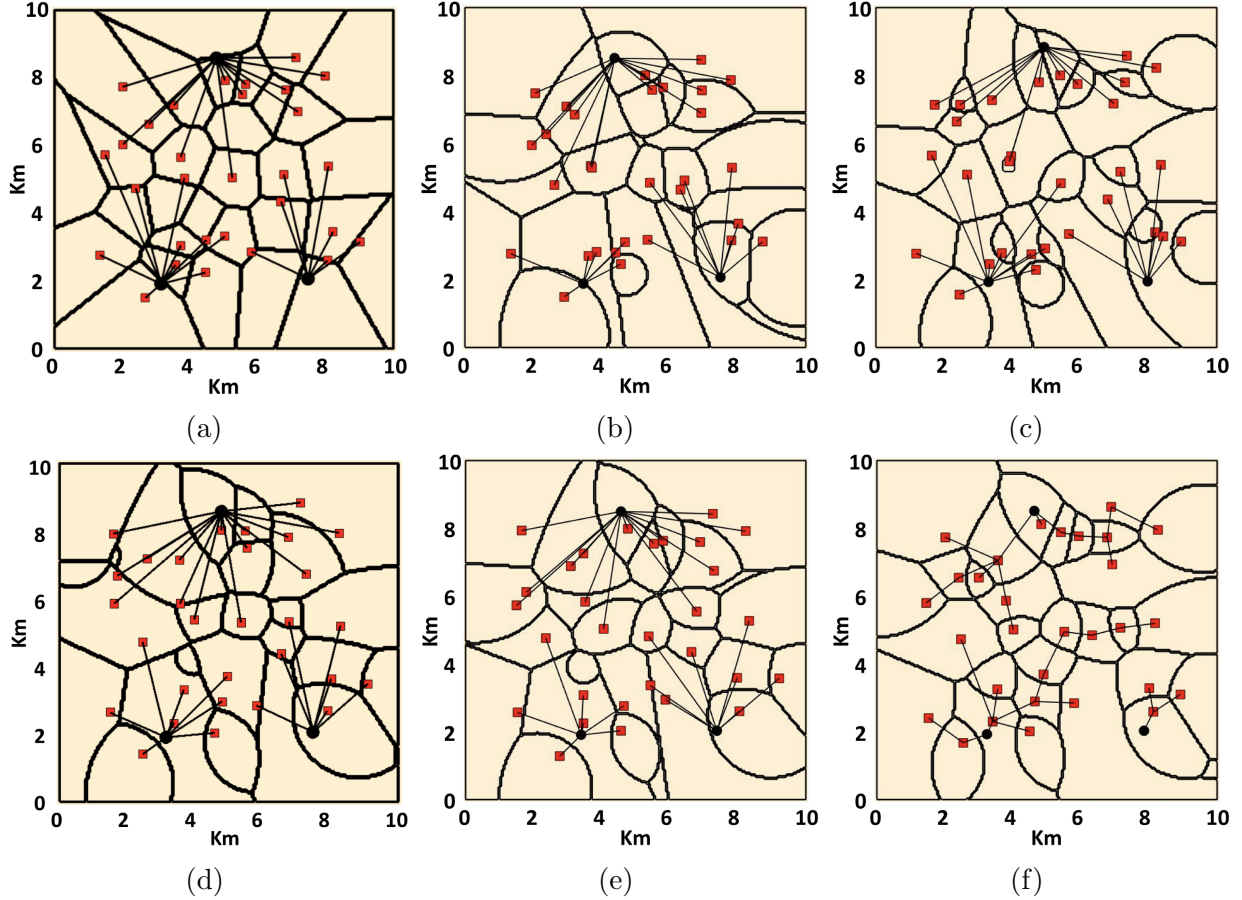
Figure 4.4: Node deployment for different algorithms and the mixture of Gaussian sensor density function. (a) BCBS (b) Lloyd-α (c) OMF (d) VCOND (e) VFA (f) LORL.

and 4.8 verify that the MERL algorithm achieves a lower total power consumption compared to the LORL algorithm although it does not guaranttee any individual power constraint.

4.8 Conclusion

In this work, a heterogeneous multi-hop wireless sensor network is discussed where data is collected from densely deployed sensors and transferred to heterogeneous fusion centers using heterogeneous access points as relay nodes. We modeled the minimum communication power consumption of such networks as an optimization problem, and studied the necessary

conditions of optimal deployment under both static and mobile network settings. A novel generalized Voronoi diagram is proposed to provide the best cell partition for the heterogeneous multi-hop network. When manual deployment is feasible, the necessary conditions of optimal deployment are explored under the static network setup, and accordingly a Routing-aware Lloyd algorithm is proposed to deploy nodes. However, when static placement is not doable, the necessary conditions of the optimal deployment are studied under a mobile network setting where nodes move from their initial locations to their optimal positions. We consider both total and individual movement energy constraints and formulate them as resource allocation and lifetime optimizations, respectively. Based on the derived necessary conditions, we propose Movement-Efficient Routing-aware Lloyd and Lifetime-Optimized Routing-aware Lloyd algorithms to deploy nodes under total and individual energy constraints, respectively. Simulation results show that our proposed RL, MERL, and LORL algorithms significantly save communication power in such networks and provide superior results compared to other methods in the literature.

Chapter 5

Node Deployment in Heterogeneous Rayleigh Fading Sensor Networks

5.1   Introduction

With recent technological advances in communication, sensing, computing, and battery capacity, wireless sensor networks (WSNs) have attracted widespread attention and have been used is numerous applications such as military applications [33], precision agriculture [1], healthcare monitoring [16], and industrial monitoring [5]. The primary utilization of WSN is to monitor physical phenomena such as environmental conditions, target positions, etc. inside a field of interest. Equipped with sensing and communication units, sensor nodes provide an interface with the physical environment and transmit the sensed information to dedicated base stations (BSs) through wireless radios [109, 118]. Sensor nodes are susceptible to failure due to factors such as adverse environmental condition and breakdown in the onboard electronics; however, battery power depletion is the most pivotal factor since sensors are driven by battery that are infeasible to replenish, especially in hostile environments [32].

Therefore, energy efficiency is considered the most crucial quality-of-service (QoS) metric for functionality of WSNs and longevity of their life span [72]. The network's energy consumption consists of different parts including the communication, computation, and sensing energy components [114, 67, 95]; however, empirical measurements have demonstrated that the dominating element is the communication energy [103]. Thus, once sensor nodes are placed in their predetermined positions for monitoring purposes, access points (APs) are deployed to facilitate the communication and connect sensor nodes to their corresponding base stations using various routing schemes [29].

Improving the energy-efficiency of WSNs is an active area of research and various methods have been proposed for this purpose. Some methods, like flat routing, hierarchical routing, and location-based routing, aim at finding the optimal path to reach a base station for sensory data [89, 10, 76, 75, 88]. Another strategy to improve the energy-efficiency and lifetime of WSNs is scheduling active and sleep modes for sensors [101, 85, 59]. One line of research that has attracted significant attention in the literature is energy-efficient node deployment due to its critical role in resource utilization and network lifetime. This is because electromagnetic wave propagation diminishes as a power law function of the distance between the transmitter and receiver; thus, the required transmission energy to guarantee a certain signal-to-noise ratio (SNR) at the receiver node highly depends on the distance and placement of network nodes.

Node deployment algorithms can be categorized in many different ways. Some techniques are developed offline and executed in a centralized manner [2] while others are distributed and are based on the assumption that each node has only local information about the state of other nodes [18, 3]. Based on nodes' mobility, WSNs can also be categorized as either static or mobile where a rich set of node deployment algorithms is developed for each category. Static node deployment methods aim to calculate optimal node positions a priori and assume that nodes will be placed at their predetermined locations [56, 55, 38, 57]; however, mobile

node deployment techniques assume that starting from an initial location, each node moves toward its optimal position [57, 98, 19, 39, 2, 120]. Node deployment algorithms can also be viewed based on whether they are stochastic or deterministic. Random deployment is preferable in hostile and inaccessible environments or when the network's size is very large [6] while deterministic methods are favorable for smaller networks, especially when manual placement is feasible since deterministic deployment algorithms often outperform their stochastic counterparts [6, 84].

The optimal node deployment in WSNs highly depends on the hardware setup. WSNs can be identified as either homogeneous WSNs [10, 21, 41, 40], where network nodes share the same hardware properties such as the antenna gain, storage, sensitivity, etc., or heterogeneous WSNs [79, 51, 56, 55, 38, 57] for which nodes, in general, have different characteristics. The optimal deployment in homogeneous WSNs is studied in [41, 40]; however, homogeneous WSNs do not represent inherent challenges that exist in their heterogeneous counterparts, namely, unlike Voronoi regions in homogeneous settings, the optimal regions in heterogeneous WSNs may not be convex, star-shaped, or connected. Node deployment in heterogeneous WSNs is studied in [56, 55, 38]; however, these studies along with the majority of the work in the literature consider a very simplistic radio energy model that does not reflect the real-world characteristics of the environment in which these networks are deployed. In addition, the randomness of the communication channel due to the fading process is usually ignored. Consequently, the resulting node deployment underestimates the actual energy consumption of the network which can significantly diminish the sustainability and durability of these networks.

With energy-efficiency being a major design concern in most WSNs, finding the optimal node deployment is an active area of research. In this work, we study heterogeneous Rayleigh fading sensor networks in details and aim to provide state-of-the-art algorithms to deploy nodes. The main motivation of this work is to take into account the small-scale fading and

the exponential dependence of the required transmission energy on the rate in heterogeneous WSNs. The main contributions of the paper are summarized below:

- We consider a communication energy model that incorporates both large-scale path-loss signal attenuation and small-scale signal variation due to Rayleigh fading, and takes the heterogeneous characteristics of network nodes into account;

- Having an outage probability constraint on all communication channels, we provide theoretical necessary conditions for an optimal deployment, cell partitioning, and data routing protocol, and design an iterative algorithm to deploy nodes such that not only is the communication power consumption minimized in the resulting WSN, but also all communication channels are guaranteed to have an outage probability below the given threshold;

- By marginalizing the stochasticity of the channel capacity due to the Rayleigh fading process and considering the ergodic capacity for all wireless links, we derive the necessary conditions of optimal deployment and design an energy-efficient algorithm to deploy nodes.

The rest of the paper is organized as follows. The system model and problem formulation are discussed in Section 5.2. In Section 5.3, the optimal deployment in heterogeneous Rayleigh fading WSNs under outage probability constraints on communication channels is studied and an iterative algorithm based on the obtained necessary conditions is provided. The optimal deployment in heterogeneous WSNs given ergodic capacity constraints on all wireless links and the corresponding deployment algorithm are studied in Section 5.4. Simulation results and concluding remarks are provided in Sections 5.5 and 5.6, respectively.

5.2 System Model

We consider a heterogeneous WSN that consists of homogeneous sensors, N heterogeneous APs, and M heterogeneous BSs. The target region $\Omega \subseteq \mathbb{R}^2$ is a convex polygon including its interior. In particular, each sensor transmits its data to an AP which acts as a relay node and forwards the collected information to BSs. We denote the set of node indices for APs and BSs by $\mathcal{I}_{AP} = \{1, \cdots, N\}$ and $\mathcal{I}_{BS} = \{1, \cdots, M\}$, respectively. While access points and base stations are characterized as a set of $(N + M)$ discrete points within the target region, the distribution of densely deployed sensors are described via a continuous and differentiable function $f : \Omega \longrightarrow \mathbb{R}^+$ such that $\int_W f(\omega)d\omega$ is the total number of sensors within the region $W \subseteq \Omega$. Thus, the total amount of data gathered by sensors within the region W in one time unit is equal to $R_b \int_W f(\omega)d\omega$ in which the bit-rate R_b is a constant due to the homogeneity of sensors [41]. Throughout this paper, we assume that each sensor only transmits its data to one AP. Consequently, the target region Ω is partitioned into N disjoint regions $\mathbf{W} = (W_1, \cdots, W_N) \subseteq \Omega^N$ such that for each $n \in \mathcal{I}_{AP}$, AP n collects data from sensors within the region $W_n \subseteq \Omega$. For any $n \in \mathcal{I}_{AP}$ and $m \in \mathcal{I}_{BS}$, let $p_n \in \Omega$ and $q_m \in \Omega$ denote the location of AP n and BS m, respectively. In addition, let $\mathbf{P} = (p_1, \cdots, p_N) \in \mathbb{R}^{N \times 2}$ and $\mathbf{Q} = (q_1, \cdots, q_M) \in \mathbb{R}^{M \times 2}$ denote the collective deployment of APs and BSs, respectively.

In addition to AP deployment $\mathbf{P}$, BS deployment $\mathbf{Q}$, and cell partitioning $\mathbf{W}$, the performance of a WSN heavily depends on the routing protocol by which data is transferred from sensors to base stations. Our network in this paper can be regarded as a directed bipartite graph where the vertex set can be partitioned into two disjoint subsets containing access points and base stations, respectively, and each edge from AP n to BS m is associated with a non-negative value $F_{n,m}$ (bits/s) denoting the flow of data from AP n to BS m. An example of one such graph is depicted in Fig. 5.1. Thus, the routing protocol can be characterized by a flow matrix $\mathbf{F} = [F_{n,m}]_{N \times M}$ where $F_{n,m}$ denotes the amount of data transmitted from AP n to BS m in one time unit. Since each AP, say n, transmits all the received data, the in-flow
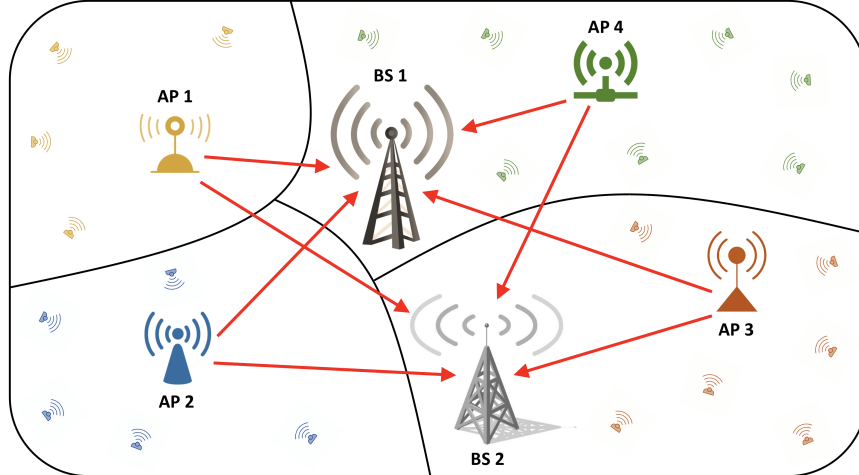
Figure 5.1: The system model and network architecture.

value should be equal to the out-flow value, i.e., $R_b \int_{W_n} f(\omega)d\omega = \sum_{m=1}^{M} F_{n,m}$. Note that instead of directly specifying the flow $F_{n,m}$ from AP n to BS m, we can specify the ratio of out-flow from AP n that goes to BS m, i.e., $r_{n,m} = \frac{F_{n,m}}{\sum_{j=1}^{M} F_{n,j}}$. By definition, it readily follows that $r_{n,m} \in [0,1]$ and $\sum_{m=1}^{M} r_{n,m} = 1$ since the in-flow to each AP is equal to its out-flow. In particular, the flow matrix $\mathbf{F}$ can be uniquely determined by the cell partitioning $\mathbf{W}$ and the normalized flow matrix $\mathbf{R} = [r_{n,m}]_{N \times M}$.

In this paper, we consider a slow fading channel in which the channel gain is stochastic but remains constant in each frame. We also assume that the receiver can track the fading process, i.e., coherent reception and the transmitter has no knowledge of the channel realization except for its statistical properties. For a channel realization h, the maximum communication rate with arbitrarily small error probability is given by $\log(1 + |h|^2 \gamma)$ bits/s/Hz, where γ represents the received signal-to-noise ratio (SNR) due to large-scale propagation effects. For a Rayleigh fading channel, the fading gain is a standard complex normal random variable, i.e., $h \sim \mathcal{CN}(0,1)$; therefore, $|h|^2$ has an exponential distribution with parameter 1. Due to stochasticity of the channel realization, the decoding error probability cannot become arbitrarily small regardless of the code used by the transmitter [53]. Hence, the primary objective in this paper is to find an optimal deployment that minimizes the wireless trans-

mission power consumption of the WSN subject to a given outage probability threshold. For a given data flow $F_{n,m}$, the outage probability is given by [53]:

$$p_{\text{out}_{n,m}}(F_{n,m}) = \mathbb{P}\left\{B \log\left(1 + |h|^2 \gamma_{n,m}\right) < F_{n,m}\right\}.$$ (5.1)

Similarly, the outage probability for the link between a sensor located at $\omega \in \Omega$ and AP n is:

$$p_{\text{out}_{\omega,n}}(R_b) = \mathbb{P}\left\{B \log\left(1 + |h|^2 \gamma_{\omega,n}\right) < R_b\right\}.$$ (5.2)

The received SNR is proportional to the transmit power, i.e., $\gamma \propto P_t \times d^{-\alpha}$ where d is the distance between the transmitter and receiver, and $2 \leq \alpha \leq 5$ is the large-scale path loss exponent [46]. We consider the Friis free space loss equation, i.e., $\alpha = 2$. More precisely, if AP n sends a signal with transmission power $P_{\text{transmit}}^{(n,m)}$, the received signal power at BS m, i.e., $P_{\text{receive}}^{(n,m)}$, is

$$P_{\text{receive}}^{(n,m)} = P_{\text{transmit}}^{(n,m)} \times \frac{G_{t_n} G_{r_m} \lambda_c^2}{(4\pi)^2 \|p_n - q_m\|^2 L_n},$$ (5.3)

where G_{t_n} is the transmitter antenna gain of AP n, G_{r_m} is the receiver antenna gain of BS m, λ_c is the wavelength of the carrier signal, and L_n denotes all other losses that are not related to the propagation loss such as loss at the antennas, filters, transmission line attenuation, etc. Therefore, for the spectral noise density of σ Watts/Hz, the received SNR $\gamma_{n,m}$ is given by:

$$\gamma_{n,m} = \frac{P_{\text{receive}}^{(n,m)}}{\sigma B} = P_{\text{transmit}}^{(n,m)} \times \frac{G_{t_n} G_{r_m} \lambda_c^2}{\sigma B (4\pi)^2 \|p_n - q_m\|^2 L_n}.$$ (5.4)

Similarly, for a sensor located at $\omega \in \Omega$, sending a signal with transmission signal power $P_{\text{transmit}}^{(\omega,n)}$, the received SNR $\gamma_{\omega,n}$ at AP n is given by:

$$\gamma_{\omega,n} = \frac{P_{\text{receive}}^{(\omega,n)}}{\sigma B} = P_{\text{transmit}}^{(\omega,n)} \times \frac{G_{t_{\text{sensor}}} G_{r_n} \lambda_c^2}{\sigma B \left(4\pi\right)^2 \|p_n - \omega\|^2 L_{\text{sensor}}}, \tag{5.5}$$

where $G_{t_{\text{sensor}}}$ and L_{sensor} are the common transmitter antenna gain and system loss of the homogeneous sensors, respectively. For a given outage probability threshold of ϵ, our goal is to find the optimal WSN deployment that minimizes the total wireless transmission power consumption of the network subject to all channels having an outage probability of less than or equal to ϵ. Hence, our primary objective function can be written as:

$$\mathcal{D}_1\left(\mathbf{P}, \mathbf{Q}, \mathbf{W}, \mathbf{R}\right) = \sum_{n=1}^{N} \int_{W_n} P_{\text{transmit}}^{(\omega,n)} f(\omega) d\omega + \lambda \sum_{n=1}^{N} \sum_{m=1}^{M} P_{\text{transmit}}^{(n,m)} \tag{5.6}$$

$$\text{s.t.} \quad p_{\text{out}_{n,m}}\left(F_{n,m}\right) \le \epsilon \quad \text{and} \quad p_{\text{out}_{\omega,n}}\left(R_b\right) \le \epsilon, \qquad \forall n \in \mathcal{I}_{AP}, \ m \in \mathcal{I}_{BS}, \tag{5.7}$$

where the Lagrangian multiplier $\lambda \ge 0$ provides a trade-off between the sensor transmission power $\sum_{n=1}^{N} \int_{W_n} P_{\text{transmit}}^{(\omega,n)} f(\omega) d\omega$ and AP transmission power $\sum_{n=1}^{N} \sum_{m=1}^{M} P_{\text{transmit}}^{(n,m)}$. Our primary goal is to minimize the constrained objective function in Eqs. (5.6) and (5.7) over node deployments $\mathbf{P}$ and $\mathbf{Q}$, cell partitioning $\mathbf{W}$, and normalized flow matrix $\mathbf{R}$.

An alternative way to address the stochasticity of the channel is to think of the channel as allowing $B \log\left(1 + |h|^2 \gamma\right)$ bits/s flow of data to pass when the fading gain is h and solve for the ergodic capacity of all wireless links in the network. More precisely, our secondary goal is to find the optimal transmission power values for each sensor and AP node such that the transmission power in each wireless link can, on average, allow the flow of data in that link to pass through.

For a Rayleigh flat-fading wireless link from AP n to BS m with an average received SNR $\gamma_{n,m}$, the ergodic capacity admits the following closed-form formula [96]:

$$C_{\text{erg}} = B \log_2(e) \times e^{\frac{1}{\gamma_{n,m}}} \times E_1\left(\frac{1}{\gamma_{n,m}}\right), \tag{5.8}$$

where $E_1(.)$ is the exponential integral of order 1 defined as:

$$E_1(z) = \int_1^\infty \frac{e^{-zx}}{x} dx, \tag{5.9}$$

for $\text{Re}\{z\} > 0$. Therefore, using Eq. (5.8), the transmission power that, on average, allows the flow $F_{n,m}$ bits/s to pass through this wireless link can be calculated as

$$F_{n,m} = B \log_2(e) \times e^{\frac{1}{\gamma_{n,m}}} \times E_1\left(\frac{1}{\gamma_{n,m}}\right), \tag{5.10}$$

$$\gamma_{n,m} = \frac{1}{U^{-1}\left(\frac{F_{n,m}}{B \log_2(e)}\right)}, \tag{5.11}$$

where $U(x) = e^x \times E_1(x)$. Hence, the AP transmission power is given by:

$$P_{\text{erg. trans.}}^{(n,m)} = \frac{\sigma B (4\pi)^2 \|p_n - q_m\|^2 L_n}{G_{t_n} G_{r_m} \lambda_c^2 \times U^{-1}\left(\frac{F_{n,m}}{B \log_2(e)}\right)}. \tag{5.12}$$

Similarly, the sensor transmission power that can, on average, allow the flow R_b bits/s to pass through the wireless link from sensor ω to AP n is given by:

$$P_{\text{erg. trans.}}^{(\omega,n)} = \frac{\sigma B (4\pi)^2 \|p_n - \omega\|^2 L_{\text{sensor}}}{G_{t_{\text{sensor}}} G_{r_n} \lambda_c^2 \times U^{-1}\left(\frac{R_b}{B \log_2(e)}\right)}. \tag{5.13}$$

Thus, the total wireless power consumption under the ergodic capacity assumption is

$$\mathcal{D}_2\left(\mathbf{P}, \mathbf{Q}, \mathbf{W}, \mathbf{R}\right) = \sum_{n=1}^{N} \int_{W_n} P_{\text{erg. trans.}}^{(\omega,n)} f(\omega) d\omega + \lambda \sum_{n=1}^{N} \sum_{m=1}^{M} P_{\text{erg. trans.}}^{(n,m)}, \tag{5.14}$$

where $\lambda \geq 0$ is the Lagrangian multiplier. Our secondary goal is to minimize the objective

function in Eq. (5.14) over node deployments $\mathbf{P}$, $\mathbf{Q}$, cell partitioning $\mathbf{W}$, and normalized flow matrix $\mathbf{R}$. In the next section, we focus on our primary objective function and study the optimal node deployment under outage probability constraint on wireless links. In Section 5.4, we consider our secondary objective function and study the optimal node deployment that minimizes the average network transmission power consumption under ergodic capacity assumption.

5.3 Optimal Deployment under Outage Probability Constraint

In this section, we focus on our primary objective function and aim to minimize the wireless power consumption $\mathcal{D}_1$ in Eq. (5.6) subject to outage probability constraints given in Eq. (5.7). Our goal is to find the optimal deployment $\mathbf{P}^* = (p_1^*, \cdots, p_N^*)$ and $\mathbf{Q}^* = (q_1^*, \cdots, q_M^*)$, cell partitioning $\mathbf{W}^* = (W_1^*, \cdots, W_N^*)$, and the normalized flow matrix $\mathbf{R}^* = \left[r_{n,m}^*\right]_{N \times M}$ that minimize the wireless transmission power consumption of the network. Note that the optimal value for each of the four variables $\mathbf{P}$, $\mathbf{Q}$, $\mathbf{W}$, and $\mathbf{R}$ depends on the value of the other three and this optimization problem is NP-hard. Our aim is to derive the necessary conditions of optimality and devise an algorithm that iteratively optimizes the value of each variable while the other variables are held fixed. We accomplish this goal in the following three steps:

Step 1 [optimizing P and Q while W and R are fixed]: First, we rewrite the objective function $\mathcal{D}_1$ according to the constraints given in Eq. (5.7). For a wireless link with flow $F_{n,m}$ from AP n to BS m, we have:

$$\mathbb{P}\left\{|h|^2 < \frac{2^{\frac{F_{n,m}}{B}} - 1}{\gamma_{n,m}}\right\} \leq \epsilon. \tag{5.15}$$

Since $|h|^2$ has an exponential distribution with parameter 1, Eq. (5.15) can be simplified to:

$$\gamma_{n,m} \geq \frac{2^{\frac{F_{n,m}}{B}} - 1}{\ln\left(\frac{1}{1-\epsilon}\right)}. \tag{5.16}$$

Using Eq. (5.4), we can rewrite Eq. (5.16) as follows:

$$
\begin{aligned}
P_{\text{transmit}}^{(n,m)} &\geq \frac{\sigma B \left(4\pi\right)^2 L_n \times \|p_n - q_m\|^2 \times \left(2^{\frac{F_{n,m}}{B}} - 1\right)}{G_{t_n} G_{r_m} \lambda_c^2 \times \ln\left(\frac{1}{1-\epsilon}\right)} \\
&= \frac{b_{n,m}}{\ln\left(\frac{1}{1-\epsilon}\right)} \|p_n - q_m\|^2 \times \left(2^{\frac{F_{n,m}}{B}} - 1\right),
\end{aligned} \tag{5.17}
$$

where $b_{n,m} = \frac{\sigma B \times (4\pi)^2 \times L_n}{G_{t_n} \times G_{r_m} \times \lambda_c^2}$. Hence, Eq. (5.17) yields a lower bound on the required transmission power at AP n that guarantees an outage probability no greater than ϵ at the corresponding base station. Note that the minimum transmission power occurs when $P_{\text{transmit}}^{(n,m)}$ is equal to its lower bound in Eq. (5.17) which corresponds to having an outage probability of $p_{\text{out}_{n,m}}\left(F_{n,m}\right) = \epsilon$. Similarly, for a sensor located at ω that transmits its data to AP n, we have:

$$
\begin{aligned}
P_{\text{transmit}}^{(\omega,n)} &\geq \frac{\sigma B \left(4\pi\right)^2 L_{\text{sensor}} \times \|p_n - \omega\|^2 \times \left(2^{\frac{R_b}{B}} - 1\right)}{G_{t_{\text{sensor}}} G_{r_n} \lambda_c^2 \times \ln\left(\frac{1}{1-\epsilon}\right)} \\
&= \frac{a_n}{\ln\left(\frac{1}{1-\epsilon}\right)} \|p_n - \omega\|^2 \left(2^{\frac{R_b}{B}} - 1\right),
\end{aligned} \tag{5.18}
$$

where $a_n = \frac{\sigma B \times (4\pi)^2 \times L_{\text{sensor}}}{G_{t_{\text{sensor}}} \times G_{r_n} \times \lambda_c^2}$. Using Eqs. (5.17) and (5.18), we can rewrite the objective function $\mathcal{D}_1$ in Eq. (5.6) as follows:

$$
\begin{aligned}
\mathcal{D}_1\left(\mathbf{P}, \mathbf{Q}, \mathbf{W}, \mathbf{R}\right) =& \sum_{n=1}^{N} \int_{W_n} \frac{a_n}{\ln\left(\frac{1}{1-\epsilon}\right)} \|p_n - \omega\|^2 \left(2^{\frac{R_b}{B}} - 1\right) f(\omega) d\omega \\
&+ \lambda \sum_{n=1}^{N} \sum_{m=1}^{M} \frac{b_{n,m}}{\ln\left(\frac{1}{1-\epsilon}\right)} \|p_n - q_m\|^2 \left(2^{\frac{F_{n,m}}{B}} - 1\right).
\end{aligned} \tag{5.19}
$$

Now, for a fixed $\mathbf{W}$ and $\mathbf{R}$, the optimal deployment is given by the following proposition.

Proposition 14. *The necessary conditions for the optimal AP and BS deployment* $\mathbf{P}^*$ *and* $\mathbf{Q}^*$ *in a heterogeneous WSN with wireless transmission power consumption defined in Eq. (5.6) and outage probability constraint ϵ on all wireless links are given by:*

$$p_n^* = \frac{a_n\left(2^{\frac{R_b}{B}} - 1\right)v_n c_n + \lambda \sum_{m=1}^{M} b_{n,m}\left(2^{\frac{F_{n,m}}{B}} - 1\right)q_m^*}{a_n\left(2^{\frac{R_b}{B}} - 1\right)v_n + \lambda \sum_{m=1}^{M} b_{n,m}\left(2^{\frac{F_{n,m}}{B}} - 1\right)}, \qquad \forall n \in \mathcal{I}_{AP}, \qquad (5.20)$$

$$q_m^* = \frac{\sum_{n=1}^{N} b_{n,m}\left(2^{\frac{F_{n,m}}{B}} - 1\right)p_n^*}{\sum_{n=1}^{N} b_{n,m}\left(2^{\frac{F_{n,m}}{B}} - 1\right)}, \qquad \forall m \in \mathcal{I}_{BS}, \qquad (5.21)$$

where $v_n = \int_{W_n} f(\omega)d\omega$ and $c_n = \frac{\int_{W_n} \omega f(\omega)d\omega}{\int_{W_n} f(\omega)d\omega}$ are the volume and centroid of the region W_n, respectively. The proof of Proposition 14 is provided in Appendix E.1.

Step 2 [optimizing W while P, Q, and R are fixed]: First, we study the properties of region boundaries in an optimal cell partitioning $\mathbf{W}^*$. Note that while $\mathbf{F}$ can be uniquely determined by $\mathbf{W}$ and $\mathbf{R}$, it only depends on the volumes of regions and not their actual geometric shape. More precisely, if we let $V = (v_1, \cdots, v_N)$ where v_n is the volume of region W_n, then $\mathbf{F}$ can be uniquely calculated by V and $\mathbf{R}$ as well. Therefore, Eq. (5.19) indicates that APs' transmission power only depends on the volume of regions and not their geometrical shape. In other words, we can manipulate region boundaries in order to reduce the sensors' power consumption in Eq. (5.19) and by extension the total power consumption $\mathcal{D}_1$ since by keeping the region volumes fixed, APs' power consumption remains unchanged. Using this intuition, we have:

Lemma 9. *Let $\mathbf{W}^* = (W_1^*, \cdots, W_N^*)$ be an optimal cell partitioning that minimizes the constrained objective function $\mathcal{D}_1$ in Eqs. (5.6) and (5.7) for a given node deployment and data routing. Let $\delta_{i,j}^* = W_i^* \cap W_j^*$ be the boundary between neighboring regions W_i^* and W_j^*. Then, $\delta_{i,j}^*$ is either a segment perpendicular to the line $\overline{p_i p_j}$ if $a_i = a_j$ or an arc with its center placed at $c = \frac{a_i p_i - a_j p_j}{a_i - a_j}$ if $a_i \neq a_j$.*

The proof of Lemma 9 is provided in Appendix E.2.

Let $h_{i,j}^*$ be the intersection point between the optimal boundary $\delta_{i,j}^*$ and the segment $\overline{p_i p_j}$ in Lemma 9. The following proposition provides the necessary condition on the location of $h_{i,j}^*$.

Proposition 15. *Let* $\mathbf{W}^* = (W_1^*, \cdots, W_N^*)$ *be an optimal cell partitioning that minimizes the constrained objective function* $\mathcal{D}_1$ *in Eqs. (5.6) and (5.7) for a given node deployment* $\mathbf{P}$, $\mathbf{Q}$, *and data routing* $\mathbf{R}$. *Let* $\delta_{i,j}^* = W_i^* \cap W_j^*$ *be the boundary between neighboring regions* W_i^* *and* W_j^* *which intersects the line* $\overline{p_i p_j}$ *at point* $h_{i,j}^*$. *Then we have:*

$$
a_i \left\| p_i - h_{i,j}^* \right\|^2 \left(2^{\frac{R_b}{B}} - 1 \right) + \lambda \sum_{t=1}^{M} \frac{\ln(2)}{B} \times R_b \times r_{i,t} \times b_{i,t} \left\| p_i - q_t \right\|^2 \times 2^{\frac{r_{i,t} R_b v_i^*}{B}}
$$

$$
= a_j \left\| p_j - h_{i,j}^* \right\|^2 \left(2^{\frac{R_b}{B}} - 1 \right) + \lambda \sum_{t=1}^{M} \frac{\ln(2)}{B} \times R_b \times r_{j,t} \times b_{j,t} \left\| p_j - q_t \right\|^2 \times 2^{\frac{r_{j,t} R_b v_j^*}{B}}. \quad (5.22)
$$

The proof of Proposition 15 is provided in Appendix E.3.

Step 3 [optimizing R while P, Q, and W are fixed]: Note that for a given deployment $\mathbf{P}$, $\mathbf{Q}$, and cell partitioning $\mathbf{W}$, the sensor power consumption is fixed and $\mathbf{R}$ only affects the AP power consumption in Eq. (5.19). Since the cell partitioning $\mathbf{W}$ is fixed and each AP directly transmits its data to base stations, the optimization problem can be split into N objective functions, one for each AP, and they can be optimized separately. More specifically, for AP n, we need to optimize the following objective function:

$$
\arg\min_{F_{n,1} \cdots F_{n,M}} \sum_{m=1}^{M} \frac{b_{n,m}}{\ln\left(\frac{1}{1-\epsilon}\right)} \left\| p_n - q_m \right\|^2 \times \left(2^{\frac{F_{n,m}}{B}} - 1 \right), \quad (5.23)
$$

$$
\text{s.t. } \sum_{m=1}^{M} F_{n,m} = \int_{W_n} R_b f(\omega) d\omega = R_b v_n, \quad (5.24)
$$

$$
F_{n,m} \geq 0 \text{ for all } m \in \mathcal{I}_{BS}. \quad (5.25)
$$

Note that when the sum of exponents is fixed, the minimum of the sum of exponentials

Algorithm 6: Optimal routing in heterogeneous WSNs with outage probability constraint

Input: Node deployment $\mathbf{P}, \mathbf{Q}$;
Cell partitioning $\mathbf{W}$;
Set $n = 1$;

Set $C_0 = \frac{1}{M}\left[\frac{R_b v_n}{B} + \sum_{m=1}^{M}\left[\log_2\left(b_{n,m}\right) + 2\log_2\left(\|\mathbf{p_n} - \mathbf{q_m}\|\right)\right]\right]$;
Set $I_L^{(0)} = \varnothing$ and $I_U^{(0)} = \{1, \cdots, M\}$;
Set iteration counter $k = 0$;

Increase k by 1;

Let $I_L^{(k)} = \{m \mid \log_2\left(b_{n,m}\right) + 2\log_2\left(\|\mathbf{p_n} - \mathbf{q_m}\|\right) > C_{k-1}, \ 1 \leq m \leq M\}$;
Let $I_U^{(k)} = \{1, \cdots, M\} \setminus I_L^{(k)}$;

Calculate $C_k = \dfrac{M \times C_0 - \sum_{m \in I_L^{(k)}}\left[\log_2\left(b_{n,m}\right) + 2\log_2\left(\|\mathbf{p_n} - \mathbf{q_m}\|\right)\right]}{\left|I_U^{(k)}\right|}$;

is $I_L^{(k)} = I_L^{(k-1)}$?   No

Yes

Set $F_{n,m} = 0$ for all $m \in I_L^{(k)}$;
Set $F_{n,m} = B \times \left(C_k - \left[\log_2\left(b_{n,m}\right) + 2\log_2\left(\|\mathbf{p_n} - \mathbf{q_m}\|\right)\right]\right)$ for all $m \in I_U^{(k)}$;

Increase n by 1;

No   is $n > N$?

Yes

Obtain the normalized flow matrix $\mathbf{R}$ from the flow matrix $\mathbf{F}$.
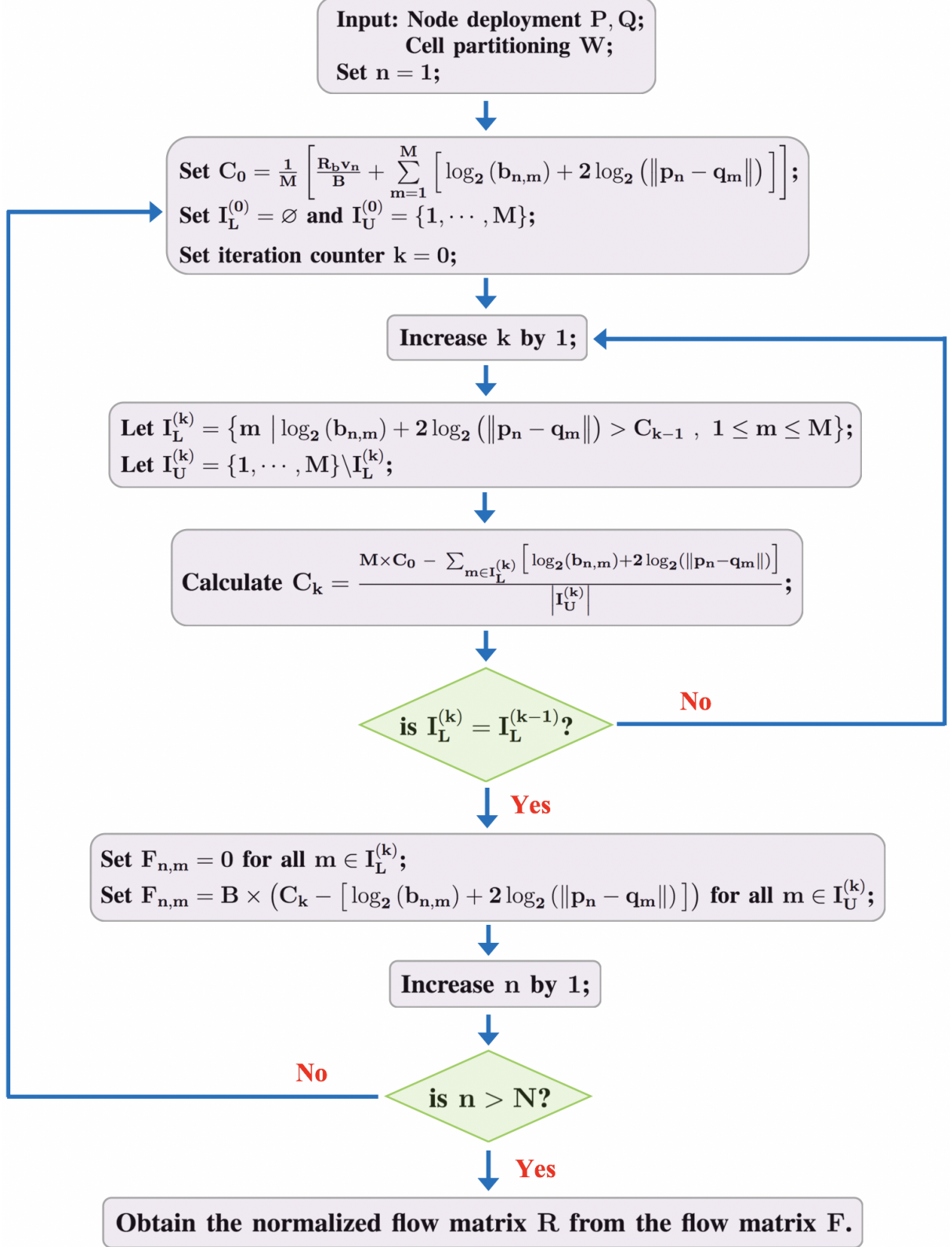
with the same base occurs when all exponents are equal. For instance, if for three variables x, y, and z we have $x + y + z = c$, then the minimum of $2^x + 2^y + 2^z$ occurs when $x = y = z = \frac{c}{3}$. Using this intuition and the fact that all elements of the flow matrix are non-negative, we propose the following algorithm that yields the optimal solution to the constrained optimization problem in Eqs. (5.23)-(5.25) for each AP n. Note that once the optimal flow matrix $\mathbf{F}^*$ is obtained, the corresponding normalized flow matrix $\mathbf{R}^*$ can be calculated from the definition.

Proposition 16. *For a given node deployment* $\mathbf{P}$*,* $\mathbf{Q}$*, and cell partitioning* $\mathbf{W}$*, Algorithm 6 yields the optimal normalized flow matrix* $\mathbf{R}^* = \arg\min_{\mathbf{R}} \mathcal{D}_1 (\mathbf{P}, \mathbf{Q}, \mathbf{W}, \mathbf{R})$ *for the heterogeneous WSN under the outage probability constraints in Eq. (5.7).*

The proof of Proposition 16 is provided in Appendix E.4.

Now, inspired by the Lloyd Algorithm [69], we propose Algorithm 7, named Power-Optimized Outage-aware Lloyd (POOL) Algorithm, to optimize node deployment, cell partitioning, and data routing in our heterogeneous WSN and minimize the wireless communication power consumption in Eq. (5.6) under outage probability constraints given in Eq. (5.7).

Proposition 17. *The POOL algorithm is an iterative improvement algorithm, i.e., the objective function* $\mathcal{D}_1$ *is non-increasing and the algorithm converges.*

The proof of Proposition 17 is provided in Appendix E.5.

5.4 Optimal Deployment under Ergodic Capacity Assumption

In this section, we consider our secondary objective function and aim to minimize the wireless communication power consumption $\mathcal{D}_2$ in Eq. (5.14) over node deployment, cell partitioning,

Algorithm 7: Power-Optimized Outage-aware Lloyd Algorithm

Initialize the node deployment P and Q;
Initialize the cell partitioning W;
Initialize the normalized flow matrix R;

For each $n \in \{1, \cdots, N\}$, set:
$p_n = \frac{\int_{W_n} \omega f(\omega) d\omega}{\int_{W_n} f(\omega) d\omega}$;

For each $n \in \{1, \cdots, N\}$, set:
$W_n = \{\omega \mid a_n \|p_n - \omega\|^2 \leq a_k \|p_k - \omega\|^2 \text{ for all } 1 \leq k \leq N\}$;

Converged?   **No**

Yes

Use the Lloyd algorithm with respect to AP locations to deploy M base stations;

Update R according to Algorithm 6;

Update P and Q according to Proposition 14;

Randomly select neighboring regions W_i and W_j;

Use line search to find $h_{i,j}$ that satisfies Proposition 15;

Adjust the boundary $\delta_{i,j} = W_i \cap W_j$ according to $h_{i,j}$;

Converged?   **No**

Yes

Update R according to Algorithm 6;

No   Converged?

Yes

Return P, Q, W, and R.

and data routing. We fulfill this aim by deriving the necessary conditions for an optimal deployment, cell partitioning, and data routing that minimize the network's power consumption under ergodic capacity assumption. Then, based on these necessary conditions, we design an iterative algorithm to find such an optimal deployment. This goal is realized in the following three steps.

Step 1 [optimizing P and Q while W and R are fixed]: We begin by rewriting the objective function in Eq. (5.14) as

$$
\mathcal{D}_2\left(\mathbf{P}, \mathbf{Q}, \mathbf{W}, \mathbf{R}\right) = \sum_{n=1}^{N} \int_{W_n} \frac{a_n}{U^{-1}\left(\frac{R_b}{B\log_2(e)}\right)} \|p_n - \omega\|^2 f(\omega) d\omega
$$
$$
+ \lambda \sum_{n=1}^{N} \sum_{m=1}^{M} \frac{b_{n,m}}{U^{-1}\left(\frac{F_{n,m}}{B\log_2(e)}\right)} \|p_n - q_m\|^2, \tag{5.26}
$$

where $a_n = \frac{\sigma B \times (4\pi)^2 \times L_{\text{sensor}}}{G_{t_{\text{sensor}}} \times G_{r_n} \times \lambda_c^2}$ and $b_{n,m} = \frac{\sigma B \times (4\pi)^2 \times L_n}{G_{t_n} \times G_{r_m} \times \lambda_c^2}$. Now, for a fixed cell partitioning and data routing, the necessary condition for an optimal deployment is given by the following proposition.

Proposition 18. *For a fixed* $\mathbf{W}$ *and* $\mathbf{R}$*, the necessary conditions for the optimal AP and BS deployment* $\mathbf{P}^*$ *and* $\mathbf{Q}^*$ *in a heterogeneous WSN with wireless transmission power consumption defined in Eq. (5.14) and ergodic capacity assumption on all wireless links are given by:*

$$
p_n^* = \frac{\frac{a_n v_n}{U^{-1}\left(\frac{R_b}{B\log_2(e)}\right)} \times c_n + \lambda \sum_{m=1}^{M} \frac{b_{n,m}}{U^{-1}\left(\frac{F_{n,m}}{B\log_2(e)}\right)} \times q_m^*}{\frac{a_n v_n}{U^{-1}\left(\frac{R_b}{B\log_2(e)}\right)} + \lambda \sum_{m=1}^{M} \frac{b_{n,m}}{U^{-1}\left(\frac{F_{n,m}}{B\log_2(e)}\right)}}, \qquad \forall n \in \mathcal{I}_{AP}, \tag{5.27}
$$

$$
q_m^* = \frac{\sum_{n=1}^{N} \frac{b_{n,m}}{U^{-1}\left(\frac{F_{n,m}}{B\log_2(e)}\right)} \times p_n^*}{\sum_{n=1}^{N} \frac{b_{n,m}}{U^{-1}\left(\frac{F_{n,m}}{B\log_2(e)}\right)}}, \qquad \forall m \in \mathcal{I}_{BS}, \tag{5.28}
$$

where v_n *and* c_n *are the volumes and centroid of* W_n*, respectively. The proof of Proposition 18 is provided in Appendix E.6.*

Step 2 [optimizing W while P, Q, and R are fixed]: The cell partitioning $\mathbf{W}$ affects the sensor power consumption in Eq. (5.26) through integrating over cells W_n for $n \in \{1, \cdots, N\}$; thus, both volume and shape of each cell influence the sensor power consumption. In contrast, the cell partitioning affects the AP power consumption through the flow matrix $\mathbf{F}$ which only depends on the volume of regions and not their shape. Hence, by keeping the volumes constant, one can adjust the region boundaries to reduce the sensor power consumption while the AP power consumption is held fixed. This leads to the following property of optimal region boundaries.

Lemma 10. *For a given node deployment and data routing, let $\mathbf{W}^* = (W_1^*, \cdots, W_N^*)$ be an optimal cell partitioning that minimizes the objective function $\mathcal{D}_2$ in Eq. (5.14). If $\delta_{i,j}^* = W_i^* \cap W_j^*$ is the boundary between neighboring regions W_i^* and W_j^*, then $\delta_{i,j}^*$ is either a segment if $a_i = a_j$ or an arc with its center placed at $c = \frac{a_i p_i - a_j p_j}{a_i - a_j}$ if $a_i \neq a_j$.*

The proof of Lemma 10 is provided in Appendix E.7.

Using Lemma 10, the necessary condition for an optimal deployment is derived as follows.

Proposition 19. *Let $\mathbf{W}^* = (W_1^*, \cdots, W_N^*)$ be the optimal cell partitioning that minimizes the objective function $\mathcal{D}_2$ in Eq. (5.14) for a given node deployment $\mathbf{P}$, $\mathbf{Q}$, and data routing $\mathbf{R}$. Let $\delta_{i,j}^* = W_i^* \cap W_j^*$ be the boundary between neighboring regions W_i^* and W_j^* and let $h_{i,j}^*$ be the intersection point of the line $\overline{p_i p_j}$ with $\delta_{i,j}^*$. Then, we have:*

$$
\frac{a_i}{U^{-1}\left(\frac{R_b}{B \log_2(e)}\right)} \|p_i - h_{i,j}^*\|^2 + \lambda \sum_{t=1}^{M} \frac{b_{i,t}\|p_i - q_t\|^2 \times \frac{r_{i,t} R_b}{B \log_2(e)}}{U^{-1}\left(\frac{r_{i,t} R_b v_i^*}{B \log_2(e)}\right)\left[1 - \frac{r_{i,t} R_b v_i^*}{B \log_2(e)} \times U^{-1}\left(\frac{r_{i,t} R_b v_i^*}{B \log_2(e)}\right)\right]}
$$
$$
= \frac{a_j}{U^{-1}\left(\frac{R_b}{B \log_2(e)}\right)} \|p_j - h_{i,j}^*\|^2 + \lambda \sum_{t=1}^{M} \frac{b_{j,t}\|p_j - q_t\|^2 \times \frac{r_{j,t} R_b}{B \log_2(e)}}{U^{-1}\left(\frac{r_{j,t} R_b v_j^*}{B \log_2(e)}\right)\left[1 - \frac{r_{j,t} R_b v_j^*}{B \log_2(e)} \times U^{-1}\left(\frac{r_{j,t} R_b v_j^*}{B \log_2(e)}\right)\right]}.
$$

$$(5.29)$$

The proof is provided in Appendix E.8.

Step 3 [optimizing R while P, Q, and W are fixed]: Note that the data routing **R** only affects the AP power consumption in Eq. (5.26) and it does not change the sensor power consumption. Since the cell partitioning, and thus the total volume of data that each AP transmits is fixed, optimizing **R** translates into each AP adjusting its data transmission independent of other AP nodes. For each AP, say n, we have the following objective function:

$$\arg\min_{F_{n,1}\cdots F_{n,M}} \sum_{m=1}^{M} \frac{b_{n,m}}{U^{-1}\left(\frac{F_{n,m}}{B\log_2(e)}\right)} \|p_n - q_m\|^2, \tag{5.30}$$

$$\text{s.t.} \sum_{m=1}^{M} F_{n,m} = \int_{W_n} R_b f(\omega)d\omega = R_b v_n, \tag{5.31}$$

$$F_{n,m} \geq 0 \text{ for all } m \in \mathcal{I}_{BS}. \tag{5.32}$$

To make the above optimization problem tractable, we resort to a common optimization strategy that seeks to minimize the upper bound on the objective function instead of directly optimizing the objective function itself. For this purpose, first, we aim to provide an upper bound on the AP n's power consumption in Eq. (5.30).

Lemma 11. *Let $U(x) = e^x \times E_1(x)$ where $E_1(x)$ is the exponential integral of order 1 defined in Eq. (5.9). Then, we have:*

$$e^x - 1 < \frac{1}{U^{-1}(x)} < \frac{e^{2x} - 1}{2}. \tag{5.33}$$

The proof is provided in Appendix E.9.

Using Lemma 11, we have the following upper bound on the objective function in Eq. (5.30).

$$\arg\min_{F_{n,1}\cdots F_{n,M}} \sum_{m=1}^{M} b_{n,m}\|p_n - q_m\|^2 \times \frac{e^{\frac{2F_{n,m}}{B\log_2(e)}} - 1}{2}, \tag{5.34}$$

$$\text{s.t.} \sum_{m=1}^{M} F_{n,m} = \int_{W_n} R_b f(\omega)d\omega = R_b v_n, \tag{5.35}$$

$$F_{n,m} \geq 0 \text{ for all } m \in \mathcal{I}_{BS}. \tag{5.36}$$

The following algorithm provides a systematic approach to yield the optimal solution to the constrained optimization problem in Eqs. (5.34)-(5.36).

Proposition 20. *For a given node deployment* $\mathbf{P}$, $\mathbf{Q}$, *and cell partitioning* $\mathbf{W}$, *Algorithm 8 yields the optimal normalized flow matrix that minimizes the upper bound in Eq. (5.34) on the AP n's power consumption under ergodic capacity assumption.*

The proof is provided in Appendix E.10.

Using properties we obtained in this section, a Power-Efficient Ergodic-based Lloyd (PEEL) Algorithm, as outlined in Algorithm 9, is proposed to minimize the wireless communication power consumption in Eq. (5.14) over node deployment, cell partitioning, and data routing.

Proposition 21. *The PEEL algorithm is an iterative improvement algorithm and converges.*

The proof is provided in Appendix E.11.

5.5   Experiments

Simulations are performed for a heterogeneous Rayleigh fading sensor network consisting of 15 APs, 3 BSs, and 1000 sensors. The sensors are uniformly distributed over the target region Ω which is a square area of size 10km $\times$ 10km. The bit-rate and the carrier wavelength are set to $R_b = 30$Kbps and $\lambda_c = 3$m, respectively. We consider no system loss, i.e., $L_{\text{sensor}} = L_n = 1$ for all $n \in \mathcal{I}_{AP}$, and a transmitter antenna gain of $G_{t_{\text{sensor}}} = 1$ for all homogeneous sensors. We denote the transmitter and receiver antenna gains of AP n by $G_{t_n}^{(\text{AP})}$ and $G_{r_n}^{(\text{AP})}$, respectively, and the receiver antenna gain of BS m by $G_{r_m}^{(\text{BS})}$. Let us denote

Algorithm 8: Optimal data routing in two-tier WSNs under ergodic capacity assumption

Input: Node deployment $\mathbf{P}, \mathbf{Q}$;
Cell partitioning $\mathbf{W}$;
Set $\mathbf{n} = 1$;

$\downarrow$

Set $S_0 = \frac{1}{M}\left[\frac{2R_b v_n}{B\log_2(e)} + \sum_{m=1}^{M}\left[\ln(b_{n,m}) + 2\ln\big(\|p_n - q_m\|\big)\right]\right]$;
Set $J_L^{(0)} = \varnothing$ and $J_U^{(0)} = \{1, \cdots, M\}$;
Set iteration counter $k = 0$;

$\downarrow$

Increase k by 1;

$\downarrow$

Let $J_L^{(k)} = \big\{m \mid S_{k-1} < \ln(b_{n,m}) + 2\ln\big(\|p_n - q_m\|\big), \ 1 \le m \le M\big\}$;
Let $J_U^{(k)} = \{1, \cdots, M\} \backslash J_L^{(k)}$;

$\downarrow$

Calculate $S_k = \dfrac{M \times S_0 - \sum_{m \in J_L^{(k)}}\left[\ln(b_{n,m}) + 2\ln\big(\|p_n - q_m\|\big)\right]}{\big|J_U^{(k)}\big|}$;

$\downarrow$

is $J_L^{(k)} = J_L^{(k-1)}$? — **No**

Yes $\downarrow$

Set $F_{n,m} = 0$ for all $m \in J_L^{(k)}$;
Set $F_{n,m} = \frac{B\log_2(e)}{2} \times \big(S_k - \big[\ln(b_{n,m}) + 2\ln\big(\|p_n - q_m\|\big)\big]\big)$ for all $m \in J_U^{(k)}$;

$\downarrow$

Increase n by 1;

$\downarrow$

No — **is $n > N$?**

Yes $\downarrow$

Obtain the normalized flow matrix $\mathbf{R}$ from the flow matrix $\mathbf{F}$.
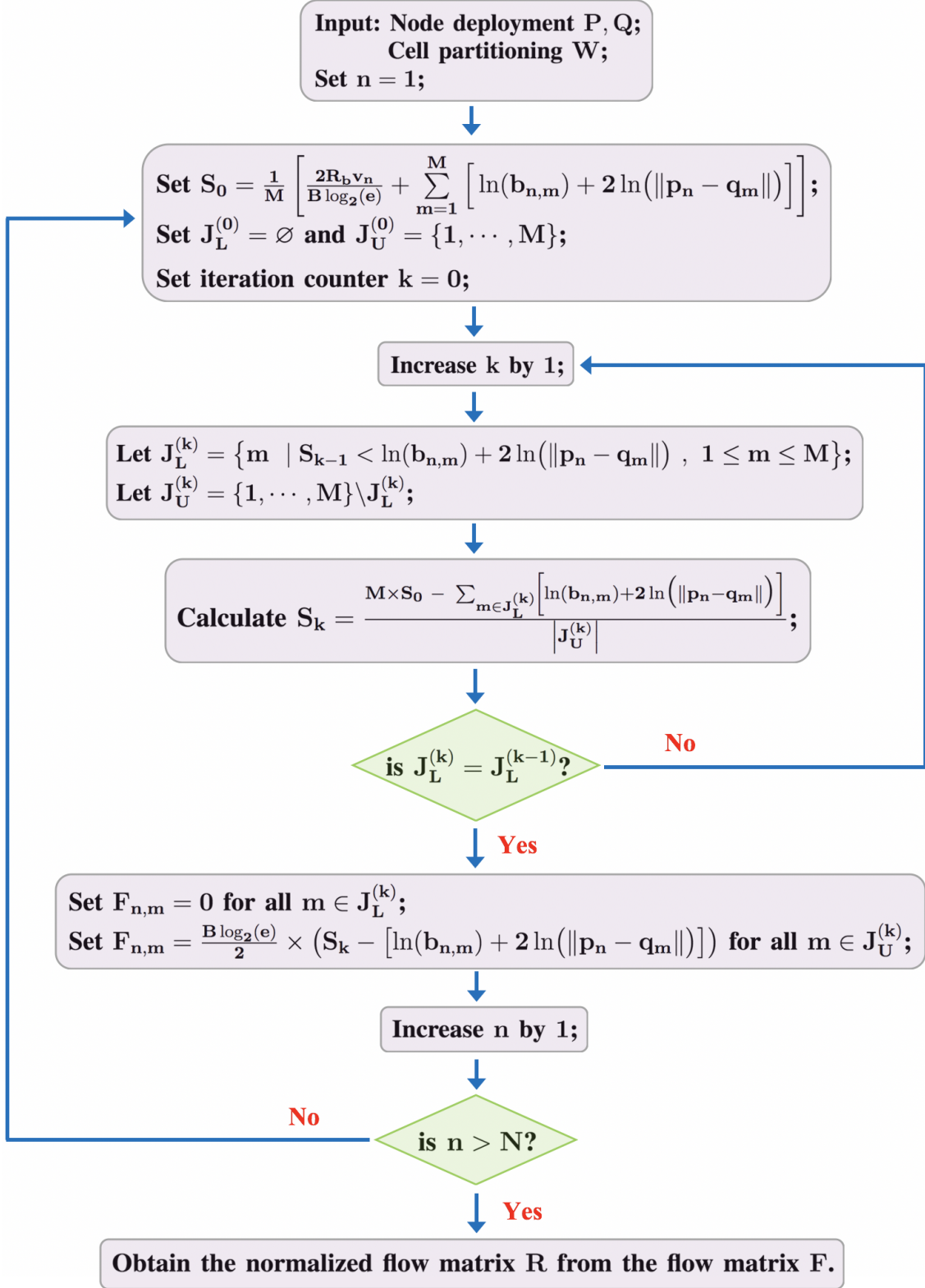
Algorithm 9: Power-Efficient Ergodic-based Lloyd Algorithm

Initialize the node deployment P and Q;
Initialize the cell partitioning W;
Initialize the normalized flow matrix R;

For each $n \in \{1, \cdots, N\}$, set:
$p_n = \frac{\int_{W_n} \omega f(\omega) d\omega}{\int_{W_n} f(\omega) d\omega}$;

For each $n \in \{1, \cdots, N\}$, set:
$W_n = \{\omega \mid a_n \|p_n - \omega\|^2 \le a_k \|p_k - \omega\|^2 \text{ for all } 1 \le k \le N\}$;

Converged?

No

Yes

Use the Lloyd algorithm with respect to AP locations to deploy M base stations;

Update R according to Algorithm 8;

Update P and Q according to Proposition 18;

Randomly select neighboring regions W_i and W_j;

Use line search to find $h_{i,j}$ that satisfies Proposition 19;

Adjust the boundary $\delta_{i,j} = W_i \cap W_j$ according to $h_{i,j}$;

Converged?

No

Yes

Calculate R' according to Algorithm 8;

is $\mathcal{D}_2(P, Q, W, R') < \mathcal{D}_2(P, Q, W, R)$?

No

Yes

Set $R = R'$;

Converged?

No

Yes

Return P, Q, W, and R.

$\mathcal{S}_1 = \{1, 2, 3, 4, 8, 9, 10\}$, $\mathcal{S}_2 = \{1, 2, 5, 6, 8, 9, 12, 13\}$, and $\mathcal{S}_3 = \{1, 2\}$. Then, we set:

$$G_{t_n}^{(\text{AP})} = \begin{cases} 2 & \text{if } n \in \mathcal{S}_1 \\ 4 & \text{otherwise} \end{cases} , \quad G_{r_n}^{(\text{AP})} = \begin{cases} 2 & \text{if } n \in \mathcal{S}_2 \\ 4 & \text{otherwise} \end{cases} , \quad G_{r_m}^{(\text{BS})} = \begin{cases} 2 & \text{if } m \in \mathcal{S}_3 \\ 4 & \text{otherwise.} \end{cases} \quad (5.37)$$

We assume that all communication channels have a spectral width of $B = 500\text{KHz}$ and a spectral noise density of $\sigma = 2 \times 10^{-17}$ Watts/Hz. Note that the parameters a_n and $b_{n,m}$ can be calculated from the experimental setup that is outlined above. For instance, we have $b_{6,2} = \frac{\sigma B \times (4\pi)^2 \times L_6}{G_{t_6}^{(\text{AP})} \times G_{r_2}^{(\text{BS})} \times \lambda_c^2} \simeq 2.19 \times 10^{-11}$ Watts/m^2. The Lagrangian multiplier is set to $\lambda = 0.25$. In Section 5.5.1, we carry out the simulations for our primary objective function $\mathcal{D}_1$ in Eqs. (5.6) and (5.7) where we have imposed an outage probability constraint of $\epsilon = 1\%$ on all wireless links. Subsequently, in Section 5.5.2, we perform the simulations for our secondary objective function $\mathcal{D}_2$ in Eq. (5.14) and compare our proposed algorithms with state-of-the-art methods in the literature.

5.5.1   Heterogeneous WSNs with Outage Probability Constraints

In this section, we compare our proposed POOL Algorithm with cluster formation (CF) Algorithm [17], heterogeneous two-tier Lloyd (HTTL) Algorithm [56], particle swarm optimization (PSO) Algorithm [23], and virtual force (VFA) Algorithm [120]. The main motivation behind choosing these methods for comparison purposes is that they represent state-of-the-art methods in different strategy categories used by researchers for node deployment problems. The CF algorithm falls within the category of methods that take a graph-theoretic approach for load balancing and energy efficiency. The HTTL algorithm belongs to the family of geometric-based methods in which the target region is partitioned into several regions, one for each network node, based on a predefined measure of closeness. The PSO algorithm represents the class of meta-heuristic node deployment techniques in which optimization

tools are used to find optimal node positions. Finally, the VFA algorithm is a prominent example of force-based techniques and has inspired numerous methods that achieve optimal deployment by applying virtual forces to relocate nodes. Table 5.1 summarizes the weighted transmission power consumption of the heterogeneous WSN outlined above for the CF, HTTL, POOL, PSO, and VFA algorithms. The POOL algorithm leads to a 590mW weighted power consumption value and outperforms all other methods. Notably, the POOL algorithm achieves a power consumption value that is less than half of the second best algorithm, i.e., the HTTL algorithm. This in turn prolongs the network lifetime by more than a factor of 2.

Table 5.1: Weighted power (W) comparison between different methods ($\mathcal{D}_1$)

Method	CF	HTTL	**POOL**	PSO	VFA
Weighted Power Consumption	3.11	1.27	**0.59**	4.61	1.95

Fig. 5.3 shows the final node deployment results where APs and BSs are denoted by red squares and black circles, respectively. Next, we study the trade-off between sensors' and APs' power consumption that is parameterized by λ in Eq. (5.6). For small values of λ, sensor power consumption is the dominant component of $\mathcal{D}_1$; thus, it is more paramount to reduce the sensors' power consumption rather than APs' power consumption to minimize $\mathcal{D}_1$. However, increasing λ puts more weight on the APs' power consumption. This effect is demonstrated in Fig. 5.2a where for the same initial node deployment, we increase the value of λ from 0 to 1. As expected, increasing λ reduces the APs' power consumption but increases the sensors' power consumption. Eq. (5.20) provides an alternative intuitive explanation for this observation because as λ increases, APs tend to be closer to BSs and farther away from centroids and sensors.
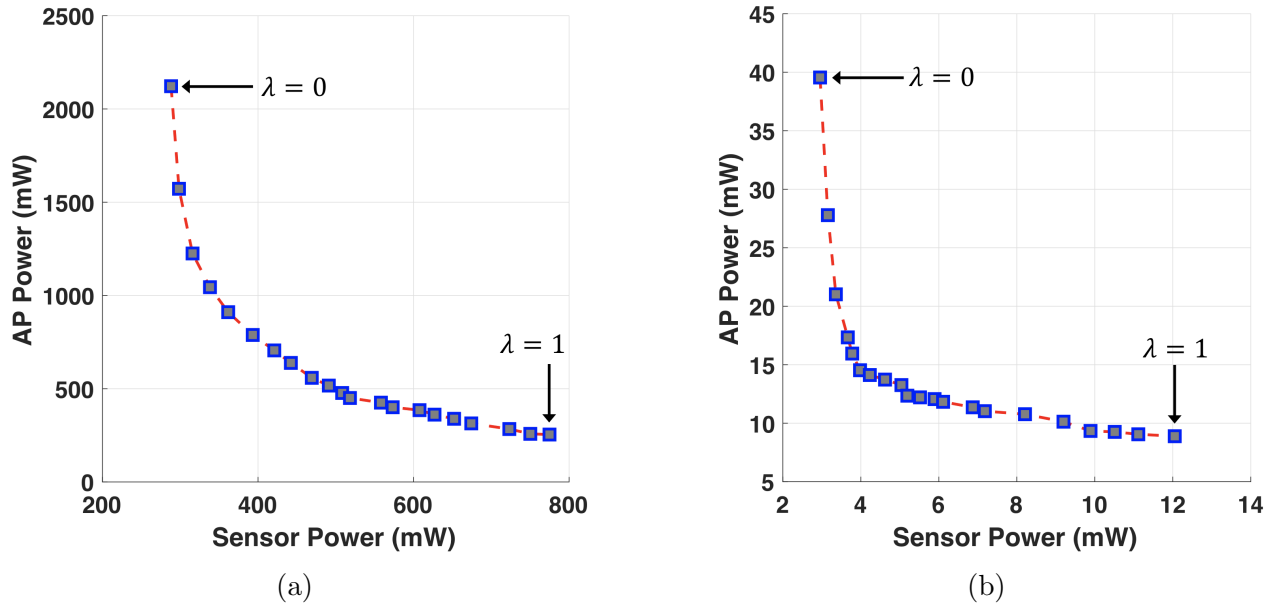
Figure 5.2: AP-Sensor power trade-off for (a) POOL Algorithm (b) PEEL Algorithm.
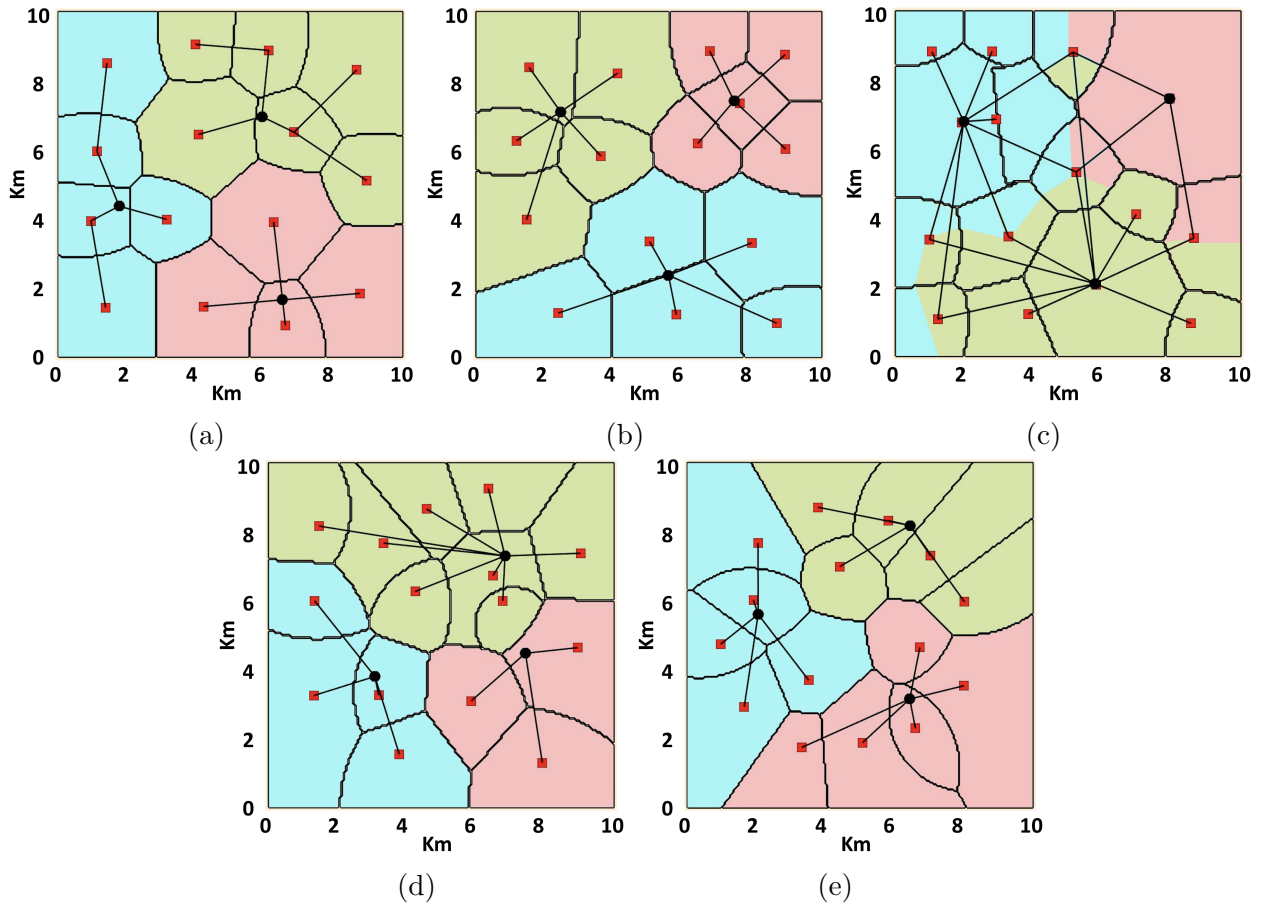
Figure 5.3: Node deployment for different algorithms. (a) CF (b) HTTL (c) POOL (d) PSO (e) VFA.

5.5.2 Heterogeneous WSNs under Ergodic Capacity Assumption

Here, we compare our proposed PEEL algorithm with the CF, HTTL, PSO, and VFA algorithms introduced in Section 5.5.1. However, instead of restricting all wireless links to have an outage probability below $\epsilon = 1\%$, we consider the ergodic capacity for all communication channels. The result for each method can then be interpreted as the amount of power that can, on average, allow the flow of data in each link to pass through.

The weighted power consumption of these methods for the heterogeneous WSN under consideration is provided in Table 5.2. The PEEL algorithm outperforms other methods and achieves a total weighted power consumption of 8.61mW. In particular, the PEEL algorithm improves the performance of the second best algorithm by more than a factor of 2 and yields a more sustainable WSN architecture. The AP-sensor power trade-off for the PEEL algorithm is depicted in Fig. 5.2b where for a fixed initial node deployment, λ is increased from 0 to 1. Similar to what we observed for the POOL algorithm in Fig. 5.2a, increasing λ puts more weight on the APs' power consumption and makes it more important to optimize. This can also be inferred from Eq. (5.27) where APs become closer to BSs and farther from centroids as λ increases.

Table 5.2: Weighted power (mW) comparison ($\mathcal{D}_2$)

Method	CF	HTTL	**PEEL**	PSO	VFA
Weighted Power Consumption	177.56	17.94	**8.61**	96.37	22.62

Some key factors contributing to the superior performance of both POOL and PEEL algorithms are worth noting: While according to the Shannon's capacity formula, the required SNR for an error-free information transmission grows exponentially with the required bit-rate, most methods in the literature consider a linear approximation to this exponential behavior. Such a linear approximation results in an underestimation of the actual power

consumption. In contrast, our approach in this work takes the exponential relationship between SNR and bit-rate into account. Another contributing factor is that this exponential relationship between the required transmission power and the flow of data is exploited in finding the optimal routing for data transfer in Algorithms 6 and 8 using Lemma 16.

5.6 Conclusion

A heterogeneous Rayleigh fading sensor network is presented and discussed in which a set of access points act as relay nodes to facilitate the transfer of sensory data from sensors to base stations by the means of wireless communication. By considering both large-scale and small-scale propagation effects on the communication channels, our goal is to minimize the wireless transmission power consumption of the network for two different perspectives on the stochasticity of the channel: First, we impose a threshold on the outage probability of all wireless links and aim to minimize the network's power consumption under such outage probability constraints. Second, we consider the ergodic capacity for all channels and aim to determine the optimal required transmission power for each sensor or access point such that the allocated transmission power to each channel can, on average, allow the flow of data in that channel to pass through. For each perspective, we derive the theoretical necessary conditions for the optimal deployment, cell partitioning, and data routing that minimizes the network's power consumption and devise an iterative algorithm accordingly to deploy nodes. Simulation results show that our proposed node deployment algorithms significantly reduce the communication power consumption in such networks and achieve superior performance compared to other techniques in the literature.

Bibliography

[1] A. Z. Abbasi, N. Islam, Z. A. Shaikh, et al. A review of wireless sensors and networks' applications in agriculture. *Computer Standards & Interfaces*, 36(2):263–270, 2014.

[2] M. Abo-Zahhad, N. Sabor, S. Sasaki, and S. M. Ahmed. A centralized immune-voronoi deployment algorithm for coverage maximization and energy conservation in mobile wireless sensor networks. *Information Fusion*, 30:36–51, 2016.

[3] M. S. Aliyu, A. H. Abdullah, H. Chizari, T. Sabbah, and A. Altameem. Coverage enhancement algorithms for distributed mobile sensors deployment in wireless sensor networks. *International Journal of Distributed Sensor Networks*, 12(3):9169236, 2016.

[4] G. Anastasi, M. Conti, M. Di Francesco, and A. Passarella. Energy conservation in wireless sensor networks: A survey. *Ad hoc networks*, 7(3):537–568, 2009.

[5] J. Aponte-Luis, J. A. Gómez-Galán, F. Gómez-Bravo, M. Sánchez-Raya, J. Alcina-Espigado, and P. M. Teixido-Rovira. An efficient wireless sensor network for industrial monitoring and control. *Sensors*, 18(1):182, 2018.

[6] F. Aznoli and N. J. Navimipour. Deployment strategies in the wireless sensor networks: systematic literature review, classification, and current trends. *Wireless Personal Communications*, 95(2):819–846, 2017.

[7] X. Bai, S. Kumar, D. Xuan, Z. Yun, and T. H. Lai. Deploying wireless sensors to achieve both coverage and connectivity. In *Proceedings of the 7th ACM international symposium on Mobile ad hoc networking and computing*, pages 131–142, 2006.

[8] J. Bang-Jensen and G. Z. Gutin. *Digraphs: theory, algorithms and applications*. Springer Science & Business Media, 2008.

[9] R. Bellman. On a routing problem. *Quarterly of applied mathematics*, 16(1):87–90, 1958.

[10] M. Benaddy, B. El Habil, M. El Ouali, O. El Meslouhi, and S. Krit. A mutlipath routing algorithm for wireless sensor networks under distance and energy consumption constraints for reliable data transmission. In *2017 International Conference on Engineering & MIS (ICEMIS)*, pages 1–4. IEEE, 2017.

[11] B. Boots, K. Sugihara, S. N. Chiu, and A. Okabe. *Spatial tessellations: concepts and applications of Voronoi diagrams.* John Wiley & Sons, 2009.

[12] N. Boufares, Y. B. Saied, and L. A. Saidane. Improved distributed virtual forces algorithm for 3d terrains coverage in mobile wireless sensor networks. In *2018 IEEE/ACS 15th International Conference on Computer Systems and Applications (AICCSA),* pages 1–8. IEEE, 2018.

[13] A. Breitenmoser, M. Schwager, J.-C. Metzger, R. Siegwart, and D. Rus. Voronoi coverage of non-convex environments with a group of networked robots. In *2010 IEEE international conference on robotics and automation,* pages 4982–4989. IEEE, 2010.

[14] B. Cao, J. Zhao, Z. Lv, X. Liu, X. Kang, and S. Yang. Deployment optimization for 3d industrial wireless sensor networks based on particle swarm optimizers with distributed parallelism. *Journal of Network and Computer Applications,* 103:225–238, 2018.

[15] J.-H. Chang and L. Tassiulas. Energy conserving routing in wireless ad-hoc networks. In *Proceedings IEEE INFOCOM 2000. Conference on Computer Communications. Nineteenth Annual Joint Conference of the IEEE Computer and Communications Societies (Cat. No. 00CH37064),* volume 1, pages 22–31. IEEE, 2000.

[16] Y.-J. Chang, C.-H. Chen, L.-F. Lin, R.-P. Han, W.-T. Huang, and G.-C. Lee. Wireless sensor networks for vital signs monitoring: Application in a nursing home. *International Journal of Distributed Sensor Networks,* 8(11):685107, 2012.

[17] P. Chatterjee and N. Das. Multiple sink deployment in multi-hop wireless sensor networks to enhance lifetime. In *2015 Applications and Innovations in Mobile Computing (AIMoC),* pages 48–54. IEEE, 2015.

[18] P. Chatterjee, S. C. Ghosh, and N. Das. Load balanced coverage with graded node deployment in wireless sensor networks. *IEEE Transactions on Multi-Scale Computing Systems,* 3(2):100–112, 2017.

[19] S. Chellappan, W. Gu, X. Bai, D. Xuan, B. Ma, and K. Zhang. Deploying wireless sensor networks under limited mobility constraints. *IEEE Transactions on Mobile Computing,* 6(10):1142–1157, 2007.

[20] A. Chunawale and S. Sirsikar. Minimization of average energy consumption to prolong lifetime of wireless sensor network. In *2014 IEEE Global Conference on Wireless Computing & Networking (GCWCN),* pages 244–248. IEEE, 2014.

[21] J. Cortes, S. Martinez, and F. Bullo. Spatially-distributed coverage optimization and control with limited-range interactions. *ESAIM: Control, Optimisation and Calculus of Variations,* 11(4):691–719, 2005.

[22] J. Cortes, S. Martinez, T. Karatas, and F. Bullo. Coverage control for mobile sensing networks. *IEEE Transactions on robotics and Automation,* 20(2):243–255, 2004.

[23] D. R. Dandekar and P. Deshmukh. Energy balancing multiple sink optimal deployment in multi-hop wireless sensor networks. In *2013 3rd IEEE International Advance Computing Conference (IACC)*, pages 408–412. IEEE, 2013.

[24] D. S. Deif and Y. Gadallah. Classification of wireless sensor networks deployment techniques. *IEEE Communications Surveys & Tutorials*, 16(2):834–855, 2013.

[25] D. S. Deif and Y. Gadallah. An ant colony optimization approach for the deployment of reliable wireless sensor networks. *IEEE Access*, 5:10744–10756, 2017.

[26] X. Deng, Z. Yu, R. Tang, X. Qian, K. Yuan, and S. Liu. An optimized node deployment solution based on a virtual spring force algorithm for wireless sensor network applications. *Sensors*, 19(8):1817, 2019.

[27] D. Djenouri and M. Bagaa. Energy-aware constrained relay node deployment for sustainable wireless sensor networks. *IEEE Transactions on Sustainable Computing*, 2(1):30–42, 2017.

[28] Y. El Khamlichi, A. Tahiri, A. Abtoy, I. Medina-Bulo, and F. Palomo-Lozano. A hybrid algorithm for optimal wireless sensor network deployment with the minimum number of sensor nodes. *Algorithms*, 10(3):80, 2017.

[29] Z. A. Eu and H.-P. Tan. Adaptive opportunistic routing protocol for energy harvesting wireless sensor networks. In *2012 IEEE international conference on communications (ICC)*, pages 318–322. IEEE, 2012.

[30] W. Fang, X. Song, X. Wu, J. Sun, and M. Hu. Novel efficient deployment schemes for sensor coverage in mobile wireless sensor networks. *Information Fusion*, 41:25–36, 2018.

[31] H. Farman, H. Javed, J. Ahmad, B. Jan, and M. Zeeshan. Grid-based hybrid network deployment approach for energy efficient wireless sensor networks. *Journal of Sensors*, 2016, 2016.

[32] M. Farsi, M. A. Elhosseini, M. Badawy, H. A. Ali, and H. Z. Eldin. Deployment techniques in wireless sensor networks, coverage and connectivity: A survey. *Ieee Access*, 7:28940–28954, 2019.

[33] E. Felemban. Advanced border intrusion detection and surveillance using wireless sensor network technology. *International Journal of Communications, Network and System Sciences*, 6(5):251–259, 2013.

[34] L. R. Ford Jr. Network flow theory. Technical report, Rand Corp Santa Monica Ca, 1956.

[35] W. Gautschi. Some elementary inequalities relating to the gamma and incomplete gamma function. *J. Math. Phys*, 38(1):77–81, 1959.

[36] M. S. Ghahroudi, A. Shahrabi, and T. Boutaleb. Voronoi-based cooperative node deployment algorithm in mobile sensor networks. In *2020 IEEE 91st Vehicular Technology Conference (VTC2020-Spring)*, pages 1–5. IEEE, 2020.

[37] A. Goldsmith. *Wireless communications*. Cambridge university press, 2005.

[38] J. Guo and H. Jafarkhani. Sensor deployment with limited communication range in homogeneous and heterogeneous wireless sensor networks. *IEEE Transactions on Wireless Communications*, 15(10):6771–6784, 2016.

[39] J. Guo and H. Jafarkhani. Movement-efficient sensor deployment in wireless sensor networks with limited communication range. *IEEE Transactions on Wireless Communications*, 18(7):3469–3484, 2019.

[40] J. Guo, S. Karimi-Bidhendi, and H. Jafarkhani. Energy-efficient node deployment in wireless ad-hoc sensor networks. In *ICC 2020-2020 IEEE International Conference on Communications (ICC)*, pages 1–6. IEEE, 2020.

[41] J. Guo, E. Koyuncu, and H. Jafarkhani. A source coding perspective on node deployment in two-tier networks. *IEEE Transactions on Communications*, 66(7):3035–3049, 2018.

[42] J. Guo, P. Walk, and H. Jafarkhani. Quantizers with parameterized distortion measures. In *2019 Data Compression Conference (DCC)*, pages 339–348. IEEE, 2019.

[43] J. Guo, P. Walk, and H. Jafarkhani. Optimal deployments of uavs with directional antennas for a power-efficient coverage. *IEEE Transactions on Communications*, 68(8):5159–5174, 2020.

[44] S. K. Gupta, P. Kuila, and P. K. Jana. Genetic algorithm for k-connected relay node placement in wireless sensor networks. In *Proceedings of the second international conference on computer and communication technologies*, pages 721–729. Springer, 2016.

[45] A. Gusrialdi and L. Zeng. Distributed deployment algorithms for robotic visual sensor networks in non-convex environment. In *2011 International Conference on Networking, Sensing and Control*, pages 445–450. IEEE, 2011.

[46] M. Haenggi. Energy-balancing strategies for wireless sensor networks. In *Proceedings of the 2003 International Symposium on Circuits and Systems, 2003. ISCAS'03.*, volume 4, pages IV–IV. IEEE, 2003.

[47] J. Han, J. Pei, and M. Kamber. *Data mining: concepts and techniques*. Elsevier, 2011.

[48] J. Hao, G. Duan, B. Zhang, and C. Li. An energy-efficient on-demand multicast routing protocol for wireless ad hoc and sensor networks. In *2013 IEEE Global Communications Conference (GLOBECOM)*, pages 4650–4655. IEEE, 2013.

[49] W. B. Heinzelman. *Application-specific protocol architectures for wireless networks*. PhD thesis, Massachusetts Institute of Technology, 2000.

[50] T. S. Helal, P. Mozumdar, and L. Akter. Evaluating the performance of optimal control based sensor deployment algorithms for realistic terrain model. In *8th International Conference on Electrical and Computer Engineering*, pages 741–744. IEEE, 2014.

[51] Y. T. Hou, Y. Shi, H. D. Sherali, and S. F. Midkiff. On energy provisioning and relay node placement for wireless sensor networks. *IEEE Transactions on Wireless Communications*, 4(5):2579–2590, 2005.

[52] C. Hu, X. Wang, Z. Yang, J. Zhang, Y. Xu, and X. Gao. A geometry study on the capacity of wireless networks via percolation. *IEEE Transactions on Communications*, 58(10):2916–2925, 2010.

[53] H. Jafarkhani. *Space-Time Coding: Theory and Practice.* Cambridge University Press, 2005.

[54] T. K. Jain, D. S. Saini, and S. V. Bhooshan. Lifetime optimization of a multiple sink wireless sensor network through energy balancing. *journal of Sensors*, 2015, Jan 2015.

[55] S. Karimi-Bidhendi, J. Guo, and H. Jafarkhani. Using quantization to deploy heterogeneous nodes in two-tier wireless sensor networks. In *2019 IEEE International Symposium on Information Theory (ISIT)*, pages 1502–1506. IEEE, 2019.

[56] S. Karimi-Bidhendi, J. Guo, and H. Jafarkhani. Energy-efficient node deployment in heterogeneous two-tier wireless sensor networks with limited communication range. *IEEE Transactions on Wireless Communications*, 20(1):40–55, 2020.

[57] S. Karimi-Bidhendi, J. Guo, and H. Jafarkhani. Energy-efficient deployment in static and mobile heterogeneous multi-hop wireless sensor networks. *IEEE Transactions on Wireless Communications*, 2021.

[58] V. Kawadia and P. Kumar. Power control and clustering in ad hoc networks. In *IEEE INFOCOM 2003. Twenty-second Annual Joint Conference of the IEEE Computer and Communications Societies (IEEE Cat. No. 03CH37428)*, volume 1, pages 459–469. IEEE, 2003.

[59] M. N. Khan, H. U. Rahman, M. A. Almaiah, M. Z. Khan, A. Khan, M. Raza, M. Al-Zahrani, O. Almomani, and R. Khan. Improving energy efficiency with content-based adaptive and dynamic scheduling in wireless sensor networks. *IEEE Access*, 8:176495–176520, 2020.

[60] E. Koyuncu and H. Jafarkhani. On the minimum average distortion of quantizers with index-dependent distortion measures. *IEEE Transactions on Signal Processing*, 65(17):4655–4669, 2017.

[61] E. Koyuncu and H. Jafarkhani. Asynchronous local construction of bounded-degree network topologies using only neighborhood information. *IEEE Transactions on Communications*, 67(3):2101–2113, 2018.

[62] E. Koyuncu, M. Shabanighazikelayeh, and H. Seferoglu. Deployment and trajectory optimization of uavs: A quantization theory approach. *IEEE Transactions on Wireless Communications*, 17(12):8531–8546, 2018.

[63] F. Li, J. Luo, S. Xin, and Y. He. Autonomous deployment of wireless sensor networks for optimal coverage with directional sensing model. *Computer Networks*, 108:120–132, 2016.

[64] X. Li, Y. Mao, and Y. Liang. A survey on topology control in wireless sensor networks. In *2008 10th International Conference on Control, Automation, Robotics and Vision*, pages 251–255. IEEE, 2008.

[65] W.-H. Liao, S.-C. Kuai, and M.-S. Lin. An energy-efficient sensor deployment scheme for wireless sensor networks using ant colony optimization algorithm. *Wireless Personal Communications*, 82(4):2135–2153, 2015.

[66] C. Liu, Z. Zhao, W. Qu, T. Qiu, and A. K. Sangaiah. A distributed node deployment algorithm for underwater wireless sensor networks based on virtual forces. *Journal of Systems Architecture*, 97:9–19, 2019.

[67] W. Liu, X. Zhou, S. Durrani, H. Mehrpouyan, and S. D. Blostein. Energy harvesting wireless sensor networks: Delay analysis considering energy costs of sensing and transmission. *IEEE Transactions on Wireless Communications*, 15(7):4635–4650, 2016.

[68] X. Liu. Coverage with connectivity in wireless sensor networks. In *2006 3rd International Conference on Broadband Communications, Networks and Systems*, pages 1–8. IEEE, 2006.

[69] S. Lloyd. Least squares quantization in pcm. *IEEE transactions on information theory*, 28(2):129–137, 1982.

[70] H. Mahboubi and A. G. Aghdam. Distributed deployment algorithms for coverage improvement in a network of wireless mobile sensors: Relocation by virtual force. *IEEE Transactions on Control of Network Systems*, 4(4):736–748, 2016.

[71] M. Maksimović and V. Milošević. Evaluating the optimal sensor placement for smoke detection. *Yugoslav journal of operations research*, 26(1):33–50, 2016.

[72] M. A. Matin and M. Islam. Overview of wireless sensor network. *Wireless sensor networks-technology and protocols*, 1(3), 2012.

[73] S. Meguerdichian, F. Koushanfar, M. Potkonjak, and M. B. Srivastava. Coverage problems in wireless ad-hoc sensor networks. In *Proceedings IEEE INFOCOM 2001. Conference on computer communications. Twentieth annual joint conference of the IEEE computer and communications society (Cat. No. 01CH37213)*, volume 3, pages 1380–1387. IEEE, 2001.

[74] S. Meguerdichian, F. Koushanfar, G. Qu, and M. Potkonjak. Exposure in wireless ad-hoc sensor networks. In *Proceedings of the 7th annual international conference on Mobile computing and networking*, pages 139–150, 2001.

[75] H. Mostafaei. Energy-efficient algorithm for reliable routing of wireless sensor networks. *IEEE Transactions on Industrial Electronics*, 66(7):5567–5575, 2018.

[76] C. Nakas, D. Kandris, and G. Visvardis. Energy efficient routing in wireless sensor networks: A comprehensive survey. *Algorithms*, 13(3):72, 2020.

[77] K. Nantomah. On some bounds for the exponential integral function. *Journal of Nepal Mathematical Society*, 4(2):28–34, 2021.

[78] S. Narayanaswamy, V. Kawadia, R. S. Sreenivas, and P. Kumar. Power control in ad-hoc networks: Theory, architecture, algorithm and implementation of the compow protocol. In *European wireless conference*, volume 2002, pages 156–162. Florence, Italy, 2002.

[79] M. Noori and M. Ardakani. Design of heterogeneous sensor networks with lifetime and coverage considerations. *IEEE Wireless Communications Letters*, 1(3):193–196, 2012.

[80] C. Öztürk, D. Karaboğa, and B. GÖRKEMLİ. Artificial bee colony algorithm for dynamic deployment of wireless sensor networks. *Turkish Journal of Electrical Engineering & Computer Sciences*, 20(2):255–262, 2012.

[81] B. Paul. *Kinematics and dynamics of planar machinery*. Prentice Hall, 1979.

[82] B. Paul and P. Barkan. Kinematics and dynamics of planar machinery. 1980.

[83] R. Poli, J. Kennedy, and T. Blackwell. Particle swarm optimization. *Swarm intelligence*, 1(1):33–57, 2007.

[84] R. Priyadarshi, B. Gupta, and A. Anurag. Deployment techniques in wireless sensor networks: a survey, classification, challenges, and future research issues. *The Journal of Supercomputing*, 76(9):7333–7373, 2020.

[85] S. Radhika and P. Rangarajan. Fuzzy based sleep scheduling algorithm with machine learning techniques to enhance energy efficiency in wireless sensor networks. *Wireless Personal Communications*, 118(4):3025–3044, 2021.

[86] A. Rakavi, M. Manikandan, and K. Hariharan. Grid based mobile sensor node deployment for improving area coverage in wireless sensor networks. In *2015 3rd international conference on signal processing, communication and networking (ICSCN)*, pages 1–5. IEEE, 2015.

[87] M. A. Razzaque and S. Dobson. Energy-efficient sensing in wireless sensor networks using compressed sensing. *Sensors*, 14(2):2822–2859, 2014.

[88] M. Sajwan, D. Gosain, and A. K. Sharma. Hybrid energy-efficient multi-path routing for wireless sensor networks. *Computers & Electrical Engineering*, 67:96–113, 2018.

[89] S. Saranya and M. Princy. Routing techniques in sensor network–a survey. *Procedia engineering*, 38:2739–2747, 2012.

[90] M. R. Senouci, A. Mellouk, and A. Aissani. An analysis of intrinsic properties of stochastic node placement in sensor networks. In *2012 IEEE Global Communications Conference (GLOBECOM)*, pages 494–499. IEEE, 2012.

[91] M. R. Senouci, A. Mellouk, and A. Aissani. Random deployment of wireless sensor networks: a survey and approach. *International Journal of Ad Hoc and Ubiquitous Computing*, 15(1-3):133–146, 2014.

[92] M. R. Senouci, A. Mellouk, and K. Assnoune. Localized movement-assisted sensordeployment algorithm for holedetection and healing. *IEEE Transactions on parallel and distributed systems*, 25(5):1267–1277, 2013.

[93] M. Shabanighazikelayeh and E. Koyuncu. Outage-optimized deployment of uavs. In *2019 IEEE 30th Annual International Symposium on Personal, Indoor and Mobile Radio Communications (PIMRC)*, pages 1–6. IEEE, 2019.

[94] S. S. Shams, M. A. H. Chowdhury, K.-H. Kim, and N. B. Lee. A fast approximation algorithm for relay node placement in double-tiered wireless sensor network. In *MILCOM 2008-2008 IEEE Military Communications Conference*, pages 1–6. IEEE, 2008.

[95] Z. Sheng, C. Mahapatra, V. C. Leung, M. Chen, and P. K. Sahu. Energy efficient cooperative computing in mobile wireless sensor networks. *IEEE Transactions on Cloud Computing*, 6(1):114–126, 2015.

[96] H. Shin and J. H. Lee. Closed-form formulas for ergodic capacity of mimo rayleigh fading channels. In *IEEE International Conference on Communications, 2003. ICC'03.*, volume 5, pages 2996–3000. IEEE, 2003.

[97] R. Singh and M. S. Manu. An energy efficient grid based static node deployment strategy for wireless sensor networks. *International Journal of Electronics and Information Engineering*, 7(1):32–40, 2017.

[98] Y. Song, B. Wang, Z. Shi, K. R. Pattipati, and S. Gupta. Distributed algorithms for energy-efficient even self-deployment in mobile sensor networks. *IEEE Transactions on Mobile Computing*, 13(5):1035–1047, 2013.

[99] Y. Su, L. Guo, Z. Jin, and X. Fu. A voronoi-based optimized depth adjustment deployment scheme for underwater acoustic sensor networks. *IEEE Sensors Journal*, 20(22):13849–13860, 2020.

[100] Z. Vincze, R. Vida, and A. Vidacs. Deploying multiple sinks in multi-hop wireless sensor networks. In *IEEE international conference on pervasive services*, pages 55–63. IEEE, 2007.

[101] R. Wan, N. Xiong, et al. An energy-efficient sleep scheduling mechanism with similarity measure for wireless sensor networks. *Human-centric Computing and Information Sciences*, 8(1):1–22, 2018.

[102] G. Wang, M. J. Irwin, P. Berman, H. Fu, and T. La Porta. Optimizing sensor movement planning for energy efficiency. In *Proceedings of the 2005 international symposium on Low power electronics and design*, pages 215–220, Aug 2005.

[103] M. M. Warrier and A. Kumar. Energy efficient routing in wireless sensor networks: A survey. In *2016 International Conference on Wireless Communications, Signal Processing and Networking (WiSPNET)*, pages 1987–1992. IEEE, 2016.

[104] C.-H. Wu, K.-C. Lee, and Y.-C. Chung. A delaunay triangulation based method for wireless sensor network deployment. *Computer Communications*, 30(14-15):2744–2752, 2007.

[105] J. Wu and S. Yang. Optimal movement-assisted sensor deployment and its extensions in wireless sensor networks. *Simulation Modelling Practice and Theory*, 15(4):383–399, Apr 2007.

[106] G. Xing, X. Wang, Y. Zhang, C. Lu, R. Pless, and C. Gill. Integrated coverage and connectivity configuration for energy conservation in sensor networks. *ACM Transactions on Sensor Networks (TOSN)*, 1(1):36–72, 2005.

[107] Z. Xinlian and Q. Wenhao. Sensor network energy saving sleep scheduling algorithm research. In *2014 International Conference on Information and Communications Technologies (ICT 2014)*, pages 1–5. IET, 2014.

[108] L. Yang, J. Liang, and W. Liu. Radar sensor (rs) deployment for multi-target detection. In *2014 Sixth International Conference on Wireless Communications and Signal Processing (WCSP)*, pages 1–5. IEEE, 2014.

[109] J. Yick, B. Mukherjee, and D. Ghosal. Wireless sensor network survey. *Computer networks*, 52(12):2292–2330, 2008.

[110] Y. Yoo and D. Agrawal. Mobile sensor relocation to prolong the lifetime of wireless sensor networks. In *VTC spring 2008-IEEE vehicular technology conference*, pages 193–197. IEEE, 2008.

[111] Y. Yoon and Y.-H. Kim. An efficient genetic algorithm for maximum coverage deployment in wireless sensor networks. *IEEE Transactions on Cybernetics*, 43(5):1473–1483, 2013.

[112] O. Younis and S. Fahmy. Distributed clustering in ad-hoc sensor networks: A hybrid, energy-efficient approach. In *IEEE INFOCOM 2004*, volume 1. IEEE, 2004.

[113] H. Yousefi'zadeh, H. Jafarkhani, and J. Kazemitabar. A study of connectivity in mimo fading ad-hoc networks. *Journal of Communications and Networks*, 11(1):47–56, 2009.

[114] H. Yousefi'zadeh, H. Jafarkhani, and M. Moshfeghi. Power optimization of wireless media systems with space-time block codes. *IEEE Transactions on Image Processing*, 13(7):873–884, 2004.

[115] B. Zafar, Z. H. Mir, S. S. Shams, M. Ikram, W. A. Baig, K.-H. Kim, and S.-W. Yoo. On improved relay nodes placement in two-tiered wireless sensor networks. In *MILCOM 2009-2009 IEEE Military Communications Conference*, pages 1–7. IEEE, 2009.

[116] H. ZainEldin, M. Badawy, M. Elhosseini, H. Arafat, and A. Abraham. An improved dynamic deployment technique based-on genetic algorithm (iddt-ga) for maximizing coverage in wireless sensor networks. *Journal of Ambient Intelligence and Humanized Computing*, 11(10):4177–4194, 2020.

[117] X.-Q. Zhao, M. Liu, Y.-P. Cui, and Y.-D. Yao. A deployment optimization algorithm for wsns based on adaptive virtual force disturbance sparrow search. In *2021 4th International Conference on Artificial Intelligence and Pattern Recognition*, pages 472–478, 2021.

[118] J. Zheng and A. Jamalipour. *Wireless sensor networks: a networking perspective*. John Wiley & Sons, 2009.

[119] F. Zhou, J. Gao, X. Fan, and K. An. Covering algorithm for different obstacles and moving obstacle in wireless sensor networks. *IEEE Internet of Things Journal*, 5(5):3305–3315, 2018.

[120] Y. Zou and K. Chakrabarty. Sensor deployment and target localization in distributed sensor networks. *ACM Transactions on Embedded Computing Systems (TECS)*, 3(1):61–91, 2004.

Appendix A

Supplementary Proofs for Chapter 1

A.1   Proof of Proposition 1

For $U = (S_1, S_2, ..., S_N)$, The left hand side of (1.7) can be written as:

$$
\begin{aligned}
D(P, Q, U, T) &= \sum_{n=1}^{N} \int_{S_n} (a_n ||p_n - w||^2 + \beta b_{n,T(n)} ||p_n - q_{T(n)}||^2) f(w) dw \\
&\geq \sum_{n=1}^{N} \int_{S_n} \min_j (a_j ||p_j - w||^2 + \beta b_{j,T(j)} ||p_j - q_{T(j)}||^2) f(w) dw \\
&= \int_{\Omega} \min_j (a_j ||p_j - w||^2 + \beta b_{j,T(j)} ||p_j - q_{T(j)}||^2) f(w) dw \\
&= \sum_{n=1}^{N} \int_{V_n} \min_j (a_j ||p_j - w||^2 + \beta b_{j,T(j)} ||p_j - q_{T(j)}||^2) f(w) dw \\
&= \sum_{n=1}^{N} \int_{V_n} (a_n ||p_n - w||^2 + \beta b_{n,T(n)} ||p_n - q_{T(n)}||^2) f(w) dw \\
&= D(P, Q, \mathbf{V}, T) \tag{A.1}
\end{aligned}
$$

Hence, the generalized Voronoi diagram is the optimal partition for any given deployment (P, Q, T). ∎

A.2   Proof of Lemma 1

Given N APs and M FCs ($M < N$), first we demonstrate that there exists an optimal node deployment such as $\left(\widehat{P}, \widehat{Q}, \widehat{\mathbf{R}}, \widehat{T}\right)$ in which each FC has at most one connected AP at the same location, i.e., for each $m \in \mathcal{I}_\mathcal{B}$, the cardinality of the set $\{n | \widehat{T}(n) = m, \widehat{p}_n = \widehat{q}_m\}$ is less than or equal to 1. For this purpose, we consider an optimal node deployment $(P^*, Q^*, \mathbf{R}^*, T^*)$ and assume that there exist at least two distinct indices $n_1, n_2 \in \mathcal{I}_\mathcal{A}$ and an index $m \in \mathcal{I}_\mathcal{B}$ such that $T^*(n_1) = T^*(n_2) = m$, and $p_{n_1}^* = p_{n_2}^* = q_m^*$. Without loss of generality, we can assume that $a_{n_1} \leq a_{n_2}$. We have:

$$D_{n_1} = \int_{R_{n_1}^*} (a_{n_1} ||p_{n_1}^* - w||^2 + \beta b_{n_1, m} ||p_{n_1}^* - q_m^*||^2) f(w) dw$$

$$= \int_{R_{n_1}^*} \left(a_{n_1} ||p_{n_1}^* - w||^2\right) f(w) dw \qquad (A.2)$$

$$D_{n_2} = \int_{R_{n_2}^*} (a_{n_2} ||p_{n_2}^* - w||^2 + \beta b_{n_2, m} ||p_{n_2}^* - q_m^*||^2) f(w) dw$$

$$= \int_{R_{n_2}^*} \left(a_{n_2} ||p_{n_2}^* - w||^2\right) f(w) dw \qquad (A.3)$$

Hence, we have:

$$D_{n_1} + D_{n_2} = \int_{R_{n_1}^*} \left(a_{n_1} ||p_{n_1}^* - w||^2\right) f(w) dw + \int_{R_{n_2}^*} \left(a_{n_2} ||p_{n_2}^* - w||^2\right) f(w) dw$$

$$\geq \int_{R_{n_1}^*} \left(a_{n_1} ||p_{n_1}^* - w||^2\right) f(w) dw + \int_{R_{n_2}^*} \left(a_{n_1} ||p_{n_1}^* - w||^2\right) f(w) dw$$

$$= \int_{R_{n_1}^* \bigcup R_{n_2}^*} \left(a_{n_1} ||p_{n_1}^* - w||^2\right) f(w) dw \qquad (A.4)$$

Eq. (A.4) implies that if we update the cell partition for AP n_1 to be $R_{n_1}^* \bigcup R_{n_2}^*$, and place the AP n_2 to an arbitrary location different from q_m^* with a corresponding zero volume cell partition, the resulting distortion will not increase, and the obtained node deployment is

129

also optimal. Note that in this newly obtained optimal distortion, AP n_2 is not in the same location as FC m anymore. This procedure is continued until we reach an optimal deployment in which each FC has at most one connected AP upon it. Let us denote this optimal node deployment via $\left(\widehat{P}, \widehat{Q}, \widehat{\mathbf{R}}, \widehat{T}\right)$.

Since $M < N$ and each FC has at most one AP upon it, there exists an index $k \in \mathcal{I}_{\mathcal{A}}$ such that $\widehat{p}_k \neq \widehat{q}_{\widehat{T}(k)}$. In order to show that the optimal two-tier distortion with N APs and $M + 1$ FCs is less than that of N APs and M FCs, it is sufficient to construct a node deployment with N APs and $M + 1$ FCs such as $(P'', Q'', \mathbf{R}'', T'')$ that achieves lower distortion than $D\left(\widehat{P}, \widehat{Q}, \widehat{\mathbf{R}}, \widehat{T}\right)$. For each $n \in \mathcal{I}_{\mathcal{A}}$, let $\widehat{v}_n$ denote the volume of the region $\widehat{R}_n$, i.e., $\widehat{v}_n = \int_{\widehat{R}_n} f(w)dw$. We consider two different cases: (i) If $\widehat{v}_k > 0$, then we set $P'' = \widehat{P}$, $Q'' = \left(\widehat{q}_1, \widehat{q}_2, ..., \widehat{q}_M, q''_{M+1} = \widehat{p}_k\right)$, $\mathbf{R}'' = \widehat{\mathbf{R}}$ and $T''(n) = \widehat{T}(n)$ for $n \neq k$ and $T''(k) = M + 1$. Note that

$$
\begin{aligned}
&\int_{\widehat{R}_k} \left(a_k ||\widehat{p}_k - w||^2 + \beta b_{k,\widehat{T}(k)} ||\widehat{p}_k - \widehat{q}_{\widehat{T}(k)}||^2\right) f(w)dw \\
&> \int_{\widehat{R}_k} \left(a_k ||\widehat{p}_k - w||^2\right) f(w)dw \\
&= \int_{\widehat{R}_k} \left(a_k ||\widehat{p}_k - w||^2 + \beta b_{k,M+1} ||\widehat{p}_k - q''_{M+1}||^2\right) f(w)dw
\end{aligned}
\tag{A.5}
$$

implies that in the new deployment $(P'', Q'', \mathbf{R}'', T'')$, the contribution of the AP k to the total distortion has decreased. Since the contribution of other APs to the distortion has not changed, we have $D(P'', Q'', \mathbf{R}'', T'') < D\left(\widehat{P}, \widehat{Q}, \widehat{\mathbf{R}}, \widehat{T}\right)$ and the proof is complete. (ii) If $\widehat{v}_k = 0$, then AP k does not contribute to the optimal distortion $D\left(\widehat{P}, \widehat{Q}, \widehat{\mathbf{R}}, \widehat{T}\right)$, and it can be placed anywhere within the target region Ω. Since the set $\{\widehat{p}_1, ..., \widehat{p}_N, \widehat{q}_1, ..., \widehat{q}_M\}$ has zero measure, clearly there exists a point $x \in \Omega$ and a threshold $\delta \in \mathbb{R}^+$ such that $\mathcal{B}(x, \delta) = \{w \in \Omega | ||x - w|| \leq \delta\}$ does not include any point from the set $\{\widehat{p}_1, ..., \widehat{p}_N, \widehat{q}_1, ..., \widehat{q}_M\}$. Since $f(.)$ is positive, continuous and differentiable over Ω, for each $0 < \epsilon < \delta$ the region $\mathcal{B}(x, \epsilon) = \{w \in \Omega | ||w - x|| \leq \epsilon\}$ has positive volume, i.e., $\int_{\mathcal{B}(x,\delta)} f(w)dw > 0$. Given $0 < \epsilon < \delta$, assume

that:

$$\mathcal{B}(x,\epsilon) \subset \widehat{R}_n \tag{A.6}$$

for some $n \in \mathcal{I}_\mathcal{A}$; therefore, the contribution of the region $\mathcal{B}(x,\epsilon)$ to the total distortion $D\left(\widehat{P},\widehat{Q},\widehat{\mathbf{R}},\widehat{T}\right)$ is equal to:

$$\int_{\mathcal{B}(x,\epsilon)} \left(a_n||\widehat{p}_n - w||^2 + \beta b_{n,\widehat{T}(n)}||\widehat{p}_n - \widehat{q}_{\widehat{T}(n)}||^2 \right) f(w)dw \tag{A.7}$$

As $\epsilon \longrightarrow 0$, (A.7) can be approximated as:

$$\Delta_n \times \int_{\mathcal{B}(x,\epsilon)} f(w)dw \tag{A.8}$$

where $\Delta_n = \left(a_n||\widehat{p}_n - x||^2 + \beta b_{n,\widehat{T}(n)}||\widehat{p}_n - \widehat{q}_{\widehat{T}(n)}||^2 \right)$. If we set $p_k'' = q_{M+1}'' = x$ and $R_k'' = \mathcal{B}(x,\epsilon)$ and $T''(k) = M+1$, then the contribution of the region $\mathcal{B}(x,\epsilon)$ to the total distortion $D\left(P'',Q'',\mathbf{R}'',T''\right)$ is equal to:

$$\begin{aligned}
&\int_{\mathcal{B}(x,\epsilon)} \left(a_k||p_k'' - w||^2 + \beta b_{k,M+1}||p_k'' - q_{M+1}''||^2 \right) f(w)dw \\
&= a_k \int_{\mathcal{B}(x,\epsilon)} \left(||x - w||^2 \right) f(w)dw
\end{aligned} \tag{A.9}$$

The below equation for the ratio of distortions in (A.8) and (A.9)

$$\lim_{\epsilon \longrightarrow 0} \frac{a_k \int_{\mathcal{B}(x,\epsilon)} \left(||x - w||^2 \right) f(w)dw}{\Delta_n \times \int_{\mathcal{B}(x,\epsilon)} f(w)dw} = 0 \tag{A.10}$$

implies that there exists an $\epsilon^* \in (0,\delta)$ such that the contribution of the region $\mathcal{B}(x,\epsilon^*)$ to the total distortion in $D\left(P'',Q'',\mathbf{R}'',T''\right)$ will be less than that of $D\left(\widehat{P},\widehat{Q},\widehat{\mathbf{R}},\widehat{T}\right)$. Hence, we set $P'' = (p_1'',p_2'',...,p_N'')$ where $p_i'' = \widehat{p}_i$ for $i \neq k$, and $p_k'' = x$. Also, we set $Q'' = \left(\widehat{q}_1,\widehat{q}_2,...,\widehat{q}_M,q_{M+1}'' = x\right)$. The partitioning $\mathbf{R}'' = (R_1'',...,R_N'')$ is defined as $R_i'' = \widehat{R}_i$ for $i \neq k$

and $i \neq n$, $R_k'' = \mathcal{B}(x, \epsilon^*)$ and $R_n'' = \widehat{R}_n - \mathcal{B}(x, \epsilon^*)$. Finally, we set $T''(i) = \widehat{T}(i)$ for $i \neq k$ and $T''(k) = M + 1$. As mentioned earlier, the two-tier distortion $D\left(P'', Q'', \mathbf{R}'', T''\right)$ is less than $D\left(\widehat{P}, \widehat{Q}, \widehat{\mathbf{R}}, \widehat{T}\right)$. Note that if the region $\mathcal{B}(x, \epsilon)$ is a subset of more than one region, Eqs. (A.6) to (A.8) and (A.10) can be modified accordingly and a similar argument can be made to show that the resulting distortion will be improved in the new deployment, and the proof is complete. ∎

A.3 Proof of Corollary 1

Assume that there exists an index $m \in \mathcal{I}_\mathcal{B}$ in the optimal node deployment $(P^*, Q^*, \mathbf{R}^*, T^*)$ such that $\bigcup_{n:T^*(n)=m} R_n^*$ has zero volume. Consider the node deployment $(P', Q', \mathbf{R}', T')$ where $P' = P^*$, $Q' = \left(q_1^*, ..., q_{m-1}^*, q_{m+1}^*, ..., q_M^*\right)$, $\mathbf{R}' = \mathbf{R}^*$ and $T'(i) = T^*(i)$ for indices $i \in \mathcal{I}_\mathcal{A}$ such that $T^*(i) \neq m$. Note that for indices $i \in \mathcal{I}_\mathcal{A}$ such that $T^*(i) = m$, we can define $T'(i)$ arbitrarily because the corresponding regions R_i' have zero volume. Since $\bigcup_{n:T^*(n)=m} R_n^*$ has zero volume, we have:

$$D\left(P', Q', \mathbf{R}', T'\right) = D\left(P^*, Q^*, \mathbf{R}^*, T^*\right) \tag{A.11}$$

which is in contradiction with Lemma 1 since the optimal node deployment $(P^*, Q^*, \mathbf{R}^*, T^*)$ for N APs and M FCs has not improved the node deployment $(P', Q', \mathbf{R}', T')$ for N APs and $M-1$ FCs in terms of distortion. Hence the proof is complete. ∎

A.4 Proof of Proposition 2

First, we study the shape of the Voronoi regions in (1.5). Let $\mathcal{B}(c, r) = \{\omega \mid \|\omega - c\| \leq r\}$ be a disk centered at c with radius r in two-dimensional space. In particular, $\mathcal{B}(c, r) = \emptyset$ when

$r \leq 0$. Let $\mathcal{HS} = \{\omega | A\omega + B \leq 0\}$ be a half space, where $A \in \mathbb{R}^2$ is a vector and $B \in \mathbb{R}$ is a constant. For $i, j \in \mathcal{I_A}$, we define

$$
\begin{aligned}
V_{ij}(P, Q, T) \triangleq \{\omega | a_i ||p_i - w||^2 + \beta b_{i,T(i)} ||p_i - q_{T(i)}||^2 \leq \\
a_j ||p_j - w||^2 + \beta b_{j,T(j)} ||p_j - q_{T(j)}||^2\}
\end{aligned}
\tag{A.12}
$$

to be the pairwise Voronoi region of AP i where only AP i and j are considered. Then, AP i's Voronoi region can be represented as $V_i(P, Q) = \left[\bigcap_{j \neq i} V_{ij}(P, Q)\right] \bigcap \Omega$. Let (ω_x, ω_y), (p_{ix}, p_{iy}), and (p_{jx}, p_{jy}) be the coordinates of ω, p_i and p_j, respectively. Expanding the inequality in (A.12) results in

$$
\begin{aligned}
(a_i - a_j)(\omega_x^2 + \omega_y^2) - 2(a_i p_{ix} - a_j p_{jx})\omega_x \\
- 2(a_i p_{iy} - a_j p_{jy})\omega_y + a_i ||p_i||^2 - a_j ||p_j||^2 \\
+ \beta b_{i,T(i)} ||p_i - q_{T(i)}||^2 - \beta b_{j,T(j)} ||p_j - q_{T(j)}||^2 \leq 0
\end{aligned}
\tag{A.13}
$$

When $a_i = a_j$, the pairwise Voronoi region is a half space, i.e., $V_{ij} = \{A_{ij}\omega + B_{ij} \leq 0\}$, where $A_{ij} = a_j p_j - a_i p_i$ and $B_{ij} = \frac{\left(a_i ||p_i||^2 - a_j ||p_j||^2 + \beta b_{i,T(i)} ||p_i - q_{T(i)}||^2 - \beta b_{j,T(j)} ||p_j - q_{T(j)}||^2\right)}{2}$. When $a_i > a_j$, V_{ij} is represented as:

$$
(\omega - c_{ij})^2 \leq L_{ij}.
\tag{A.14}
$$

When $a_i < a_j$, V_{ij} is represented as:

$$
(\omega - c_{ij})^2 \geq L_{ij},
\tag{A.15}
$$

where

$$
c_{ij} = \left(\frac{a_i p_{ix} - a_j p_{jx}}{a_i - a_j}, \frac{a_i p_{iy} - a_j p_{jy}}{a_i - a_j}\right) = \frac{a_i p_i - a_j p_j}{a_i - a_j}
\tag{A.16}
$$

$$L_{ij} = \frac{a_i a_j \|p_i - p_j\|^2}{(a_i - a_j)^2} - \beta \times \frac{b_{i,T(i)} \|p_i - q_{T(i)}\|^2 - b_{j,T(j)} \|p_j - q_{T(j)}\|^2}{(a_i - a_j)} \tag{A.17}$$

For $L_{ij} \geq 0$, we define the radius r_{ij} as:

$$r_{ij} = \begin{cases} \sqrt{L_{ij}}, & L_{ij} \geq 0 \\ \\ 0, & L_{ij} < 0 \end{cases} \tag{A.18}$$

Therefore, the pairwise Voronoi region V_{ij} is derived:

$$V_{ij} = \Omega \cap \begin{cases} \mathcal{HS}(A_{ij}, B_{ij}) & , a_i = a_j \\ \\ \mathcal{B}(c_{ij}, r_{ij}) & , a_i > a_j, L_{ij} \geq 0 \\ \\ \varnothing & , a_i > a_j, L_{ij} < 0 \\ \\ \mathcal{B}^c(c_{ij}, r_{ij}) & , a_i < a_j, L_{ij} \geq 0 \\ \\ \mathbb{R}^2 & , a_i < a_j, L_{ij} < 0 \end{cases} \tag{A.19}$$

where $\mathcal{B}^c(c_{ij}, r_{ij})$ is the complementary of $\mathcal{B}(c_{ij}, r_{ij})$. Note that for two distinct indices such as $i, j \in \mathcal{I}_\mathcal{A}$, if $a_i > a_j$ and $L_{ij} < 0$, then two regions $\Omega \cap \mathcal{B}(c_{ij}, r_{ij})$ and $\varnothing$ differ only in one point, i.e., c_{ij}. Similarly, for $a_i < a_j$ and $L_{ij} < 0$, two regions $\Omega \cap \mathcal{B}^c(c_{ij}, r_{ij})$ and Ω differ only in one point c_{ij}. Hence, if we define:

$$\overline{V}_k = \left[\bigcap_{i:a_k > a_i} \mathcal{B}(c_{ki}, r_{ki}) \right] \bigcap \left[\bigcap_{i:a_k = a_i} \mathcal{HS}(A_{ki}, B_{ki}) \right] \bigcap \left[\bigcap_{i:a_k < a_i} \mathcal{B}^c(c_{ki}, r_{ki}) \right] \bigcap \Omega \tag{A.20}$$

then two regions $\overline{V}_k$ and V_k differ only in finite number of points. As a result, integrals over both $\overline{V}_k$ and V_k have the same value since the density function f is continuous and differentiable, and removing finite number of points from the integral region does not change the integral value. Note that if V_k is empty, the Proposition 1 in [38] holds since the integral over an empty region is zero. If V_k is not empty, the same arguments as in Appendix A of

[38] can be replicated since $\overline{V}_k$ in (A.20) is similar to Eq. (31) in [38].

Using parallel axis theorem, the two-tier distortion can be written as:

$$
\begin{aligned}
D\left(P,Q,\mathbf{V},T\right) &= \sum_{n=1}^{N} \int_{V_n} \left(a_n ||p_n - w||^2 + \beta b_{n,T(n)} ||p_n - q_{T(n)}||^2 \right) f(w) dw \\
&= \sum_{n=1}^{N} \left(\int_{V_n} a_n ||c_n - w||^2 f(w) dw + a_n ||p_n - c_n||^2 v_n \right. \\
&\quad \left. + \beta b_{n,T(n)} ||p_n - q_{T(n)}||^2 v_n \right)
\end{aligned}
\tag{A.21}
$$

Using Proposition 1 in [38], since the optimal deployment (P^*, Q^*) satisfies zero gradient, we take the partial derivatives of Eq. (A.21) as follows:

$$
\begin{aligned}
\frac{\partial D}{\partial p_n^*} &= 2 \left[a_n (p_n^* - c_n^*) + \beta b_{n,T^*(n)} (p_n^* - q_{T^*(n)}^*) \right] v_n^* = 0 \\
\frac{\partial D}{\partial q_m^*} &= 2 \sum_{n:T^*(n)=m} \beta b_{n,m} (q_m^* - p_n^*) v_n^* = 0
\end{aligned}
\tag{A.22}
$$

By solving Eq. (A.22), we have the following necessary conditions:

$$
p_n^* = \frac{a_n c_n^* + \beta b_{n,T^*(n)} q_{T^*(n)}^*}{a_n + \beta b_{n,T^*(n)}}
\tag{A.23}
$$

$$
q_m^* = \frac{\sum_{n:T^*(n)=m} b_{n,m} p_n^* v_n^*}{\sum_{n:T^*(n)=m} b_{n,m} v_n^*}
\tag{A.24}
$$

and the proof is complete. ∎

A.5 Proof of Convergence for the HTTL algorithm

In what follows, we demonstrate that none of the four steps in the HTTL algorithm will increase the two-tier distortion. Given P, Q and $\mathbf{R}$, updating the index map T according to (1.4) minimizes the total distortion, i.e., the two-tier distortion will not increase by the first

step. Moreover, given P, Q and T, Proposition 1 indicates that updating $\mathbf{R}$ according to (1.5) and (1.6) gives the best partitioning; thus, the second step of the HTTL algorithm will not increase the distortion. Below equality follows from straightforward algebraic calculations and we omit the proof here:

$$\sum_{n:T(n)=m} b_{n,m} v_n ||p_n - q_m||^2 = \sum_{n:T(n)=m} b_{n,m} v_n (||p_n - q'_m||^2 + ||q_m - q'_m||^2) \tag{A.25}$$

for $q'_m = \frac{\sum_{n:T(n)=m} b_{n,m} p_n v_n}{\sum_{n:T(n)=m} b_{n,m} v_n}$. The contribution of FC m to the total distortion can then be rewritten as:

$$\sum_{n:T(n)=m} \int_{R_n} \left(a_n ||p_n - w||^2 + \beta b_{n,m} ||p_n - q_m||^2 \right) f(w) dw$$

$$= \sum_{n:T(n)=m} \int_{R_n} a_n ||p_n - w||^2 f(w) dw + \beta \left(\sum_{n:T(n)=m} b_{n,m} v_n \right) ||q_m - q'_m||^2$$

$$+ \beta \left(\sum_{n:T(n)=m} b_{n,m} v_n ||p_n - q'_m||^2 \right) \tag{A.26}$$

Now, given P, $\mathbf{R}$ and T, the first and third terms in right hand side of (A.26) are constant and moving q_m toward q'_m will not increase the distortion in (A.26). Therefore, the third step of the HTTL algorithm will not increase the total two-tier distortion as well.

The following equation can be easily verified using straightforward algebraic computations and we omit the proof here:

$$a_n ||p_n - w||^2 + \beta b_{n,m} ||p_n - q_m||^2$$

$$= (a_n + \beta b_{n,m}) \left\| p_n - \frac{(a_n w + \beta b_{n,m} q_m)}{a_n + \beta b_{n,m}} \right\|^2$$

$$+ \frac{\beta a_n b_{n,m}}{a_n + \beta b_{n,m}} ||w - q_m||^2 \tag{A.27}$$

For each index $n \in \mathcal{I}_A$ and the corresponding index $m = T(n)$, we can rewrite the contribu-

tion of AP n to the total distortion as:

$$\int_{R_n} \left(a_n ||p_n - w||^2 + \beta b_{n,m} ||p_n - q_m||^2 \right) f(w)dw$$

$$= \int_{R_n} \left[(a_n + \beta b_{n,m}) \left|\left| p_n - \frac{(a_n w + \beta b_{n,m} q_m)}{a_n + \beta b_{n,m}} \right|\right|^2 + \frac{\beta a_n b_{n,m}}{a_n + \beta b_{n,m}} ||w - q_m||^2 \right] f(w)dw$$

$$= \int_{R_n} \left[\frac{a_n^2}{a_n + \beta b_{n,m}} \left|\left| \frac{(a_n + \beta b_{n,m})\, p_n - \beta b_{n,m} q_m}{a_n} - w \right|\right|^2 \right.$$
$$\left. + \frac{\beta a_n b_{n,m}}{a_n + \beta b_{n,m}} ||w - q_m||^2 \right] f(w)dw$$

$$= \int_{R_n} \left[\frac{a_n^2}{a_n + \beta b_{n,m}} \left(\left|\left| \frac{(a_n + \beta b_{n,m})\, p_n - \beta b_{n,m} q_m}{a_n} - c_n \right|\right|^2 \right.\right.$$
$$\left.\left. + ||c_n - w||^2 \right) + \frac{\beta a_n b_{n,m}}{a_n + \beta b_{n,m}} ||w - q_m||^2 \right] f(w)dw$$

$$= \int_{R_n} \left[\frac{a_n^2}{a_n + \beta b_{n,m}} ||c_n - w||^2 + (a_n + \beta b_{n,m}) \left|\left| p_n - \frac{a_n c_n + \beta b_{n,m} q_m}{a_n + \beta b_{n,m}} \right|\right|^2 \right.$$
$$\left. + \frac{\beta a_n b_{n,m}}{a_n + \beta b_{n,m}} ||w - q_m||^2 \right] f(w)dw$$

$$= \frac{a_n^2}{a_n + \beta b_{n,m}} \int_{R_n} ||c_n - w||^2 f(w)dw + (a_n + \beta b_{n,m}) ||p_n - p_n'||^2 v_n$$
$$+ \frac{\beta a_n b_{n,m}}{a_n + \beta b_{n,m}} \int_{R_n} ||w - q_m||^2 f(w)dw \qquad \text{(A.28)}$$

where $p_n' = \frac{a_n c_n + \beta b_{n,m} q_m}{a_n + \beta b_{n,m}}$. Note that the first equality in (A.28) comes from (A.27), and the third equality follows from the parallel axis theorem. Now, given Q, $\mathbf{R}$ and T, the first and third terms in (A.28) are constant and moving p_n toward p_n' will not increase the second term in (A.28). Hence, the fourth step of the HTTL algorithm will not increase the total distortion either. So, the HTTL algorithm generates a sequence of positive non-increasing distortion values and thus, it converges. Note that if distortion remains the same after an iteration of the algorithm, it means that non of the four steps have decreased distortion and the algorithm has already reached an optimal deployment. ∎

Appendix B

Supplementary Proofs for Chapter 2

B.1   Proof of Proposition 3

For $U = (S_1, S_2, ..., S_N)$, the left-hand side of (2.9) can be written as:

$$\overline{\mathcal{P}}(P, Q, U, T) = \sum_{n=1}^{N} \int_{S_n} (a_n \|p_n - w\|^2$$

$$+ \beta b_{n,T(n)} \|p_n - q_{T(n)}\|^2) f(w) dw \geq \sum_{n=1}^{N} \int_{S_n} \min_{j} (a_j \|p_j - w\|^2$$

$$+ \beta b_{j,T(j)} \|p_j - q_{T(j)}\|^2) f(w) dw = \int_{\Omega} \min_{j} (a_j \|p_j - w\|^2$$

$$+ \beta b_{j,T(j)} \|p_j - q_{T(j)}\|^2) f(w) dw = \sum_{n=1}^{N} \int_{V_n} \min_{j} (a_j \|p_j - w\|^2$$

$$+ \beta b_{j,T(j)} \|p_j - q_{T(j)}\|^2) f(w) dw = \sum_{n=1}^{N} \int_{V_n} (a_n \|p_n - w\|^2$$

$$+ \beta b_{n,T(n)} \|p_n - q_{T(n)}\|^2) f(w) dw = \overline{\mathcal{P}}(P, Q, \mathbf{V}, T).$$

Hence, the generalized Voronoi diagram is the optimal partition for any deployment (P, Q, T). ∎

B.2 Proof of Lemma 2

Given N APs and M FCs ($M < N$), first we demonstrate that there exists an optimal node deployment such as $\left(\widehat{P}, \widehat{Q}, \widehat{\mathbf{R}}, \widehat{T}\right)$ in which each FC has at most one connected AP at the same location, i.e., for each $m \in \mathcal{I}_{\mathcal{B}}$, the cardinality of the set $\{n|\widehat{T}(n) = m, \widehat{p}_n = \widehat{q}_m\}$ is less than or equal to 1. For this purpose, we consider an optimal node deployment $(P^*, Q^*, \mathbf{R}^*, T^*)$ and assume that there exist at least two distinct indices $n_1, n_2 \in \mathcal{I}_{\mathcal{A}}$ and an index $m \in \mathcal{I}_{\mathcal{B}}$ such that $T^*(n_1) = T^*(n_2) = m$, and $p_{n_1}^* = p_{n_2}^* = q_m^*$. We have:

$$
\begin{aligned}
\overline{\mathcal{P}}_{n_1} &= \int_{R_{n_1}^*} (a_{n_1}\|p_{n_1}^* - w\|^2 + \beta b_{n_1,m}\|p_{n_1}^* - q_m^*\|^2) f(w) dw \\
&= \int_{R_{n_1}^*} a_{n_1}\|p_{n_1}^* - w\|^2 f(w) dw,
\end{aligned}
\tag{B.1}
$$

$$
\begin{aligned}
\overline{\mathcal{P}}_{n_2} &= \int_{R_{n_2}^*} (a_{n_2}\|p_{n_2}^* - w\|^2 + \beta b_{n_2,m}\|p_{n_2}^* - q_m^*\|^2) f(w) dw \\
&= \int_{R_{n_2}^*} a_{n_2}\|p_{n_2}^* - w\|^2 f(w) dw.
\end{aligned}
\tag{B.2}
$$

Without loss of generality, we can assume that $a_{n_1} \leq a_{n_2}$. Hence, we have:

$$
\begin{aligned}
\overline{\mathcal{P}}_{n_1} + \overline{\mathcal{P}}_{n_2} &= \int_{R_{n_1}^*} a_{n_1}\|p_{n_1}^* - w\|^2 f(w) dw + \int_{R_{n_2}^*} a_{n_2}\|p_{n_2}^* - w\|^2 f(w) dw \\
&\geq \int_{R_{n_1}^*} a_{n_1}\|p_{n_1}^* - w\|^2 f(w) dw + \int_{R_{n_2}^*} a_{n_1}\|p_{n_1}^* - w\|^2 f(w) dw \\
&= \int_{R_{n_1}^* \bigcup R_{n_2}^*} a_{n_1}\|p_{n_1}^* - w\|^2 f(w) dw,
\end{aligned}
$$

which implies that if we update the cell partition for AP n_1 to be $R_{n_1}^* \bigcup R_{n_2}^*$, and place the AP n_2 to an arbitrary location different from q_m^* with a corresponding zero volume cell partition, the resulting power consumption will not increase, and the obtained node deployment is also optimal. Note that in this newly obtained optimal power consumption, AP n_2 is not in the

same location as FC m anymore. This procedure is continued until we reach an optimal deployment, denoted via $\left(\widehat{P}, \widehat{Q}, \widehat{\mathbf{R}}, \widehat{T}\right)$, in which each FC has at most one connected AP upon it.

Since $M < N$ and each FC has at most one AP upon it, there exists an index $k \in \mathcal{I}_A$ such that $\widehat{p}_k \neq \widehat{q}_{\widehat{T}(k)}$. In order to show that the optimal two-tier power consumption with N APs and $M + 1$ FCs is less than that of N APs and M FCs, it is sufficient to construct a node deployment with N APs and $M + 1$ FCs such as $(P'', Q'', \mathbf{R}'', T'')$ that achieves lower power consumption than $\overline{\mathcal{P}}\left(\widehat{P}, \widehat{Q}, \widehat{\mathbf{R}}, \widehat{T}\right)$. For each $n \in \mathcal{I}_A$, let $\widehat{v}_n = \int_{\widehat{R}_n} f(w) dw$ denote the volume of the region $\widehat{R}_n$. We consider two cases: (i) If $\widehat{v}_k > 0$, then we set $P'' = \widehat{P}$, $Q'' = \left(\widehat{q}_1, \widehat{q}_2, ..., \widehat{q}_M, q''_{M+1} = \widehat{p}_k\right)$, $\mathbf{R}'' = \widehat{\mathbf{R}}$ and $T''(n) = \widehat{T}(n)$ for $n \neq k$ and $T''(k) = M + 1$. Note that

$$
\int_{\widehat{R}_k} \left(a_k \|\widehat{p}_k - w\|^2 + \beta b_{k,\widehat{T}(k)} \|\widehat{p}_k - \widehat{q}_{\widehat{T}(k)}\|^2\right) f(w) dw
$$
$$
> \int_{\widehat{R}_k} \left(a_k \|\widehat{p}_k - w\|^2\right) f(w) dw = \int_{\widehat{R}_k} \left(a_k \|\widehat{p}_k - w\|^2 + \beta b_{k,M+1} \|\widehat{p}_k - q''_{M+1}\|^2\right) f(w) dw
$$
$$
\tag{B.3}
$$

implies that in the deployment $(P'', Q'', \mathbf{R}'', T'')$, the contribution of the AP k to the total power consumption has decreased. Since the contribution of other APs to the power consumption has not changed, we have $\overline{\mathcal{P}}(P'', Q'', \mathbf{R}'', T'') < \overline{\mathcal{P}}\left(\widehat{P}, \widehat{Q}, \widehat{\mathbf{R}}, \widehat{T}\right)$ and the proof is complete. (ii) If $\widehat{v}_k = 0$, then AP k does not contribute to the optimal power consumption $\overline{\mathcal{P}}\left(\widehat{P}, \widehat{Q}, \widehat{\mathbf{R}}, \widehat{T}\right)$, and it can be placed anywhere within the target region Ω. Since the set $\{\widehat{p}_1, ..., \widehat{p}_N, \widehat{q}_1, ..., \widehat{q}_M\}$ has zero measure, there exists a point $x \in \Omega$ and a threshold $\delta \in \mathbb{R}^+$ such that $\mathcal{B}(x, \delta) = \{w \in \Omega | \|x - w\| \leq \delta\}$ does not include any point from the set $\{\widehat{p}_1, ..., \widehat{p}_N, \widehat{q}_1, ..., \widehat{q}_M\}$. Since $f(.)$ is positive, continuous and differentiable over Ω, for each $0 < \epsilon < \delta$ the region $\mathcal{B}(x, \epsilon) = \{w \in \Omega | \|w - x\| \leq \epsilon\}$ has positive volume, i.e., $\int_{\mathcal{B}(x,\delta)} f(w) dw > 0$. Given $0 < \epsilon < \delta$, assume that:

$$\mathcal{B}(x, \epsilon) \subset \widehat{R}_n, \tag{B.4}$$

for some $n \in \mathcal{I}_A$; therefore, the contribution of the region $\mathcal{B}(x, \epsilon)$ to the total power consumption $\overline{\mathcal{P}}\left(\widehat{P}, \widehat{Q}, \widehat{\mathbf{R}}, \widehat{T}\right)$ is equal to:

$$\int_{\mathcal{B}(x,\epsilon)} \left(a_n \|\widehat{p}_n - w\|^2 + \beta b_{n,\widehat{T}(n)} \|\widehat{p}_n - \widehat{q}_{\widehat{T}(n)}\|^2 \right) f(w)dw. \tag{B.5}$$

As $\epsilon \longrightarrow 0$, (B.5) can be approximated as:

$$\Delta_n \times \int_{\mathcal{B}(x,\epsilon)} f(w)dw, \tag{B.6}$$

where $\Delta_n = \left(a_n \|\widehat{p}_n - x\|^2 + \beta b_{n,\widehat{T}(n)} \|\widehat{p}_n - \widehat{q}_{\widehat{T}(n)}\|^2 \right)$. If we set $p_k'' = q_{M+1}'' = x$ and $R_k'' = \mathcal{B}(x, \epsilon)$ and $T''(k) = M+1$, then the contribution of the region $\mathcal{B}(x, \epsilon)$ to the total power consumption $\overline{\mathcal{P}}\left(P'', Q'', \mathbf{R}'', T''\right)$ is equal to:

$$\int_{\mathcal{B}(x,\epsilon)} \left(a_k \|p_k'' - w\|^2 + \beta b_{k,M+1} \|p_k'' - q_{M+1}''\|^2 \right) f(w)dw$$

$$= a_k \int_{\mathcal{B}(x,\epsilon)} \left(\|x - w\|^2 \right) f(w)dw. \tag{B.7}$$

The below equation for the ratio of power consumption in (B.6) and (B.7)

$$\lim_{\epsilon \longrightarrow 0} \frac{a_k \int_{\mathcal{B}(x,\epsilon)} \left(\|x - w\|^2 \right) f(w)dw}{\Delta_n \times \int_{\mathcal{B}(x,\epsilon)} f(w)dw} = 0 \tag{B.8}$$

implies that there exists an $\epsilon^* \in (0, \delta)$ such that the contribution of the region $\mathcal{B}(x, \epsilon^*)$ to the total power in $\overline{\mathcal{P}}\left(P'', Q'', \mathbf{R}'', T''\right)$ will be less than that of $\overline{\mathcal{P}}\left(\widehat{P}, \widehat{Q}, \widehat{\mathbf{R}}, \widehat{T}\right)$. Hence, we set $P'' = (p_1'', p_2'', ..., p_N'')$ where $p_i'' = \widehat{p}_i$ for $i \neq k$, and $p_k'' = x$. Also, we set $Q'' = \left(\widehat{q}_1, \widehat{q}_2, ..., \widehat{q}_M, q_{M+1}'' = x \right)$. The partitioning $\mathbf{R}'' = (R_1'', ..., R_N'')$ is defined as $R_i'' = \widehat{R}_i$ for $i \neq k$

and $i \neq n$, $R''_k = \mathcal{B}(x, \epsilon^*)$ and $R''_n = \widehat{R}_n - \mathcal{B}(x, \epsilon^*)$. Finally, we set $T''(i) = \widehat{T}(i)$ for $i \neq k$ and $T''(k) = M + 1$. As mentioned earlier, the two-tier power consumption $\overline{\mathcal{P}}(P'', Q'', \mathbf{R}'', T'')$ is less than $\overline{\mathcal{P}}\left(\widehat{P}, \widehat{Q}, \widehat{\mathbf{R}}, \widehat{T}\right)$. Note that if the region $\mathcal{B}(x, \epsilon)$ is a subset of more than one region, (B.4) to (B.6) and (B.8) can be modified accordingly and a similar argument shows that the resulting power consumption will be improved in the new deployment, and the proof is complete. ∎

B.3   Proof of Corollary 2

Assume that there exists an index $m \in \mathcal{I}_\mathcal{B}$ in the optimal node deployment $(P^*, Q^*, \mathbf{R}^*, T^*)$ such that $\bigcup_{n:T^*(n)=m} R_n^*$ has zero volume. Consider the node deployment $(P', Q', \mathbf{R}', T')$ where $P' = P^*$, $Q' = \left(q_1^*, ..., q_{m-1}^*, q_{m+1}^*, ..., q_M^*\right)$, $\mathbf{R}' = \mathbf{R}^*$ and $T'(i) = T^*(i)$ for indices $i \in \mathcal{I}_\mathcal{A}$ such that $T^*(i) \neq m$. Note that for indices $i \in \mathcal{I}_\mathcal{A}$ such that $T^*(i) = m$, we can define $T'(i)$ arbitrarily because the corresponding regions R'_i have zero volume. Since $\bigcup_{n:T^*(n)=m} R_n^*$ has zero volume, we have $\overline{\mathcal{P}}(P', Q', \mathbf{R}', T') = \overline{\mathcal{P}}(P^*, Q^*, \mathbf{R}^*, T^*)$ which is in contradiction with Lemma 1 since the optimal node deployment $(P^*, Q^*, \mathbf{R}^*, T^*)$ for N APs and M FCs has not improved the node deployment $(P', Q', \mathbf{R}', T')$ for N APs and $M - 1$ FCs in terms of power consumption. ∎

B.4   Proof of Proposition 4

First, we study the shape of the Voronoi regions in (2.7). Let $\mathcal{B}(c, r) = \{\omega | \|\omega - c\| \leq r\}$ be a disk centered at c with radius r in two-dimensional space. In particular, $\mathcal{B}(c, r) = \varnothing$ when $r \leq 0$. Let $\mathcal{HS}(A, B) = \{\omega | A\omega + B \leq 0\}$ be a half space, where $A \in \mathbb{R}^2$ is a vector and $B \in \mathbb{R}$ is a constant. For $i, j \in \mathcal{I}_\mathcal{A}$, we define

$$V_{ij}(P, Q, T) \triangleq \{w | a_i \|p_i - w\|^2 + \beta b_{i,T(i)} \|p_i - q_{T(i)}\|^2$$

$$\leq a_j \|p_j - w\|^2 + \beta b_{j,T(j)} \|p_j - q_{T(j)}\|^2\} \tag{B.9}$$

to be the pairwise Voronoi region of AP i where only AP i and j are considered. Then, AP i's Voronoi region can be represented as $V_i(P, Q) = \left[\bigcap_{j \neq i} V_{ij}(P, Q) \right] \bigcap \Omega$. By expanding (B.9) and straightforward algebraic calculations, the pairwise Voronoi region V_{ij} is derived as:

$$V_{ij} = \Omega \cap \begin{cases} \mathcal{HS}\left(A_{ij}, B_{ij}\right) & , a_i = a_j \\ \mathcal{B}\left(c_{ij}, r_{ij}\right) & , a_i > a_j, L_{ij} \geq 0 \\ \varnothing & , a_i > a_j, L_{ij} < 0 \\ \mathcal{B}^c\left(c_{ij}, r_{ij}\right) & , a_i < a_j, L_{ij} \geq 0 \\ \mathbb{R}^2 & , a_i < a_j, L_{ij} < 0 \end{cases} \tag{B.10}$$

where $A_{ij} = a_j p_j - a_i p_i$, $B_{ij} = \frac{\left(a_i \|p_i\|^2 - a_j \|p_j\|^2 + \beta b_{i,T(i)} \|p_i - q_{T(i)}\|^2 - \beta b_{j,T(j)} \|p_j - q_{T(j)}\|^2\right)}{2}$, $c_{ij} = \frac{a_i p_i - a_j p_j}{a_i - a_j}$, $L_{ij} = \frac{a_i a_j \|p_i - p_j\|^2}{(a_i - a_j)^2} - \beta \times \frac{b_{i,T(i)} \|p_i - q_{T(i)}\|^2 - b_{j,T(j)} \|p_j - q_{T(j)}\|^2}{(a_i - a_j)}$, $r_{ij} = \sqrt{\max\left(L_{ij}, 0\right)}$, and $\mathcal{B}^c(c_{ij}, r_{ij})$ is the complementary of $\mathcal{B}(c_{ij}, r_{ij})$. Note that for two distinct indices such as $i, j \in \mathcal{I_A}$, if $a_i > a_j$ and $L_{ij} < 0$, then two regions $\Omega \cap \mathcal{B}(c_{ij}, r_{ij})$ and $\varnothing$ differ only in the point c_{ij}. Similarly, for $a_i < a_j$ and $L_{ij} < 0$, two regions $\Omega \cap \mathcal{B}^c(c_{ij}, r_{ij})$ and Ω differ only in the point c_{ij}. If we define:

$$\overline{V}_k = \left[\bigcap_{i:a_k > a_i} \mathcal{B}(c_{ki}, r_{ki}) \right] \bigcap \left[\bigcap_{i:a_k = a_i} \mathcal{HS}(A_{ki}, B_{ki}) \right] \bigcap \left[\bigcap_{i:a_k < a_i} \mathcal{B}^c(c_{ki}, r_{ki}) \right] \bigcap \Omega, \tag{B.11}$$

then two regions $\overline{V}_k$ and V_k differ only in finite number of points. As a result, integrals over both $\overline{V}_k$ and V_k have the same value since the density function f is continuous and

differentiable, and removing finite number of points from the integral region does not change the integral value. Note that if V_k is empty, the Proposition 1 in [38] holds since the integral over an empty region is zero. If V_k is not empty, the same arguments as in Appendix A of [38] can be replicated since $\overline{V}_k$ in (B.11) is similar to (31) in [38].

Using parallel axis theorem [82], the two-tier power consumption can be written as:

$$\overline{\mathcal{P}}(P,Q,\mathbf{V},T) = \sum_{n=1}^{N} \int_{V_n} \left(a_n \|p_n - w\|^2 + \beta b_{n,T(n)} \|p_n - q_{T(n)}\|^2 \right) f(w) dw$$

$$= \sum_{n=1}^{N} \left(\int_{V_n} a_n \|c_n - w\|^2 f(w) dw + a_n \|p_n - c_n\|^2 v_n + \beta b_{n,T(n)} \|p_n - q_{T(n)}\|^2 v_n \right). \quad (B.12)$$

Using Proposition 1 in [38], since the optimal deployment (P^*, Q^*) satisfies zero gradient, we take the partial derivatives of (B.12) as follows:

$$\frac{\partial \overline{\mathcal{P}}}{\partial p_n^*} = 2 \left[a_n(p_n^* - c_n^*) + \beta b_{n,T^*(n)}(p_n^* - q_{T^*(n)}^*) \right] v_n^* = 0,$$

$$\frac{\partial \overline{\mathcal{P}}}{\partial q_m^*} = 2 \sum_{n:T^*(n)=m} \beta b_{n,m}(q_m^* - p_n^*) v_n^* = 0. \quad (B.13)$$

By solving (B.13), we have the following necessary conditions:

$$p_n^* = \frac{a_n c_n^* + \beta b_{n,T^*(n)} q_{T^*(n)}^*}{a_n + \beta b_{n,T^*(n)}},$$

$$q_m^* = \frac{\sum_{n:T^*(n)=m} b_{n,m} p_n^* v_n^*}{\sum_{n:T^*(n)=m} b_{n,m} v_n^*}, \quad (B.14)$$

and the proof is complete. ∎

B.5 Proof of Lemma 3

Using Lemma 3 in [42], it can be easily shown that the optimal quantization regions are two closed intervals. Without loss of generality, let $\mathbf{R} = \{R_1, R_2\}$, where $R_1 = [0, r]$ and $R_2 = [r, 1]$ be the optimal partitioning. Thus, we have $c_1 = \frac{r}{2}$ and $c_2 = \frac{1+r}{2}$. Using (2.11), we have:

$$
\begin{aligned}
p_1 &= \frac{a_1 c_1 + \beta b_{1,1} q}{a_1 + \beta b_{1,1}} = \frac{r + 2\beta' q}{2(1 + \beta')}, \\
p_2 &= \frac{a_2 c_2 + \beta b_{2,1} q}{a_2 + \beta b_{2,1}} = \frac{1 + r + 2\beta' q}{2(1 + \beta')},
\end{aligned}
\tag{B.15}
$$

where $\beta' = \beta \times \kappa$. Therefore, the two-tier power in the regions R_1 and R_2 are given by:

$$
\begin{aligned}
\overline{\mathcal{P}}_1 &= a_1 \int_0^r \left[\left(\frac{r + 2\beta' q}{2(1 + \beta')} - w \right)^2 + \beta' \frac{(r - 2q)^2}{4(1 + \beta')^2} \right] dw, \\
\overline{\mathcal{P}}_2 &= a_2 \int_r^1 \left[\left(\frac{1 + r + 2\beta' q}{2(1 + \beta')} - w \right)^2 + \beta' \frac{(1 + r - 2q)^2}{4(1 + \beta')^2} \right] dw,
\end{aligned}
\tag{B.16}
$$

and $\overline{\mathcal{P}}(r, q) = \overline{\mathcal{P}}_1 + \overline{\mathcal{P}}_2$ is the total two-tier power consumption. Simplifying (B.16) yields:

$$
\begin{aligned}
\overline{\mathcal{P}}_1 &= \frac{a_1 r}{4(1 + \beta')^2} \times \bigg(\beta' (r - 2q)^2 + \frac{1}{3} \times \Big[(r + 2\beta' q)^2 \\
&\quad + (r + 2\beta' q)(2\beta'(q - r) - r) + (2\beta'(q - r) - r)^2 \Big] \bigg), \\
\overline{\mathcal{P}}_2 &= \frac{a_2(1 - r)}{4(1 + \beta')^2} \times \bigg(\beta' (1 + r - 2q)^2 + \frac{1}{3} \times \Big[((1 - r) + 2\beta'(q - r))^2 \\
&\quad + ((1 - r) + 2\beta'(q - r))((r - 1) + 2\beta'(q - 1)) + ((r - 1) + 2\beta'(q - 1))^2 \Big] \bigg). \quad \text{(B.17)}
\end{aligned}
$$

Since both $\overline{\mathcal{P}}_1(r, q)$ and $\overline{\mathcal{P}}_2(r, q)$ are continuous and differentiable functions of r and q, the minimum occurs either at zero gradients, given by:

$$
\frac{\partial \overline{\mathcal{P}}}{\partial q} = 0 \quad , \quad \frac{\partial \overline{\mathcal{P}}}{\partial r} = 0.
\tag{B.18}
$$

or at the boundaries, i.e., $q, r \in \{0, 1\}$. First, we focus on the zero gradient equations. Simplifying (B.18) yields the following:

$$q = \frac{a_1 r^2 + a_2(1 - r^2)}{2\left(a_1 r + a_2(1 - r)\right)},$$
(B.19)

$$3\left(4\beta' + 1\right)\left(a_1 - a_2\right) r^2 + 12\beta'\left(a_1 - a_2\right) q^2$$
$$- 24\beta'\left(a_1 - a_2\right) qr + 3a_2(2r - 1) = 0. \quad \text{(B.20)}$$

If $a_1 = a_2$, then the unique solution to (B.19) and (B.20) is $q = r = \frac{1}{2}$; otherwise, by substituting (B.19) in (B.20) we have the following fourth order polynomial equation:

$$(a_1 - a_2)^3\left(\beta' + 1\right) r^4 + 4a_2\left(a_1 - a_2\right)^2\left(\beta' + 1\right) r^3 \tag{B.21}$$
$$+ \left[\left(4\beta' + 5\right) a_2^2\left(a_1 - a_2\right) - \left(2\beta' + 1\right) a_2 \times \left(a_1 - a_2\right)^2\right] r^2$$
$$+ 2a_2^2\left[a_2 - \left(2\beta' + 1\right)\left(a_1 - a_2\right)\right] r + a_2^2\left[\beta'\left(a_1 - a_2\right) - a_2\right] = 0.$$

Solving (B.21) and substituting the roots into (B.19) gives the following pairs of solutions to (B.18):

$$
\begin{aligned}
r_1 &= \frac{1}{1 + \sqrt{\frac{a_1}{a_2}}} \quad , \quad q_1 = \frac{1}{1 + \sqrt{\frac{a_1}{a_2}}}, \\
r_2 &= \frac{1}{1 - \sqrt{\frac{a_1}{a_2}}} \quad , \quad q_2 = \frac{1}{1 - \sqrt{\frac{a_1}{a_2}}}, \\
r_3 &= \frac{1 - \sqrt{\frac{\beta'}{\beta'+1}}\sqrt{\frac{a_1}{a_2}}}{1 - \frac{a_1}{a_2}} \quad , \quad q_3 = \frac{1 - \left(\frac{\sqrt{\frac{\beta'}{\beta'+1}} + \sqrt{\frac{\beta'+1}{\beta'}}}{2}\right)\sqrt{\frac{a_1}{a_2}}}{1 - \frac{a_1}{a_2}}, \\
r_4 &= \frac{1 + \sqrt{\frac{\beta'}{\beta'+1}}\sqrt{\frac{a_1}{a_2}}}{1 - \frac{a_1}{a_2}} \quad , \quad q_4 = \frac{1 + \left(\frac{\sqrt{\frac{\beta'}{\beta'+1}} + \sqrt{\frac{\beta'+1}{\beta'}}}{2}\right)\sqrt{\frac{a_1}{a_2}}}{1 - \frac{a_1}{a_2}},
\end{aligned}
$$
(B.22)

which in turn, leads to the four possible power consumption values $\overline{\mathcal{P}}(r_i, q_i)$ for $i \in \{1, 2, 3, 4\}$. By comparing all four feasible powers, it can be shown via straightforward algebraic calculations that $\overline{\mathcal{P}}(r_1, q_1)$ is always the minimum among the four candidate solutions. Therefore, the optimal FC location and partitioning are given by q_1 and $\mathbf{R} = \{R_1 = [0, r_1], R_2 = [r_1, 1]\}$, respectively. Using (B.15), the optimal AP locations can be calculated accordingly. Now, we consider the boundary case of $q, r \in \{0, 1\}$. Note that $r \in \{0, 1\}$ means that one of the regions is empty, i.e., the whole target region $\Omega = [0, 1]$ sends its data to the stronger AP. As a result, we can achieve the optimal power consumption of $\frac{\min(a_1, a_2)}{12}$ by placing the stronger AP and the FC at the centroid of Ω. The weaker AP will be used only if:

$$\overline{\mathcal{P}}(r_1, q_1) < \frac{a_1}{12} \quad , \quad \overline{\mathcal{P}}(r_1, q_1) < \frac{a_2}{12}. \tag{B.23}$$

Solving (B.23) yields the necessary and sufficient condition given in (2.12). Therefore, if the condition in (2.12) holds, both APs are useful and the optimal power consumption is given by $\overline{\mathcal{P}}(r_1, q_1)$ as it is given in (2.13); otherwise, using only the stronger AP yields a lower power consumption value given in (2.14) and the proof is complete. ∎

B.6   Proof of Proposition 5

In what follows, we demonstrate that none of the four steps in the HTTL algorithm will increase the two-tier power consumption. Given P, Q and $\mathbf{R}$, updating the index map T according to (2.6) minimizes the total power consumption, i.e., the two-tier power consumption will not increase by the first step. Moreover, given P, Q and T, Proposition 3 indicates that updating $\mathbf{R}$ according to (2.7) and (2.8) provides the best partitioning; thus, the second step of the HTTL algorithm will not increase the power consumption either. We need the following equality, which can be derived from simple algebra, to continue the proof.

$$\sum_{n:T(n)=m} b_{n,m} v_n \|p_n - q_m\|^2 = \sum_{n:T(n)=m} b_{n,m} v_n (\|p_n - q'_m\|^2 + \|q_m - q'_m\|^2), \quad \text{(B.24)}$$

where $q'_m = \frac{\sum_{n:T(n)=m} b_{n,m} p_n v_n}{\sum_{n:T(n)=m} b_{n,m} v_n}$. Now, the contribution of FC m to the total power consumption can then be rewritten as:

$$\sum_{n:T(n)=m} \int_{R_n} \left(a_n \|p_n - w\|^2 + \beta b_{n,m} \|p_n - q_m\|^2 \right) f(w) dw$$

$$= \sum_{n:T(n)=m} \int_{R_n} a_n \|p_n - w\|^2 f(w) dw + \beta \left(\sum_{n:T(n)=m} b_{n,m} v_n \right) \|q_m - q'_m\|^2$$

$$+ \beta \left(\sum_{n:T(n)=m} b_{n,m} v_n \|p_n - q'_m\|^2 \right). \tag{B.25}$$

Now, given P, $\mathbf{R}$ and T, the first and third terms in the right hand side of (B.25) are constant and moving q_m toward q'_m will not increase the power consumption in (B.25). Therefore, the third step of the HTTL algorithm will not increase the total two-tier power consumption as well. We use the following equality to simplify the calculation:

$$a_n \|p_n - w\|^2 + \beta b_{n,m} \|p_n - q_m\|^2 = (a_n + \beta b_{n,m}) \times$$

$$\left\| p_n - \frac{(a_n w + \beta b_{n,m} q_m)}{a_n + \beta b_{n,m}} \right\|^2 + \frac{\beta a_n b_{n,m}}{a_n + \beta b_{n,m}} \|w - q_m\|^2. \tag{B.26}$$

Using (B.26), for each index $n \in \mathcal{I}_A$ and the corresponding index $m = T(n)$, we can rewrite the contribution of AP n to the total power consumption as:

$$\int_{R_n} (a_n \|p_n - w\|^2 + \beta b_{n,m} \|p_n - q_m\|^2) f(w) dw$$

$$\overset{(a)}{=} \int_{R_n} \left[(a_n + \beta b_{n,m}) \left\| p_n - \frac{(a_n w + \beta b_{n,m} q_m)}{a_n + \beta b_{n,m}} \right\|^2 + \frac{\beta a_n b_{n,m}}{a_n + \beta b_{n,m}} \times \|w - q_m\|^2 \right] f(w) dw$$

$$
\overset{(b)}{=} \int_{R_n} \left[\frac{a_n^2}{a_n + \beta b_{n,m}} \times \left\| \frac{(a_n + \beta b_{n,m})p_n - \beta b_{n,m} q_m}{a_n} - w \right\|^2 \right.
$$
$$
\left. + \frac{\beta a_n b_{n,m}}{a_n + \beta b_{n,m}} \|w - q_m\|^2 \right] f(w) dw
$$
$$
\overset{(c)}{=} \int_{R_n} \left[\frac{a_n^2}{a_n + \beta b_{n,m}} \times \left(\left\| \frac{(a_n + \beta b_{n,m})p_n - \beta b_{n,m} q_m}{a_n} - c_n \right\|^2 \right. \right.
$$
$$
\left. \left. + \|c_n - w\|^2 \right) + \frac{\beta a_n b_{n,m}}{a_n + \beta b_{n,m}} \|w - q_m\|^2 \right] f(w) dw
$$
$$
\overset{(d)}{=} \int_{R_n} \left[\frac{a_n^2}{a_n + \beta b_{n,m}} \|c_n - w\|^2 + (a_n + \beta b_{n,m}) \times \right.
$$
$$
\left. \left\| p_n - \frac{a_n c_n + \beta b_{n,m} q_m}{a_n + \beta b_{n,m}} \right\|^2 + \frac{\beta a_n b_{n,m}}{a_n + \beta b_{n,m}} \|w - q_m\|^2 \right] f(w) dw
$$
$$
\overset{(e)}{=} \frac{a_n^2}{a_n + \beta b_{n,m}} \int_{R_n} \|c_n - w\|^2 f(w) dw + (a_n + \beta b_{n,m}) \|p_n - p_n'\|^2 v_n
$$
$$
+ \frac{\beta a_n b_{n,m}}{a_n + \beta b_{n,m}} \int_{R_n} \|w - q_m\|^2 f(w) dw, \tag{B.27}
$$

where $p_n' = \frac{a_n c_n + \beta b_{n,m} q_m}{a_n + \beta b_{n,m}}$. Note that Equality (a) in (B.27) comes from (B.26), and Equality (c) follows from the parallel axis theorem. Now, given Q, $\mathbf{R}$ and T, the first and third terms in the right hand side of Equality (e) in (B.27) are constants and moving p_n toward p_n' will not increase the second term in (B.27). Hence, the fourth step of the HTTL algorithm will not increase the total power consumption either. So, the HTTL algorithm generates a sequence of positive non-increasing power consumption values and thus, it converges. Note that if power consumption remains the same after an iteration of the algorithm, it means that none of the four steps has decreased the power consumption and the algorithm has already reached an optimal deployment. ∎

B.7 Proof of Lemma 4

Note that $\overline{\mathcal{P}}^{\mathcal{S}}(P, \mathbf{R})$ defined in (2.1) is the distortion of a one-tier quantizer with parameters $a_1, \ldots, a_N$, node positioning $P = (p_1, \ldots, p_N)$ and partitioning $\mathbf{R} = (R_1, \ldots, R_N)$; thus, the

minimum value that $\overline{\mathcal{P}}^{\mathcal{S}}(P, \mathbf{R})$ can achieve is D_N given in (2.15), i.e., $\overline{\mathcal{P}}^{\mathcal{S}} \in [D_N, +\infty)$ which is the domain of the function $A(s)$.

Let $\mathcal{F}(s)$ be the set of all feasible solutions for the power pair $(s, A(s))$. We can rewrite (2.3) as:

$$A(s) = \inf_{(P,Q,\mathbf{R},T) \in \mathcal{F}(s)} \overline{\mathcal{P}}^{\mathcal{A}}(P, Q, \mathbf{R}, T). \tag{B.28}$$

It is self-evident that for two values of s_1 and s_2 such that $D_N \leq s_1 < s_2$, we have $\mathcal{F}(s_1) \subseteq \mathcal{F}(s_2)$, which implies that $A(s_1) \geq A(s_2)$, i.e., $A(s)$ is a non-increasing function.

Without loss of generality, we assume that $a_1 \leq a_2 \leq \ldots \leq a_N$. If $s \in [D_M, +\infty)$, then $A(s) = 0$ since if $X^* = (x_1^*, \ldots, x_M^*)$ and $\mathbf{R}^* = (R_1^*, \ldots, R_M^*)$ is the optimal deployment that achieves D_M in (2.15), then the deployment $(P, Q, \mathbf{R}, T)$ where $P = (x_1^*, \ldots, x_M^*, x_1^*, x_1^*, \ldots, x_1^*)$, $Q = (x_1^*, \ldots, x_M^*)$, $\mathbf{R} = (R_1^*, \ldots, R_M^*, \varnothing, \varnothing, \ldots, \varnothing)$ and $T^*(i) = i$ for each $i \in \mathcal{I}_\mathcal{B}$ and $T^*(i) = 1$ for each $i \in \mathcal{I}_\mathcal{A} - \mathcal{I}_\mathcal{B}$ is a feasible solution for which $\overline{\mathcal{P}}^{\mathcal{S}}(P, \mathbf{R}) = D_M \leq s$ and $A(s) = 0$. If $s \in [D_N, D_M)$, then the inequality $\overline{\mathcal{P}}^{\mathcal{S}}(P, \mathbf{R}) \leq s$ implies that $\overline{\mathcal{P}}^{\mathcal{S}}(P, \mathbf{R}) < D_M$, i.e., optimal APs should have at least $M + 1$ different positions; therefore, the optimal AP power cannot be zero and the proof is complete. ∎

B.8   Proof of Lemma 5

Note that the pair $(s, \mathbf{R})$ belongs to the domain of $A(s, \mathbf{R})$ if and only if there exists a node positioning P such that $\overline{\mathcal{P}}^{\mathcal{S}}(P, \mathbf{R}) \leq s$. Since we have $\overline{\mathcal{P}}^{\mathcal{S}}(P, \mathbf{R}) \geq \mathcal{H}(\mathbf{R})$ for any fixed partitioning $\mathbf{R}$, the domain of the function $A(s, \mathbf{R})$ is $\{(s, \mathbf{R}) | s \geq \mathcal{H}(\mathbf{R})\}$.

First, we show that $\mathcal{J}(\mathbf{R})$ is the minimum value of the quantity $\sum_{n=1}^{N} \int_{R_n} a_n \|x - w\|^2 f(w) dw$ for a fixed $\mathbf{R}$. Using parallel axis theorem, we have:

$$\sum_{n=1}^{N} \int_{R_n} a_n \|x - w\|^2 f(w) dw =$$

$$\sum_{n=1}^{N} a_n \|x - c_n\|^2 v_n + \sum_{n=1}^{N} \int_{R_n} a_n \|c_n - w\|^2 f(w) dw, \quad \text{(B.29)}$$

where c_n is the centroid of the region R_n. Taking the derivative of (B.29) yields:

$$\frac{\partial}{\partial x} \sum_{n=1}^{N} \int_{R_n} a_n \|x - w\|^2 f(w) dw = \sum_{n=1}^{N} 2a_n (x - c_n) v_n = 0, \quad \text{(B.30)}$$

i.e., $x^* = \frac{\sum_{n=1}^{N} a_n v_n c_n}{\sum_{n=1}^{N} a_n v_n}$ where v_n is the volume of R_n. Substituting x^* into (B.29) yields:

$$\mathcal{J}(\mathbf{R}) = \min_x \sum_{n=1}^{N} \int_{R_n} a_n \|x - w\|^2 f(w) dw. \quad \text{(B.31)}$$

If $s \in [\mathcal{J}(\mathbf{R}), +\infty)$ then $A(s, \mathbf{R}) = 0$ because for the deployment $P = (p_1, \ldots, p_N) = (x^*, \ldots, x^*)$ and $Q = (q) = (x^*)$, we have $\overline{\mathcal{P}}^{\mathcal{S}}(P, \mathbf{R}) = \mathcal{J}(\mathbf{R}) \leq s$ and $\overline{\mathcal{P}}^{\mathcal{A}}(P, Q, \mathbf{R}, T) = 0$. Now, we determine the value of $A(s, \mathbf{R})$ for $s \in [\mathcal{H}(\mathbf{R}), \mathcal{J}(\mathbf{R}))$. We have:

$$\overline{\mathcal{P}}^{\mathcal{A}}(P, Q, \mathbf{R}, T) = \sum_{n=1}^{N} \int_{R_n} b_{n,1} \|p_n - q\|^2 f(w) dw$$

$$= \sum_{n=1}^{N} b_{n,1} \|p_n - q\|^2 v_n$$

$$= \kappa \sum_{n=1}^{N} a_n \|p_n - q\|^2 v_n$$

$$= \kappa \sum_{n=1}^{N} \|p_n \sqrt{a_n v_n} - q \sqrt{a_n v_n}\|^2$$

$$= \kappa \times \|\tilde{\mathbf{p}} - \tilde{\mathbf{q}}\|^2, \quad \text{(B.32)}$$

where $\tilde{\mathbf{p}} = \left(p_1 \sqrt{a_1 v_1}, \ldots, p_N \sqrt{a_N v_N}\right)$ and $\tilde{\mathbf{q}} = \left(q \sqrt{a_1 v_1}, \ldots, q \sqrt{a_N v_N}\right)$. Similarly, we can

rewrite the Sensor-power function as:

$$\overline{\mathcal{P}}^{\mathcal{S}}(P, \mathbf{R}) = \sum_{n=1}^{N} \int_{R_n} a_n \|p_n - w\|^2 f(w) dw$$

$$= \sum_{n=1}^{N} a_n \|p_n - c_n\|^2 v_n + \mathcal{H}(\mathbf{R})$$

$$= \sum_{n=1}^{N} \|p_n \sqrt{a_n v_n} - c_n \sqrt{a_n v_n}\|^2 + \mathcal{H}(\mathbf{R}) \qquad \text{(B.33)}$$

$$= \|\tilde{\mathbf{p}} - \tilde{\mathbf{c}}\|^2 + \mathcal{H}(\mathbf{R}),$$

where $\tilde{\mathbf{c}} = \left(c_1 \sqrt{a_1 v_1}, \ldots, c_N \sqrt{a_N v_N}\right)$. Note that $\mathcal{H}(\mathbf{R})$ is a constant since $\mathbf{R}$ is fixed. Therefore, we have:

$$A(s, \mathbf{R}) = \inf_{(\tilde{\mathbf{p}}, \tilde{\mathbf{q}}) : \|\tilde{\mathbf{p}} - \tilde{\mathbf{c}}\|^2 \leq (s - \mathcal{H}(\mathbf{R}))} \kappa \times \|\tilde{\mathbf{p}} - \tilde{\mathbf{q}}\|^2. \qquad \text{(B.34)}$$

Note that for any fixed value of $\tilde{\mathbf{q}}$, (B.34) implies that we want to minimize the distance from the point $\tilde{\mathbf{p}}$ to $\tilde{\mathbf{q}}$ while it remains within a radius of $\sqrt{s - \mathcal{H}(\mathbf{R})}$ of the point $\tilde{\mathbf{c}}$. By using a simple geometric reasoning, it can be shown that $\tilde{\mathbf{p}}$ lies on the segment connecting $\tilde{\mathbf{c}}$ to $\tilde{\mathbf{q}}$, i.e., there exists a coefficient $\lambda \geq 0$ for which we have:

$$\tilde{\mathbf{p}} = \frac{\tilde{\mathbf{q}} + \lambda \tilde{\mathbf{c}}}{1 + \lambda}, \qquad \text{(B.35)}$$

i.e., for any $\tilde{\mathbf{q}}$, the constraint in (B.34) is equivalent to:

$$\lambda : (1 + \lambda)^2 \geq \frac{\|\tilde{\mathbf{q}} - \tilde{\mathbf{c}}\|^2}{s - \mathcal{H}(\mathbf{R})}. \qquad \text{(B.36)}$$

Therefore, (B.34) can be rewritten as:

$$A(s, \mathbf{R}) = \inf_{Q} \inf_{\lambda : (1+\lambda)^2 \geq \frac{\|\tilde{\mathbf{q}} - \tilde{\mathbf{c}}\|^2}{s - \mathcal{H}(\mathbf{R})}} \kappa \times \left\| \frac{\tilde{\mathbf{q}} + \lambda \tilde{\mathbf{c}}}{1 + \lambda} - \tilde{\mathbf{q}} \right\|^2$$

$$= \inf_{\lambda:(1+\lambda)^2 \geq \frac{\sum_{n=1}^{N} a_n \|q - c_n\|^2 v_n}{s - \mathcal{H}(\mathbf{R})}} \inf_{q} G(q, \lambda), \tag{B.37}$$

where:

$$G(q, \lambda) = \kappa \times \sum_{n=1}^{N} a_n \left\| \frac{q + \lambda c_n}{1 + \lambda} - q \right\|^2 v_n$$

$$= \kappa \times \left(\frac{\lambda}{1 + \lambda} \right)^2 \sum_{n=1}^{N} a_n \|c_n - q\|^2 v_n. \tag{B.38}$$

Taking the derivative of $G(q)$ w.r.t. the FC location q yields:

$$\frac{\partial G(q, \lambda)}{\partial q} = \kappa \times \left(\frac{\lambda}{1 + \lambda} \right)^2 \sum_{n=1}^{N} 2 a_n v_n (q - c_n) = 0, \tag{B.39}$$

i.e., $q^* = \frac{\sum_{n=1}^{N} a_n v_n c_n}{\sum_{n=1}^{N} a_n v_n}$. By substituting q^* into (B.37), we have:

$$A(s, \mathbf{R}) = \inf_{\lambda:\lambda \geq \sqrt{\frac{\sum_{n=1}^{N} a_n \|q^* - c_n\|^2 v_n}{s - \mathcal{H}(\mathbf{R})} - 1}} G(q^*, \lambda). \tag{B.40}$$

Since $G(q^*, \lambda)$ depends on λ through the coefficient $\left(\frac{\lambda}{1+\lambda} \right)^2$ that increases with λ, the infimum in (B.40) occurs for:

$$\begin{aligned} \lambda^* &= \sqrt{\frac{\sum_{n=1}^{N} a_n \|q^* - c_n\|^2 v_n}{s - \mathcal{H}(\mathbf{R})} - 1} \\ &= \sqrt{\frac{\mathcal{J}(\mathbf{R}) - \mathcal{H}(\mathbf{R})}{s - \mathcal{H}(\mathbf{R})} - 1}, \end{aligned} \tag{B.41}$$

where the second equality follows from the parallel axis theorem. Substituting λ^* into (B.40) yields the formula in (2.17) for $A(s, \mathbf{R})$ and the proof is complete. ∎

B.9   Proof of Lemma 6

Note that the constrained optimization in (2.3) is equivalent to the unconstrained optimization in (2.5). As we showed earlier in Appendix B.5, if the condition in (2.12) holds, the optimal partitioning is two closed intervals $[0, r^*]$ and $[r^*, 1]$ where the FC is located at $r^* = q^* = \frac{1}{1+\sqrt{\frac{a_1}{a_2}}}$, in which case we have:

$$
\mathcal{J}(\mathbf{R}) - \mathcal{H}(\mathbf{R}) = \sum_{n=1}^{2} a_n \|q^* - c_n\|^2 v_n
$$

$$
= \frac{1}{4} \times \left[a_1 q^{*3} + a_2 (1-q^*)^3 \right], \tag{B.42}
$$

$$
s - \mathcal{H}(\mathbf{R}) = s - \int_0^{q^*} a_1 \left\| \frac{q^*}{2} - w \right\|^2 f(w) dw - \int_{q^*}^1 a_2 \left\| \frac{1+q^*}{2} - w \right\|^2 f(w) dw
$$

$$
= s - \frac{1}{12} \left[a_1 q^{*3} + a_2 (1-q^*)^3 \right]. \tag{B.43}
$$

Substituting (B.42) and (B.43) into (2.17) yields (2.19) for $\frac{1}{12} \left(\frac{\sqrt{a_1 a_2}}{\sqrt{a_1} + \sqrt{a_2}} \right)^2 \leq s \leq \frac{1}{3} \left(\frac{\sqrt{a_1 a_2}}{\sqrt{a_1} + \sqrt{a_2}} \right)^2$. However, if the condition in (2.12) does not hold, the optimal partitioning is when the region corresponding to the weaker AP is empty, and both FC q and the stronger AP are located at the centroid of the target space; hence, $A(s) = 0$ and $\overline{\mathcal{P}}^{\mathcal{S}}(P, \mathbf{R}) = \frac{\min(a_1, a_2)}{12}$. Since $\frac{\min(a_1, a_2)}{12} \leq \frac{1}{3} \left(\frac{\sqrt{a_1 a_2}}{\sqrt{a_1} + \sqrt{a_2}} \right)^2$ with equality if and only if $a_1 = a_2$, (2.19) is only valid for $\frac{1}{12} \left(\frac{\sqrt{a_1 a_2}}{\sqrt{a_1} + \sqrt{a_2}} \right)^2 \leq s < \frac{\min(a_1, a_2)}{12}$, and $A(s) = 0$ for $s \geq \frac{\min(a_1, a_2)}{12}$. ∎

B.10   Proof of Proposition 6

In what follows, we prove that none of the four steps in the Limited-HTTL algorthim will increase the two-tier power consumption. Note that APs in the set $\{n | T(n) = -1\}$ are nei-

ther used for target region partitioning, nor they contribute to the total power consumption; hence, given P, Q and R, updating the index map T according to (2.23) will not increase the power consumption. Furthermore, partitioning the target region according to the generalized Voronoi diagram is the best partitioning according to Proposition 3, and the two-tier power consumption will not be increased by the second stage of Limited-HTTL Algorithm.

Next, for a given P, R and T, (B.25) indicates that decreasing the distance between q_m and $q'_m = \frac{\sum_{n:T(n)=m} b_{n,m} p_n v_n}{\sum_{n:T(n)=m} b_{n,m} v_n}$ will decrease the two-tier power consumption. Note that moving FC m to $\widehat{q}_m$ will not increase the power consumption since $\|\widehat{q}_m - q'_m\| \leq \|q_m - q'_m\|$, and $\widehat{q}_m$ is still in the communication range of APs associated to FC m. Finally, (B.27) implies that decreasing the distance between p_n and $p'_n = \frac{a_n c_n + \beta b_{n,m} q_m}{a_n + \beta b_{n,m}}$ will decrease the two-tier power consumption. Note that moving AP n to $\widehat{p}_n$ will not increase the power consumption since $\|\widehat{p}_n - p'_n\| \leq \|p_n - p'_n\|$, and $\widehat{p}_n$ is still in the communication range of the FC $q_{T(n)}$. Since none of the above four stages will increase the power consumption, Limited-HTTL Algorithm generates a sequence of positive non-increasing power consumption values and thus, it converges. ∎

Appendix C

Supplementary Proofs for Chapter 3

C.1 Proof of Theorem 3.1

Using parallel axis theorem, we can rewrite the cost function in (3.5) as:

$$
\begin{aligned}
D(\mathbf{P}, \mathbf{W}, \mathbf{S}) = & \sum_{i=1}^{N} \int_{W_i} \|c_i - \omega\|^2 f(\omega) d\omega + \|p_i - c_i\|^2 v_i \\
& + \lambda \rho \sum_{i=1}^{N} \sum_{j=1}^{N} F_{i,j} + \lambda \beta \sum_{i=1}^{N} \sum_{j=1}^{N+M} \|p_i - p_j\|^2 F_{i,j},
\end{aligned}
\tag{C.1}
$$

where $F_{i,j} = F_{i,j}(\mathbf{W}, \mathbf{S})$, $v_i = \int_{W_i} f(\omega) d\omega$ is the Lebesgue measure (volume) of W_i and $c_i = \frac{\int_{W_i} \omega f(\omega) d\omega}{\int_{W_i} f(\omega) d\omega}$ is the centroid of W_i. Let $\mathbf{P}^* = (p_1^*, \ldots, p_{N+M}^*)^T$, $\mathbf{W}^* = (W_1^*, \ldots, W_N^*)^T$, and $\mathbf{S}^* = [s_{i,j}^*]$ denote, respectively, the optimal node deployment, cell partitioning and normalized flow matrix. According to [11], each cell in the power diagram is either empty or a convex polygon; thus, we can take the gradient of the objective function $D(\mathbf{P}, \mathbf{W}, \mathbf{S})$ using Proposition A.1. in [21]. It is self-evident that the cost function in (3.5) is continuously

differentiable. Therefore, $D(\mathbf{P}, \mathbf{W}, \mathbf{S})$ achieves zero-gradient at the optimal point $(\mathbf{P}^*, \mathbf{W}^*, \mathbf{S}^*)$. The partial derivative of (C.1) with respect to p_i is provided in (C.2), on top of the next page. By solving the zero-gradient equation, we obtain:

$$
\frac{\partial D(\mathbf{P}, \mathbf{W}, \mathbf{S})}{\partial p_i} = \begin{cases} 2(p_i - c_i)v_i + 2\lambda\beta \sum\limits_{j=1}^{N+M} (p_i - p_j)F_{i,j} + 2\lambda\beta \sum\limits_{j=1}^{N} (p_i - p_j)F_{j,i}, & \forall i \in \mathcal{I}_S \\ 2\lambda\beta \sum\limits_{j=1}^{N} (p_i - p_j)F_{j,i}, & \forall i \in \mathcal{I}_F \end{cases}
$$

$$(C.2)$$

$$
p_i^* = \begin{cases} \dfrac{c_i^* v_i^* + \lambda\beta \sum\limits_{j=1}^{N+M} F_{i,j}^* p_j^* + \lambda\beta \sum\limits_{j=1}^{N} F_{j,i}^* p_j^*}{v_i^* + \lambda\beta \left(\sum\limits_{j=1}^{N+M} F_{i,j}^* + \sum\limits_{j=1}^{N} F_{j,i}^* \right)}, & i \in \mathcal{I}_S \\ \dfrac{\sum\limits_{j=1}^{N} F_{j,i}^* p_j^*}{\sum\limits_{j=1}^{N} F_{j,i}^*}, & i \in \mathcal{I}_F \end{cases}
$$

$$(C.3)$$

where v_i^* and c_i^* are, respectively, the volume and centroid of W_i^*, and $F_{i,j}^* = F_{i,j}(\mathbf{W}^*, \mathbf{S}^*)$.

As shown at the beginning of Sec. 3.3, given the optimal deployment $\mathbf{P}^*$ and the optimal normalized flow matrix $\mathbf{S}^*$, the optimal cell partitioning is given by the power diagram $\mathbf{W}^* = \mathcal{V}(\mathbf{P}^*, \mathbf{S}^*)$, indicating (3.16). Similarly, given the optimal deployment $\mathbf{P}^*$ and the optimal cell partitioning $\mathbf{W}^*$, the optimal normalized flow matrix is $\mathbf{S}^* = \mathcal{R}(\mathbf{P}^*, \mathbf{W}^*)$, indicating (3.17). Substituting (3.16) and (3.17) into (C.3), we get (3.14) and (3.15) and the proof is complete. ∎

C.2 Proof of Theorem 3.2

Note that when $\mathbf{W}$, $\mathbf{S}$, and $\{p_j\}_{j \neq i}$ are fixed, the cost function in (C.1) is a convex function of p_i; thus, by solving the zero-gradient equation, we have the following unique minimizer:

$$
p_i = \begin{cases} \dfrac{c_i v_i + \lambda \beta \sum\limits_{j=1}^{N+M} F_{i,j} p_j + \lambda \beta \sum\limits_{j=1}^{N} F_{j,i} p_j}{v_i + \lambda \beta \left(\sum\limits_{j=1}^{N+M} F_{i,j} + \sum\limits_{j=1}^{N} F_{j,i} \right)}, & i \in \mathcal{I}_S \\[4ex] \dfrac{\sum\limits_{j=1}^{N} F_{j,i} p_j}{\sum\limits_{j=1}^{N} F_{j,i}}, & i \in \mathcal{I}_F \end{cases}
\tag{C.4}
$$

where c_i and v_i are centroid and volume of W_i, respectively. Therefore, moving sensors and FCs according to Lines 10 and 13 of Algorithm 1 does not increase the cost function. Since $\mathcal{R}(\mathbf{P}, \mathbf{W})$ is the optimal normalized flow matrix for a given node deployment $\mathbf{P}$ and cell partitioning $\mathbf{W}$, updating $\mathbf{S}$ according to Line 15 of Algorithm 1 does not increase the cost function either. As mentioned earlier, given the node deployment $\mathbf{P}$ and normalized flow matrix $\mathbf{S}$, the optimal cell partitioning is given by the power diagram $\mathcal{V}(\mathbf{P}, \mathbf{S})$; hence, updating the cell partitioning according to Line 17 of Algorithm 1 also does not increase the cost function. Since the parameters $\mathbf{P}$, $\mathbf{W}$ and $\mathbf{S}$ are updated only in Lines 10, 13, 15 and 17 of RL Algorithm, the cost function is non-increasing. In addition, the cost function is lower bounded by 0, i.e., $D(\mathbf{P}, \mathbf{W}, \mathbf{S}) \geq 0$. As a result, RL Algorithm is an iterative improvement algorithm and it converges. ∎

Appendix D

Supplementary Proofs for Chapter 4

D.1 Proof of Lemma 7

The AP power coefficient $g_n(\mathbf{P}, \mathbf{S})$ defined in Eq. (4.8) is the power consumption for transmitting 1 bit data from AP n to the FCs. This includes both the transmission power at each node, including AP n, on the paths connecting AP n to the FCs, and the receiver power at each node, excluding AP n, on the paths connecting AP n to the FCs. Since $R_b \int_{W_n} f(\omega) d\omega$ is the total amount of data collected by AP n from sensors within the region W_n in a unit time, the term $g_n(\mathbf{P}, \mathbf{S}) R_b \int_{W_n} f(\omega) d\omega$ is the required communication power for transmitting the sensory data collected within the region W_n from AP n to the FCs. Hence, the left-hand-side of Eq. (4.10) is the required communication power for transmitting the sensory data collected within the target region from APs to FCs. This can be decomposed into the APs' total transmission power in addition to the required receiver power for the data to reach FCs from AP nodes. This proves Eq. (4.10) since the right-hand-side of Eq. (4.10) can be rewritten as $\overline{\mathcal{P}}_{\mathcal{A}}^{T} + \sum_{i=1}^{N} \sum_{j=1}^{N} \rho_j F_{i,j}(\mathbf{W}, \mathbf{S})$, i.e. the sum of APs' total transmission power and the receiver power for all links (i, j) connecting AP i and AP j. ∎

D.2 Proof of Proposition 7

Using Eq. (4.11), we have:

$$
\begin{aligned}
\mathcal{D}\left(\mathbf{P}, \mathbf{W}, \mathbf{S}\right) &= \sum_{n=1}^{N} \int_{W_n} \left(\eta_n \|p_n - \omega\|^2 R_b + \lambda g_n\left(\mathbf{P}, \mathbf{S}\right) R_b + \lambda \rho_n R_b \right) f(\omega) d\omega \\
&\geq \sum_{n=1}^{N} \int_{W_n} \min_{j} \left(\eta_j \|p_j - \omega\|^2 R_b + \lambda g_j\left(\mathbf{P}, \mathbf{S}\right) R_b + \lambda \rho_j R_b \right) f(\omega) d\omega \\
&= \int_{\Omega} \min_{j} \left(\eta_j \|p_j - \omega\|^2 R_b + \lambda g_j\left(\mathbf{P}, \mathbf{S}\right) R_b + \lambda \rho_j R_b \right) f(\omega) d\omega \\
&= \sum_{n=1}^{N} \int_{\mathcal{V}_n} \min_{j} \left(\eta_j \|p_j - \omega\|^2 R_b + \lambda g_j\left(\mathbf{P}, \mathbf{S}\right) R_b + \lambda \rho_j R_b \right) f(\omega) d\omega \\
&= \sum_{n=1}^{N} \int_{\mathcal{V}_n} \left(\eta_n \|p_n - \omega\|^2 R_b + \lambda g_n\left(\mathbf{P}, \mathbf{S}\right) R_b + \lambda \rho_n R_b \right) f(\omega) d\omega \\
&= \mathcal{D}\left(\mathbf{P}, \mathcal{V}\left(\mathbf{P}, \mathbf{S}\right), \mathbf{S}\right).
\end{aligned}
\tag{D.1}
$$

Hence, the generalized Voronoi diagram provides the optimal cell partitioning for any given node deployment $\mathbf{P}$ and normalized flow matrix $\mathbf{S}$. ∎

D.3 Proof of Proposition 8

Eq. (4.19) is a direct implication of Proposition 7. Eq. (4.20) is directly followed from Eq. (4.15). Here, we prove Eq. (4.18) for the optimal locations of APs and FCs. First, we study the shape of the Voronoi regions in (4.12). Let $\mathcal{B}(c, r) = \{\omega | \|\omega - c\| \leq r\}$ be a disk centered at c with radius r in two-dimensional space. In particular, $\mathcal{B}(c, r) = \varnothing$ when $r < 0$. Let $\mathcal{HS}(a, b) = \{\omega | a \cdot \omega + b \leq 0\}$ be a half space, where $a \in \mathbb{R}^2$ is a vector and $b \in \mathbb{R}$ is a constant. For $i, j \in \mathcal{I}_A$, we define

$$
\mathcal{V}_{ij}(\mathbf{P}, \mathbf{S}) \triangleq \{\omega | \eta_i \|p_i - \omega\|^2 + \lambda g_i\left(\mathbf{P}, \mathbf{S}\right) + \lambda \rho_i \leq \eta_j \|p_j - \omega\|^2 + \lambda g_j\left(\mathbf{P}, \mathbf{S}\right) + \lambda \rho_j\} \tag{D.2}
$$

to be the pairwise Voronoi region of AP i where only APs i and j are considered. Then, AP i's Voronoi region can be represented as $\mathcal{V}_i(\mathbf{P}, \mathbf{S}) = \left[\bigcap_{j \neq i} \mathcal{V}_{ij}(\mathbf{P}, \mathbf{S})\right] \bigcap \Omega$. By expanding (D.2) and straightforward algebraic calculations, the pairwise Voronoi region $\mathcal{V}_{ij}$ is derived as:

$$
V_{ij} = \Omega \cap
\begin{cases}
\mathcal{HS}\left(a_{ij}, b_{ij}\right) & , \eta_i = \eta_j \\[1mm]
\mathcal{B}\left(c_{ij}, r_{ij}\right) & , \eta_i > \eta_j, L_{ij} \geq 0 \\[1mm]
\varnothing & , \eta_i > \eta_j, L_{ij} < 0 \\[1mm]
\mathcal{B}^c\left(c_{ij}, r_{ij}\right) & , \eta_i < \eta_j, L_{ij} \geq 0 \\[1mm]
\mathbb{R}^2 & , \eta_i < \eta_j, L_{ij} < 0
\end{cases}
\tag{D.3}
$$

where $a_{ij} = \eta_j p_j - \eta_i p_i$, $b_{ij} = \frac{\left(\eta_i \|p_i\|^2 - \eta_j \|p_j\|^2 + \lambda g_i(\mathbf{P},\mathbf{S}) + \lambda \rho_i - \lambda g_j(\mathbf{P},\mathbf{S}) - \lambda \rho_j\right)}{2}$, $c_{ij} = \frac{\eta_i p_i - \eta_j p_j}{\eta_i - \eta_j}$, $L_{ij} = \frac{\eta_i \eta_j \|p_i - p_j\|^2}{(\eta_i - \eta_j)^2} - \lambda \times \frac{g_i(\mathbf{P},\mathbf{S}) + \rho_i - g_j(\mathbf{P},\mathbf{S}) - \rho_j}{(\eta_i - \eta_j)}$, $r_{ij} = \sqrt{\max\left(L_{ij}, 0\right)}$, and $\mathcal{B}^c(c_{ij}, r_{ij})$ is the complementary of $\mathcal{B}(c_{ij}, r_{ij})$. Note that for two distinct indices such as $i, j \in \mathcal{I}_\mathcal{A}$, if $\eta_i > \eta_j$ and $L_{ij} < 0$, then two regions $\Omega \cap \mathcal{B}(c_{ij}, r_{ij})$ and $\varnothing$ differ only in the point c_{ij}. Similarly, for $\eta_i < \eta_j$ and $L_{ij} < 0$, two regions $\Omega \cap \mathcal{B}^c(c_{ij}, r_{ij})$ and Ω differ only in the point c_{ij}. If we define:

$$
\overline{V}_k = \left[\bigcap_{i:\eta_k > \eta_i} \mathcal{B}(c_{ki}, r_{ki})\right] \bigcap \left[\bigcap_{i:\eta_k = \eta_i} \mathcal{HS}(a_{ki}, b_{ki})\right] \bigcap \left[\bigcap_{i:\eta_k < \eta_i} \mathcal{B}^c(c_{ki}, r_{ki})\right] \bigcap \Omega,
\tag{D.4}
$$

then two regions $\overline{V}_k$ and V_k differ only in finite number of points. As a result, integrals over both $\overline{V}_k$ and V_k have the same value since the density function f is continuous and differentiable, and removing finite number of points from the integral region does not change the integral value. Note that if V_k is empty, the Proposition 1 in [38] holds since the integral over an empty region is zero. If V_k is not empty, the same arguments as in Appendix A of [38] can be replicated since $\overline{V}_k$ in (D.4) is similar to (31) in [38].

Using parallel axis theorem [81], the heterogeneous multi-hop communication power con-

161

sumption can be written as:

$$
\begin{aligned}
\mathcal{D}\left(\mathbf{P}, \mathbf{W}, \mathbf{S}\right) = &\sum_{n=1}^{N} \int_{W_n} \eta_n \|c_n - \omega\|^2 R_b f(\omega) d\omega \\
&+ \sum_{n=1}^{N} \eta_n \|p_n - c_n\|^2 R_b v_n \\
&+ \lambda \sum_{i=1}^{N} \sum_{j=1}^{N+M} \beta_{i,j} \|p_i - p_j\|^2 F_{i,j}\left(\mathbf{W}, \mathbf{S}\right) \\
&+ \lambda \sum_{n=1}^{N} \rho_n \left[\sum_{i=1}^{N} F_{i,n}\left(\mathbf{W}, \mathbf{S}\right) + R_b \int_{W_n} f(\omega) d\omega \right],
\end{aligned}
\tag{D.5}
$$

where $v_n = v\left(W_n\right)$ and c_n are the volume and centroid of the region W_n, respectively. Using Proposition 1 in [38], since the optimal deployment $\mathbf{P}^*$ should have a zero gradient, we take the partial derivatives of (D.5) with respect to node locations. For each $i \in \mathcal{I}_A$, we have

$$
\frac{\partial \mathcal{D}}{\partial p_i^*} = 2\eta_i (p_i^* - c_i^*) R_b v_i^* + 2\lambda \sum_{j=1}^{N+M} \beta_{i,j}(p_i^* - p_j^*) F_{i,j}^* + 2\lambda \sum_{j=1}^{N} \beta_{j,i}(p_i^* - p_j^*) F_{j,i}^* = 0, \quad \text{(D.6)}
$$

and for each $i \in \mathcal{I}_{\mathcal{F}}$, we have

$$
\frac{\partial \mathcal{D}}{\partial p_i^*} = 2\lambda \sum_{j=1}^{N} \beta_{j,i}(p_i^* - p_j^*) F_{j,i}^* = 0.
\tag{D.7}
$$

By solving Eqs. (D.6) and (D.7), we obtain Eq. (4.18) and the proof is complete. ■

D.4   Proof of Proposition 9

Note that RL Algorithm iterates between three steps. In what follows, we show that none of these steps will increase the objective function $\mathcal{D}\left(\mathbf{P}, \mathbf{W}, \mathbf{S}\right)$. For a fixed node deployment $\mathbf{P}$ and normalized flow matrix $\mathbf{S}$, the cell partitioning $\mathbf{W}$ is updated according to Eq. (4.19) which was shown to be optimal for a given $\mathbf{P}$ and $\mathbf{S}$ in Proposition 7. Therefore, the first

step of RL Algorithm does not increase the objective function. Next, since $\mathcal{R}(\mathbf{P}, \mathbf{W})$ is the optimal normalized flow matrix for a given node deployment $\mathbf{P}$ and cell partitioning $\mathbf{W}$, the second step of RL Algorithm does not increase the objective function either. Finally, note that when $\mathbf{W}$, $\mathbf{S}$ and $\{p_j\}_{j \neq i}$ are fixed, the objective function $\mathcal{D}(\mathbf{P}, \mathbf{W}, \mathbf{S})$ in Eq. (4.4) is a convex function of the node position p_i; hence, by solving the zero-gradient equations and updating the node locations according to the Eq. (4.18), the objective function does not increase. Therefore, the objective function of RL Algorithm is nonincreasing. In addition, the objective function is lower bounded by 0, i.e., $\mathcal{D}(\mathbf{P}, \mathbf{W}, \mathbf{S}) \geq 0$. As a result, RL Algorithm is an iterative improvement algorithm and it converges. ∎

D.5   Proof of Lemma 8

Before going through the proof, we state the following lemma:

Lemma 12. *Given a set of points $q_i \in \mathbb{R}^2$ and non-negative scalar weights a_i for $i \in \{1, \cdots, K\}$, and a scalar m, the geometric locus of the point $p \in \mathbb{R}^2$ such that the equality*

$$\sum_{i=1}^{K} a_i \|p - q_i\|^2 = m \tag{D.8}$$

holds, is either an empty set, a single point, or a circle centered at the point $c = \frac{\sum_{i=1}^{K} a_i q_i}{\sum_{i=1}^{K} a_i}$.

Proof: Let $p = (p_x, p_y)$ and $q_i = (q_{i,x}, q_{i,y})$. Then, we can rewrite Eq. (D.8) as

$$\left(\sum_{i=1}^{K} a_i\right) (p_x^2 + p_y^2) - 2\left(\sum_{i=1}^{K} a_i q_{i,x}\right) p_x - 2\left(\sum_{i=1}^{K} a_i q_{i,y}\right) p_y = m - \sum_{i=1}^{K} a_i \|q_i\|^2. \tag{D.9}$$

By manipulating both sides, we can rewrite Eq. (D.9) as follows:

163

$$\left[p_x - \frac{\sum\limits_{i=1}^{K} a_i q_{i,x}}{\sum\limits_{i=1}^{K} a_i} \right]^2 + \left[p_y - \frac{\sum\limits_{i=1}^{K} a_i q_{i,y}}{\sum\limits_{i=1}^{K} a_i} \right]^2 = \frac{m - \sum\limits_{i=1}^{K} a_i \|q_i\|^2}{\sum\limits_{i=1}^{K} a_i} + \frac{\left(\sum\limits_{i=1}^{K} a_i q_{i,x}\right)^2 + \left(\sum\limits_{i=1}^{K} a_i q_{i,y}\right)^2}{\left(\sum\limits_{i=1}^{K} a_i\right)^2}.$$

(D.10)

Hence, the geometric locus of the point $p = (p_x, p_y)$ is an empty set or a single point if the right-hand-side of Eq. (D.10) is negative or zero, respectively; otherwise, the geometric locus is a circle centered at the point c with the radius r where

$$c = \frac{\sum_{i=1}^{K} a_i q_i}{\sum_{i=1}^{K} a_i},$$

(D.11)

$$r = \sqrt{\frac{m - \sum_{i=1}^{K} a_i \|q_i\|^2}{\sum_{i=1}^{K} a_i} + \frac{\left(\sum_{i=1}^{K} a_i q_{i,x}\right)^2 + \left(\sum_{i=1}^{K} a_i q_{i,y}\right)^2}{\left(\sum_{i=1}^{K} a_i\right)^2}},$$

(D.12)

and Lemma 12 is proved.   ∎

Corollary 3. *If the geometric locus in Lemma 12 is a circle centered at c with radius r, then for any point p within this circle we have $\sum_{i=1}^{K} a_i \|p - q_i\|^2 < m$, i.e. moving the point p inside this circle reduces the weighted squared sum in Eq. (D.8).*

Now, assume that there exists at least one node, say n, for which Eq. (4.27) in Lemma 8 does not hold for an optimal node deployment $\mathbf{P}^*$, cell partitioning $\mathbf{W}^*$ and normalized flow matrix $\mathbf{S}^*$, i.e. p_n^* does not lie on the segment $\overline{z_n^* \tilde{p}_n}$. We aim to find another deployment such as $\mathbf{P}'$, $\mathbf{W}'$ and $\mathbf{S}'$ so that $E(\mathbf{P}') \leq \gamma$ and $\mathcal{D}(\mathbf{P}', \mathbf{W}', \mathbf{S}') < \mathcal{D}(\mathbf{P}^*, \mathbf{W}^*, \mathbf{S}^*)$; hence, contradicting the optimality assumption of $\mathbf{P}^*$, $\mathbf{W}^*$ and $\mathbf{S}^*$, and concluding that Eq. (4.27) holds for all nodes. For this purpose, let $\mathbf{W}' = \mathbf{W}^*$, $\mathbf{S}' = \mathbf{S}^*$ and $p_i' = p_i^*$ for all $i \in \mathcal{I}_\mathcal{A} \bigcup \mathcal{I}_\mathcal{F} \backslash \{n\}$. We aim to determine the node location p_n' accordingly. Using the parallel axis theorem [81], we

can rewrite $\mathcal{D}\left(\mathbf{P}^*, \mathbf{W}^*, \mathbf{S}^*\right)$ as:

$$\mathcal{D}\left(\mathbf{P}^*, \mathbf{W}^*, \mathbf{S}^*\right) = \sum_{i=1}^{N} \int_{W_i^*} \eta_i \|c_i^* - \omega\|^2 R_b f(\omega) d\omega + \sum_{i=1}^{N} \eta_i R_b v_i^* \|p_i^* - c_i^*\|^2$$
$$+ \lambda \sum_{i=1}^{N} \sum_{j=1}^{N+M} \beta_{i,j} \|p_i^* - p_j^*\|^2 F_{i,j}\left(\mathbf{W}^*, \mathbf{S}^*\right) + \lambda \overline{\mathcal{P}}_{\mathcal{A}}^{R}\left(\mathbf{W}^*, \mathbf{S}^*\right), \qquad \text{(D.13)}$$

where v_i^* and c_i^* are the volume and centroid of the region W_i^*, respectively. In what follows, we assume that $n \in \mathcal{I}_{\mathcal{A}}$, i.e. node n is an AP. Similar proof can be carried out for $n \in \mathcal{I}_{\mathcal{F}}$. Note that Eq. (D.13) can be split as $\mathcal{D}\left(\mathbf{P}^*, \mathbf{W}^*, \mathbf{S}^*\right) = \mathcal{D}_1\left(\mathbf{P}^*, \mathbf{W}^*, \mathbf{S}^*\right) + \mathcal{D}_2\left(\mathbf{P}^*, \mathbf{W}^*, \mathbf{S}^*\right)$, where

$$\mathcal{D}_1(\mathbf{P}^*, \mathbf{W}^*, \mathbf{S}^*) = \eta_n R_b v_n^* \|p_n^* - c_n^*\|^2 + \sum_{j=1}^{N+M} \lambda \beta_{n,j} F_{n,j}^* \|p_n^* - p_j^*\|^2 + \sum_{j=1}^{N} \lambda \beta_{j,n} F_{j,n}^* \|p_n^* - p_j^*\|^2,$$

$$\text{(D.14)}$$

i.e. $\mathcal{D}_1$ includes those terms in Eq. (D.13) that involve p_n^*. In particular, regardless of the node n's position, we have $\mathcal{D}_2\left(\mathbf{P}^*, \mathbf{W}^*, \mathbf{S}^*\right) = \mathcal{D}_2\left(\mathbf{P}', \mathbf{W}', \mathbf{S}'\right)$. According to Lemma 12, the geometric locus of points such as p_n^* for which the value of $\mathcal{D}_1\left(\mathbf{P}^*, \mathbf{W}^*, \mathbf{S}^*\right)$ in Eq. (D.14) remains the same is a circle Φ_n^* centered at the point $z_n^* = z_n\left(\mathbf{P}^*, \mathbf{W}^*, \mathbf{S}^*\right)$ defined in Eq. (4.16), with radius $r_n^* = \|z_n^* - p_n^*\|$. Note that if $\|z_n^* - \tilde{p}_n\| < \|z_n^* - p_n^*\|$, then setting $p_n' = \tilde{p}_n$ not only leads to the movement energy $E\left(\mathbf{P}'\right) < E\left(\mathbf{P}^*\right)$, but also results in $\mathcal{D}_1\left(\mathbf{P}', \mathbf{W}', \mathbf{S}'\right) < \mathcal{D}_1\left(\mathbf{P}^*, \mathbf{W}^*, \mathbf{S}^*\right)$ since p_n' lies inside Φ_n^*. Therefore, we have $\mathcal{D}\left(\mathbf{P}', \mathbf{W}', \mathbf{S}'\right) < \mathcal{D}\left(\mathbf{P}^*, \mathbf{W}^*, \mathbf{S}^*\right)$ which is in contradiction with the optimality of $\mathbf{P}^*$, $\mathbf{W}^*$ and $\mathbf{S}^*$; hence, we have $\|z_n^* - \tilde{p}_n\| \geq \|z_n^* - p_n^*\|$. Let $\hat{p}_n$ be the intersection point of the circle Φ_n^* and segment $\overline{z_n^* \tilde{p}_n}$. Since $\|\tilde{p}_n - \hat{p}_n\| < \|\tilde{p}_n - p_n^*\|$, there exists an $\epsilon_n \in \mathbb{R}^+$ such that $\|\tilde{p}_n - \hat{p}_n\| + \epsilon_n < \|\tilde{p}_n - p_n^*\|$. If $p_n' = \hat{p}_n + \epsilon_n \times \frac{z_n^* - \hat{p}_n}{\|z_n^* - \hat{p}_n\|}$, then not only we have $E\left(\mathbf{P}'\right) < E\left(\mathbf{P}^*\right)$ since $E\left(\mathbf{P}^*\right) - E\left(\mathbf{P}'\right) > \zeta_n \epsilon_n > 0$, but also $\mathcal{D}_1\left(\mathbf{P}', \mathbf{W}', \mathbf{S}'\right) < \mathcal{D}_1\left(\mathbf{P}^*, \mathbf{W}^*, \mathbf{S}^*\right)$ since p_n' lies inside the circle Φ_n^*. Therefore, we have $\mathcal{D}\left(\mathbf{P}', \mathbf{W}', \mathbf{S}'\right) < \mathcal{D}\left(\mathbf{P}^*, \mathbf{W}^*, \mathbf{S}^*\right)$ which contradicts the optimality of $\mathbf{P}^*$, $\mathbf{W}^*$ and $\mathbf{S}^*$ and concludes the proof. ∎

D.6 Proof of Proposition 10

If $p_i^* = z_i^*$ for all $i \in \mathcal{I}_d$, then Eq. (4.26) implies that $E(\mathbf{P}^*) = \sum_{i \in \mathcal{I}_d} \zeta_i \|\Gamma_i^*\| \leq \gamma$; hence, Eq. (4.29) reduces to the trivial statement $p_n^* = \tilde{p}_n + \Gamma_n^*$ and the proof is complete. Therefore, we assume that there exists at least one node, say n, for which $p_n^* \neq z_n^*$. Note that if any residual movement energy is left in the optimal deployment, i.e. $E(\mathbf{P}^*) < \gamma$, then there exists an $\epsilon \in \mathbb{R}^+$ such that $E(\mathbf{P}^*) + \epsilon < \gamma$ and $\bar{p}_n = p_n^* + \epsilon \times \frac{z_n^* - p_n^*}{\|z_n^* - p_n^*\|}$ lies inside the circle centered at z_n^* and radius $\|z_n^* - p_n^*\|$. Then, according to Lemma 12 and Corollary 3, by fixing the cell partitioning, normalized flow matrix and the location of all nodes except Node n, and placing Node n at $\bar{p}_n$ we can achieve a lower total multi-hop communication power without exhausting the available movement energy, which contradicts the optimality of $\mathbf{P}^*$, $\mathbf{W}^*$ and $\mathbf{S}^*$. Therefore, $p_n^* \neq z_n^*$ implies that $E(\mathbf{P}^*) = \gamma$. Now, given the optimal node deployment $\mathbf{P}^*$, $\mathbf{W}^*$ and $\mathbf{S}^*$, we construct the node deployment $\mathbf{P}'$, $\mathbf{W}'$ and $\mathbf{S}'$ as follows. Let $\mathbf{W}' = \mathbf{W}^*$, $\mathbf{S}' = \mathbf{S}^*$ and $p_i' = p_i^*$ for all $i \in \mathcal{I}_\mathcal{A} \bigcup \mathcal{I}_\mathcal{F} \backslash \{m, n\}$. Let $\epsilon_m, \epsilon_n \in \mathbb{R}^+$ be small values and define

$$p_m' = p_m^* - \epsilon_m \times \frac{z_m^* - \tilde{p}_m}{\|z_m^* - \tilde{p}_m\|} \qquad , \qquad p_n' = p_n^* + \epsilon_n \times \frac{z_n^* - \tilde{p}_n}{\|z_n^* - \tilde{p}_n\|}. \tag{D.15}$$

To satisfy the equality $E(\mathbf{P}') = \gamma$, we have $\zeta_n \epsilon_n = \zeta_m \epsilon_m$. Now, we calculate the change in the multi-hop communication power, i.e. $\mathcal{D}(\mathbf{P}', \mathbf{W}', \mathbf{S}') - \mathcal{D}(\mathbf{P}^*, \mathbf{W}^*, \mathbf{S}^*)$. Assume that Node m is fixed at p_m^* and we move Node n from p_n^* to p_n'. Note that this movement only changes the term $\mathcal{D}_1$ defined in Eq. (D.14); thus, according to Lemma 12 and Eq. (D.10), this change is proportional to the difference between the squared radii, i.e.

$$\Delta_1 = \left[\|p_n' - z_n^*\|^2 - \|p_n^* - z_n^*\|^2 \right] \times \psi_n^*, \tag{D.16}$$

where ψ_n^* is defined in Eq. (4.30). Now, with Node n placed at p_n', we move Node m from p_m^* to p_m'. Similar to the above argument, the term Δ_2 defined as

$$\Delta_2 = \left[\|p'_m - z^*_m\|^2 - \|p^*_m - z^*_m\|^2 \right] \times \psi^*_m \tag{D.17}$$

captures the change in $\mathcal{D}$ with the assumption that Node n was located at p^*_n. Now, we take into account that Node n was located at p'_n instead of p^*_n during Node m's movement.

$$\Delta_3 = \lambda \beta_{n,m} F^*_{n,m} \times \left[\left(\|p'_n - p'_m\|^2 - \|p'_n - p^*_m\|^2 \right) - \left(\|p^*_n - p'_m\|^2 - \|p^*_n - p^*_m\|^2 \right) \right] \tag{D.18}$$

$$= \lambda \beta_{n,m} F^*_{n,m} \times \left[\left(\|p'_n - p^*_m\|^2 + \epsilon^2_m - 2\epsilon_m \|p'_n - p^*_m\| \cos \angle p'_n p^*_m p'_m - \|p'_n - p^*_m\|^2 \right) \right.$$
$$\left. - \left(\|p^*_n - p'_m\|^2 - \|p^*_n - p'_m\|^2 - \epsilon^2_m - 2\epsilon_m \|p^*_n - p'_m\| \cos \angle p^*_n p'_m \tilde{p}_m \right) \right] \tag{D.19}$$

$$= \lambda \beta_{n,m} F^*_{n,m} \times \left[2\epsilon^2_m - 2\epsilon_m \left(\|p'_n - p^*_m\| \cos \angle p'_n p^*_m p'_m - \|p^*_n - p'_m\| \cos \angle p^*_n p'_m \tilde{p}_m \right) \right] \tag{D.20}$$

$$= \lambda \beta_{n,m} F^*_{n,m} \times \left[2\epsilon^2_m - 2\epsilon_m \left(\epsilon_m - \epsilon_n \cos \theta \right) \right] \tag{D.21}$$

$$= \lambda \beta_{n,m} F^*_{n,m} \times \left[2\frac{\zeta_m}{\zeta_n} \epsilon^2_m \cos \theta \right], \tag{D.22}$$

where s and $\theta = \angle z^*_n s z^*_m$ are the intersection point and the angle between the lines $\overline{z^*_n \tilde{p}_n}$ and $\overline{z^*_m \tilde{p}_m}$, respectively. Note that in Eq. (D.18), without any loss of generality, we have assumed that the direction of the flow of data, if any, is from Node n to Node m. Moreover, Eq. (D.19) follows from the law of cosines and Eq. (D.22) follows from the equation $\zeta_n \epsilon_n = \zeta_m \epsilon_m$. Hence, we have:

$$\mathcal{D}\left(\mathbf{P}', \mathbf{W}', \mathbf{S}'\right) - \mathcal{D}\left(\mathbf{P}^*, \mathbf{W}^*, \mathbf{S}^*\right) = \Delta_1 + \Delta_2 + \Delta_3 \tag{D.23}$$
$$= \left[\frac{\zeta^2_m}{\zeta^2_n} \epsilon^2_m - 2\frac{\zeta_m}{\zeta_n} \epsilon_m \|p^*_n - z^*_n\| \right] \times \psi^*_n$$
$$+ \left[\epsilon^2_m + 2\epsilon_m \|p^*_m - z^*_m\| \right] \times \psi^*_m$$
$$+ 2\lambda \beta_{n,m} F^*_{n,m} \frac{\zeta_m}{\zeta_n} \epsilon^2_m \cos \theta.$$

Due to the optimality of $\mathbf{P}^*$, $\mathbf{W}^*$ and $\mathbf{S}^*$, Eq. (D.23) should be non-negative, or equivalently:

$$\epsilon_m \left(\frac{\zeta_m^2}{\zeta_n^2} \psi_n^* + \psi_m^* + 2\lambda\beta_{n,m} F_{n,m}^* \frac{\zeta_m}{\zeta_n} \cos\theta \right) \geq 2 \left(\frac{\zeta_m}{\zeta_n} \psi_n^* \|p_n^* - z_n^*\| - \psi_m^* \|p_m^* - z_m^*\| \right). \quad \text{(D.24)}$$

According to Eq. (4.30), the term $\lambda\beta_{n,m} F_{n,m}^*$ is included in both ψ_n^* and ψ_m^*, i.e. $\psi_n^* \geq \lambda\beta_{n,m} F_{n,m}^*$ and $\psi_m^* \geq \lambda\beta_{n,m} F_{n,m}^*$; therefore, we have:

$$\frac{\zeta_m^2}{\zeta_n^2} \psi_n^* + \psi_m^* + 2\lambda\beta_{n,m} F_{n,m}^* \frac{\zeta_m}{\zeta_n} \cos\theta \geq \frac{\zeta_m^2}{\zeta_n^2} \lambda\beta_{n,m} F_{n,m}^* + \lambda\beta_{n,m} F_{n,m}^* + 2\lambda\beta_{n,m} F_{n,m}^* \frac{\zeta_m}{\zeta_n} \cos\theta$$
$$\text{(D.25)}$$

$$\geq \lambda\beta_{n,m} F_{n,m}^* \left(\frac{\zeta_m}{\zeta_n} - 1 \right)^2 \geq 0, \quad \text{(D.26)}$$

thus, the term inside the parentheses on the left hand side of Eq. (D.24) is always non-negative. Note that if the right hand side of Eq. (D.24) is strictly positive, then we can choose a small enough ϵ_m such that the inequality in Eq. (D.24) is contradicted. Hence, we have:

$$\zeta_m \psi_n^* \|p_n^* - z_n^*\| \leq \zeta_n \psi_m^* \|p_m^* - z_m^*\|. \quad \text{(D.27)}$$

By swapping the indices m and n in Eq. (D.15) and repeating the same argument, we have:

$$\zeta_m \psi_n^* \|p_n^* - z_n^*\| \geq \zeta_n \psi_m^* \|p_m^* - z_m^*\|. \quad \text{(D.28)}$$

Eqs. (D.27) and (D.28) imply that:

$$\zeta_m \psi_n^* \|p_n^* - z_n^*\| = \zeta_n \psi_m^* \|p_m^* - z_m^*\|. \quad \text{(D.29)}$$

Note that Eq. (D.15) indicates that Eq. (D.27) holds for any n but only for a dynamic index $m \in \mathcal{I}_d$, and similarly Eq. (D.28) holds for any m but only for a dynamic index $n \in \mathcal{I}_d$. Hence, Eqs. (D.27) and (D.29) imply that $\chi_m^* \geq \chi_n^*$ if $n \in \mathcal{I}_s, m \in \mathcal{I}_d$ and $\chi_m^* = \chi_n^*$ if $n, m \in \mathcal{I}_d$, and Eq. (4.28) is proved. Now, by using Eq. (D.29) and the equality $E(\mathbf{P}^*) = \gamma$, we can write:

$$\sum_{i \in \mathcal{I}_d} \zeta_i \|\Gamma_i^*\| - \gamma = \sum_{i \in \mathcal{I}_d} \zeta_i \|p_i^* - z_i^*\| = \sum_{i \in \mathcal{I}_d} \frac{\zeta_i^2 \psi_n^*}{\zeta_n \psi_i^*} \|p_n^* - z_n^*\| = \frac{\psi_n^*}{\zeta_n} \|p_n^* - z_n^*\| \sum_{i \in \mathcal{I}_d} \frac{\zeta_i^2}{\psi_i^*}, \quad \text{(D.30)}$$

or equivalently:

$$\|p_n^* - z_n^*\| = \frac{\sum_{i \in \mathcal{I}_d} \zeta_i \|\Gamma_i^*\| - \gamma}{\frac{\psi_n^*}{\zeta_n} \sum_{i \in \mathcal{I}_d} \frac{\zeta_i^2}{\psi_i^*}}. \quad \text{(D.31)}$$

Hence, we have:

$$p_n^* = \tilde{p}_n + \frac{\Gamma_n^*}{\|\Gamma_n^*\|} (\|\Gamma_n^*\| - \|p_n^* - z_n^*\|) = \tilde{p}_n + \Gamma_n^* \left(1 - \frac{\sum_{i \in \mathcal{I}_d} \zeta_i \|\Gamma_i^*\| - \gamma}{\|\Gamma_n^*\| \times \frac{\psi_n^*}{\zeta_n} \times \sum_{i \in \mathcal{I}_d} \frac{\zeta_i^2}{\psi_i^*}} \right), \quad \text{(D.32)}$$

and the proof is complete. ∎

D.7 Proof of Proposition 11

We show that none of the steps in MERL Algorithm increases the multi-hop communication power $\mathcal{D}(\mathbf{P}, \mathbf{W}, \mathbf{S})$. Since the movement energy constraint in Eq. (4.26) does not depend on the cell partitioning and normalized flow matrix, same reasoning as in Appendix D.4 shows that updating $\mathbf{W}$ and $\mathbf{S}$ according to the generalized Voronoi diagram and Bellman-Ford Algorithm, respectively, does not increase $\mathcal{D}(\mathbf{P}, \mathbf{W}, \mathbf{S})$. In what follows, we show that updating the node deployment according to steps 4 and 5 in Algorithm 4 will not increase the objective function as well. To show this, we first need the following concepts:

Let $\mathbf{P}^k = \left(p_1^k, \cdots, p_N^k, p_{N+1}^k, \cdots, p_{N+M}^k\right)$ denote the node deployment after the k-th iteration. In particular, $\mathbf{P}^0 = \tilde{\mathbf{P}}$ is the initial deployment. We define the energy allocation after the k-th iteration as $\mathbf{E}^k = \left(e_1^k, \cdots, e_N^k, e_{N+1}^k, \cdots, e_{N+M}^k\right)$ where $e_n^k = \zeta_n \|p_n^k - \tilde{p}_n\|$ is node n's movement energy consumption. Note that after the cell partitioning using the generalized Voronoi diagram, the partitions are fixed as $\mathcal{V}\left(\mathbf{P}^{k-1}, \mathbf{S}^{k-1}\right)$. Moreover, let v_n^k and c_n^k denote the volume and centroid of $\mathcal{V}_n\left(\mathbf{P}^k, \mathbf{S}^k\right)$, respectively, and define $\Gamma_n^k = z_n^k - \tilde{p}_n$ where z_n^k is expressed as in Eqs. (4.16) and (4.17). We denote the energy consumed by moving node n from its initial location to z_n^k by $\tau_n^k = \zeta_n \|\Gamma_n^k\|$, and define $\kappa_n^k = \kappa_n\left(\mathbf{P}^k, \mathbf{S}^k\right) = \frac{\zeta_n^2}{\psi_n^k}$ where ψ_n^k is given by Eq. (4.30). Finally, we define an auxiliary function $\hat{\chi}_n^k : \mathbb{R}^{N+M} \longrightarrow \mathbb{R}$ to be $\hat{\chi}_n^k\left(\mathbf{E}\right) = \frac{\tau_n^k - e_n}{\kappa_n^k}$. Note that $\hat{\chi}_n^k$ differs from χ_n defined in Eq. (4.31) in the sense that it depends on the energy allocation $\mathbf{E}$ rather than the node deployment and data routing.

Lemma 13. *Let $\mathcal{I}_d^k$ and $\mathcal{I}_s^k$ denote the set of dynamic and static nodes after the k-th iteration of the MERL algorithm, respectively. Then, we have:*

$$\hat{\chi}_i^{k-1}\left(\mathbf{E}^k\right) = \hat{\chi}_j^{k-1}\left(\mathbf{E}^k\right), \qquad \forall i, j \in \mathcal{I}_d^k \tag{D.33}$$

$$\hat{\chi}_i^{k-1}\left(\mathbf{E}^k\right) \geq \hat{\chi}_j^{k-1}\left(\mathbf{E}^k\right), \qquad \forall i \in \mathcal{I}_d^k, j \in \mathcal{I}_s^k \tag{D.34}$$

Proof: At the end of the deployment step, dynamic node n's location in the k-th iteration is:

$$p_n^k = \tilde{p}_n + \Gamma_n^{k-1}\left(1 - \frac{\sum_{i \in \mathcal{I}_d^k} \zeta_i \|\Gamma_i^{k-1}\| - \gamma}{\|\Gamma_n^{k-1}\| \times \frac{\psi_n^{k-1}}{\zeta_n} \times \sum_{i \in \mathcal{I}_d^k} \frac{\zeta_i^2}{\psi_i^{k-1}}}\right), \tag{D.35}$$

thus, its movement energy consumption is:

$$e_n^k = \zeta_n \|p_n^k - \tilde{p}_n\| = \zeta_n \|\Gamma_n^{k-1}\| \times \left\|1 - \frac{\sum_{i \in \mathcal{I}_d^k} \zeta_i \|\Gamma_i^{k-1}\| - \gamma}{\|\Gamma_n^{k-1}\| \times \frac{\psi_n^{k-1}}{\zeta_n} \times \sum_{i \in \mathcal{I}_d^k} \frac{\zeta_i^2}{\psi_i^{k-1}}}\right\| \tag{D.36}$$

$$
= \left\| \tau_n^{k-1} - \frac{\kappa_n^{k-1} \left(\sum_{i \in \mathcal{I}_d^k} \tau_i^{k-1} - \gamma \right)}{\sum_{i \in \mathcal{I}_d^k} \kappa_i^{k-1}} \right\|, \qquad \forall n \in \mathcal{I}_d^k \tag{D.37}
$$

where $\mathcal{I}_d^k$ is the set of dynamic nodes in the k-th iteration, determined by the inner loop in steps 3 and 4 of the MERL algorithm. According to this inner loop, the term inside the vertical bars in Eq. (D.37) is positive; hence, we have:

$$
e_n^k = \tau_n^{k-1} - \frac{\kappa_n^{k-1} \left(\sum_{i \in \mathcal{I}_d^k} \tau_i^{k-1} - \gamma \right)}{\sum_{i \in \mathcal{I}_d^k} \kappa_i^{k-1}}, \qquad \forall n \in \mathcal{I}_d^k. \tag{D.38}
$$

Now, by substituting Eq. (D.38) into the definition of $\hat{\chi}_n^k$, we have:

$$
\hat{\chi}_n^{k-1} \left(\mathbf{E}^k \right) = \frac{\tau_n^{k-1} - e_n^k}{\kappa_n^{k-1}} = \frac{\left[\sum_{i \in \mathcal{I}_d^k} \tau_i^{k-1} \right] - \gamma}{\sum_{i \in \mathcal{I}_d^k} \kappa_i^{k-1}}, \qquad \forall n \in \mathcal{I}_d^k. \tag{D.39}
$$

Therefore, all $\hat{\chi}_n^{k-1} \left(\mathbf{E}^k \right)$ for dynamic nodes are the same and Eq. (D.33) is proved.

In order to prove Eq. (D.34), we assume that L_k inner iterations are performed in steps 3 and 4 of the MERL algorithm to determine the dynamic node set in the k-th iteration of the algorithm. For $l \in \{ 1, \cdots, L_k \}$, let $\mathcal{J}_l^k$ be the dynamic node set after the l-th inner iteration, where k is the iteration index of the MERL algorithm. In particular, we have $\mathcal{J}_0^k = \mathcal{I}_\mathcal{A} \bigcup \mathcal{I}_\mathcal{F}$ and:

$$
\mathcal{I}_d^k = \mathcal{J}_{L_k}^k \subsetneq \mathcal{J}_{L_k-1}^k \subsetneq \cdots \subsetneq \mathcal{J}_0^k \tag{D.40}
$$

In other words, in the l-th inner iteration, nodes within the set $\mathcal{J}_{l-1}^k - \mathcal{J}_l^k$ are removed from $\mathcal{J}_{l-1}^k$ due to their non-positive energy allocation, i.e., we have:

$$
e_j^k = \tau_j^{k-1} - \frac{\kappa_j^{k-1} \left(\sum_{i \in \mathcal{J}_{l-1}^k} \tau_i^{k-1} - \gamma \right)}{\sum_{i \in \mathcal{J}_{l-1}^k} \kappa_i^{k-1}} \leq 0, \qquad \forall j \in \mathcal{J}_{l-1}^k - \mathcal{J}_l^k \tag{D.41}
$$

hence, by rearranging the terms in Eq. (D.41), and summation over all $j \in \mathcal{J}_{l-1}^k - \mathcal{J}_l^k$, we have:

$$\left(\sum_{j \in \mathcal{J}_{l-1}^k - \mathcal{J}_l^k} \tau_j^{k-1} \right) \left(\sum_{i \in \mathcal{J}_{l-1}^k} \kappa_i^{k-1} \right) \leq \left(\sum_{j \in \mathcal{J}_{l-1}^k - \mathcal{J}_l^k} \kappa_j^{k-1} \right) \left(\sum_{i \in \mathcal{J}_{l-1}^k} \tau_i^{k-1} - \gamma \right). \tag{D.42}$$

Let the auxiliary function $\tilde{\chi}^k(\mathcal{J}) = \frac{\left(\sum_{i \in \mathcal{J}} \tau_i^k \right) - \gamma}{\sum_{i \in \mathcal{J}} \kappa_i^k}$ be a mapping from the node set $\mathcal{J}$ to the real numbers. For an inner iteration index $l \in \{1, \cdots, L_k\}$, we have:

$$\tilde{\chi}^{k-1}\left(\mathcal{J}_l^k \right) - \tilde{\chi}^{k-1}\left(\mathcal{J}_{l-1}^k \right) \tag{D.43}$$

$$= \frac{\left(\sum_{i \in \mathcal{J}_l^k} \tau_i^{k-1} \right) - \gamma}{\sum_{i \in \mathcal{J}_l^k} \kappa_i^{k-1}} - \frac{\left(\sum_{i \in \mathcal{J}_{l-1}^k} \tau_i^{k-1} \right) - \gamma}{\sum_{i \in \mathcal{J}_{l-1}^k} \kappa_i^{k-1}} \tag{D.44}$$

$$= \frac{\left(\sum_{i \in \mathcal{J}_{l-1}^k} \kappa_i^{k-1} \right) \left[\left(\sum_{i \in \mathcal{J}_l^k} \tau_i^{k-1} \right) - \gamma \right] - \left(\sum_{i \in \mathcal{J}_l^k} \kappa_i^{k-1} \right) \left[\left(\sum_{i \in \mathcal{J}_{l-1}^k} \tau_i^{k-1} \right) - \gamma \right]}{\left(\sum_{i \in \mathcal{J}_l^k} \kappa_i^{k-1} \right) \left(\sum_{i \in \mathcal{J}_{l-1}^k} \kappa_i^{k-1} \right)}$$

$$\tag{D.45}$$

$$= \frac{\left(\sum_{i \in \mathcal{J}_{l-1}^k} \kappa_i^{k-1} \right) \left[\left(\sum_{i \in \mathcal{J}_{l-1}^k} \tau_i^{k-1} \right) - \left(\sum_{i \in \mathcal{J}_{l-1}^k - \mathcal{J}_l^k} \tau_i^{k-1} \right) - \gamma \right]}{\left(\sum_{i \in \mathcal{J}_l^k} \kappa_i^{k-1} \right) \left(\sum_{i \in \mathcal{J}_{l-1}^k} \kappa_i^{k-1} \right)} \tag{D.46}$$

$$- \frac{\left[\left(\sum_{i \in \mathcal{J}_{l-1}^k} \kappa_i^{k-1} \right) - \left(\sum_{i \in \mathcal{J}_{l-1}^k - \mathcal{J}_l^k} \kappa_i^{k-1} \right) \right] \left[\left(\sum_{i \in \mathcal{J}_{l-1}^k} \tau_i^{k-1} \right) - \gamma \right]}{\left(\sum_{i \in \mathcal{J}_l^k} \kappa_i^{k-1} \right) \left(\sum_{i \in \mathcal{J}_{l-1}^k} \kappa_i^{k-1} \right)} \tag{D.47}$$

$$= \frac{\left(\sum_{i \in \mathcal{J}_{l-1}^k - \mathcal{J}_l^k} \kappa_i^{k-1} \right) \left[\left(\sum_{i \in \mathcal{J}_{l-1}^k} \tau_i^{k-1} \right) - \gamma \right] - \left(\sum_{i \in \mathcal{J}_{l-1}^k - \mathcal{J}_l^k} \tau_i^{k-1} \right) \left(\sum_{i \in \mathcal{J}_{l-1}^k} \kappa_i^{k-1} \right)}{\left(\sum_{i \in \mathcal{J}_l^k} \kappa_i^{k-1} \right) \left(\sum_{i \in \mathcal{J}_{l-1}^k} \kappa_i^{k-1} \right)} \tag{D.48}$$

$$\geq 0, \tag{D.49}$$

where the last inequality follows from Eq. (D.42). Thus, we have the following ordered sequence:

$$\tilde{\chi}^{k-1}\left(\mathcal{J}_0^k \right) \leq \tilde{\chi}^{k-1}\left(\mathcal{J}_1^k \right) \leq \cdots \leq \tilde{\chi}^{k-1}\left(\mathcal{J}_{L_k}^k \right) = \tilde{\chi}^{k-1}\left(\mathcal{I}_d^k \right) = \hat{\chi}_n^{k-1}\left(\mathbf{E}^k \right), \qquad \forall n \in \mathcal{I}_d^k. \tag{D.50}$$

Let the tentative energy allocation in the l-th inner iteration be $\tilde{\mathbf{E}}^k(l) = \left(\tilde{e}_1^k(l), \cdots, \tilde{e}_{N+M}^k(l)\right)$. The tentative movement energy consumption of node n in the l-th inner iteration is given by:

$$\tilde{e}_n^k(l) = \tau_n^{k-1} - \frac{\kappa_n^{k-1} \left[\left(\sum_{i \in \mathcal{J}_l^k} \tau_i^{k-1}\right) - \gamma\right]}{\sum_{i \in \mathcal{J}_l^k} \kappa_i^{k-1}}, \qquad \forall n \in \mathcal{J}_l^k \tag{D.51}$$

hence, we can rewrite $\tilde{\chi}^{k-1}\left(\mathcal{J}_l^k\right)$ as:

$$\tilde{\chi}^{k-1}\left(\mathcal{J}_l^k\right) = \frac{\left[\left(\sum_{i \in \mathcal{J}_l^k} \tau_i^{k-1}\right) - \gamma\right]}{\sum_{i \in \mathcal{J}_l^k} \kappa_i^{k-1}} = \frac{\tau_n^{k-1} - \tilde{e}_n^k(l)}{\kappa_n^{k-1}}, \qquad \forall n \in \mathcal{J}_l^k. \tag{D.52}$$

Note that each node $j \in \mathcal{J}_{l-1}^k - \mathcal{J}_l^k$ is removed from the dynamic node set in the l-th inner iteration of the MERL algorithm due to its non-positive tentative energy $\tilde{e}_j^k(l) \leq 0$; therefore, we have $j \in \mathcal{I}_s^k$ and its allocated movement energy consumption is $e_j^k = 0$. Then, we have:

$$\hat{\chi}_j^{k-1}\left(\mathbf{E}^k\right) = \frac{\tau_j^{k-1} - e_j^k}{\kappa_j^{k-1}} = \frac{\tau_j^{k-1}}{\kappa_j^{k-1}} \leq \frac{\tau_j^{k-1} - \tilde{e}_j^k(l)}{\kappa_j^{k-1}} = \tilde{\chi}^{k-1}\left(\mathcal{J}_l^k\right), \qquad \forall j \in \mathcal{J}_{l-1}^k - \mathcal{J}_l^k. \tag{D.53}$$

Using Eqs. (D.50) and (D.53), we have:

$$\hat{\chi}_j^{k-1}\left(\mathbf{E}^k\right) \leq \hat{\chi}_i^{k-1}\left(\mathbf{E}^k\right), \qquad \forall i \in \mathcal{I}_d^k, j \in \mathcal{J}_{l-1}^k - \mathcal{J}_l^k, l \in \{1, \cdots, L_k\}. \tag{D.54}$$

Note that the static node set $\mathcal{I}_s^k$ consists of all nodes that are removed in the inner loop, i.e. $\mathcal{I}_s = \bigcup_{l \in \{1, \cdots, L_k\}} \left(\mathcal{J}_{l-1}^k - \mathcal{J}_l^k\right)$; hence, Eq. (D.34) follows from Eq. (D.54) and the proof is finished. ∎

Lemma 14. *For a fixed cell partitioning and normalized flow matrix, the node deployment* $\mathbf{P}^k$ *given by the k-th iteration of MERL Algorithm is the unique minimizer to the objective function in Eqs. (4.25) and (4.26).*

Proof: Using parallel axis theorem [81], the objective function in the k-th iteration is:

$$\mathcal{D} = \sum_{i=1}^{N} \int_{\mathcal{V}_i^{k-1}} \eta_i \|c_i^{k-1} - \omega\|^2 R_b f(\omega) d\omega + \sum_i \eta_i R_b v_i^{k-1} \|p_i - c_i^{k-1}\|^2$$

$$+ \lambda \sum_{i=1}^{N} \sum_{j=1}^{N+M} \beta_{i,j} \|p_i - p_j\|^2 F_{i,j}^{k-1} + \lambda \overline{\mathcal{P}}_{\mathcal{A}}^{R} \left(\mathbf{W}^{k-1}, \mathbf{S}^{k-1} \right). \tag{D.55}$$

For a fixed partitioning and routing, a similar reasoning as in the proof of Lemma 8 shows that node n's optimal location at the end of k-th iteration should be placed on the segment connecting its initial location $\tilde{p}_n$ to the point z_n^{k-1} given in Eqs. (4.16) and (4.17), i.e., if we denote the node n's movement energy by e_n, we have:

$$p_n(e_n) = \tilde{p}_n + \frac{e_n}{\zeta_n} \times \frac{\Gamma_n^{k-1}}{\|\Gamma_n^{k-1}\|}, \qquad \forall n \in \mathcal{I}_{\mathcal{A}} \bigcup \mathcal{I}_{\mathcal{F}}. \tag{D.56}$$

By substituting the Eq. (D.56) into Eq. (D.55), we can rewrite the objective function as:

$$\underset{\mathbf{E}}{\text{minimize}} \, \mathcal{D}(\mathbf{E})$$

$$s.t. \qquad \left(\sum_{n=1}^{N+M} e_n \right) \leq \gamma, \qquad 0 \leq e_n \leq \zeta_n \|\Gamma_n^{k-1}\|, \quad \forall n \in \mathcal{I}_{\mathcal{A}} \bigcup \mathcal{I}_{\mathcal{F}}. \tag{D.57}$$

where:

$$\mathcal{D}(\mathbf{E}) = \sum_{i=1}^{N} \int_{\mathcal{V}_i^{k-1}} \eta_i \|c_i^{k-1} - \omega\|^2 R_b f(\omega) d\omega$$

$$+ \sum_i \eta_i R_b v_i^{k-1} \left\| \tilde{p}_i + \frac{e_i}{\zeta_i} \times \frac{\Gamma_i^{k-1}}{\|\Gamma_i^{k-1}\|} - c_i^{k-1} \right\|^2$$

$$+ \lambda \sum_{i=1}^{N} \sum_{j=1}^{N+M} \beta_{i,j} \left\| \tilde{p}_i + \frac{e_i}{\zeta_i} \times \frac{\Gamma_i^{k-1}}{\|\Gamma_i^{k-1}\|} - \tilde{p}_j - \frac{e_j}{\zeta_j} \times \frac{\Gamma_j^{k-1}}{\|\Gamma_j^{k-1}\|} \right\|^2 F_{i,j}^{k-1}$$

$$+ \lambda \overline{\mathcal{P}}_{\mathcal{A}}^{R} \left(\mathbf{W}^{k-1}, \mathbf{S}^{k-1} \right), \tag{D.58}$$

Note that the objective function in Eq. (D.57) and its constraints are convex; hence, it has a

unique minimizer for a fixed partitioning and routing. If $\left(\sum_{n=1}^{N+M} \zeta_n \|\Gamma_n^{k-1}\| \right) \leq \gamma$, *then the MERL algorithm moves each node n to z_n^{k-1} without violating the total energy constraint, indicating an optimal deployment. On the other hand, if* $\left(\sum_{n=1}^{N+M} \zeta_n \|\Gamma_n^{k-1}\| \right) > \gamma$, *then nodes will run out of movement energy before they can reach to their corresponding z_n^{k-1}, and the same reasoning as in Appendix D.6 shows that* $\left(\sum_{n=1}^{N+M} e_n \right) = \gamma$. *For the fixed partitioning and routing, let* $\mathbf{E}^* = \left(e_1^*, \cdots, e_{N+M}^* \right)$ *be the optimal energy allocation for the constrained objective function in Eq. (D.57), and let* $\mathbf{P}^* = \left(p_1^*, \cdots, p_{N+M}^* \right)$ *be the corresponding optimal deployment. Assume that the movement energy allocation $\mathbf{E}^k$ in the k-th iteration is different from the optimal one, i.e., $\mathbf{E}^* \neq \mathbf{E}^k$. Since* $\left(\sum_{n=1}^{N+M} e_n^* \right) = \left(\sum_{n=1}^{N+M} e_n^k \right) = \gamma$, *there exist two distinct indices i and j such that $0 \leq e_i^k < e_i^*$ and $0 \leq e_j^* < e_j^k$. Note that $e_j^k > 0$ indicates that $j \in \mathcal{I}_d^k$, i.e., node j is a dynamic node in the k-th iteration. Therefore, using Lemma 13 we have:*

$$\frac{\zeta_i \|\Gamma_i^{k-1}\| - e_i^*}{\frac{\zeta_i^2}{\psi_i^{k-1}}} < \frac{\zeta_i \|\Gamma_i^{k-1}\| - e_i^k}{\frac{\zeta_i^2}{\psi_i^{k-1}}} \leq \frac{\zeta_j \|\Gamma_j^{k-1}\| - e_j^k}{\frac{\zeta_j^2}{\psi_j^{k-1}}} < \frac{\zeta_j \|\Gamma_j^{k-1}\| - e_j^*}{\frac{\zeta_j^2}{\psi_j^{k-1}}}. \tag{D.59}$$

Now, we consider a new energy allocation $\overline{\mathbf{E}} = (\overline{e}_1, \cdots, \overline{e}_{N+M})$, where $\overline{e}_i = e_i^* - \epsilon$, $\overline{e}_j = e_j^* + \epsilon$ and $\overline{e}_t = e_t^*$ for all $t \in \mathcal{I}_A \bigcup \mathcal{I}_F \backslash \{i, j\}$. Note that $\left(\sum_{n=1}^{N+M} \overline{e}_n \right) = \gamma$, *and for a sufficiently small positive value of ϵ, we have $0 \leq e_i^* - \epsilon = \overline{e}_i < e_i^* \leq \zeta_i \|\Gamma_i^{k-1}\|$ and $0 \leq e_j^* < \overline{e}_j = e_j^* + \epsilon \leq e_j^k \leq \zeta_j \|\Gamma_j^{k-1}\|$, i.e., $\overline{\mathbf{E}}$ satisfies the constraints in Eq. (D.57) and it is a valid energy allocation. Similar argument as in Appendix D.6, that led to the Eq. (D.27), shows that in order for the energy allocation $\overline{\mathbf{E}}$ not to achieve a lower objective function value in Eq. (D.57) than $\mathcal{D}(\mathbf{E}^*)$, which contradicts the optimality of the movement energy allocation $\mathbf{E}^*$, we should have:*

$$\zeta_i \psi_j^{k-1} \|p_j^* - z_j^{k-1}\| \leq \zeta_j \psi_i^{k-1} \|p_i^* - z_i^{k-1}\|, \tag{D.60}$$

or equivalently:

$$\frac{\zeta_j \|p_j^* - z_j^{k-1}\|}{\frac{\zeta_j^2}{\psi_j^{k-1}}} \leq \frac{\zeta_i \|p_i^* - z_i^{k-1}\|}{\frac{\zeta_i^2}{\psi_i^{k-1}}}. \tag{D.61}$$

According to Eq. (D.56), each node $n \in \mathcal{I}_\mathcal{A} \bigcup \mathcal{I}_\mathcal{F}$ is located on the segment connecting $\tilde{p}_n$ to z_n^{k-1}; hence: we can rewrite the Eq. (D.61) as:

$$\frac{\zeta_j \|\Gamma_j^{k-1}\| - e_j^*}{\frac{\zeta_j^2}{\psi_j^{k-1}}} \leq \frac{\zeta_i \|\Gamma_i^{k-1}\| - e_i^*}{\frac{\zeta_i^2}{\psi_i^{k-1}}}. \tag{D.62}$$

But Eq. (D.62) is in contradiction with Eq. (D.59); thus, the assumption $\mathbf{E}^* \neq \mathbf{E}^k$ is wrong and we have $\mathbf{E}^* = \mathbf{E}^k$, i.e. the deployment given by the MERL algorithm is the unique minimizer of the constrained objective function and the proof is complete. ∎

Now, we have enough materials to prove the convergence of the MERL algorithm. As mentioned in the beginning of the Appendix D.7, updating the partitioning and normalized flow matrix using the generalized Voronoi diagram and Bellman-Ford Algorithm, respectively, does not increase the objective function. Now, for a fixed partitioning and routing, Lemma 14 indicates that the deployment given by the MERL algorithm is the unique minimizer of the constrained objective function, i.e., the deployment step in the MERL algorithm does not increase the objective function either. Hence, the MERL algorithm generates a sequence of positive non-increasing values for the objective function $\mathcal{D}$; thus, it converges. ∎

D.8 Proof of Proposition 12

If $p_n^* = z_n^*$ is an optimal deployment $\mathbf{P}^*$, $\mathbf{W}^*$ and $\mathbf{S}^*$, then Eq. (4.34) implies that $E_n(\mathbf{P}^*) = \zeta_n \|\Gamma_n^*\| \leq \gamma_n$. Therefore, Eq. (4.35) reduces to the trivial statement $p_n^* = \tilde{p}_n + \Gamma_n^*$ and the proof is complete. Hence, we assume that $p_n^* \neq z_n^*$. Now, if any residual movement energy is

left in Node n, i.e. if $E_n(\mathbf{P}^*) < \gamma_n$, then there exists an $\epsilon_n \in \mathbb{R}^+$ such that $E_n(\mathbf{P}^*) + \epsilon_n < \gamma_n$ and the point $\bar{p}_n = p_n^* + \epsilon_n \times \frac{z_n^* - p_n^*}{\|z_n^* - p_n^*\|}$ lies inside the circle centered at z_n^* with radius $\|z_n^* - p_n^*\|$. Then, according to Lemma 12, by fixing the cell partitioning, normalized flow matrix and the location of all nodes except Node n, and placing Node n at $\bar{p}_n$, we can achieve a lower total multi-hop communication power without exhausting the available movement energy in Node n, which contradicts the optimality of $\mathbf{P}^*$, $\mathbf{W}^*$ and $\mathbf{S}^*$. Therefore, $p_n^* \neq z_n^*$ implies that $E_n(\mathbf{P}^*) = \gamma_n$, that is

$$\zeta_n \|p_n^* - \tilde{p}_n\| = \gamma_n. \tag{D.63}$$

According to Lemma 8, we have

$$p_n^* = \delta_n \tilde{p}_n + (1 - \delta_n) z_n^*, \tag{D.64}$$

where $\delta_n \in [0, 1]$, which indicates that

$$\|p_n^* - \tilde{p}_n\| = (1 - \delta_n) \|z_n^* - \tilde{p}_n\|. \tag{D.65}$$

Eqs. (D.63) and (D.65) imply that $\delta_n = 1 - \frac{\gamma_n}{\zeta_n \|z_n^* - \tilde{p}_n\|}$. Therefore, Eq. (D.64) can be written as:

$$p_n^* = \left(1 - \frac{\gamma_n}{\zeta_n \|z_n^* - \tilde{p}_n\|}\right) \tilde{p}_n + \left(\frac{\gamma_n}{\zeta_n \|z_n^* - \tilde{p}_n\|}\right) z_n^* \tag{D.66}$$

$$= \tilde{p}_n + \left(\frac{\gamma_n}{\zeta_n \|z_n^* - \tilde{p}_n\|}\right) (z_n^* - \tilde{p}_n) \tag{D.67}$$

$$= \tilde{p}_n + \frac{\gamma_n}{\zeta_n \|\Gamma_n^*\|} \Gamma_n^*. \tag{D.68}$$

Eqs. (D.63) and (D.64) imply that $\gamma_n = \zeta_n \|p_n^* - \tilde{p}_n\| \leq \zeta_n \|z_n^* - \tilde{p}_n\| = \zeta_n \|\Gamma_n^*\|$, i.e. $\frac{\gamma_n}{\zeta_n \|\Gamma_n^*\|} \leq 1$. Therefore, Eq. (D.68) can be rewritten as $p_n^* = \tilde{p}_n + \min\left(1, \frac{\gamma_n}{\zeta_n \|\Gamma_n^*\|}\right) \Gamma_n^*$ which concludes the proof. ∎

D.9 Proof of Proposition 13

In what follows, we show that none of the three steps in LORL Algorithm will increase the communication power $\mathcal{D}(\mathbf{P}, \mathbf{W}, \mathbf{S})$. Note that the movement energy constraint in Eq. (4.34) does not depend on the cell partitioning and normalized flow matrix. Hence, it can be shown via the same argument as in Appendix D.4 that updating $\mathbf{W}$ and $\mathbf{S}$ according to the generalized Voronoi diagrams and Bellman-Ford Algorithm, respectively, does not increase $\mathcal{D}(\mathbf{P}, \mathbf{W}, \mathbf{S})$. Note that for a fixed $\mathbf{W}$, $\mathbf{S}$ and $\{p_i\}_{i \neq n}$, according to Lemma 12, the geometric locus of node n for which the objective function $\mathcal{D}(\mathbf{P}, \mathbf{W}, \mathbf{S})$ remains the same is a circle Φ_n centered at z_n with radius $\|z_n - p_n\|$. Note that the update rule in Eq. (4.35) always keeps node n in its *valid region* determined by its limited movement energy, which is a circle centered at $\tilde{p}_n$ and radius $\frac{\gamma_n}{\zeta_n}$. A simple geometric reasoning indicates that by updating the position of node n according to Eq. (4.35), node n will either remain the same or move to the point inside its valid region that is closest to the point z_n, i.e., node n will either remain on the circle Φ_n or move inside it, and the objective function $\mathcal{D}(\mathbf{P}, \mathbf{W}, \mathbf{S})$ does not increase. Since the objective function has a lower bounded, i.e. $\mathcal{D}(\mathbf{P}, \mathbf{W}, \mathbf{S}) \geq 0$, and it is nonincreasing, LORL Algorithm is in iterative improvement algorithm and it converges. ∎

Appendix E

Supplementary Proofs for Chapter 5

E.1 Proof of Proposition 14

For a fixed cell partitioning $\mathbf{W}$ and data routing $\mathbf{R}$, we can rewrite the objective function $\mathcal{D}_1$ in Eq. (5.19) using the parallel axis theorem [81] as follows:

$$
\begin{aligned}
\mathcal{D}_1(\mathbf{P}, \mathbf{Q}, \mathbf{W}, \mathbf{R}) = & \sum_{n=1}^{N} \int_{W_n} \frac{a_n}{\ln\left(\frac{1}{1-\epsilon}\right)} \|c_n - \omega\|^2 \left(2^{\frac{R_b}{B}} - 1\right) f(\omega) d\omega \\
& + \sum_{n=1}^{N} \frac{a_n}{\ln\left(\frac{1}{1-\epsilon}\right)} \|p_n - c_n\|^2 \left(2^{\frac{R_b}{B}} - 1\right) v_n \\
& + \lambda \sum_{n=1}^{N} \sum_{m=1}^{M} \frac{b_{n,m}}{\ln\left(\frac{1}{1-\epsilon}\right)} \|p_n - q_m\|^2 \left(2^{\frac{F_{n,m}}{B}} - 1\right),
\end{aligned}
\tag{E.1}
$$

where v_n and c_n are the volume and centroid of region W_n, respectively. Since the optimal deployment satisfies the zero gradient condition, we take the partial derivatives of Eq. (E.1) with respect to AP and BS locations as follows. For each $n \in \mathcal{I}_{AP}$, we have:

$$\frac{\partial \mathcal{D}_1}{\partial p_n^*} = \frac{2a_n}{\ln\left(\frac{1}{1-\epsilon}\right)}\left(p_n^* - c_n\right)\left(2^{\frac{R_b}{B}} - 1\right)v_n + \lambda \sum_{m=1}^{M} \frac{2b_{n,m}}{\ln\left(\frac{1}{1-\epsilon}\right)}\left(p_n^* - q_m^*\right)\left(2^{\frac{F_{n,m}}{B}} - 1\right) = 0.$$

(E.2)

By solving Eq. (E.2), we directly obtain Eq. (5.20). Now, for each $m \in \mathcal{I}_{BS}$, we have:

$$\frac{\partial \mathcal{D}_1}{\partial q_m^*} = \lambda \sum_{n=1}^{N} \frac{2b_{n,m}}{\ln\left(\frac{1}{1-\epsilon}\right)}\left(q_m^* - p_n^*\right)\left(2^{\frac{F_{n,m}}{B}} - 1\right) = 0.$$

(E.3)

By solving Eq. (E.3), we obtain Eq. (5.21) and the proof is complete. ∎

E.2 Proof of Lemma 9

First, we prove the following lemma.

Lemma 15. *For a constant $d \in \mathbb{R}$, the geometric locus of points $\omega \in \mathbb{R}^2$ that satisfy the equation*

$$a_i\|p_i - \omega\|^2 - a_j\|p_j - \omega\|^2 = d,$$

(E.4)

is a line perpendicular to $\overline{p_i p_j}$ in case $a_i = a_j$, and either a circle centered at $c = \frac{a_i p_i - a_j p_j}{a_i - a_j}$ or an empty set in case $a_i \neq a_j$.

Proof: First, we consider the case where $a_i = a_j = a$. Let h be the projection of the point ω on the line $\overline{p_i p_j}$. Using Pythagoras' theorem, we can rewrite Eq. (E.4) as follows:

$$\left(\|p_i - h\|^2 + \|h - \omega\|^2\right) - \left(\|p_j - h\|^2 + \|h - \omega\|^2\right) = \left(\|p_i - h\|^2 - \|p_j - h\|^2\right) = \frac{d}{a},$$ (E.5)

thus, any point ω whose projection on the line $\overline{p_i p_j}$ is h satisfies Eq. (E.4). Therefore, the

geometric locus of the point ω is a line perpendicular to the line $\overline{p_i p_j}$. Now, we consider the case where $a_i \neq a_j$. Let $p = (p_x, p_y)$ and $\omega = (\omega_x, \omega_y)$. We can rewrite Eq. (E.4) as:

$$(a_i - a_j)\left(\omega_x^2 + \omega_y^2\right) - 2\left(a_i p_{ix} - a_j p_{jx}\right)\omega_x - 2\left(a_i p_{iy} - a_j p_{jy}\right)\omega_y = d - \left(a_i \|p_i\|^2 - a_j \|p_j\|^2\right) \tag{E.6}$$

or equivalently:

$$\left[\omega_x - \frac{a_i p_{ix} - a_j p_{jx}}{a_i - a_j}\right]^2 + \left[\omega_y - \frac{a_i p_{iy} - a_j p_{jy}}{a_i - a_j}\right]^2 = d', \tag{E.7}$$

where $d' = \frac{d - \left(a_i \|p_i\|^2 - a_j \|p_j\|^2\right)}{a_i - a_j} + \frac{(a_i p_{ix} - a_j p_{jx})^2 + (a_i p_{iy} - a_j p_{jy})^2}{(a_i - a_j)^2}$. Hence, the geometric locus of the point ω is either an empty set if $d' < 0$ or a circle centered at $c = \frac{a_i p_i - a_j p_j}{a_i - a_j}$ with radius $\kappa = \sqrt{d'}$ and Lemma 15 is proved. ∎

Now, we use proof by contradiction to establish Lemma 9. Let v_i^* and v_j^* be the volume of the neighboring regions W_i^* and W_j^*, respectively, and assume that the optimal boundary $\delta_{i,j}^*$ is neither a segment if $a_i = a_j$, nor an arc in case $a_i \neq a_j$. Let $m_{i,j}(\alpha) = \alpha p_i + (1 - \alpha)p_j$ and let $l_{i,j}(\alpha)$ be either a line perpendicular to $\overline{p_i p_j}$ at $m_{i,j}(\alpha)$ in case $a_i = a_j$, or a circle centered at $c_{i,j} = \frac{a_i p_i - a_j p_j}{a_i - a_j}$ and radius $\kappa_{i,j}(\alpha) = \|c_{i,j} - m_{i,j}(\alpha)\|$ in case $a_i \neq a_j$. Now, we define:

$$W_i' = \left\{\omega \mid \omega \in \Omega_{i,j}^*, a_i \|p_i - \omega\|^2 - a_j \|p_j - \omega\|^2 \leq a_i \|p_i - m_{i,j}(\alpha)\|^2 - a_j \|p_j - m_{i,j}(\alpha)\|^2\right\}, \tag{E.8}$$

$$W_j' = \left\{\omega \mid \omega \in \Omega_{i,j}^*, a_i \|p_i - \omega\|^2 - a_j \|p_j - \omega\|^2 \geq a_i \|p_i - m_{i,j}(\alpha)\|^2 - a_j \|p_j - m_{i,j}(\alpha)\|^2\right\}, \tag{E.9}$$

where $\Omega_{i,j}^* = W_i^* \cup W_j^*$, and let $v_i'(\alpha)$ and $v_j'(\alpha)$ be the volume of regions W_i' and W_j', respectively. Note that since the sensor density function $f(\omega)$ is a continuous and differentiable function, both $v_i'(\alpha)$ and $v_j'(\alpha)$ are continuous functions of α. As an intuition,

note that the geometric locus of points $\omega \in \mathbb{R}^2$, such that $a_i\|p_i - \omega\|^2 - a_j\|p_j - \omega\|^2 = a_i\|p_i - m_{i,j}(\alpha)\|^2 - a_j\|p_j - m_{i,j}(\alpha)\|^2$ holds, is $l_{i,j}(\alpha)$ according to Lemma 15. It readily follows from simple geometric reasoning that for $a_i \leq a_j$, we have $v_i' = 0$ for large enough values of α, and $v_j' = 0$ for $\alpha = \frac{a_i}{a_i - a_j}$ that leads to $\kappa_{i,j}(\alpha) = 0$. Similarly, for $a_i > a_j$, we have $v_i' = 0$ for $\alpha = \frac{a_i}{a_i - a_j}$ that leads to $\kappa_{i,j}(\alpha) = 0$, and $v_j' = 0$ for large enough values of α.

Using the above argument and the fact that $v_i'(\alpha) + v_j'(\alpha) = v_i^* + v_j^*$, it readily follows that there exists an α^* for which we have $v_i'(\alpha^*) = v_i^*$ and $v_j'(\alpha^*) = v_j^*$. Now, we define a new cell partitioning $\mathbf{W}'' = (W_1'', \cdots, W_N'')$ where $W_t'' = W_t^*$ for $t \notin \{i, j\}$, $W_i'' = W_i'(\alpha^*)$, and $W_j'' = W_j'(\alpha^*)$. Then, substituting $\mathbf{W}^*$ with $\mathbf{W}''$ will increase the objective function by:

$$
\begin{aligned}
\Delta = & \left[\sum_{n=1}^{N} \int_{W_n''} \frac{a_n}{\ln\left(\frac{1}{1-\epsilon}\right)} \|p_n - \omega\|^2 \left(2^{\frac{R_b}{B}} - 1\right) f(\omega) d\omega \right. \\
& \left. + \lambda \sum_{i=1}^{N} \sum_{j=1}^{M} \frac{b_{i,j}}{\ln\left(\frac{1}{1-\epsilon}\right)} \|p_i - q_j\|^2 \left(2^{\frac{r_{i,j} \times R_b \times v_i''}{B}} - 1\right) \right] \\
& - \left[\sum_{n=1}^{N} \int_{W_n^*} \frac{a_n}{\ln\left(\frac{1}{1-\epsilon}\right)} \|p_n - \omega\|^2 \left(2^{\frac{R_b}{B}} - 1\right) f(\omega) d\omega \right. \\
& \left. + \lambda \sum_{i=1}^{N} \sum_{j=1}^{M} \frac{b_{i,j}}{\ln\left(\frac{1}{1-\epsilon}\right)} \|p_i - q_j\|^2 \left(2^{\frac{r_{i,j} \times R_b \times v_i^*}{B}} - 1\right) \right].
\end{aligned}
\tag{E.10}
$$

Note that $W_t'' = W_t^*$ for $t \notin \{i, j\}$ and $v_t'' = v_t^*$ for all $t \in \{1, \cdots, N\}$. Hence, we have:

$$
\begin{aligned}
\frac{\Delta \times \ln\left(\frac{1}{1-\epsilon}\right)}{\left(2^{\frac{R_b}{B}} - 1\right)} = & \left[\int_{W_i''} a_i \|p_i - \omega\|^2 f(\omega) d\omega + \int_{W_j''} a_j \|p_j - \omega\|^2 f(\omega) d\omega \right] \\
& - \left[\int_{W_i^*} a_i \|p_i - \omega\|^2 f(\omega) d\omega + \int_{W_j^*} a_j \|p_j - \omega\|^2 f(\omega) d\omega \right].
\end{aligned}
\tag{E.11}
$$

Let $\mathcal{V}_1 = W_i'' \cap W_j^*$ and $\mathcal{V}_2 = W_j'' \cap W_i^*$. Note that both $\mathcal{V}_1$ and $\mathcal{V}_2$ are non-empty; otherwise, we have $W_i'' = W_i^*$ and $W_j'' = W_j^*$ which contradicts the assumption that the optimal boundary $\delta_{i,j}^*$ is not a segment or an arc. Now, we can rewrite Eq. (E.11) as follows:

$$\frac{\Delta \times \ln\left(\frac{1}{1-\epsilon}\right)}{\left(2^{\frac{R_b}{B}} - 1\right)} = \left[\int_{\mathcal{V}_1} a_i \|p_i - \omega\|^2 f(\omega)d\omega + \int_{\mathcal{V}_2} a_j \|p_j - \omega\|^2 f(\omega)d\omega\right]$$

$$- \left[\int_{\mathcal{V}_2} a_i \|p_i - \omega\|^2 f(\omega)d\omega + \int_{\mathcal{V}_1} a_j \|p_j - \omega\|^2 f(\omega)d\omega\right] \tag{E.12}$$

$$= \int_{\mathcal{V}_1} \left(a_i \|p_i - \omega\|^2 - a_j \|p_j - \omega\|^2\right) f(\omega)d\omega$$

$$+ \int_{\mathcal{V}_2} \left(a_j \|p_j - \omega\|^2 - a_i \|p_i - \omega\|^2\right) f(\omega)d\omega \tag{E.13}$$

$$< \int_{\mathcal{V}_1} \left(a_i \|p_i - m_{i,j}(\alpha^*)\|^2 - a_j \|p_j - m_{i,j}(\alpha^*)\|^2\right) f(\omega)d\omega$$

$$+ \int_{\mathcal{V}_2} \left(a_j \|p_j - m_{i,j}(\alpha^*)\|^2 - a_i \|p_i - m_{i,j}(\alpha^*)\|^2\right) f(\omega)d\omega \tag{E.14}$$

$$= \left(a_i \|p_i - m_{i,j}(\alpha^*)\|^2 - a_j \|p_j - m_{i,j}(\alpha^*)\|^2\right) \times \left(\int_{\mathcal{V}_1} f(\omega)d\omega - \int_{\mathcal{V}_2} f(\omega)d\omega\right)$$

$$\tag{E.15}$$

$$= 0, \tag{E.16}$$

where the inequality in (E.14) follows from Lemma 15 and the fact that both $\mathcal{V}_1$ and $\mathcal{V}_2$ are non-empty. Also, Eq. (E.16) follows from the fact that $\mathcal{V}_1$ and $\mathcal{V}_2$ have the same volume because $v_i'' = v_i^*$ and $v_j'' = v_j^*$. Since $0 < \epsilon < 1$ and $R_b > 0$, it follows from Eqs. (E.12)−(E.16) that

$$\frac{\Delta \times \ln\left(\frac{1}{1-\epsilon}\right)}{\left(2^{\frac{R_b}{B}} - 1\right)} < 0 \qquad \implies \qquad \Delta < 0, \tag{E.17}$$

that is, the increase in the objective function is negative. Therefore, $\mathbf{W}''$ yields a lower objective function than that of $\mathbf{W}^*$ which contradicts the optimality of $\mathbf{W}^*$ and the proof is complete. ∎

E.3 Proof of Proposition 15

According to Lemma 9, the optimal boundary $\delta_{i,j}^*$, which intersects the line $\overline{p_i p_j}$ at $h_{i,j}^*$, is either a segment if $a_i = a_j$, or an arc with its center placed at $c = \frac{a_i p_i - a_j p_j}{a_i - a_j}$ if $a_i \neq a_j$. Let α^* be the scalar that satisfies the equation $\alpha^* p_i + (1 - \alpha^*) p_j = h_{i,j}^*$. For an infinitesimal $\gamma > 0$, let $\alpha' = \alpha^* - \gamma$. Then, we define a new cell partitioning $\mathbf{W}' = \left(W_1', \cdots, W_N'\right)$ as follows:

$$W_i' = \left\{\omega \mid \omega \in \Omega_{i,j}^*, a_i \|p_i - \omega\|^2 - a_j \|p_j - \omega\|^2 \leq a_i \|p_i - h_{i,j}'\|^2 - a_j \|p_j - h_{i,j}'\|^2\right\},$$

(E.18)

$$W_j' = \left\{\omega \mid \omega \in \Omega_{i,j}^*, a_i \|p_i - \omega\|^2 - a_j \|p_j - \omega\|^2 \geq a_i \|p_i - h_{i,j}'\|^2 - a_j \|p_j - h_{i,j}'\|^2\right\},$$

(E.19)

and $W_t' = W_t^*$ for $t \notin \{i, j\}$, where $\Omega_{i,j}^* = W_i^* \cup W_j^*$ and $h_{i,j}' = \alpha' p_i + (1 - \alpha') p_j$. Note that the infinitesimal difference between α^* and α' leads to an infinitesimal difference between volumes of these new regions, i.e., $v_i' = v_i^* + dv$ and $v_j' = v_j^* - dv$, where v_i' and v_j' are the volume of W_i' and W_j', respectively, and dv is the volume of the region $dW = W_i' - W_i^* = W_j^* - W_j'$. By substituting $\mathbf{W}^*$ with $\mathbf{W}'$, the increase in sensor power consumption can be written as:

$$\Delta_1 = \int_{W_i'} \frac{a_i}{\ln\left(\frac{1}{1-\epsilon}\right)} \|p_i - \omega\|^2 \left(2^{\frac{R_b}{B}} - 1\right) f(\omega) d\omega + \int_{W_j'} \frac{a_j}{\ln\left(\frac{1}{1-\epsilon}\right)} \|p_j - \omega\|^2 \left(2^{\frac{R_b}{B}} - 1\right) f(\omega) d\omega$$
$$- \int_{W_i^*} \frac{a_i}{\ln\left(\frac{1}{1-\epsilon}\right)} \|p_i - \omega\|^2 \left(2^{\frac{R_b}{B}} - 1\right) f(\omega) d\omega - \int_{W_j^*} \frac{a_j}{\ln\left(\frac{1}{1-\epsilon}\right)} \|p_j - \omega\|^2 \left(2^{\frac{R_b}{B}} - 1\right) f(\omega) d\omega$$

(E.20)

which can be simplified as follows:

$$\Delta_1 = \int_{dW} \frac{a_i}{\ln\left(\frac{1}{1-\epsilon}\right)} \|p_i - \omega\|^2 \left(2^{\frac{R_b}{B}} - 1\right) f(\omega) d\omega - \int_{dW} \frac{a_j}{\ln\left(\frac{1}{1-\epsilon}\right)} \|p_j - \omega\|^2 \left(2^{\frac{R_b}{B}} - 1\right) f(\omega) d\omega$$

(E.21)

$$= \int_{dW} \frac{1}{\ln\left(\frac{1}{1-\epsilon}\right)} \left[a_i \|p_i - \omega\|^2 - a_j \|p_j - \omega\|^2\right] \left(2^{\frac{R_b}{B}} - 1\right) f(\omega) d\omega.$$

(E.22)

It follows from Lemma 15 and the definition of W_i' and W_j' in Eqs. (E.18) and (E.19) that for an infinitesimal region dW, we have:

$$\Delta_1 = \int_{dW} \frac{1}{\ln\left(\frac{1}{1-\epsilon}\right)} \left[a_i \|p_i - h_{i,j}^*\|^2 - a_j\|p_j - h_{i,j}^*\|^2\right]\left(2^{\frac{R_b}{B}} - 1\right)f(\omega)d\omega + \mathcal{O}(dv^2) \quad \text{(E.23)}$$

$$= \frac{1}{\ln\left(\frac{1}{1-\epsilon}\right)} \left[a_i \|p_i - h_{i,j}^*\|^2 - a_j\|p_j - h_{i,j}^*\|^2\right]\left(2^{\frac{R_b}{B}} - 1\right)dv + \mathcal{O}(dv^2). \quad \text{(E.24)}$$

Now, substituting $\mathbf{W}^*$ with $\mathbf{W}'$ results in the following increase in AP power consumption:

$$\Delta_2 = \sum_{t=1}^{M} \frac{b_{i,t}}{\ln\left(\frac{1}{1-\epsilon}\right)} \|p_i - q_t\|^2\left(2^{\frac{r_{i,t}R_b v_i'}{B}} - 1\right) + \sum_{t=1}^{M} \frac{b_{j,t}}{\ln\left(\frac{1}{1-\epsilon}\right)} \|p_j - q_t\|^2\left(2^{\frac{r_{j,t}R_b v_i'}{B}} - 1\right)$$

$$- \sum_{t=1}^{M} \frac{b_{i,t}}{\ln\left(\frac{1}{1-\epsilon}\right)} \|p_i - q_t\|^2\left(2^{\frac{r_{i,t}R_b v_i^*}{B}} - 1\right) - \sum_{t=1}^{M} \frac{b_{j,t}}{\ln\left(\frac{1}{1-\epsilon}\right)} \|p_j - q_t\|^2\left(2^{\frac{r_{j,t}R_b v_i^*}{B}} - 1\right)$$

$$\text{(E.25)}$$

$$= \sum_{t=1}^{M} \frac{b_{i,t}}{\ln\left(\frac{1}{1-\epsilon}\right)} \|p_i - q_t\|^2 \times 2^{\frac{r_{i,t}R_b v_i^*}{B}} \times \left(2^{\frac{r_{i,t}R_b dv}{B}} - 1\right)$$

$$+ \sum_{t=1}^{M} \frac{b_{j,t}}{\ln\left(\frac{1}{1-\epsilon}\right)} \|p_j - q_t\|^2 \times 2^{\frac{r_{j,t}R_b v_j^*}{B}} \times \left(2^{\frac{-r_{j,t}R_b dv}{B}} - 1\right), \quad \text{(E.26)}$$

where Eq. (E.26) follows from the relations $v_i' = v_i^* + dv$ and $v_j' = v_j^* - dv$. Using the Taylor series expansion, we can write Eq. (E.26) as follows:

$$\Delta_2 = \sum_{t=1}^{M} \frac{b_{i,t}}{\ln\left(\frac{1}{1-\epsilon}\right)} \|p_i - q_t\|^2 \times 2^{\frac{r_{i,t}R_b v_i^*}{B}} \times \ln(2) \times \frac{r_{i,t}R_b dv}{B}$$

$$- \sum_{t=1}^{M} \frac{b_{j,t}}{\ln\left(\frac{1}{1-\epsilon}\right)} \|p_j - q_t\|^2 \times 2^{\frac{r_{j,t}R_b v_j^*}{B}} \times \ln(2) \times \frac{r_{j,t}R_b dv}{B} + \mathcal{O}(dv^2), \quad \text{(E.27)}$$

where $\mathcal{O}(dv^2)$ contains terms of second and higher order in Taylor series approximation. By combining Eqs. (E.24) and (E.27), the total increase in objective function due to substituting $\mathbf{W}^*$ with $\mathbf{W}'$ is given by $\Delta = \Delta_1 + \lambda\Delta_2$, that is:

$$\Delta = \frac{1}{\ln\left(\frac{1}{1-\epsilon}\right)} \left[a_i\|p_i - h_{i,j}^*\|^2 - a_j\|p_j - h_{i,j}^*\|^2\right]\left(2^{\frac{R_b}{B}} - 1\right)dv$$

$$+ \lambda \sum_{t=1}^{M} \frac{b_{i,t}}{\ln\left(\frac{1}{1-\epsilon}\right)} \|p_i - q_t\|^2 \times 2^{\frac{r_{i,t} R_b v_i^*}{B}} \times \ln(2) \times \frac{r_{i,t} R_b dv}{B}$$

$$- \lambda \sum_{t=1}^{M} \frac{b_{j,t}}{\ln\left(\frac{1}{1-\epsilon}\right)} \|p_j - q_t\|^2 \times 2^{\frac{r_{j,t} R_b v_j^*}{B}} \times \ln(2) \times \frac{r_{j,t} R_b dv}{B} + \mathcal{O}(dv^2) \geq 0, \qquad \text{(E.28)}$$

where the last inequality follows from the optimality of $\mathbf{W}^*$. By dividing Δ by dv and taking the limit $dv \longrightarrow 0$, the term $\mathcal{O}(dv^2)$ vanishes and we have:

$$\left[a_i \|p_i - h_{i,j}^*\|^2 - a_j \|p_j - h_{i,j}^*\|^2\right]\left(2^{\frac{R_b}{B}} - 1\right)$$

$$+ \lambda \sum_{t=1}^{M} b_{i,t} \|p_i - q_t\|^2 \times 2^{\frac{r_{i,t} R_b v_i^*}{B}} \times \ln(2) \times \frac{r_{i,t} R_b}{B}$$

$$- \lambda \sum_{t=1}^{M} b_{j,t} \|p_j - q_t\|^2 \times 2^{\frac{r_{j,t} R_b v_j^*}{B}} \times \ln(2) \times \frac{r_{j,t} R_b}{B} \geq 0. \qquad \text{(E.29)}$$

By defining $\alpha'' = \alpha^* + \gamma$ for an infinitesimal $\gamma > 0$ and repeating the same procedure, we obtain:

$$\left[a_i \|p_i - h_{i,j}^*\|^2 - a_j \|p_j - h_{i,j}^*\|^2\right]\left(2^{\frac{R_b}{B}} - 1\right)$$

$$+ \lambda \sum_{t=1}^{M} b_{i,t} \|p_i - q_t\|^2 \times 2^{\frac{r_{i,t} R_b v_i^*}{B}} \times \ln(2) \times \frac{r_{i,t} R_b}{B}$$

$$- \lambda \sum_{t=1}^{M} b_{j,t} \|p_j - q_t\|^2 \times 2^{\frac{r_{j,t} R_b v_j^*}{B}} \times \ln(2) \times \frac{r_{j,t} R_b}{B} \leq 0. \qquad \text{(E.30)}$$

By combining Eqs. (E.29) and (E.30), we obtain Eq. (5.22) and the proof is complete. ∎

E.4 Proof of Proposition 16

First, we prove the following lemma.

Lemma 16. *Let $g(x) = a^x + a^{C-x}$ where $x \in [0, C]$ for $a, C \in \mathbb{R}^+$ and $a > 1$. Then, $g(.)$ is symmetric around the point $x = \frac{C}{2}$ and strictly decreasing in the interval $\left[0, \frac{C}{2}\right)$.*

Proof: The function $g(.)$ is symmetric because $g(x) = g(C - x)$. Now, by taking the derivative w.r.t. x, we have $\frac{d}{dx}g(x) = \ln(a) \times (a^x - a^{C-x})$. Since $a > 1$, we have $\frac{d}{dx}g(x) < 0$ for $x \in [0, \frac{C}{2})$ and the proof is complete. ∎

Lemma 16 readily leads to the following conclusion.

Corollary 4. *Let x_1 and x_2 be two non-negative real numbers such that $x_1 + x_2 = C$ is a constant. Then, for $a > 1$, decreasing $|x_1 - x_2|$ results in smaller $a^{x_1} + a^{x_2}$ values.*

Now, we proceed to establish Proposition 16. Note that the constrained objective function formulation in Eqs. (5.23)−(5.25) is equivalent to

$$\underset{F_{n,1},\cdots,F_{n,M}}{\arg\min} \sum_{i=1}^{M} 2^{\left[\frac{F_{n,i}}{B} + \log_2\left(b_{n,i}\|p_n - q_i\|^2\right)\right]}, \tag{E.31}$$

$$\text{s.t. } \sum_{i=1}^{M} F_{n,i} = \int_{W_n} R_b f(\omega) d\omega = R_b v_n, \quad \text{and} \quad F_{n,i} \geq 0 \text{ for all } i \in \mathcal{I}_{BS}, \tag{E.32}$$

which is equivalent to the following constrained objective function formulation:

$$\underset{x_{n,1},\cdots,x_{n,M}}{\arg\min} \sum_{i=1}^{M} 2^{x_{n,i}}, \tag{E.33}$$

$$\text{s.t. } \sum_{i=1}^{M} x_{n,i} = \frac{R_b v_n}{B} + \sum_{i=1}^{M} \log_2\left(b_{n,i}\|p_n - q_i\|^2\right) = C, \tag{E.34}$$

$$x_{n,i} \geq \log_2\left(b_{n,i}\|p_n - q_i\|^2\right) \text{ for all } i \in \{1, \cdots, M\}, \tag{E.35}$$

where $x_{n,i} = \frac{F_{n,i}}{B} + \log_2\left(b_{n,i}\|p_n - q_i\|^2\right)$. Corollary 4 indicates that for any two indices i and j, we can decrease the objective function in Eq. (E.33) by decreasing $|x_{n,i} - x_{n,j}|$ while keeping their summation constant. Thus, the minimum occurs when we have $x_{n,1} = \cdots = x_{n,M} = \frac{C}{M}$. However, this may contradict the constraint in Eq. (E.35) for some indices $i \in \{1, \cdots, M\}$. Therefore, we can always improve the objective function in Eq. (E.33) and achieve a lower value by decreasing the distance between any pair of $x_{n,i}$ and $x_{n,j}$ while

keeping their summation constant as long as the constraints in Eq. (E.35) is not contradicted. This observation results in

Corollary 5. *Let $X_n^* = (x_{n,1}^*, \cdots, x_{n,M}^*)$ be the optimal solution to the constrained objective function in Eqs. (E.33)−(E.35). Then, there exist unique sets I_L^* and I_U^* such that*

$$x_{n,i}^* = x_{n,j}^* = \overline{x}^* \ \ for \ \ \forall i,j \in I_U^*, \qquad and \qquad x_{n,i}^* = \log_2\left(b_{n,i}\|p_n - q_i\|^2\right) \ \ for \ \ \forall i \in I_L^*,$$

(E.36)

and $x_{n,i}^* > \overline{x}^*$ for all $i \in I_L^*$.

To see why the last property holds, first, let us assume that we have $x_{n,j}^* = \log_2\left(b_{n,j}\|p_n - q_j\|^2\right)$ for all $j \in I_U^*$. Since $v_n > 0$, it follows that

$$\sum_{t=1}^{M} x_{n,t}^* = \sum_{t \in I_U^*} x_{n,t}^* + \sum_{t \in I_L^*} x_{n,t}^* = \sum_{t=1}^{M} \log_2\left(b_{n,t}\|p_n - q_t\|^2\right) < C,$$

(E.37)

which is in contradiction with Eq. (E.34). Hence, there exists an index $j' \in I_U^*$ for which $x_{n,j'}^* > \log_2\left(b_{n,j'}\|p_n - q_{j'}\|^2\right)$. Now, assume that there exists an index i such that $x_{n,i}^* = \log_2\left(b_{n,i}\|p_n - q_i\|^2\right) < \overline{x}^* = x_{n,j'}^*$. Then, according to Corollary 4, we can achieve a lower objective function by replacing $x_{n,i}^*$ and $x_{n,j'}^*$ with $x_{n,i}^* + \eta$ and $x_{n,j'}^* - \eta$ for any $0 < \eta < x_{n,j'}^* - \log_2\left(b_{n,j'}\|p_n - q_{j'}\|^2\right)$, which contradicts the optimality of X^*. Thus, we have $x_{n,i}^* > \overline{x}^*$ for all $i \in I_L^*$.

Corollary 5 indicates that in an optimal solution, all $x_{n,t}^*$ values should be equal to some value $\overline{x}^*$ except for those that cannot get close enough to $\overline{x}^*$ without contradicting Eq. (E.35). Hence, the optimal solution can be found using a water filling algorithm as follows. By initializing I_L to an empty set and starting from the case in which all $x_{n,t}$ values are equal to the mean value $\overline{x} = \frac{C}{M}$, we can identify those indices such as $i \in I$ for which $x_{n,i} < \log_2\left(b_{n,i}\|p_n - q_i\|^2\right)$. Thus, I provides the first series of indices for which the value of $x_{n,i}$ cannot be reduced enough to the mean value $\overline{x}$ without contradicting the constraint in

Eq. (E.35). Therefore, the optimal value for each $i \in I$ is $x_{n,i}^* = \log_2\left(b_{n,i}\|p_n - q_i\|^2\right)$ and we update the set I_L by taking its union with the set I. Now, we can update the mean value $\overline{x}$ such that $\sum_{i \in \mathcal{I}_{BS} \backslash I_L} \overline{x} + \sum_{i \in I_L} x_{n,i}^*$ or equivalently $\left(M - |I_L|\right) \times \overline{x} + \sum_{i \in I_L} \log_2\left(b_{n,i}\|p_n - q_i\|^2\right)$ still sums to C. By using the new mean value $\overline{x}$, we can determine the next series of indices that would belong to I_L and the same procedure can be repeated. Note that in each iteration, the mean value $\overline{x}$ either decreases or stays the same and the set I_L either increases in size or stays the same. If I_L stays the same, meaning that there has been no other index that would contradict Eq. (E.35), then we have found the optimal solution and the algorithm terminates. Since $|I_L| \leq M$, the process of I_L increasing in size can continue for at most M iterations and the algorithm will finally converge to the optimal value X_n^* that satisfies Eq. (E.36) in Corollary 5. The above procedure is summarized in Algorithm 6. Note that the optimal values $F_{n,1}^*, \cdots, F_{n,M}^*$ in Eqs. (E.31) and (E.32) can then be found as $F_{n,i}^* = B \times \left[x_{n,i}^* - \log_2\left(b_{n,i}\|p_n - q_i\|^2\right)\right]$ and the proof is complete. ∎

E.5 Proof of Proposition 17

First, we aim to prove the convergence of the initialization step that is outlined in Algorithm 7. Note that the generalized Voronoi diagram $\mathcal{V}$ in Algorithm 7 provides the optimal cell partitioning for the following cost function:

$$\mathcal{D}'(\mathbf{P}, \mathbf{W}) = \sum_{n=1}^{N} \int_{W_n} a_n \|p_n - \omega\|^2 f(\omega) d\omega. \tag{E.38}$$

Thus, for a fixed AP deployment $\mathbf{P}$, updating $\mathbf{W}$ according to $\mathcal{V}$ does not increase the cost function $\mathcal{D}'$. Now, using the parallel axis theorem, we can rewrite Eq. (E.38) as follows:

$$\mathcal{D}'(\mathbf{P}, \mathbf{W}) = \sum_{n=1}^{N} \int_{W_n} a_n \|p_n - c_n\|^2 f(\omega) d\omega + \sum_{n=1}^{N} \int_{W_n} a_n \|c_n - \omega\|^2 f(\omega) d\omega. \tag{E.39}$$

Hence, for a fixed cell partitioning $\mathbf{W}$, updating $\mathbf{P}$ according to the rule $p_n = c_n = \frac{\int_{W_n} \omega f(\omega) d\omega}{\int_{W_n} f(\omega) d\omega}$ does not increase the cost function $\mathcal{D}'$ in Eq. (E.39) as well. Therefore, by iterating this process, a sequence of non-increasing $\mathcal{D}'$ values are generated and since $\mathcal{D}' \geq 0$, it will converge.

Note that base stations are initialized by applying the Lloyd algorithm to the set of AP points, which is known to converge. Finally, the normalized flow matrix $\mathbf{R}$ is updated by applying Algorithm 6, which we showed to converge in Appendix E.4. Thus, the initialization step which is outlined in Algorithm 7 will eventually converge.

Now, to establish the convergence of the POOL algorithm, we show that none of the three steps corresponding to updating the node deployment, cell partitioning, and normalized flow matrix will increase the objective function $\mathcal{D}_1$. Note that when $\mathbf{W}$, $\mathbf{R}$, $\mathbf{Q}$, and $\{p_j\}_{j \neq i}$ are fixed, the objective function $\mathcal{D}_1$ is a convex function of p_i; thus, updating p_i acccording to Eq. (5.20), which is the solution to the zero-gradient equation, does not increase the objective function. Similarly, once $\mathbf{W}$, $\mathbf{R}$, $\mathbf{P}$, and $\{q_j\}_{j \neq i}$ are fixed, $\mathcal{D}_1$ is a convex function of q_i. Therefore, updating q_i according to Eq. (5.21), which is the solution to the zero-gradient equation, does not increase $\mathcal{D}_1$. Hence, the node deployment step of the POOL algorithm does not increase the objective function. Note that the cell partitioning is updated through an iterative process where at each step, two neighboring regions such as W_i and W_j are selected and their boundary is adjusted. More precisely, in each iteration, all W_t regions for $t \notin \{i, j\}$ are held fixed and only the boundary $\delta_{i,j}$ between regions W_i and W_j is adjusted to provide another partitioning of the region $\Omega_{i,j} = W_i \cup W_j$. According to Proposition 15, this new partitioning is optimal; hence, the objective function $\mathcal{D}_1$ will not increase as a result of updating $\delta_{i,j}$. Finally, Proposition 16 indicates that updating the normalized flow matrix according to Algorithm 6 yields the optimal value of $\mathbf{R}$ and as such, $\mathcal{D}_1$ will either remain the same or decrease. Therefore, Algorithm 7 generates a non-increasing sequence of $\mathcal{D}_1$ values in each iteration, i.e., the POOL algorithm is an iterative improvement algorithm

and since $\mathcal{D}_1 \geq 0$, it will converge. ∎

E.6   Proof of Proposition 18

Using the parallel axis theorem, we can rewrite the objective function $\mathcal{D}_2$ in Eq. (5.26) as

$$\mathcal{D}_2\left(\mathbf{P}, \mathbf{Q}, \mathbf{W}, \mathbf{R}\right) = \sum_{n=1}^{N} \int_{W_n} \frac{a_n}{U^{-1}\left(\frac{R_b}{B\log_2(e)}\right)} \|c_n - \omega\|^2 f(\omega) d\omega$$

$$+ \sum_{n=1}^{N} \frac{a_n}{U^{-1}\left(\frac{R_b}{B\log_2(e)}\right)} \|p_n - c_n\|^2 v_n$$

$$+ \lambda \sum_{i=1}^{N} \sum_{j=1}^{M} \frac{b_{i,j}}{U^{-1}\left(\frac{F_{i,j}}{B\log_2(e)}\right)} \|p_i - q_j\|^2. \tag{E.40}$$

Since the optimal deployment satisfies the zero-gradient equation, for each $i \in \mathcal{I}_{AP}$, we have

$$\frac{\partial}{\partial p_i^*}\mathcal{D}_2 = \frac{2a_i}{U^{-1}\left(\frac{R_b}{B\log_2(e)}\right)}\left(p_i^* - c_i\right)v_i + \lambda \sum_{j=1}^{M} \frac{2b_{i,j}}{U^{-1}\left(\frac{F_{i,j}}{B\log_2(e)}\right)}\left(p_i^* - q_j^*\right) = 0. \tag{E.41}$$

Similarly, by taking the derivative with respect to the location of BS $i \in \mathcal{I}_{BS}$, we have

$$\frac{\partial}{\partial q_i^*}\mathcal{D}_2 = \lambda \sum_{j=1}^{N} \frac{2b_{j,i}}{U^{-1}\left(\frac{F_{j,i}}{B\log_2(e)}\right)}\left(q_i^* - p_j^*\right) = 0. \tag{E.42}$$

By solving these two zero-gradient equations, we obtain Eqs. (5.27) and (5.28) and the proof is complete. ∎

E.7 Proof of Lemma 10

The proof closely follows that of Lemma 9; thus, we borrow the notations and definitions outlined in Appendix E.2. More precisely, by using the proof by contradiction, we consider W_i' and W_j' as defined in Eqs. (E.8) and (E.9), respectively, and define the cell partitioning $\mathbf{W}''$ similarly. Now, we can rewrite Eq. (E.10) to calculate the increase in objective function $\mathcal{D}_2$ due to substituting $\mathbf{W}^*$ with $\mathbf{W}''$ as follows:

$$
\Delta = \left[\sum_{n=1}^{N} \int_{W_n''} \frac{a_n}{U^{-1}\left(\frac{R_b}{B\log_2(e)}\right)} \|p_n - \omega\|^2 f(\omega)d\omega + \lambda \sum_{i=1}^{N}\sum_{j=1}^{M} \frac{b_{i,j}}{U^{-1}\left(\frac{r_{i,j}R_b v_i''}{B\log_2(e)}\right)} \|p_i - q_j\|^2 \right]
$$
$$
- \left[\sum_{n=1}^{N} \int_{W_n^*} \frac{a_n}{U^{-1}\left(\frac{R_b}{B\log_2(e)}\right)} \|p_n - \omega\|^2 f(\omega)d\omega + \lambda \sum_{i=1}^{N}\sum_{j=1}^{M} \frac{b_{i,j}}{U^{-1}\left(\frac{r_{i,j}R_b v_i^*}{B\log_2(e)}\right)} \|p_i - q_j\|^2 \right].
$$

$$\tag{E.43}$$

Since $W_t'' = W_t^*$ for $t \notin \{i, j\}$ and $v_t'' = v_t^*$ for all $t \in \{1, \cdots, N\}$, we have:

$$
U^{-1}\left(\frac{R_b}{B\log_2(e)}\right) \times \Delta = \left[\int_{W_i''} a_i \|p_i - \omega\|^2 f(\omega)d\omega + \int_{W_j''} a_j \|p_j - \omega\|^2 f(\omega)d\omega \right]
$$
$$
- \left[\int_{W_i^*} a_i \|p_i - \omega\|^2 f(\omega)d\omega + \int_{W_j^*} a_j \|p_j - \omega\|^2 f(\omega)d\omega \right]. \quad \text{(E.44)}
$$

Note that the right-hand-side of Eq. (E.44) is the same as the right-hand-side of Eq. (E.11) which is shown to be less than zero in Eqs. (E.12)$-$(E.16). Thus, since $U^{-1}(x) > 0$ for all $x > 0$, we have

$$
U^{-1}\left(\frac{R_b}{B\log_2(e)}\right) \times \Delta < 0 \qquad \implies \qquad \Delta < 0, \tag{E.45}
$$

which contradicts the optimality of $\mathbf{W}^*$ and the proof is complete. ∎

E.8 Proof of Proposition 19

As shown in Lemma 10, the optimal boundary $\delta_{i,j}^*$ is a segment if $a_i = a_j$, or an arc with its center located at $c = \frac{a_i p_i - a_j p_j}{a_i - a_j}$ if $a_i \neq a_j$. Let $h_{i,j}^*$ be the intersection point of $\delta_{i,j}^*$ and the line $\overline{p_i p_j}$ which corresponds to the scalar α^* that satisfies the equation $\alpha^* p_i + (1 - \alpha^*) p_j = h_{i,j}^*$. For a small and positive $\gamma > 0$, let $\alpha' = \alpha^* - \gamma$ and define the new cell partitioning $\mathbf{W}' = (W_1', \cdots, W_N')$ as $W_t' = W_t^*$ for $t \notin \{i, j\}$ and

$$W_i' = \left\{ \omega \mid \omega \in \Omega_{i,j}^*, a_i \|p_i - \omega\|^2 - a_j \|p_j - \omega\|^2 \leq a_i \|p_i - h_{i,j}'\|^2 - a_j \|p_j - h_{i,j}'\|^2 \right\},$$
(E.46)

$$W_j' = \left\{ \omega \mid \omega \in \Omega_{i,j}^*, a_i \|p_i - \omega\|^2 - a_j \|p_j - \omega\|^2 \geq a_i \|p_i - h_{i,j}'\|^2 - a_j \|p_j - h_{i,j}'\|^2 \right\},$$
(E.47)

where $\Omega_{i,j}^* = W_i^* \cup W_j^*$ and $h_{i,j}' = \alpha' p_i + (1 - \alpha') p_j$. The infinitesimal difference between α^* and α' causes infinitesimal difference between volumes of regions W_i' and W_j', i.e., v_i' and v_j', and volumes of regions W_i^* and W_j^*. In other words, if dv is the volume of the region $dW = W_i' - W_i^* = W_j^* - W_j'$, we have $v_i' = v_i^* + dv$ and $v_j' = v_j^* - dv$. The increase in the sensor power consumption due to replacing $\mathbf{W}^*$ by $\mathbf{W}'$ is then given by

$$\Delta_1 = \int_{W_i'} \frac{a_i}{U^{-1}\left(\frac{R_b}{B \log_2(e)} \right)} \|p_i - \omega\|^2 f(\omega) d\omega + \int_{W_j'} \frac{a_j}{U^{-1}\left(\frac{R_b}{B \log_2(e)} \right)} \|p_j - \omega\|^2 f(\omega) d\omega$$
$$- \int_{W_i^*} \frac{a_i}{U^{-1}\left(\frac{R_b}{B \log_2(e)} \right)} \|p_i - \omega\|^2 f(\omega) d\omega - \int_{W_j^*} \frac{a_j}{U^{-1}\left(\frac{R_b}{B \log_2(e)} \right)} \|p_j - \omega\|^2 f(\omega) d\omega,$$
(E.48)

which can be simplified to

$$\Delta_1 = \int_{dW} \frac{1}{U^{-1}\left(\frac{R_b}{B \log_2(e)} \right)} \left[a_i \|p_i - \omega\|^2 - a_j \|p_j - \omega\|^2 \right] f(\omega) d\omega.$$
(E.49)

Using Lemma 15 and the definition of W_i' and W_j' in Eqs. (E.46) and (E.47), it readily follows that

$$\Delta_1 = \frac{1}{U^{-1}\left(\frac{R_b}{B\log_2(e)}\right)}\left[a_i\|p_i - h_{i,j}^*\|^2 - a_j\|p_j - h_{i,j}^*\|^2\right]dv + \mathcal{O}(dv^2), \tag{E.50}$$

where $\mathcal{O}(dv^2)$ includes terms of second and higher order. The increase in AP power consumption due to substituting $\mathbf{W}^*$ with $\mathbf{W}'$ can be written as

$$\Delta_2 = \sum_{t=1}^{M}\frac{b_{i,t}}{U^{-1}\left(\frac{r_{i,t}R_b v_i'}{B\log_2(e)}\right)}\|p_i - q_t\|^2 + \sum_{t=1}^{M}\frac{b_{j,t}}{U^{-1}\left(\frac{r_{j,t}R_b v_j'}{B\log_2(e)}\right)}\|p_j - q_t\|^2$$

$$- \sum_{t=1}^{M}\frac{b_{i,t}}{U^{-1}\left(\frac{r_{i,t}R_b v_i^*}{B\log_2(e)}\right)}\|p_i - q_t\|^2 - \sum_{t=1}^{M}\frac{b_{j,t}}{U^{-1}\left(\frac{r_{j,t}R_b v_j^*}{B\log_2(e)}\right)}\|p_j - q_t\|^2. \tag{E.51}$$

For the function $U(x) = e^x E_1(x)$, we have $\frac{d}{dx}U(x) = e^x E_1(x) + e^x \times \frac{-e^{-x}}{x} = U(x) - \frac{1}{x}$ and

$$\frac{d}{dx}\left(\frac{1}{U^{-1}(x)}\right) = \frac{-\left(U^{-1}\right)'(x)}{\left[U^{-1}(x)\right]^2} = \frac{-1}{\left[U^{-1}(x)\right]^2 \times U'\left(U^{-1}(x)\right)} = \frac{1}{U^{-1}(x)\left[1 - xU^{-1}(x)\right]}. \tag{E.52}$$

Now, using Taylor series expansion, we can rewrite Δ_2 in Eq. (E.51) as follows:

$$\Delta_2 = \sum_{t=1}^{M}\left[\frac{b_{i,t}\|p_i - q_t\|^2 \times \frac{r_{i,t}R_b}{B\log_2(e)}}{U^{-1}\left(\frac{r_{i,t}R_b v_i^*}{B\log_2(e)}\right) \times \left[1 - \frac{r_{i,t}R_b v_i^*}{B\log_2(e)} \times U^{-1}\left(\frac{r_{i,t}R_b v_i^*}{B\log_2(e)}\right)\right]}\right]dv$$

$$- \sum_{t=1}^{M}\left[\frac{b_{j,t}\|p_j - q_t\|^2 \times \frac{r_{j,t}R_b}{B\log_2(e)}}{U^{-1}\left(\frac{r_{j,t}R_b v_j^*}{B\log_2(e)}\right) \times \left[1 - \frac{r_{j,t}R_b v_j^*}{B\log_2(e)} \times U^{-1}\left(\frac{r_{j,t}R_b v_j^*}{B\log_2(e)}\right)\right]}\right]dv + \mathcal{O}(dv^2), \tag{E.53}$$

where $\mathcal{O}(dv^2)$ contains terms of second and higher order in Taylor series expansion. Thus, the total increase in the objective function is given by $\Delta = \Delta_1 + \lambda\Delta_2$. Since the cell partitioning $\mathbf{W}^*$ is optimal, the increase in the objective function due to replacing $\mathbf{W}^*$ by $\mathbf{W}'$ cannot be negative; thus, we have $\Delta \geq 0$. Therefore, by dividing Δ by $dv > 0$ and taking the limit

$dv \longrightarrow 0$, the term $\mathcal{O}(dv^2)$ vanishes and we have

$$\frac{a_i}{U^{-1}\left(\frac{R_b}{B\log_2(e)}\right)}\|p_i - h_{i,j}^*\|^2 + \lambda \sum_{t=1}^{M} \frac{b_{i,t}\|p_i - q_t\|^2 \times \frac{r_{i,t}R_b}{B\log_2(e)}}{U^{-1}\left(\frac{r_{i,t}R_b v_i^*}{B\log_2(e)}\right)\left[1 - \frac{r_{i,t}R_b v_i^*}{B\log_2(e)} \times U^{-1}\left(\frac{r_{i,t}R_b v_i^*}{B\log_2(e)}\right)\right]}$$

$$\geq \frac{a_j}{U^{-1}\left(\frac{R_b}{B\log_2(e)}\right)}\|p_j - h_{i,j}^*\|^2 + \lambda \sum_{t=1}^{M} \frac{b_{j,t}\|p_j - q_t\|^2 \times \frac{r_{j,t}R_b}{B\log_2(e)}}{U^{-1}\left(\frac{r_{j,t}R_b v_j^*}{B\log_2(e)}\right)\left[1 - \frac{r_{j,t}R_b v_j^*}{B\log_2(e)} \times U^{-1}\left(\frac{r_{j,t}R_b v_j^*}{B\log_2(e)}\right)\right]}.$$

$$\text{(E.54)}$$

Now, by defining $\alpha'' = \alpha^* + \gamma$ for an infinitesimal $\gamma > 0$ and repeating the same argument, we obtain $\Delta \leq 0$ and the inequality sign in Eq. (E.54) will be reversed, i.e., we have

$$\frac{a_i}{U^{-1}\left(\frac{R_b}{B\log_2(e)}\right)}\|p_i - h_{i,j}^*\|^2 + \lambda \sum_{t=1}^{M} \frac{b_{i,t}\|p_i - q_t\|^2 \times \frac{r_{i,t}R_b}{B\log_2(e)}}{U^{-1}\left(\frac{r_{i,t}R_b v_i^*}{B\log_2(e)}\right)\left[1 - \frac{r_{i,t}R_b v_i^*}{B\log_2(e)} \times U^{-1}\left(\frac{r_{i,t}R_b v_i^*}{B\log_2(e)}\right)\right]}$$

$$\leq \frac{a_j}{U^{-1}\left(\frac{R_b}{B\log_2(e)}\right)}\|p_j - h_{i,j}^*\|^2 + \lambda \sum_{t=1}^{M} \frac{b_{j,t}\|p_j - q_t\|^2 \times \frac{r_{j,t}R_b}{B\log_2(e)}}{U^{-1}\left(\frac{r_{j,t}R_b v_j^*}{B\log_2(e)}\right)\left[1 - \frac{r_{j,t}R_b v_j^*}{B\log_2(e)} \times U^{-1}\left(\frac{r_{j,t}R_b v_j^*}{B\log_2(e)}\right)\right]}.$$

$$\text{(E.55)}$$

The two inequalities in Eqs. (E.54) and (E.55) yield the equality in Eq. (5.29) and the proof is complete. ∎

E.9   Proof of Lemma 11

First, we show that the function $U(x)$ is strictly decreasing. For this purpose, we have:

$$\frac{d}{dx}U(x) = e^x E_1(x) + e^x \times \left(-\frac{e^{-x}}{x}\right) = e^x E_1(x) - \frac{1}{x} < 0, \tag{E.56}$$

where the last inequality follows from the inequality $xe^x E_1(x) < 1$ in [77]. Note that for $y > 0$, the function $U(y) = e^y E_1(y)$ satisfies the following inequalities [77, 35]:

$$\frac{1}{2}\ln\left(1+\frac{2}{y}\right) < U(y) < \ln\left(1+\frac{1}{y}\right). \tag{E.57}$$

It readily follows from Eq. (E.57) that both domain and range of the function $U(y)$ is $(0,\infty)$. Since $U(y)$ is strictly decreasing, it is invertible and we define $y = U^{-1}(x)$. Substituting $y = U^{-1}(x)$ and $x = U(y)$ in Eq. (E.57), we obtain:

$$\frac{1}{2}\ln\left(1+\frac{2}{U^{-1}(x)}\right) < x < \ln\left(1+\frac{1}{U^{-1}(x)}\right). \tag{E.58}$$

From Eq. (E.58) it readily follows that

$$\frac{1}{2}\ln\left(1+\frac{2}{U^{-1}(x)}\right) < x \qquad \Longrightarrow \qquad \frac{1}{U^{-1}(x)} < \frac{e^{2x}-1}{2}, \tag{E.59}$$

$$x < \ln\left(1+\frac{1}{U^{-1}(x)}\right) \qquad \Longrightarrow \qquad e^{x}-1 < \frac{1}{U^{-1}(x)}, \tag{E.60}$$

which concludes the proof. ∎

E.10 Proof of Proposition 20

The proof closely follows that of Proposition 16; thus, we borrow the notations and definitions outlined in Appendix E.4. We can rewrite the constrained objective function formulation in Eqs. (5.34)-(5.36) as

$$\arg\min_{F_{n,1},\cdots,F_{n,M}} \sum_{i=1}^{M} e^{\left[\frac{2F_{n,i}}{B\log_2(e)}+\ln\left(b_{n,i}\|p_n-q_i\|^2\right)\right]}, \tag{E.61}$$

$$\text{s.t. } \sum_{i=1}^{M} F_{n,i} = \int_{W_n} R_b f(\omega)d\omega = R_b v_n, \qquad \text{and} \qquad F_{n,i} \geq 0 \text{ for all } i \in \mathcal{I}_{BS}. \tag{E.62}$$

The above constrained objective function formulation can be rewritten as

$$\underset{x_{n,1},\cdots,x_{n,M}}{\arg\min} \sum_{i=1}^{M} e^{x_{n,i}} \tag{E.63}$$

$$\text{s.t.} \sum_{i=1}^{M} x_{n,i} = \frac{2R_b v_n}{B \log_2(e)} + \sum_{i=1}^{M} \ln\left(b_{n,i}\|p_n - q_i\|^2\right) = S, \tag{E.64}$$

$$x_{n,i} \geq \ln\left(b_{n,i}\|p_n - q_i\|^2\right) \qquad \text{for all } i \in \{1,\cdots,M\}, \tag{E.65}$$

where $x_{n,i} = \frac{2F_{n,i}}{B \log_2(e)} + \ln\left(b_{n,i}\|p_n - q_i\|^2\right)$. According to Corollary 4, the objective function in Eq. (E.63) can be decreased by reducing $|x_{n,i} - x_{n,j}|$ while keeping their summation unaltered. Hence, the minimum occurs when we have $x_{n,1} = \cdots = x_{n,M} = \frac{S}{M}$. However, it is crucial to make sure that the constraints in Eqs. (E.64) and (E.65) are not contradicted. Hence, using the same argument as in Corollary 5, we have:

Corollary 6. *Let $X_n^* = (x_{n,1}^*, \cdots, x_{n,M}^*)$ be the optimal solution to the constrained objective function in Eqs. (E.63)–(E.65). Then, there exist unique sets J_L^* and J_U^* such that*

$$x_{n,i}^* = x_{n,j}^* = \overline{x}^* \ \text{ for } \ \forall i,j \in J_U^*, \quad \text{and} \quad x_{n,i}^* = \ln\left(b_{n,i}\|p_n - q_i\|^2\right) \ \text{ for } \ \forall i \in J_L^*, \tag{E.66}$$

and $x_{n,i}^* > \overline{x}^*$ for all $i \in J_L^*$.

Corollary 6 indicates that all $x_{n,i}^*$ values are equal to some value $\overline{x}^*$ in the optimal solution except the ones that cannot get close enough to $\overline{x}^*$ without contradicting the constraint in Eq. (E.65). Hence, the same arguments and the water filling algorithm explained in Appendix E.4, with the modification of replacing $\log_2(.)$ with natural logarithm, can be used to determine the optimal solution. This procedure is exactly what is outlined in Algorithm 8 which concludes the proof. ∎

E.11 Proof of Proposition 21

The proof of convergence for the initialization step is similar to that of Proposition 17 in Appendix E.5 and is omitted here. In what follows, we demonstrate that none of the three steps in the PEEL algorithm will increase the objective function $\mathcal{D}_2$. Note that the term in Eq. (5.27) is the solution to the zero-gradient equation; thus, for a fixed $\mathbf{W}$, $\mathbf{R}$, $\mathbf{Q}$, and $\{p_j\}_{j \neq i}$, updating p_i according to Eq. (5.27) does not increase the objective function. Similarly, updating q_i according to Eq. (5.28) does not increase the objective function. Therefore, updating node deployment according to the PEEL Algorithm will not increase $\mathcal{D}_2$. Note that cell partitioning is updated iteratively in the PEEL algorithm as follows: in each iteration, two adjacent regions are selected and their common boundary is adjusted according to the optimal necessary condition; thus, the objective function either remains the same or decreases at each iteration. In the last step, the optimal routing that minimizes the upper bound on AP power consumption is calculated. If the resulting routing leads to a decrease in the original objective function, it will be preserved; otherwise, it will be discarded. Hence, the objective function does not increase as a result of the data routing update rule. Hence, Algorithm 9 generates a non-increasing sequence of $\mathcal{D}_2$ values, which proves its convergence since $\mathcal{D}_2$ is bounded from below by 0. ∎